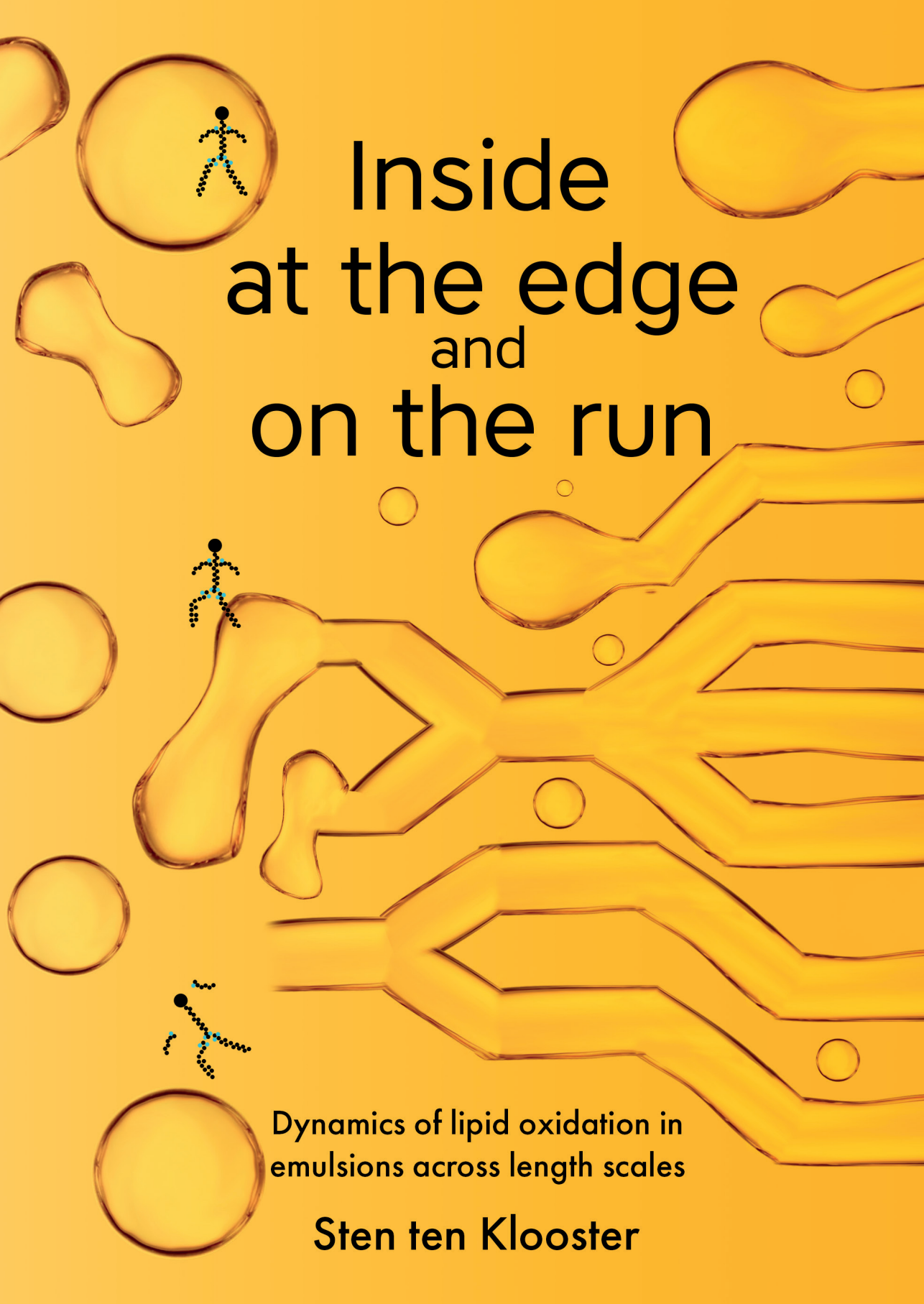
Inside
at the edge
and
on the run
Dynamics of lipid oxidation in
emulsions across length scales
Sten ten Klooster

Propositions

1. Short-chain 4-hydroperoxyenals are mobile and reactive lipid oxidation intermediates in emulsions.
   (this thesis)

2. Ignoring co-oxidation biases the current interpretation of lipid oxidation.
   (this thesis)

3. Well-being in the scientific community will improve by embracing being coached as much as athletes are.

4. Food technologists spoon-feed their customers.

5. A scientific presentation without an entertaining format is not worth listening to.

6. Cherishing naivety is essential for making scientific progress.

7. Healthy diets are dangerous for pharmaceutical businesses.

8. Consumers underestimate the value of food processing.

Propositions belonging to the thesis, entitled

Inside, at the edge, and on the run; Dynamics of lipid oxidation in emulsions across length scales

Sten ten Klooster Wageningen, 9-6-23

Inside, at the edge, and on the run

Dynamics of lipid oxidation in emulsions across length scales

Sten ten Klooster

Promotor
Prof. Dr C.G.P.H. Schroën
Personal chair, Laboratory of Food Process Engineering
Wageningen University & Research
University of Twente, Enschede

Co-promotor
Dr C.C. Berton-Carabin
Associate professor, Laboratory of Food Process Engineering
Wageningen University & Research
Research Director
INRAE, Nantes, France

Other members
Prof. Dr V. Fogliano, Wageningen University & Research
Dr T.E. Kodger, Wageningen University & Research
Prof. Dr K. Schwarz, Christian-Albrechts-Universität zu Kiel, Germany
Dr M. Laguerre, Naturex, Avignon, France

This research was conducted under the auspices of VLAG Graduate School (Biobased, Biomolecular, Chemical, Food, and Nutrition sciences).

Inside, at the edge, and on the run

Dynamics of lipid oxidation in emulsions across length scales

Sten ten Klooster

Thesis

Submitted in fulfilment of the requirements for the degree of doctor
at Wageningen University
By the authority of the Rector Magnificus,
Prof. Dr A.P.J. Mol,
in the presence of the
Thesis Committee appointed by the Academic Board
to be defended in public
on Friday 9 June 2023
at 1.30 p.m. in the Omnia Auditorium.

Sten ten Klooster
Inside, at the edge, and on the run
Dynamics of lipid oxidation in emulsions across length scales
240 Pages

PhD thesis, Wageningen University, Wageningen, the Netherlands (2023)
With references and summary in English

ISBN: 978-94-6447-624-8
DOI: https://doi.org/10.18174/589594

Content

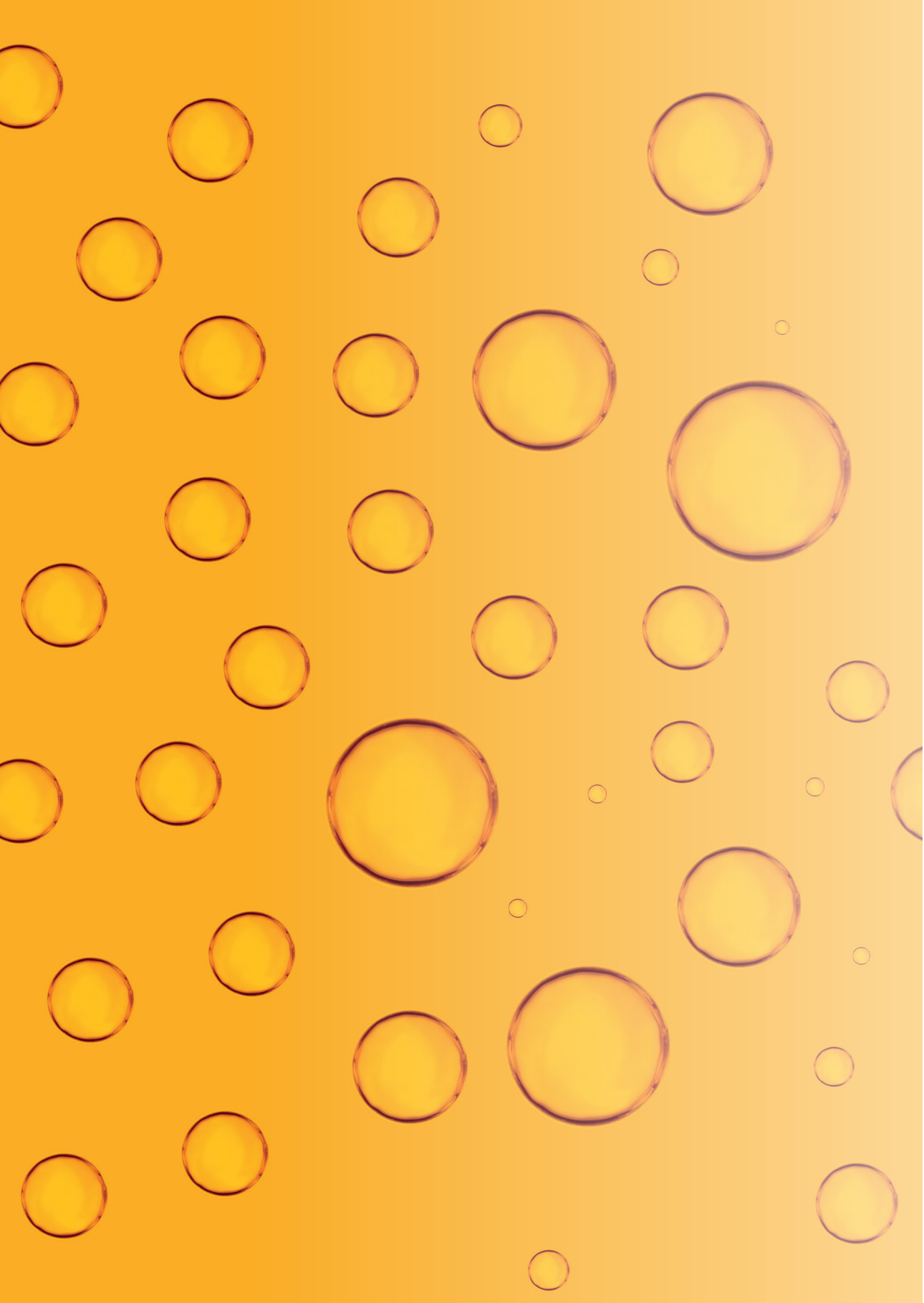

Chapter 1

Introduction and thesis outline

Introduction

An early 'experiment' on emulsion production dates back to 1756. It took place in a kitchen, where a meal was prepared to celebrate the victory of the duke of Richelieu on the Brits at Port Mahon, on the island of Minorca. Due to the lack of cream, the chef was probably somewhat desperate to try to use olive oil instead, which surprisingly led to a 'stable' sauce. Moreover, the sauce was very well-received by the guests. Based on the location where the successful experiment took place, this home-made emulsion sauce was called 'Mahonaisse'. This experiment has had way more impact than the French chef could ever have imagined, although it took another two centuries before chemists figured out how it was possible to mix two liquids that are, in essence, immiscible. From there, the number of emulsion applications skyrocketed, leading to many emulsion products, such as: sauces, paints, sunscreen, cosmetics, and ointments, as we know them in our daily lives.

Ever since the first emulsions that were made, obtaining a visually homogeneous system out of incompatible components has remained challenging. In relation to the Mahonaisse, some challenges are: why did olive oil and water not phase separate? What component in the egg led to this stability? How long could the product be eaten safely? And for how long was it still tasty? As is generally known now, the stability of emulsion products is highly influenced by their ingredients and by the emulsification process used to prepare them (McClements, 2004); yet, suppressing both physical and lipid oxidation instabilities in emulsion products remains challenging because these dynamic processes are not that well-understood. This thesis is dedicated to shed light on how dynamic processes occurring across a wide length scale contribute to lipid oxidation. For this, we developed highly dedicated experimental set-ups that are touched upon in this introduction.

1.1 Emulsification processes

Since the liquid phases constituting emulsions are immiscible, shear is commonly used to create droplets of the dispersed phase in the continuous phase. In this way, a large interface between both liquids (oil and water) is created, which is in the order of several square meters per gram of dispersed phase (Berton-Carabin et al., 2018). The production processes of emulsions are generally divided into two steps. First, the oil and water are mixed gently, resulting in a coarse emulsion with relatively large droplets. These droplets are then further broken-down into smaller droplets by intensive shearing, resulting in a fine emulsion. The shear can be generated by different types of process equipment. In rotor-

stator devices, this is achieved by a rotating unit that moves at high frequencies in close proximity to a static unit, which causes the liquid to be forced through the shallow gap in between them (Figure 1.1a). In high-pressure homogenisers, the shear is generated by pressurizing the coarse emulsion through a narrow constriction (Figure 1.1b). The high shear rate in these devices causes the coarse droplets to be elongated, which then break up into smaller entities due to the instability of such an elongated droplet. The final droplet size in the freshly prepared emulsion is influenced by the amount of shear introduced into the system, the interfacial tension between the oil and water phases and possible rapid recoalescence of previously formed droplets. Emulsifiers have a key role in small droplet formation because of their adsorption at oil-water interfaces during the process, which decreases the interfacial tension and helps preventing rapid recoalescence (Walstra, 1993).

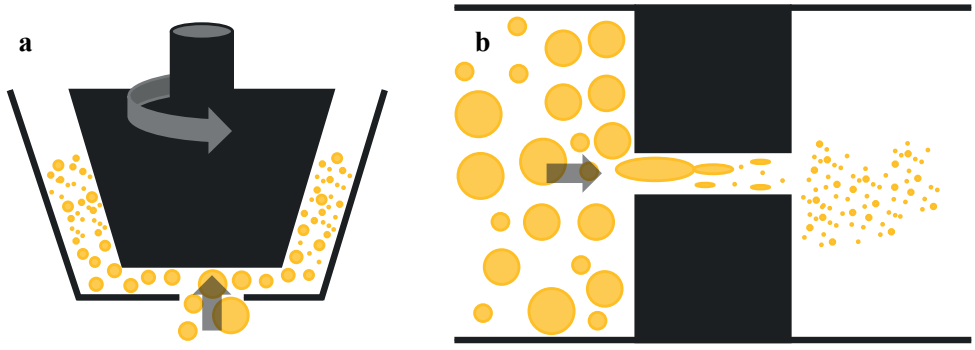

Figure 1.1. Schematic representations of: a rotor-stator homogenisation device (a) and a high-pressure homogenisation device (b).

The current emulsification processes are not recognized for their control over droplet size; the droplet size distributions can even span up to three orders of magnitude (McClements, 2004; Saito et al., 2006). Besides, the large shear forces dissipate for 90-99% as heat, which makes the processes largely inefficient and energy-intensive (McClements, 2004). Additionally, this may lead to degradation of heat- and shear-sensitive components (Charcosset et al., 2004). This may impair the functionality and stability of the products, which are highly influenced by the impact of the homogenisation process on the droplet size distribution (McClements, 2004; Neves et al., 2017; Walstra, 1993).

1.2 Physical stability

Emulsions are thermodynamically unstable and tend to destabilise via different mechanisms over time. The driving force for some of these destabilisation

mechanisms is the high interfacial energy of the system (ΔG, J), which is defined as:

$$\Delta G = \Delta A \cdot \gamma \tag{1.1}$$

where γ is the interfacial tension between oil and water (N/M), and ΔA is the change in interfacial area (m^2) (McClements, 2004). Over time, the emulsion system is driven to reduce free energy, which can occur through a reduction of γ or A. The interfacial tension can be reduced through adsorption and/or conformational reorganisation of emulsifiers at the oil-water interface, and A can decrease through droplet coalescence (Figure 1.2a). The latter can ultimately lead to complete phase separation. Coalescence can be prevented through the use of emulsifiers that exert steric and/or electrostatic repulsion. Emulsifiers that form highly elastic interfacial layers can also be advantageous to mitigate coalescence (Botti et al., 2022). These layers allow for very fast relaxation of the interfacial film towards its initial state when subjected to a deformation, which may counteract the onset of coalescence.

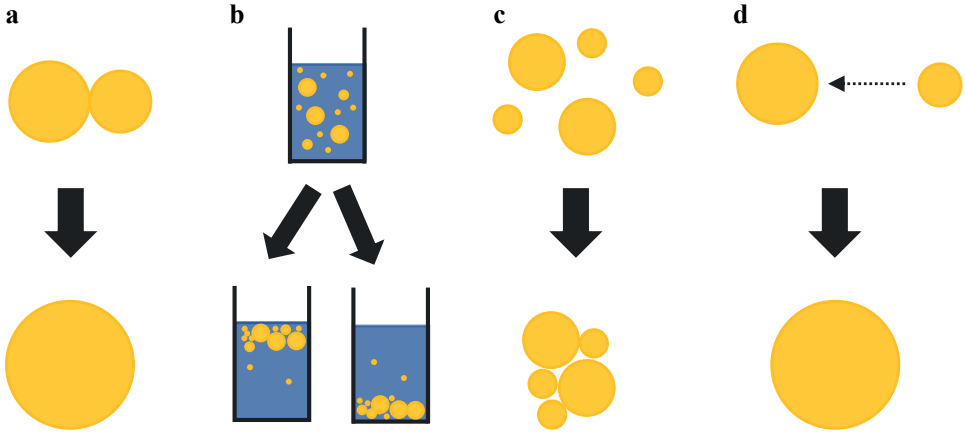

Figure 1.2. Schematic representations of physical instability mechanisms that may play a role during incubation of emulsions: coalescence (a), creaming (b, left), sedimentation (b, right), flocculation (c), and Ostwald ripening (d).

Another well-known physical destabilisation mechanism is creaming/sedimentation (Figure 1.2b), which is often undesired because of the resulting heterogeneous visual appearance. Creaming/sedimentation can be governed by multiple parameters, captured in the Stokes equation, which is valid for dilute systems:

$$v = \frac{2\,(\rho_d - \rho_c)\,g\,r^2}{9\,\eta_c} \tag{1.2}$$

where v is the velocity (m/s) at which the droplets cream or sediment, ρ_d and ρ_c are the density (kg/m^3)) of the dispersed and continuous phase, respectively, g is the gravitational acceleration (m/s^2), r is the radius of the droplet (m), and η_c is the viscosity of the continuous phase (kg/(m s)). Since v scales with r^2 (Equation 1.2), creaming/sedimentation can be effectively mitigated by producing small droplets, which can be achieved using relatively large shear forces. When droplets stick together without coalescing, flocs are formed. Flocs have an increased effective droplet size (Figure 1.2c), which thereby enhances creaming or sedimentation. An increased droplet size can also be caused by the destabilisation mechanism called Ostwald ripening (Figure 1.2d). This occurs by diffusion of dispersed material through the continuous phase from smaller to larger droplets, and this mechanism is driven by the higher Laplace pressure of the smaller droplets. The exchange of components between droplets can also occur without an increase and/or decrease in droplet size, which is then called compositional ripening (Weiss et al., 2000). The kinetics of Ostwald and compositional ripening depend on the solubility and diffusion of the dispersed phase components in the continuous phase (Weiss et al., 2000), which can be enhanced by structures present in the continuous phase such as surfactant micelles (Villeneuve et al., 2021).

1.3 Oxidative stability

Polyunsaturated fatty acids (PUFAs), in particular the omega-3 series, are often incorporated in emulsions because they are known to have beneficial health effects. Examples of such beneficial effects can be found in relation to cardiovascular diseases and the brain development of infants (Ganesan et al., 2014; Lien et al., 2018). The Food and Agriculture Organisation (FAO) has even set recommendations to increase the consumption of PUFAs and in particular omega-3 PUFAs (Joint, 2010; Vannice et al., 2014). The downside of incorporating PUFAs into food is that PUFAs are particularly sensitive to lipid oxidation, resulting in a loss of nutritionally relevant compounds and in off-flavour formation, which impairs the shelf life. Lipid oxidation can be mitigated by using modified atmosphere packaging, low temperature storage, and/or (synthetic) antioxidants. These measures are somewhat effective, but they cannot completely prevent the occurrence of oxidative reactions, which implies that a systematic basis for robust and predictable mitigation strategies is still missing. Furthermore, to comply with clean label trends, the use of synthetic additives, including antioxidants, needs to be reduced and ideally abolished (Berton-Carabin et al., 2014).

Lipid oxidation is a complex, cascaded reaction that is classically divided in three stages: initiation, propagation, and termination (Bolland, 1946). During initiation a lipid radical is formed, for example by hydrogen abstraction from an unsaturated lipid ($L^{\bullet}$), which can then react with oxygen to form a peroxyl radical ($LOO^{\bullet}$). During the propagation stage, a peroxyl radical abstracts a hydrogen from another unsaturated lipid, which results in a hydroperoxide (LOOH) and a new lipid radical ($L^{\bullet}$). The lipid radical can start the reaction all over again, which is why this reaction is qualified as autocatalytic. Hydroperoxides are primary lipid oxidation products and can decompose to secondary oxidation products, such as aldehydes (LO). Those aldehydes cause the formation of undesired flavours and odours. In the termination phase, radicals react together to form non-radical products (e.g., polymers). In the last decades, lipid oxidation chemistry research has expanded to include reactions between iron and hydroperoxides. These reactions provide $LO^{\bullet}$- and $LOO^{\bullet}$-radicals that can cause propagation of lipid oxidation (Forney et al., 1982; Schaich, 1992). It is expected that when hydroperoxides are present at the interface (Nuchi et al., 2002), this leads to reactions with metal cations, which results in the formation of radicals that propagate the lipid oxidation reaction.

Recently, spatiotemporal aspects of lipid oxidation in emulsions have been put forward, which is expected to lead to effective strategies to counteract lipid oxidation (Laguerre et al., 2020). For example, amphiphilic radical scavenging antioxidants were found to be most effective in emulsions, whereas hydrophilic antioxidants were most effective in bulk oils (Laguerre et al., 2009; Porter et al., 1989). This was postulated to be a result of their partitioning because a radical scavenging antioxidant can only be effective if it is at the place where lipid oxidation is initiated (Laguerre et al., 2015). For emulsions, this location is the oil-water interface (Losada Barreiro et al., 2013; Romsted et al., 2013). For bulk oils, antioxidants have to partition towards the prooxidant association colloids, such as reverse micelles, which implies that they need to be hydrophilic (Homma et al., 2015). The effectiveness of antioxidants has been shown to be complex and highly dependent on the emulsion system (Alemán et al., 2015), but ideally the antioxidant is mobile and at the right place at the right time (Laguerre et al., 2015).

Complex questions arising from the latter are: What is the right place? What is the right time? The answers will differ depending on the structure of a product, examples are: bulk oil, wet emulsions, dried emulsions, or something in between (Gumus et al., 2021; McClements et al., 2000; Villeneuve et al., 2021). As mentioned above, for wet emulsions, there is a general consensus that lipid

oxidation is mainly initiated at the oil-water interface. One would therefore expect that increasing the surface area by making smaller droplets would increase lipid oxidation. However, varying the specific surface area without simultaneously varying other parameters is impossible with conventional emulsification techniques (Berton-Carabin et al., 2014; Sørensen et al., 2007). In addition, it remains unexplored which reactions take place at the interface, and how these reactions influence the cascaded oxidation reaction. This knowledge – and analytical gap – have led to studies with contradicting conclusions regarding the effect of droplet size on lipid oxidation (Berton-Carabin et al., 2014). As evoked earlier, emulsions are often polydisperse systems with typical droplet size distributions that cover several orders of magnitude. This means that if such an oil droplet size dependency of the reaction applies, lipid oxidation in emulsions is highly heterogenous. Fast-oxidising droplets have been postulated to accelerate lipid oxidation in nearby droplets as well (Laguerre et al., 2017, 2020; Li et al., 2020), although direct evidence is lacking. To get a full understanding of how oxidation in one droplet can be affected by another, the use of kinetic modelling can be helpful (Schroën et al., 2022a). It is clear that there is still a lot to be discovered regarding: which reactions are taking place in which droplets, at which specific locations in droplets, at which rates, and how reactions are interconnected. To shed light on some of these complex research questions, we needed to exploit advanced analytical techniques to improve the localisation, visualisation, quantification, and qualification of oxidation in emulsions. In addition, we needed to develop an alternative emulsification technology to have control over the droplet size, as is further described below.

1.4 Microfluidic emulsification

The limited control over the droplet size of conventional emulsification techniques, and the high energy required, have generated a scientific interest for alternative emulsification processes, such as membrane emulsification (Nakashima, 1991) and microfluidic techniques (Vladisavljević et al., 2012). Spontaneous microfluidic emulsification is a gentle technology that can be used for the production of very monodisperse droplets at 20 times lower energy input than conventional techniques (Charcosset et al., 2004; Kawakatsu et al., 1997), which is also a potential asset for preserving temperature-labile ingredients. Spontaneous microfluidic emulsification operates by pushing the to-be-dispersed phase through a narrow connection into a (deeper) channel containing the continuous phase (Figure 1.3). Droplets are generated spontaneously by the interfacial tension force (Sugiura et al., 2002). The productivities that can be reached currently are less than a millilitre per hour (for droplets < 10 μm), which makes application as an analytical tool possible,

e.g., to study emulsion physical stability (Hinderink et al., 2021; Khalid et al., 2014, 2017; Krebs et al., 2012). To have sufficient sample to perform physical stability or lipid oxidation experiments in a food context, it was necessary to look at upscaling options for the production of relatively small droplets (< 10 μm) as well as for larger droplets (10-50 μm).

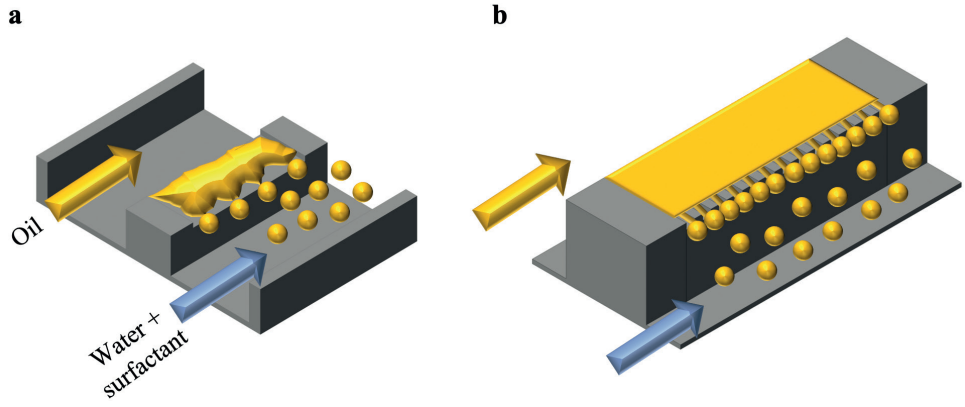

Figure 1.3. Schematic representations of microfluidic emulsification devices: EDGE (Edge-based Droplet Generation) (a) and Partitioned EDGE (b). Figure is redrawn based on images from (Şahin, 2016).

Within the field of microfluidic emulsification, essential insights have been obtained regarding the role of viscosity and interfacial tension of the fluids in the droplet formation mechanisms (Kobayashi et al., 2003; Schroën et al., 2015; Van Dijke et al., 2010, 2008; Vladisavljević et al., 2012). The next challenge is to exploit this knowledge to study and optimise emulsion productivity based on the design of microfluidic emulsification devices. Previously, increasing productivity has been mainly achieved by numbering up the amount of droplet formation units. In a few cases, upscaling was achieved by optimising the chip design (Sahin et al., 2015). In the work of Sahin and co-workers, the latter approach improved the productivity with a factor of 100 compared to their previous microfluidic emulsification device (Figure 1.3a & b) (van Dijke et al., 2010b).

The production of highly monodisperse droplets at reasonable throughputs is of relevance for one of the aims of this thesis because it will aid in clarifying: which reactions are taking place in which droplets, at which specific locations, at which rates, and how those reactions are influenced by which phenomena.

1.5 Research aim and approach

Even though our knowledge of emulsion products has increased dramatically

since the 'Mahonaisse', lipid oxidation and physical destabilisation are still widely acknowledged as major concerns in the (food) industry; unexpected fluctuations in the shelf life of products when changing product formulation are still common place. This highlights that there is a clear need for a deeper understanding of lipid oxidation in complex food systems. The aim of this thesis is to understand the oxidative stability of emulsions on a fundamental level. The research carried out in this thesis will assess the physical and oxidative stability of emulsions by advanced analytical set-ups providing data on where lipid oxidation is happening, and which reaction products are formed, and thus contribute to improving food emulsions. As a first step, microfluidic devices have to be upscaled to improve our control over droplet sizes for which elucidation of the droplet formation mechanisms is required. Next, we study lipid oxidation in well-defined droplets, which are prepared with microfluidic devices. The oxidation mechanisms in the well-defined emulsions are compared to those in model emulsions, which are prepared with conventional lab-scale emulsification processes. Colloidal structures across various length scales may play a role in the lipid oxidation reaction, and we, therefore, studied their involvement via advanced analytical techniques such as: confocal laser microscopy, transmission electron microscopy, and nuclear magnetic resonance.

1.6 Thesis outline

The outline of this thesis is described below per chapter and summarised in Figure 1.4.

In **Chapter 2**, an upscaled microfluidic emulsification chip containing 75,000 droplet formation units is presented. Via a proof-of-concept study, preparing hexadecane droplets of 10 μm, it is shown that productivity can be improved greatly through smart microfluidic chip design. The design of microfluidic emulsification chip is further discussed in **Chapter 3**, where an upgraded chip is presented with which we were able to systematically make monodisperse droplets, of different sizes, using different droplet formation mechanisms. This chapter elaborates on production of monodisperse emulsions relevant for food-related research questions. The very monodisperse droplets produced with the chips from Chapter 3 enable a systematic study regarding the effect of droplet size on lipid oxidation in a surfactant-stabilised model emulsion, as reported in **Chapter 4**. Unlike monodisperse microfluidic-made emulsions, the size difference between the smallest and the largest droplets in model emulsions can be in the order of a factor 1000. In **Chapter 5**, this is investigated in the light of both the oxidative and physical stability of the smallest droplets' population, which were tracked and visualised by advanced cryo-transmission

electron microscopy. A direct comparison between emulsions prepared with microfluidics and with conventional emulsification techniques is then made in **Chapter 6**. An advanced confocal laser scanning microscopy set-up allows for comparing lipid and protein oxidation status of droplets present in the same sample. In literature, it has been suggested that small droplets and micelles are able to transfer components between oil droplets, which would propagate lipid oxidation. Therefore, we investigate this in **Chapter 7** for surfactant-stabilised model food emulsions. Since these emulsions are often dried to extend their shelf life, we also address how this process and the resulting structural changes affect lipid oxidation in **Chapter 8**, where we especially focus on the effectiveness of antioxidants. Finally, in **Chapter 9**, the findings of this thesis regarding droplet formation and lipid oxidation are discussed in a broader context, which will provide an answer to the compelling question: 'Is microfluidic emulsification only a powerful analytical tool, or can it also be a means to produce stable emulsions on larger scale?'

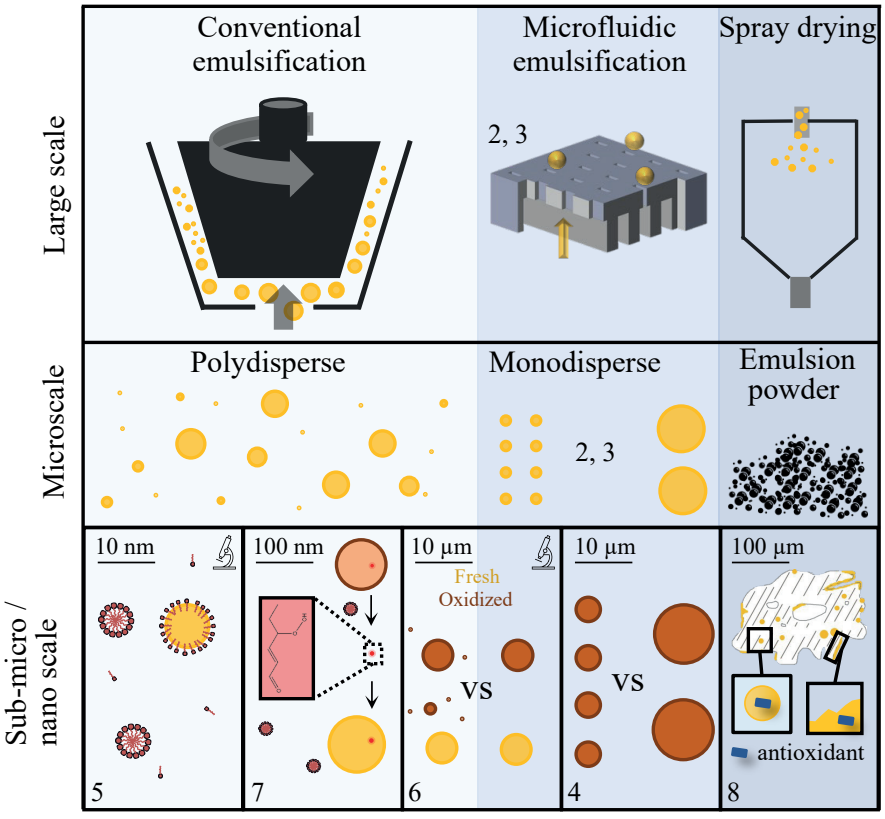

Figure 1.4. Overview of the different chapters in this thesis. Yellow and brown colours correspond to oxidised and non-oxidised droplets, respectively. The small red dot represents 4-hydroperoxy-2-hexenal, which is a small secondary lipid oxidation product.

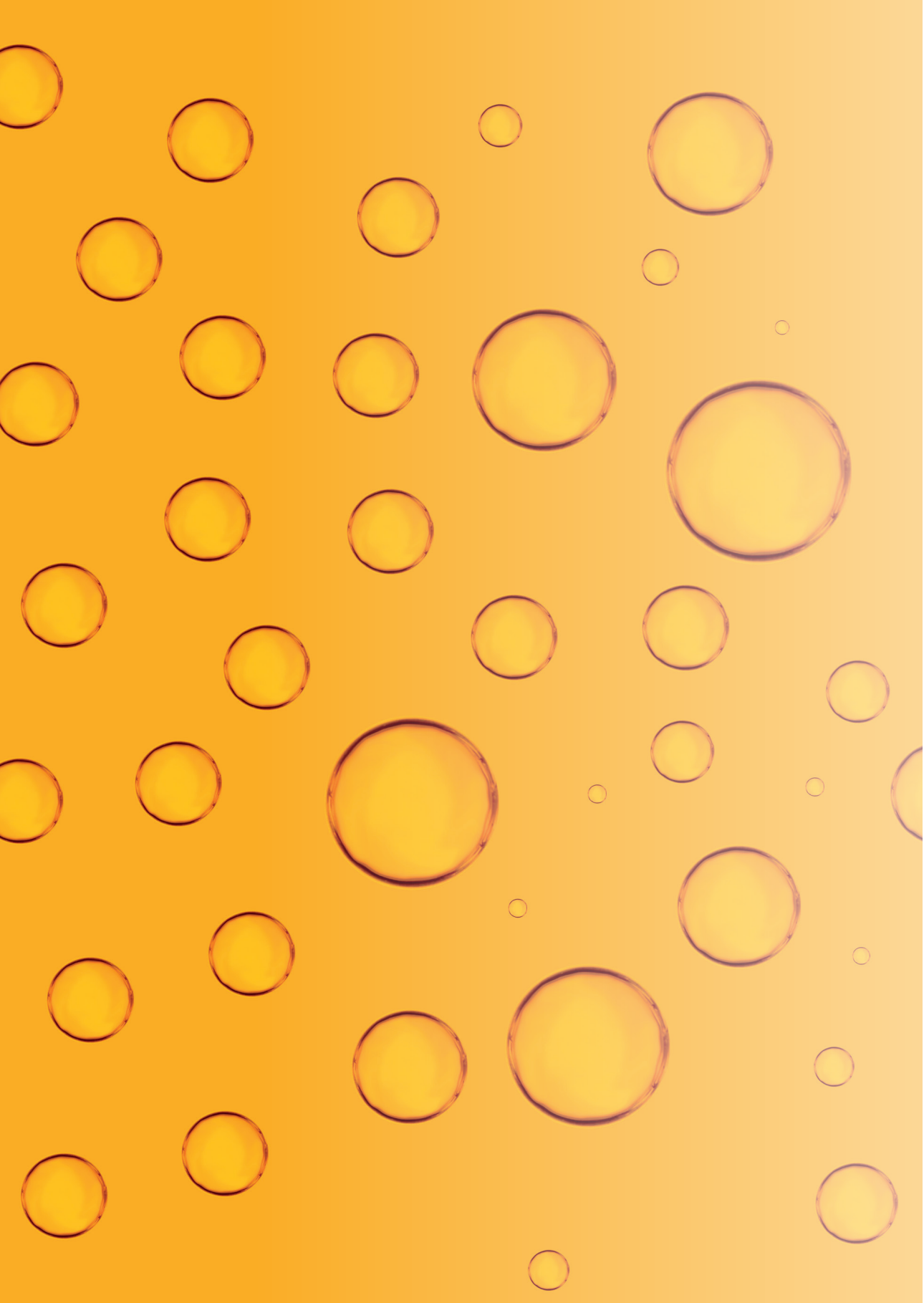

Chapter 2

Upscaling microfluidic emulsification: the importance of sub-structure design in EDGE devices

This chapter was published as:
S. ten Klooster, J. van Den Berg, C. Berton-Carabin, J. de Ruiter, K. Schroën: *Upscaling microfluidic emulsification: the importance of sub-structure design in EDGE devices*, Chemical Engineering Science 261 (2022), 117993.

Abstract

When used for emulsion production, microfluidics are known for their low energy usage and droplet monodispersity. However, current throughputs need to be improved to realise larger scale microfluidic emulsion production. In this chapter, we present the upscaled device called Multi EDGE with a proof of concept study in which we produce 10-µm hexadecane droplets in a 0.5-wt.% SDS solution at 0.3 m^3/m^2h. The design of the dispersed phase supply channels is crucial, since a higher flow resistance causes a higher blow-up pressure and faster pore refilling. In turn, this results in high droplet formation frequencies of > 1800 droplet s^{-1} per droplet formation unit, compared to maximally 60 droplet s^{-1} per droplet formation unit for devices with low-resistance substructure, which are limited by the refilling process. The fluxes and small droplets of Multi EDGE, show that these devices have potential for upscaling, especially when the substructure is designed properly.

2.1 Introduction

To produce emulsion products, such as mayonnaise, sunscreen and paint, the energy input may exceed the energy input needed for creation of the interface by a factor twenty or more (Charcosset et al., 2004; Gijsbertsen-Abrahamse et al., 2004). Another disadvantage of conventional high-shear emulsification techniques is that they cause local fluctuations of energy density and cavitation, which makes it is hard to regulate the droplet sizes precisely, leading to emulsions with wide droplet size distributions that are inherently less stable (Persson et al., 2014). These emulsification processes may lead to loss of protein functionality and the onset of lipid oxidation that influence chemical product stability in a negative way (Guo et al., 2020; Neves et al., 2017).

Compared to classic emulsification technologies, microfluidic emulsification is more subtle and enables production of emulsions with a controlled droplet size, while preserving the nativity of the ingredients (Neves et al., 2017; Zhu et al., 2017). Microfluidic emulsification have been used for the interpretation of results in research areas such as biology, chemistry, and particle synthesis, through the monodisperse droplets that are generated (Conchouso et al., 2014; Shen et al., 2016; Theberge et al., 2010).

Microfluidic emulsification starts by pushing the dispersed phase through a narrow channel until it reaches the continuous phase channel. Next, the dispersed phase adopts a droplet-like shape and snaps off, which occurs either spontaneously or due to the shear of the continuous phase flow. The microfluidic devices that operate by shear of the continuous phase flow (e.g., T- and Y-junctions, flow-focussing and co-flow devices) require very accurate flow control over the two phases, which is rather difficult when multiple droplet formation units operate in close proximity (Vladisavljević et al., 2012; Zhu et al., 2017). In spontaneous microfluidic emulsification techniques, snap-off occurs because of a difference in Laplace pressure, and only one phase has to be controlled precisely, which makes it more practical (Kawakatsu et al., 1997; Schroën et al., 2015).

Currently, microfluidic emulsification is mostly applied at a small scale a few mL per hour for droplets with a size relevant to food production (< 10 μm) (Schroën et al., 2015). For an industrial scale production of typically 20 m^3 per hour, many channels (in the order of billions) have to be operated in parallel, and therefore the major challenge for microfluidic emulsification is to scale up by numbering up (Gijsbertsen-Abrahamse et al., 2004; Schroën et al., 2015; van Dijke et al., 2009;

Vladisavljević et al., 2018). A few successes have been reported in literature, such as: EDGE (Edge-based Droplet GEneration)(van Dijke et al., 2009, 2010a), (asymmetric) straight-through arrays (Kobayashi et al., 2008, 2009), Millipede (Amstad et al., 2016; Ofner et al., 2017), microchannels (Kobayashi et al., 2012; Vladisavljević et al., 2018), and STEP emulsification (Stolovicki et al., 2018). Not all these devices have shown the production of small droplets (~ 10 μm) that we target here.

Recently, we have introduced a novel microfluidic emulsification device called Partitioned EDGE (Sahin et al., 2015), which is an improved version of regular EDGE, and we explored its droplet formation mechanism (Deng et al., 2021; ten Klooster et al., 2019). The productivity of these devices is determined by the fraction of active droplet formation units (DFUs), the droplet formation frequency per DFU, and the droplet size (larger droplets can be made at higher overall productivity (Stolovicki et al., 2018)). Besides, the surfactant as well as the viscosities of both phases affect the productivity (Sahin et al., 2016; Van Dijke et al., 2010; van Dijke et al., 2010a).

When upscaling microfluidic emulsification devices, it is in principle desired to make the dispersed phase supply channels as short as possible to save space on the chip. Until now, the effect of sub-structure geometry on the production rates in spontaneous upscaled devices has never been considered to be relevant to the best of our knowledge. In this chapter, we present a device called Multi EDGE. It was manufactured with state-of-the-art clean-room technologies and contains 75,000 DFUs. We report the performance of Multi EDGE for oil-in-water (O/W) emulsification and discuss its suitability for larger scale production. Here, we compare its productivity per DFU (DFU productivity) with the small scale Partitioned EDGE, which has 125 DFUs with the same DFU structure and a different sub-structure (Sahin et al., 2015). Next, we compare overall productivity (L/m^2h) between devices. The productivity of Multi EDGE is relatively high compared to that of other devices from literature. Furthermore, we explain how the sub-structure can be used to improve this further, therewith highlighting an aspect of microfluidics design that is generally not considered.

2.2 Materials and methods

2.2.1 Materials

Hexadecane (ReagentPlus® 99%, Zwijndrecht, the Netherlands) was used as the to-be-dispersed phase and 0.5 wt.% sodium dodecyl sulphate (SDS, Merck, Darmstadt, Germany) as the emulsifier. Ultrapure water (18.2 MΩ) was used

for all experiments and prepared using a Milli-Q system (Millipore Corporation, Billerica, MA, USA).

2.2.2 Microfluidic emulsification devices

In this research, we used Multi EDGE, an upscaled microfluidic emulsification device and compared its productivity per DFU with Partitioned EDGE. Partitioned EDGE and Multi EDGE have several similarities: (i) the droplet formation unit consists of a 3D structure, with a pore ending in a deeper continuous phase channel where the droplets were formed, (ii) the geometry of the DFUs has equal dimensions, and (iii) there is no cross-flow needed for droplet formation. The differences between the chips are in the amount of DFUs and the geometry of the sub-structures (Table 2.1), which is further explained below.

Table 2.1. Specifications of Partitioned EDGE and Multi EDGE devices.

EDGE Type	Micro-plateaus (DFUs)			Main plateaus	
	n_{mi} (per main plateau)	Dimensions $L \cdot W \cdot H$ [µm]	Spacing $S_1 \cdot S_2$ [µm]	n	Dimensions $l \cdot w \cdot h$ [µm]
Partitioned EDGE	25	30 · 10 · 2	10 · —	1	170 · 500 · 2
Multi EDGE	250	30 · 10 · 2	10 · 20	300	370 · 6,000 · 10

Partitioned EDGE

Partitioned EDGE has a shallow connection between the deeper continuous and dispersed phase channels (Figure 2.1 a & b) (Sahin et al., 2015; ten Klooster et al., 2019). The shallow connection consists of a main plateau and multiple micro-plateaus. Partitioned EDGE has 25 micro-plateaus, which are the DFUs, with a length, width and height of 30, 10, and 2 µm, respectively (Figure 2.1 and Table 2.1). Fabrication of the Partitioned EDGE chips was done by Micronit Microfluidics, Enschede, The Netherlands, which is explained in detail in a previous paper (Sahin et al., 2015). The chip was placed in a chip holder from Micronit (Fluidic Connect PRO Chip Holder with 4515 Inserts, Micronit Microfluidics, Enschede, The Netherlands), and connected with standard tubing.

Multi EDGE

Silicon substrates of 400-µm thickness were used to fabricate the Multi EDGE chips (Figure 2.1c & d). In the substrate, the micro- and the main plateaus were fabricated through deep reactive ion etching (Cytocentrics B.V., The Netherlands); the dimensions of the micro-plateaus (DFUs) were 10 · 2 µm (width · height). The Multi EDGE chip was placed in a custom-made module constructed by the technical workshop of Wageningen University. The Multi EDGE chip was 10 · 10 mm, and the part containing the DFUs was 5 · 6 mm, of which the effective pore area was 5% (surface porosity based on DFUs). The overall, area-based

productivity (in L/m²h) was calculated based on the area that contained the DFUs (5 · 6 mm), as is commonly done in literature (Kobayashi et al., 2005c). The main difference in device geometry between Multi EDGE and Partitioned EDGE was the height of the main plateaus (*h*) (Table 2.1). Technical limitations did not allow us to etch the main plateaus as shallow as the micro-plateaus (10 µm vs 2 µm). To research the effect of this change in substructure, we compared the droplet sizes and productivity per DFU with Partitioned EDGE that was described in the section above.

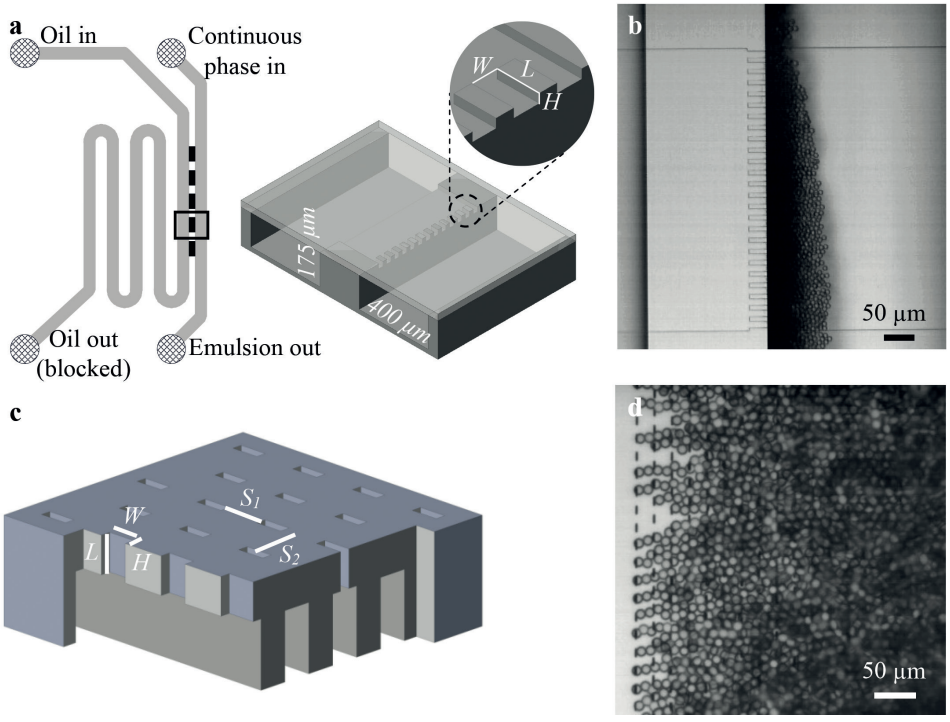

Figure 2.1. (a) The Partitioned EDGE chip layout with five plateaus (black rectangles in left image), placed between the deep continuous and to-be-dispersed phase channels, and a close-up sketch of the micro-plateaus with their characteristic dimensions labelled in the middle circle (W=width, L=length and H=height). (b) Partitioned EDGE during emulsification. (c) Schematic 3D representation of Multi EDGE. (d) Multi EDGE during emulsification.

We did not observe monodisperse droplet formation with a Multi EDGE chip, which had dimensions of 5 · 2 µm (width · height) micro-plateaus. In other publications about STEP and microchannel emulsification, it was shown both experimentally and theoretically that the minimum aspect ratio of micro-plateaus (width / height, Figure 2.1) has to be larger than ~ 2.6 for monodisperse droplet formation (Kobayashi et al., 2004b; Montessori et al., 2019). Possibly this effect also plays a role in EDGE chips.

2.2.3 Cleaning of the devices

Both devices were thoroughly cleaned prior to operation to ensure their hydrophilicity and suitability for O/W emulsification (Van Dijke et al., 2008). Since the devices had a different configuration, they could not be cleaned in the same way. The Multi EDGE device was cleaned by flushing ethanol through the chip, and subsequently subjecting to plasma oxidation. The Partitioned EDGE device was cleaned by flushing ethanol through the chip and sonicating in ethanol. Next, It was baked in an ashing furnace (Carbolite AAF-1100, Carbolite Gero, Derbyshire, United Kingdom) at 500 °C for 2 h.

2.2.4 Operation of the devices

Once cleaned, the devices could be used. First, the dispersed and continuous phases were prepared, using hexadecane and 0.5 wt.% SDS in water, respectively. Next, each microfluidic chip was placed in its own holder. The continuous phase was then run through each chip to wet the device. After this, the oil was pushed in across the plateau, and the formed droplets were carried away by the cross-flowing continuous phase (Figure 2.1b & d). The cross-flow is oriented along the width of the DFUs in Partitioned EDGE and along the height of the DFU in Multi EDGE. The cross-flow is not needed for droplet formation, but only required to carry away the formed droplets that otherwise obscure observation. The flows were controlled through a microfluidic control system (Elveflow®, France), and droplet formation was monitored by using an inverted microscope (Axiovert 200 MAT, Carl Zeiss B.V., The Netherlands) connected to a high-speed camera (MotionPro HS-4, IDT Inc., USA) (maximum frame rate used for recording was 5,000 Hz, maximum precision was 7.8 pixels μm^{-1}). High resolution videos were made with a high-speed camera (FASTCAM SA-Z, Photron Limited, Japan) at a frame rate of 100,000 frames per second and with a resolution of 0.973 μm/pixel to measure the time needed for droplet formation. Please note: for Multi EDGE we used top-view recordings (Figure 2.1d), since we cannot look through the (silicon) channels.

2.2.5 Droplet size measurements

For both chips, 20–50 droplets per droplet size data point were analysed by image analysis software to determine the average droplet size and size distribution, as was done previously (Sahin et al., 2015; ten Klooster et al., 2019). Given the monodispersity of the droplets, this is an appropriate measurement method. This method has been compared to static light scattering previously and good agreement was found (van Dijke et al., 2010b). The size distribution of the droplets was expressed in the form of coefficient of variation, CV, which was defined as:

$$\mathrm{CV} = \frac{\sigma}{d_{dr}}\, x\, 100 \tag{2.1}$$

where σ is the standard deviation of the droplet diameters and d_{dr} is the number-average droplet diameter. Droplets with a CV below 10% were considered monodisperse, which is based on previous research (Sahin et al., 2016; van Dijke et al., 2009).

2.2.6 Measuring down time and necking time

High resolution images at a maximum frame rate of 100,000 frames s^{-1} were used to determine the down time (DFU filling) and necking time (actual droplet formation). The number of frames between the start of dispersed phase leaping into the deeper continuous phase channel and breakage of the neck was divided by the frame rate to obtain the necking time. The down time was determined in a similar way, starting with the neck breakage, and finishing with the dispersed phase leaping into the continuous phase channel again. This was done for several locations over the chip and for three droplets per DFU.

2.2.7 Flow resistance calculation

To compare various designs, the flow resistances are calculated. The flow resistance (R) of a rectangular channel can be calculated with a Hagen-Poiseuille equation:

$$R = \frac{12\eta_d l}{1 - 0.63(\frac{h}{w})} \frac{1}{h^3 w} \tag{2.2}$$

where η_d is the dispersed phase viscosity, l the length, h the height and w the width of the channel. Equation 2.2 was used to calculate the flow resistance of a micro-plateau and main plateau separately. The flow resistance of the main and micro-plateaus together (R_t) was defined as:

$$R_t = \frac{R_{mi}}{n_{mi}} + R_{ma} \tag{2.3}$$

where R_{mi} is the flow resistance of the micro-plateau, n_{mi} is the number of micro-plateaus per main plateau and R_{ma} is the flow resistance of the main plateaus. The flow resistance of the whole shallow connection, expressed per micro-plateau ($R_{t,mi}$) was calculated as:

$$R_{t,mi} = R_t \cdot n_{mi} \tag{2.4}$$

2.3. Results and discussion

We compared the droplet sizes and maximum productivity of the upscaled Multi EDGE (Figure 2.1c & d) with the small scale Partitioned EDGE (Figure 2.1a & b). The productivity of Multi EDGE was expressed per DFU (DFU productivity) to compare with Partitioned EDGE, and per area (overall productivity) to compare with devices from literature.

2.3.1 Emulsion production with Multi EDGE

In this section, we first describe the results for Multi EDGE (10 · 2 μm micro-plateaus); monodisperse hexadecane droplets were successfully produced over 8 h, which was the maximum time that we attempted due to lab closing hours. Also a recent publication showed that long-term stable production of dichloromethane droplets (25 μm) with silicon microchannel (STEP) emulsification devices was possible (Vladisavljević et al., 2018). Droplet formation in Multi EDGE started at 95 mbar, and droplet size remained constant at 11.0 μm and monodisperse up to 130 mbar with a CV of < 10% (Figure 2.2a, insert). Above 130 mbar, a few DFUs started to produce polydisperse droplets that are roughly one order of magnitude larger in diameter, whereas the majority of DFUs still formed small monodisperse droplets. With increasing pressure, more DFUs show this so-called blow-up behaviour, indicated by the vertical solid line (Figure 2.2a). Both droplet formation frequency per DFU (Figure 2.2b) and the number of active micro-plateaus (Figure 2.2c) increased linearly with pressure, up to the point at which blow-up started occurring. Thus, the flux per area increased quadratically with pressure till it reached blow-up (Figure 2.2d). At this pressure (130 mbar), 93% of the micro-plateaus were active with an average frequency of 58 Hz per micro-plateau, amounting to 313 L of oil per m^2h (assuming uniform performance over the entire surface of the device). This value is similar to values reported for STEP devices, where 91% of the channels were active during production of 25-μm droplets (Vladisavljević et al., 2018). Multi EDGE will be further compared to other devices reported in literature in section 2.3.3.

2.3.2 Comparison of Multi EDGE with Partitioned EDGE

Both devices showed a start of droplet formation at a dispersed phase pressure of 95 mbar (dashed vertical line Figure 2.2a), which therefore does not seem to be substantially influenced by the sub-structure design (more specifically, the main plateau height). For Partitioned EDGE, insufficient droplets were formed to measure the droplet size accurately, and therefore there is no data point at 95 mbar for Partitioned EDGE (Figure 2.2a). This so-called breakthrough pressure

is determined by the Laplace pressure, $P_{LP} = \gamma\ (1/R_1 + 1/R_2)\ \cos(\theta)$ of the meniscus (with radii R_1 and R_2) inside the micro-plateau working in the direction opposite to the applied pressure (P_{app}). Since the breakthrough pressure, the width, and height of the micro-plateaus (and thus R_1 and R_2) were constant, the devices should have a similar contact angle (θ). A contact angle increase of 10° may decrease the breakthrough pressure by ~ 5 mbar. The contact angle also influences on the productivity (Maan et al., 2013b), since it can reduce blow-up pressure (Van Dijke et al., 2008), and thus decrease maximum productivity even by a factor two (Eggersdorfer et al., 2018). The low breakthrough pressure of 95 mbar indicates that – at least at low pressures – SDS adsorbed to the hexadecane-water meniscus, and thereby γ may reach as low as 8 mN/m (equilibrium value) compared to ~ 44 mN/m for an interface free of surfactant (Muijlwijk et al., 2016). When using the same components and concentrations in a Y-junction, it has been shown that the equilibrium interfacial tension was reached after ~ 0.01 s, and a first reduction in interfacial tension was observed after < 0.001 s (Muijlwijk et al., 2016). This implies that the reduction in interfacial tension can be much faster than the droplet formation time at low droplet formation rates (< 10 s^{-1}), although it may not be fast enough at high droplet formation rates (> 1,000 s^{-1}) (ten Klooster et al., 2019).

The droplet sizes produced by Multi EDGE and Partitioned EDGE at the blow-up pressure were 11.0 and 9.8 μm, respectively. Droplet sizes have been shown to depend on DFU height (Van Dijke et al., 2010), which we kept as constant as possible at 2 μm for both devices. The droplets were indeed rather similar in size; slight differences may have occurred due to slightly different dimensions. DFU activation increased with pressure for both Multi EDGE and Partitioned EDGE, but did not seem to be influenced by main plateau height (Figure 2.2c). As explained earlier, the DFUs start to become active when P_{app} exceeds P_{LP}, and since the DFUs have equal dimensions, our hypothesis was that all pores become active at this breakthrough pressure of 95 mbar. In reality, about three times the breakthrough pressure was required for an activity of 100% (Figure 2.2c). Similar effects were described by Abrahamse and co-workers for cross-flow membrane emulsification; as soon as the dispersed phase flows through one DFU, this prevents the neighbour DFUs from becoming active (Abrahamse et al., 2002).

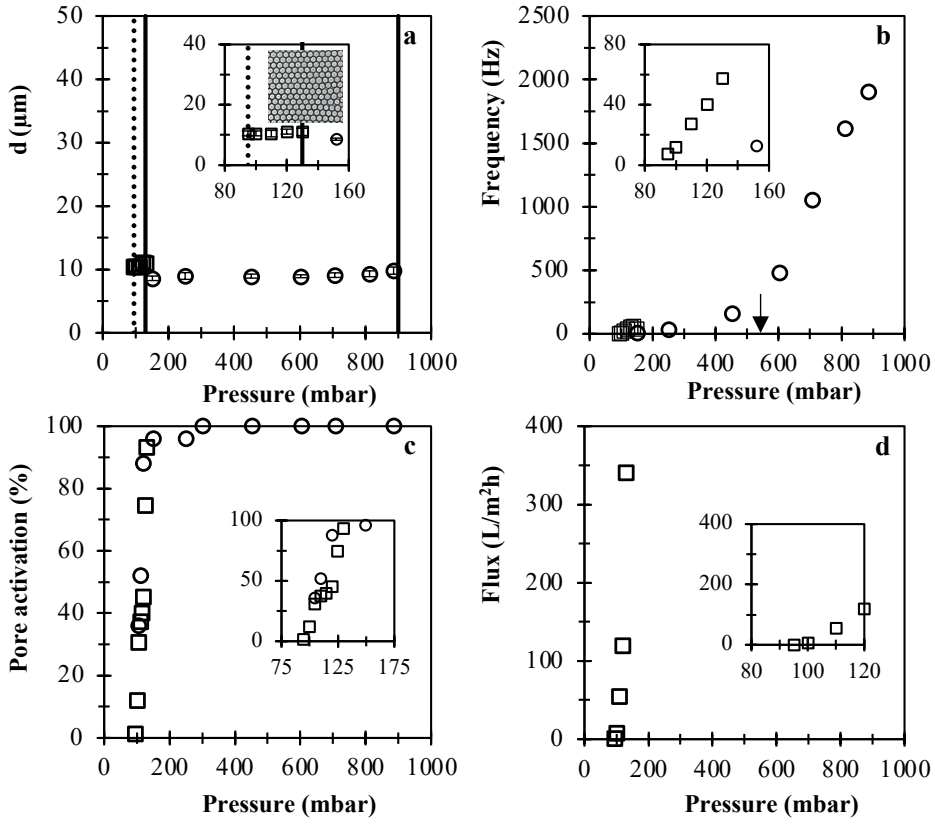

Figure 2.2. Effect of dispersed phase pressure on: droplet size – *d* – (a), droplet formation frequency (b), pore activation (c), and hexadecane flux (d) for Partitioned EDGE (○) and Multi EDGE (□). The dashed vertical lines (in (a)) denote the breakthrough pressure; the solid lines (in (a)) the blow-up pressures. The arrow in (b) indicates the LaPlace pressure of the meniscus when no surfactant is adsorbed. Error bars in (a) denote standard deviations.

When increasing the pressure beyond the breakthrough pressure for Multi EDGE, the droplet formation frequency per DFU initially increased faster compared to Partitioned EDGE (initial slopes in Figure 2.2b), which is caused by the lower flow resistance of the main plateau in Multi EDGE. Just before blow-up, the maximum droplet formation frequency per DFU was ~ 30 times higher for Partitioned EDGE (blow-up pressure of 900 mbar) compared with Multi EDGE (blow-up pressure of 130 mbar). When including the slight difference in droplet size, the DFU productivity of hexadecane droplets by Partitioned EDGE was ~ 22 times higher.

To further improve the performance of microfluidic emulsification devices, we next identify the cause of the lower DFU productivity and blow-up pressure of

Multi EDGE. To do so, we divide droplet formation into two stages: (i) necking and (ii) down time. During necking, the dispersed phase leaps into the deeper continuous phase channel, where it adopts a droplet-like shape, which is still connected to the fluid on the plateau via a 'neck'. When the neck collapses (due to interfacial tension forces), the droplet is detached and with that the necking stage is finished (Figure 2.3a-c). Modelling studies have been performed leading to identification of local flow profiles (Montessori et al., 2018, 2019; Van Dijke et al., 2010, 2008; van Dijke et al., 2010c). During the down time, the meniscus first retreats into the micro-plateau after which the DFU refills (Figure 2.3c-e). The latter only occurs when there is a positive pressure difference, which is defined as:

$$\Delta P_p = P_{app} - P_{LP} \tag{2.5}$$

So, to obtain a short down time, which is desired because this will increase the productivity, ΔP_p needs to be high, which is the case when P_{app} is high and/or P_{LP} is low; the first factor is determined by the blow-up pressure, and the latter is determined by the extent of surfactant adsorption at the interface. The down time ends when the dispersed phase leaps into the continuous phase channel again (Figure 2.3e).

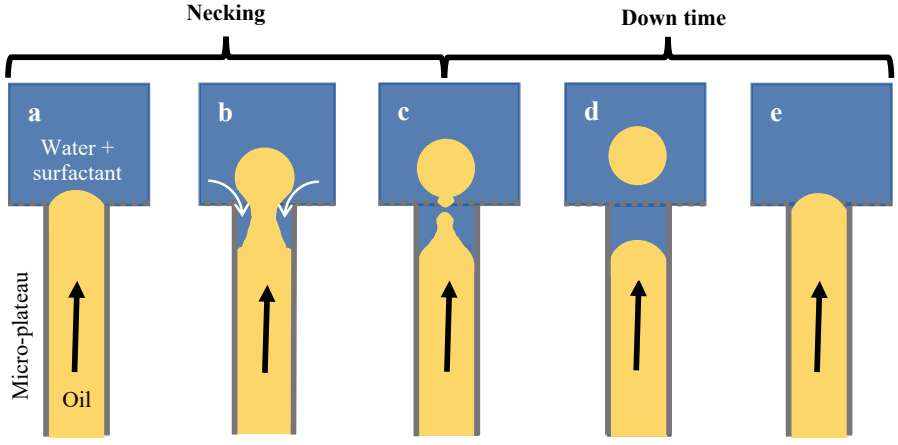

Figure 2.3. The two stages of droplet formation; a-b-c depict necking and c-d-e depict down time.

We measured necking and down times for both Multi EDGE and Partitioned EDGE at the highest pressures before blow-up ($P_{blow\text{-}up}$) (Table 2.2). These results show that at high dispersed phase pressures, the down time is a substantial part of droplet formation. At lower pressures, the ratio of down/necking time would have been even higher because surfactant adsorption would be required to initiate refilling of the DFU. We found a down time of 16 ms for Multi EDGE

versus 0.2 ms for Partitioned EDGE at $P_{blow\text{-}up}$, which was the main cause for differences in productivity. The necking times were more comparable, although Partitioned EDGE is still considerably faster as Multi EDGE (Table 2.2). So, ΔP_p will be higher in Partitioned EDGE than in Multi EDGE, which indicates that for Partitioned EDGE P_{app} is relatively high, and/or P_{LP} is relatively low.

Table 2.2. The droplet formation time, necking time, down time and the ratio between the down and necking time at the maximum productivity before blow-up, with standard deviations for Partitioned EDGE and Multi EDGE.

Chip	Drop formation time (ms)	Necking time (ms)	Down time (ms)	Ratio down / necking time
Multi EDGE	17 ± 2.1	1.5 ± 0.30	16 ± 2.1	10 ± 2.5
Partitioned EDGE	0.52 ± 0.021	0.33 ± 0.065	0.19 ± 0.069	0.59 ± 0.23

We can calculate the average P_{LP} over the total droplet formation (necking + down time) from:

$$P_{LP} = P_{app} - \phi_{tot} \cdot R_{t,mi} \tag{2.6}$$

ϕ_{tot} (DFU flow rate) was calculated by multiplying the DFU frequency with the droplet volume; for $R_{t,mi}$ (the flow resistance of the whole shallow connection per micro-plateau, Equation 2.4) and P_{app} we used values in Table 2.3). This results in an average P_{LP} of 122 mbar for Multi EDGE and 330 mbar for Partitioned EDGE. For both devices this is higher than the breakthrough pressure of 95 mbar, which indicates that the interfacial tension during down time is highly dynamic: just after droplet formation (Figure 2.3c) barely any SDS has adsorbed yet, but over time SDS adsorption will occur (provided that the down time is long enough as would be the case in Multi EDGE), and the interfacial tension will gradually decrease (Figure 2.3c-3e). When the applied pressure is higher than the P_{LP} of a *bare* hexadecane-water interface, the meniscus barely moves backwards after droplet formation (Figure 2.3c) and immediately starts moving forward (Figure 2.3d & e). This phenomenon was also used to explain the sudden exponential increase in bubble formation frequency when the applied pressure was higher than the P_{LP} of a *bare* air-water interface (Deng et al., 2021). In line with those results, we observed an increased productivity around an applied pressure of 530 mbar (Figure 2.2b; arrow), which corresponds to the P_{LP} of a *bare* hexadecane-water meniscus ($P_{LP,\max}$) (Figure 2.3d).

Table 2.3. The total flow resistance expressed for one micro-plateau ($R_{t,mi}$), the blow-up pressures ($P_{blow\text{-}up}$), and the Laplace counter pressures (P_{LP}) (as calculated by Equation 2.6) with standard deviations for Partitioned EDGE and Multi EDGE.

EDGE type	$R_{t,mi}$ (Pa s/m^3)	P_{app} (mbar)	P_{LP} (mbar)
Partitioned EDGE	$6.2 \cdot 10^{16}$	900 ± 20	122
Multi EDGE	$1.9 \cdot 10^{16}$	130 ± 10	330

In contrast, for applied pressures below the Laplace pressure of a *bare* hexadecane-water interface, the meniscus will even momentarily move backwards, and droplet formation can only start if the Laplace pressure is lowered through SDS adsorption (Figure 2.3c & d). The subsequent forward motion is slow when the pressure difference is small resulting in a long down time. With Equation 2.6 we calculated an average P_{LP} for droplet formation, but we expect the P_{LP} during down time to be even higher than that because during the necking stage there is not an effective P_{LP} (Appendix). We expect that the average P_{LP} of the meniscus (Figure 2.3d) for Partitioned EDGE during down time is close to that of a bare hexadecane-water interface ($P_{LP,max}$ of 530 mbar). This also implies that the time-average ΔP_p for Multi EDGE in the situation shown in Figure 2.3d & e is probably only a few mbar. For Partitioned EDGE this was probably a few hundred mbar, which means that the relative difference in ΔP_p between the devices was in the order of a factor of one hundred. The forward motion of the menisci (Figure 2.3d & e) is determined by the pressure difference divided by the flow resistance of the device (Equation 2.6). Since Multi EDGE has a 3.3 times lower $R_{t,mi}$ (Equation 2.6, Table 2.3), the actual difference in forward motion of the menisci between the devices would be in the order of 100/3.3, when operated at their maximum productivity. To summarise, the low flow resistance of Multi EDGE caused that at low pressures the viscous force already exceeds the interfacial tension force, resulting in a low blow-up pressure. The low blow-up pressure leads to a low ΔP_p, and therefore a long down time, leading to a low droplet formation frequency.

As mentioned, there was a factor five difference in necking time between Multi EDGE and Partitioned EDGE (Table 2.2). It was previously shown for bubbles that the necking time decreases with increasing applied pressure (Deng et al., 2021). We estimated the blow-up pressure of Multi EDGE with the Hagen-Poiseuille equation, based on the flow during necking of Partitioned EDGE. The values we calculate for Multi EDGE are high (270 mbar) compared to what we measured (130 mbar) (Appendix). This value is lower than $P_{LP,\max}$, and therefore ΔP_p during down time would still be relatively low. This would result in a long down time, which would reduce the DFU productivity of Multi EDGE, again stressing the importance of the flow resistance of the sub-structure. The difference between the calculated blow-up pressure and measured blow-up pressure of Multi EDGE may be due to a difference in contact angle between the devices; in literature it has been suggested that an increase of 10° in contact angle can lead to a factor two difference in maximum productivity (Eggersdorfer et al., 2018). In addition, the difference in height between main and micro-plateau for Multi EDGE may have influenced the flow profile of the dispersed phase inside the micro-plateau

and affect the instability needed for droplet formation (Figure 2.3b & c). For microchannels with diameters of a few hundred μm operated at low Reynolds numbers (< 1) the entrance length is close to the hydraulic diameter. If we translate this directly through to our channels, this would imply an entrance length of around 3 μm (Galvis et al., 2012), which could be relevant given the device dimensions. To elucidate this, the sub-structure geometry should be systematically varied.

A special feature in Partitioned EDGE is that far beyond the blow-up pressure, large droplets are formed by the physical force that neighbouring droplets exert on each other by direct contact, and as this happens in a cascade fashion, this leads to a monodisperse emulsion (ten Klooster et al., 2019). This was not observed for Multi EDGE, and most probably this has to do with the fact that in Multi EDGE the droplet formation units are positioned further apart, and the forming droplets are less confined as in Partitioned EDGE. Furthermore, at blow-up, slightly less droplet formation units are active, therewith increasing the average distance, and reducing the chance of interaction (Figure 2.1).

2.3.3 Comparing Multi EDGE with other devices

Compared to Multi EDGE, straight-through microchannels (MCs) are the most similar upscaled microfluidic emulsification devices (Figure 2.4). MCs receive the to be disperse phase by individual narrow channels that are all connected to the same general feeding area (Figure 2.4a), whereas EDGE devices receive the to be dispersed phase from a common (main) plateau (Figure 2.4b). These differences in device geometry are thought to influence DFU activity. For asymmetric straight-through MCs, the fraction of active channels increases with oil viscosity. For instance, 50% and 95% of the channels were active for the preparation of ~ 30 μm tetradecane (viscosity of ~ 3 mPa s) and soybean oil droplets (typical viscosity of 50-60 mPa s), respectively (Vladisavljević et al., 2011). According to the reasoning that we used before for EGDE devices (Equation 2.5), the high viscosity oil will flow more slowly, which increases the chances for activation of neighbouring DFUs (Abrahamse et al., 2002). In line with this, the DFU activation of symmetric straight-through MCs decreased to 12% when making smaller (9.8 μm) soybean oil droplets, which is probably caused by the higher applied pressures needed to overcome the Laplace pressure of the meniscus in this narrower channel (Figure 2.3d) (Kobayashi et al., 2008). In EDGE devices, early blow-up is prevented by the flow resistance of the substructure, which increases pore activation (Figure 2.2c). This is an important lead for microfluidic design (e.g. making longer DFUs).

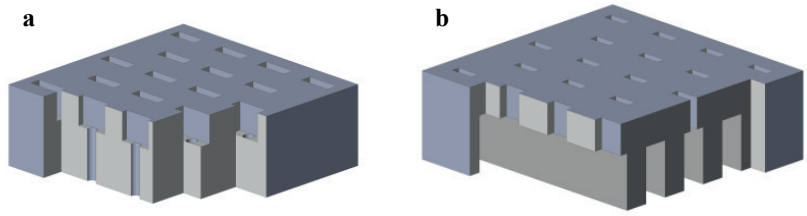

Figure 2.4. Schematic 3D representation of asymmetric straight-through MCs (a) in comparison with Multi EDGE (b). Oil is pushed through the circular channels at the bottom and droplets form at the top.

For small droplet (~ 10 μm) production, Multi EDGE devices seem to hold a competitive advantage due to their high micro-plateau activation (93%). Ideally, we would like to compare the throughput of EDGE and MCs for similar droplet sizes and oil viscosities, but we could not find this combination in literature. However, a derived comparison is possible. In MCs studies a throughput of 2700 L/m^2h was found for 30-μm tetradecane droplets, and it was suggested that the throughput would be an order of magnitude lower when 10-μm droplets are targeted (Vladisavljević et al., 2011). Therefore, we think that the current Multi EDGE design, with its 313 L/m^2h throughput for 10-μm hexadecane droplets, performs similarly to straight-through MCs.

We have also shown that there is still considerable room for improvement for Multi EDGE, and this may also be the case for straight-through MCs. As discussed earlier, if the frequencies obtained with partitioned EDGE can be reached in Multi EDGE by increasing the flow resistance of the device, this would imply approximately a 20 times higher DFU productivity. In addition, when using hexadecane as the dispersed phase in a regular EDGE device, productivity increased by a factor forty when using 5 wt.% of α-lactalbumin (a dairy protein) as an emulsifier instead of 0.5 wt.% of SDS (Sahin et al., 2016). These effects clearly indicate that much higher productivity is feasible when product formulation is used as an additional variable.

2.3.4 Outlook for upscaling microfluidic emulsification devices

All of the above shows that the design of microfluidic emulsification devices are of utmost importance to improve overall productivity. DFU productivity can be increased by increasing flow resistance of the dispersed phase sub-structure. This will lead to a blow-up pressure that is substantially higher than the Laplace pressure of the empty interface. The pressure difference of such a device will always be positive, and droplets can be formed without the need for emulsifier adsorption taking place, which reduces down time and droplet formation time greatly. This will allow the DFU frequency to steeply increase (as shown

in Figure 2.2b for the Partitioned EDGE). A similar effect may be achieved by increasing the surfactant concentration, since this will decrease the interfacial tension faster during down time, which increases the pressure difference.

If the DFUs do not get a sufficient supply of emulsifier, this will have two negative consequences: (i) coalescence may occur, which negatively impacts droplet monodispersity and (ii) droplet formation might not be taking place at downstream pores if SDS gets depleted; the interfacial tension of these menisci (Figure 2.3d) will be close to the interfacial tension of a bare oil-water interface, which is higher than the blow-up pressure in the case of Multi EDGE, which could result in inactive DFUs. Therefore, we recommend to estimate how much emulsifier the droplet generator needs, which can be achieved by multiplying the formation frequency of droplets per DFU (58 s^{-1} for Multi EDGE) with the amount of active pores (70,000) the surface area of one droplet ($3.8 \cdot 10^{-10}$ m^2) and the interfacial load ($\sim$ 1 mg m^{-2}) (Berton-Carabin et al., 2014). So, for Multi EDGE that would be $1.5 \cdot 10^{-6}$ g/s. If an SDS concentration of 5 g/L is used, the lowest possible continuous phase flow rate to cover all droplets with SDS would be 1.1 mL per hour, and one would need to apply a flow rate of several times this amount for two reasons: (i) the droplets are formed at locations of low continuous phase flow, and it is undesirable to deplete the surfactant concentration there and (ii) to decrease the interfacial tension faster during down time, which promotes droplet formation as explained above.

2.4 Conclusion

In this chapter, we have shown that Multi EDGE devices enable stable production of 10-µm monodisperse hexadecane droplets at $\sim$ 0.31 m^3/m^2h over long periods of time, which brings the device close to industrially relevant values. Designing upscaled microfluidic emulsification devices should be done wisely to further increase the productivity, which can be done by increasing the flow resistance of the dispersed phase sub-structure. The required pressure to reach maximum production (before blow-up occurs) is then higher, which leads to a larger driving force for refilling of the droplet formation unit, therewith effectively increasing the throughput. The down time can be minimized if the blow-up pressure is higher than the bare oil-water Laplace pressure of the meniscus in the droplet formation unit. If that is the case, surfactant adsorption is not required for refilling the droplet formation unit, which makes the refill fast. To make most out of the insights generated in this chapter, current limitations in microfluidic chip design need to be mitigated, and we would like to challenge construction companies to help us make Multi EDGE a break-through technology.

2.5 Appendix

2.5.1 Flow during necking and counter pressure

The flow during necking can be determined by recording the time the necking stage takes (t_{neck}) and the volume of the final droplet (V_{drop}):

$$\phi_{n,experimental} = \frac{V_{drop}}{t_{neck}} \quad \text{(A2.1)}$$

V_{drop} is determined as described in the main text and t_{neck} is determined by dividing the number of frames that the necking stage takes by the frame rate. The flow during necking was measured for Partitioned EDGE at blow-up and compared with the theoretical flow during necking, which can be determined by the Hagen-Poiseuille equation:

$$\phi_{n,theory} = \frac{P_{app}}{R_{t,mi}} \quad \text{(A2.2)}$$

The results for $\phi_{n,\ theory}$ and $\phi_{n,\ experimental}$ differ only by 2%, which suggests that there is no effective counter pressure during necking (Table A2.1).

2.5.2 Calculated blow-up pressure

The blow-up pressure has been argued to be the pressure at which the viscous forces from the dispersed phase flow start to dominate over the interfacial tension force in the neck (Dangla et al., 2013). Since differences in sub-structure of the EDGE devices are not expected to influence the interfacial tension force in the neck, we would expect that the flow during necking at blow-up would be the same for Partitioned EDGE and Multi EDGE. Since the section above shows that there is not an effective counter pressure during necking, we can rewrite Equation A2.2 to find the theoretical blow-up pressure of Multi EDGE, based on the maximum flow during necking for Partitioned EDGE($\phi_{n,\ experimental}$) and flow resistance calculated for one micro-plateau of Multi EDGE ($R_{t,\ mi}$):

$$P_{blow-up} = \phi_{n,\ experimental} \cdot R_{t,mi} \quad \text{(A2.3)}$$

When using the $\phi_{n,\ experimental}$ from Partitioned EDGE (Table A2.1) and the $R_{t,mi}$ from Multi EDGE (Table 2.3, main text), we find a theoretical blow-up pressure for Multi EDGE of 270 mbar. This is higher than the experimentally determined blow-up pressure of 130 mbar. As described in the main text, this could be due to a difference in contact angle of Multi EDGE and Partitioned EDGE or due to a different flow profile caused by the main plateau dimensions (especially the height).

Table A2.1. Results of flow during necking for Partitioned EDGE at blow-up.

Necking flow	V_{drop} **(ml)**	t_{neck} **(ms)**	P_{app} **(Pa)**	$R_{t,mi}$ **(Pa s/m^3)**	ϕ_n **(ml/s)**
Experimental	$4.96 \cdot 10^{-10}$	0.335	-	-	$1.48 \cdot 10^{-6}$
Theory	-	-	$9.0 \cdot 10^{4}$	$6.22 \cdot 10^{16}$	$1.45 \cdot 10^{-6}$

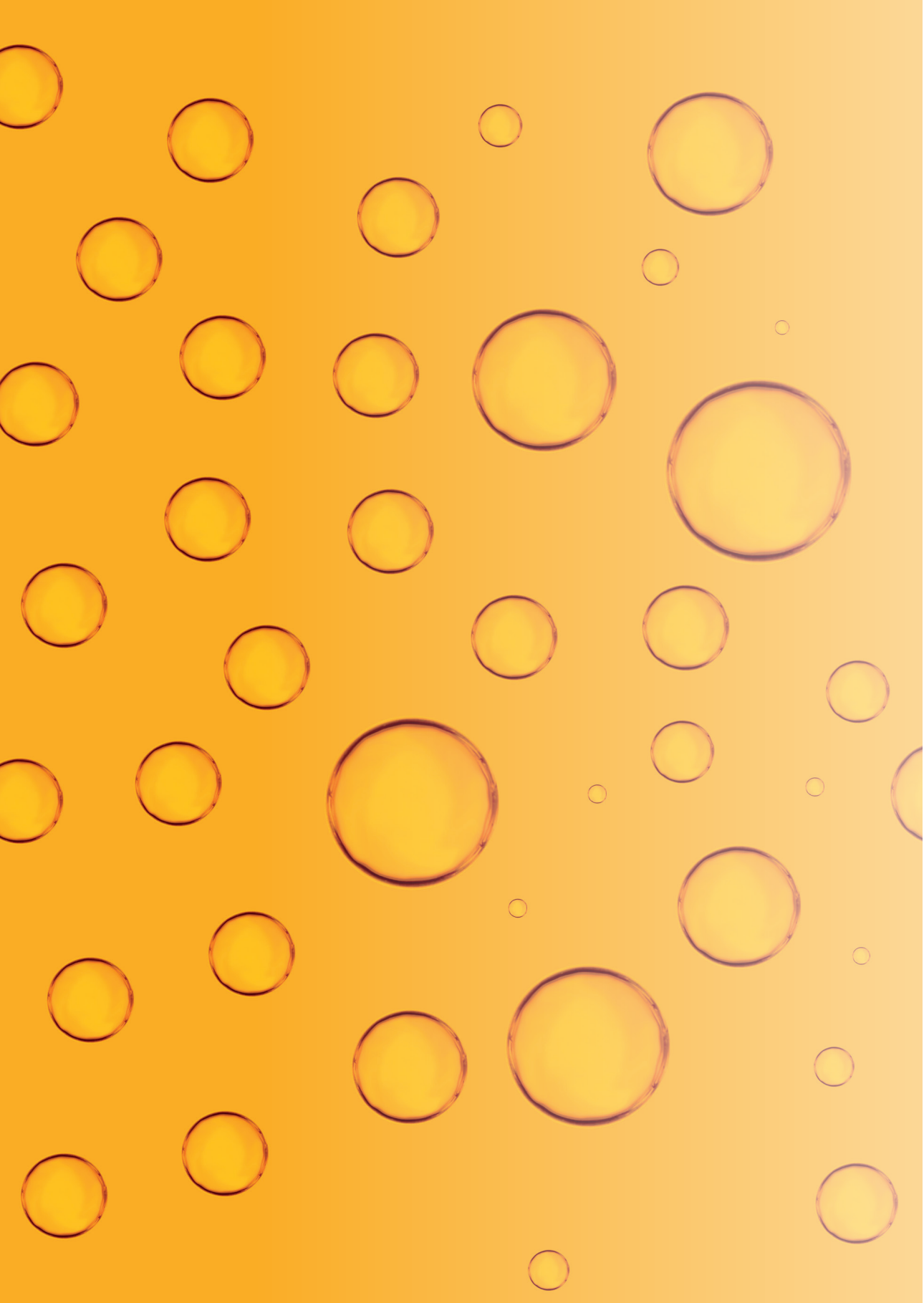

Chapter 3

Design insights for upscaling spontaneous microfluidic emulsification devices based on behaviour of the Upscaled Partitioned EDGE device

This chapter was published as:
S. ten Klooster, C. Berton-Carabin, K. Schroën: *Design insights for upscaling spontaneous microfluidic emulsification devices based on behaviour of the Upscaled Partitioned EDGE device*, Food Research International (2022), 112365.

Abstract

Microfluidic emulsification has the potential to produce emulsions with very controlled droplet sizes in a subtle manner. To support in unleashing this potential, we provide guidelines regarding upscaling based on the performance of Upscale Partitioned EDGE (UPE) devices, using rapeseed oil as the to-be-dispersed phase and whey proteins as the emulsifier. The UPE_{5x1} device (11,000 droplet formation units (DFUs) of 5 · 1 μm) produced 3.5-μm droplets (CV 3.2%) at 0.3 mL/h; UPE_{10x2} (8,000 DFUs of 10 · 2 μm) produced 7-μm droplets (CV 3.2%) at 0.5 mL/h, and at higher pressures, 32-μm droplets (CV 3-4%) at 4 mL/h. These productivities are relatively high compared to those of other devices reported in literature (e.g., Microchannel, Tsukuba and Millipede, Harvard).

Based on these results, and on others from literature, we conclude that: (i) the continuous phase channel dimensions need to be chosen such that they allow for gradual filling of this channel with droplets without decreasing the pressure over the droplet formation units significantly; (ii) the dispersed phase supply channel design should create a wide stable droplet formation pressure range to increase productivity; and (iii) higher productivities can be obtained through the choice of the ingredients used; low viscosity oil and an emulsifier that increases the interfacial tension without negatively affecting device wettability is preferred (e.g., whey protein out-performs Tween 20). These results and design guidelines are expected to contribute to the first food emulsion products prepared with microfluidics.

3.1 Introduction

Microfluidic emulsification is an emerging technique to produce, amongst others, food and pharma emulsions with a highly controlled droplet size in a very subtle manner (Schroën et al., 2015; Zhu et al., 2017). It is also an excellent tool to perform high throughput experiments in the fields of biology and chemistry compared to conventional approaches (Neves et al., 2017; Shang et al., 2017; Teh et al., 2008). Besides, microfluidic emulsification has also been widely used in food science as analytical tools to study e.g. lipid oxidation (Neves et al., 2017), emulsion physical stability (Hinderink et al., 2021; Krebs et al., 2012; Muijlwijk et al., 2017), and so on, as recently reviewed (Schroën et al., 2021).

In microfluidic emulsification devices, a dispersed phase is contacted with a continuous phase in a controlled manner by making use of very small channels (van Dijke et al., 2010c). As a result, a droplet is formed either spontaneously or due to the shear exerted by the continuous phase flow. The disadvantage of microfluidic devices that operate by such shear forces (e.g., T- and Y-junctions, flow-focussing and co-flow devices) is that the flow of both phases has to be controlled very precisely to make monodisperse droplets, which complicates tuning droplet size and reaching a specific concentration of oil in the final emulsion (Vladisavljević et al., 2012; Zhu et al., 2017). Spontaneous microfluidic emulsification devices are more practical for scale-up because droplet formation occurs through a change in Laplace pressure of the dispersed phase, which is also the only phase that needs to be controlled precisely (Kawakatsu et al., 1997; Schroën et al., 2015).

In literature, several upscaled spontaneous microfluidic emulsification devices can be found, all with a specific device geometry. It is difficult to compare these devices because different assessment criteria exist: droplet size (often smaller droplets are desired), droplet monodispersity (often assessed by the coefficient of variation (CV)), droplet formation frequency per active droplet formation unit (DFU), fraction of active DFUs, productivity per unit area (L/m^2h), or the actual oil throughput; additionally, throughputs per DFU are higher when producing larger droplets (Stolovicki et al., 2018). The intrinsic properties of the components used also influence productivity: for example, the higher the continuous and dispersed phase viscosities, the lower the productivity (Kobayashi et al., 2009; Van Dijke et al., 2010; Vladisavljević et al., 2011). In addition, a higher oil-water interfacial tension usually leads to a higher productivity (Kobayashi et al., 2005c). This (dynamic) oil-water interfacial tension is also affected by the emulsifier type and concentration. Besides, the

emulsifier can change the wetting of the channel walls, which may lead to a higher productivity (Sahin et al., 2016). The differences in assessment criteria and in experimental set-ups make it rather difficult to compare studies fairly.

In this chapter, we focus on droplets that are below 10 μm, and thus relevant for food applications; it would be even more favourable from the point of product physical stability if we could produce droplets that are smaller than 5 μm and for some products even below 1 μm (Gijsbertsen-Abrahamse et al., 2004; Leal-Calderon et al., 2007). Devices capable of producing droplets < 5 μm have been reported, but the productivities were very low (10^{-3} mL oil per h), which limits the options for characterising the obtained emulsion (Kobayashi et al., 2001, 2007). Here, we present a device called Upscaled Partitioned EDGE (UPE), which can be flexibly deployed to make different droplet sizes and oil volume fractions, starting from different emulsifiers: Tween 20 and whey proteins as prominent representatives of food-grade surfactant and protein emulsifiers, respectively. We use several assessment criteria such as droplet sizes, true oil droplet production (mL/h) and productivity per chip area (L/m^2h) that are normalised where possible (e.g., for dispersed phase viscosity (Van Dijke et al., 2010)) to compare our device with other upscaled devices in literature. Finally, we provide guidelines for the design and operation of upscaled microfluidic emulsification devices.

3.2 Materials and methods

3.2.1 Materials

Rapeseed oil was kindly provided by Unilever (Wageningen, the Netherlands) and stripped with alumina powder (MP EcoChromet ALUMINA N, Activity: Super I, Biomedicals) to remove surface-active impurities and endogenous antioxidants (Berton et al., 2011a). Whey protein isolate (WPI), purity 97.0–98.4% (BiPro®, Davisco, Switzerland) and Tween 20 (Sigma-Aldrich, Zwijndrecht, the Netherlands) were used as emulsifiers. Sodium phosphate monobasic dihydrate and sodium phosphate dibasic dihydrate (Sigma-Aldrich, Zwijndrecht, the Netherlands) were used to make the phosphate buffer (pH 7.0). For cleaning the chips, we used ethanol, purity 96% v/v (VWR International B.V., Amsterdam, the Netherlands) and piranha solution, which is a 3:1 v/v ratio of sulphuric acid, purity 96% (Sigma-Aldrich, Zwijndrecht, the Netherlands) and 35 wt.% hydrogen peroxide (Sigma-Aldrich, Zwijndrecht, the Netherlands). Assay reagent for measuring the triglyceride (TAG) content and a standard containing TAGs (Triglycerides liquicolor mono kit) were purchased from HUMAN (HUMAN Gesellschaft für Biochemica und Diagnostica mbH,

Wiesbaden, Germany). Ultrapure water (18.2 MΩ) was used for all experiments and prepared using a Milli-Q system (Millipore Corporation, Billerica, MA, USA).

3.2.2 Chip design

The Upscaled Partitioned EDGE (Edge-based droplet generation) (UPE) microfluidic chips were designed in our lab and produced in glass by deep reactive ion etching (DRIE) (Micronit Microfluidics, Enschede, The Netherlands). The relatively deep continuous and dispersed phase channels and the shallow plateaus, including the micro-plateaus (droplet formation units: DFUs), were etched into two separate glass substrates, which were later bonded together and diced. In the relatively long and deep continuous phase channel, the droplets were formed and collected. The layout of the microchips is shown in Figure 3.1; the dimensions of the micro-plateaus are specified in Table 3.1.

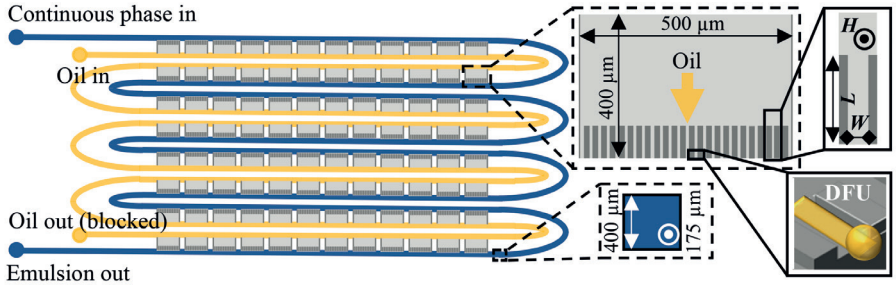

Figure 3.1. Top-view design of the Upscaled Partitioned EDGE chips used in this research. The blue 'twisted road' channel is the continuous phase channel, and the yellow 'twisted road' channel is the to-be-dispersed phase channel. The grey rectangular areas in between these channels are the main plateaus that contain the micro-plateaus with the Droplet Formation Units (DFU). A 3D representation of a DFU is shown in the right lower corner, showing oil – in yellow –, being pushed out of the DFU and forming a droplet, which is ready to detach. Dimensions of the DFUs are in Table 3.1. This illustration is not to scale; only 12 out of the 42 main plateaus are shown per row.

Table 3.1. Characteristic dimensions of the Upscaled Partitioned EDGE devices.

Coding used	Dimensions of micro-plateaus [$L \cdot W \cdot H$] [µm]	Number of main plateaus [-]	Number of micro-plateaus per main plateau [–]	Total number of micro-plateaus (DFUs) [-]
UPE_{5x1}	40 · 5 · 1	336	33	11,088
UPE_{10x2}	40 · 10 · 2	336	24	8,064

3.2.3 Continuous and dispersed phase preparation

The day before emulsion production with the microfluidic chips, the emulsifier (either 5.0 wt.% WPI or 2 wt.% Tween 20) was dissolved in 10 mM phosphate buffer (pH = 7.0) and gently stirred overnight at 4 °C. Prior to use, the dispersed and continuous phase liquids were filtered using a 0.22-µm filter (Minisart

High-Flow, Sartorius Stedim Biotech GmbH, Goettingen, Germany).

3.2.4 Chip cleaning

The cleaning of the chips is one of the most critical points in microfluidic emulsification; if the chip is not properly cleaned, the productivity can be reduced (Zhang et al., 2015). After each experiment was completed, the chips (including the plateaus) were flushed with ethanol, sonicated in ethanol for 90 min and then in water for 10 min. Next, the chip was baked in an oven at 500 °C for 2 h. The chip was stored until the day before the experiment. The day before the experiment, the chip was sonicated (Branson 1800, Brookfield, CT, USA) in a glass beaker with piranha (1:3 v/v mixture of sulphuric acid and 35% hydrogen peroxide) for 90 min followed by 90 min sonication in ultrapure water, and it was left in ultrapure water overnight. On the day of the experiment, the chip was rinsed with ultrapure water to remove any leftovers of cleaning chemicals from the channels.

3.2.5 Chip operation

Once cleaned, the device may be used. The microfluidic chip was placed in a chip holder from Micronit (Fluidic Connect PRO Chip Holder with 4515 Inserts, Micronit Microfluidics, Enschede, The Netherlands). After the main channels were wetted with the continuous phase by flowing this phase into the chip gently, the oil was pushed into the dispersed phase channel. When rinsed thoroughly, the dispersed phase outlet was blocked (Figure 3.1). Next, the dispersed phase was pressurized across the plateau, through the micro-plateaus and finally through the DFUs. At the DFUs, droplets were formed that were carried away by the cross-flowing continuous phase (Figure 3.1). This cross-flow will not influence droplet size since the cross-flow is not needed for droplet formation in these devices (Sahin et al., 2015). The pressures, and thereby the flows, were controlled through a microfluidic control system (Elveflow OB1, MK3, Elveflow®, France), and droplet formation was monitored by using an inverted microscope (Axiovert 200 MAT, Carl Zeiss B.V., The Netherlands), which was connected to a high-speed camera (FASTCAM SA-Z, Photron Limited, Japan). The maximum frame rate was 100,000 frames per s, and the resolution was 0.973 or 0.402 μm/pixel.

3.2.6 Productivity

The maximum emulsion productivity was measured by determining droplet size in combination with the droplet formation frequencies and by the actual oil content (approximately 5 wt.%) of the collected emulsions. Both methods are described below.

Droplet sizes and frequencies
The productivity was determined by multiplying the average droplet volume (section 3.2.7) with the average droplet formation frequency per DFU and with the amount of DFUs per chip (Table 3.1). The average droplet formation frequency was determined by using a custom-written script in image analysis software (Matlab R2019B) on high-speed recordings during production. The recordings were taken at several locations on the chip and at several time points during production to ensure representative data.

Triglyceride content of collected emulsions
In addition, the productivity was determined by weighing the amount of emulsion collected over time, and measuring the oil content using a colorimetric method to determine the triglyceride (TAG) content (Triglycerides Liquicolor Mono kit, HUMAN) (Jacobs et al., 1960; Trinder, 1969). In brief, the samples were diluted to a range of 0.5-4 g/L. Next, the droplets were broken up in smaller droplets by sonification with the Branson Sonifier SFX550 (Brookfield, CT, USA) equipped with a sonication tip 1/8′ tapered microtip (Branson, Brookfield, CT, USA) at an amplitude of 35% for 15 s. This was done because a large amount of oil-water interface was required to hydrolyse the triglycerides and thereby obtain accurate results using this assay kit. The droplet size distribution of the broken droplets was independent of the initial droplet size (Figure A3.1a). Next, about 20 µL of sample were weighed into a 2-mL microtube, and 1 mL of assay reagent was added. The assay reagent content was: 50 mmol/L PIPES buffer (pH 7.5), 5 mmol/L 4-chlorophenol, 0.25 mmol/L 4-aminoantipyrine, 4.5 mmol/L magnesium ions, 2 mmol/L ATP, 1.3 U/mL lipases, 0.5 U/mL peroxidase, 0.4 U/mL glycerol kinase, and 1.5 U/mL glycerol-3-phosphate oxidase. The samples were incubated in a heating block at 800 rpm for 20 minutes at 20 °C. Next, the absorbance was measured at a wavelength of 500 nm. A calibration curve was generated with TAG dispersions with known concentrations ranging from 0.5-4 g/L. Finally, the productivity was calculated based on the amount of collected sample and its TAG content.

3.2.7 Droplet sizes measurements

Image analysis
A small volume (3 µL) of sample was taken from the collected emulsions and analysed using a Carl Zeiss Axioscope A1 optical microscope (Carl Zeiss BV, Breda, the Netherlands) equipped with a camera (AxioCam Mrc5). At least 75 droplets per data point were analysed using a custom-written script in image analysis software (Matlab R2019b) to determine the average droplet size, which is sufficient when droplets are very monodisperse (Deng et al., 2021).

With this script, the droplet diameter is calculated from the circumference of the droplet. Since the droplet volume scales with the droplet diameter to the power of three, a small systematic error leads to a large error in productivity (section 3.2.6); therefore, as a check, the centre-to-centre distance of clustered droplets was determined, and with that a correction factor could be calculated (Table A3.1). The productivities determined by the different methods described above (section 3.2.6) were in line with each other (Figure A3.1b); therefore, confirming the appropriateness of the methods used.

Statistics droplet sizes
The size distribution of the droplets was expressed as a coefficient of variation, CV, which was defined as:

$$\mathrm{CV} = \frac{\sigma}{d_{dr}} \cdot 100 \tag{3.1}$$

where σ is the standard deviation of the droplet diameters, and d_{dr} is the number-average droplet diameter. Based on previous research, droplets with a CV below 10% can be considered monodisperse (van Dijke et al., 2009).

3.2.8 Viscosity measurements

The viscosity of the rapeseed oil used was measured at 22 °C (the lab temperature) with a rheometer (Anton Paar Physica MCR 301, Anton Paar, Oosterhout, the Netherlands) at a shear rate of 100 s^{-1}.

3.2.9 Calculations

The pressure difference (ΔP) working over the DFUs is calculated as the applied pressure over the dispersed phase minus the applied pressure over the continuous phase.

The flow resistances (R) of the devices can be calculated with a Hagen-Poiseuille-based equation for a rectangular channel:

$$R = \frac{12\eta l}{1 - 0.63(\frac{h}{w})} \frac{1}{h^3 w} \tag{3.2}$$

where η is the viscosity, l the length, h the height and w the width of the channel, respectively. Equation 3.2 was used to calculate the flow resistance of a micro-plateau (actual DFU) and the main plateau separately. The total flow resistance of main and micro-plateaus (R_t) was defined as:

$$R_t = \frac{R_{mi}}{n_{mi}} + R_{ma} \tag{3.3}$$

where R_{mi} is the flow resistance of the micro-plateau, n_{mi} is the number of micro-plateaus per main plateau and R_{ma} is the flow resistance of the main plateaus. The flow resistance of the whole shallow connection, expressed per micro-plateau ($R_{t,mi}$), was calculated as:

$$R_{t,mi} = R_t \cdot n_{mi} \tag{3.4}$$

This flow resistance was then used to calculated the flow (ϕ) at a certain pressure (P):

$$\phi = \frac{P - P_{LP}}{R_{t,mi}} \tag{3.5}$$

The Laplace pressure (P_{LP}) of a *bare* oil-water interface can be calculated by:

$$P_{LP} = \gamma_b \left(\frac{1}{r_1} + \frac{1}{r_2}\right) \tag{3.6}$$

where γ_b is the interfacial tension of the *bare* oil-water interface, r_1 and r_2 the radii of curvature of the meniscus inside the micro-plateau, in this case, half the width and half the height (of the DFUs).

3.3 Results and discussion

In section 3.3.1 & 3.3.2, the performance of the Upscaled Partitioned EDGE (UPE) device is discussed and in section 3.3.3, UPE is compared with other upscaled devices from literature. Section 3.3.4 provides guidelines for upscaling spontaneous microfluidic emulsification devices.

3.3.1 Operation of UPE

The chips, with 8,000-11,000 DFUs (Table 3.1), were operated by first pushing the continuous phase in the respective channel, after which the applied pressure over the dispersed phase was increased until the oil flows over the shallow plateaus at the so-called breakthrough pressure (Figure 3.2a), which equals the Laplace pressure of the oil-water meniscus that works in the opposite direction (van Dijke et al., 2009). Upon further increasing the pressure, droplet formation started, and the droplet formation frequency increased with pressure, whereas the droplet size was barely affected (Figure 3.2b & c) (Sahin et al., 2015). When the pressure was further increased, the so-called blow-up pressure was reached, above which larger monodisperse droplets were formed through a physical push by neighbouring droplets in a cascaded fashion (Figure 3.2d) (ten Klooster et al., 2019).

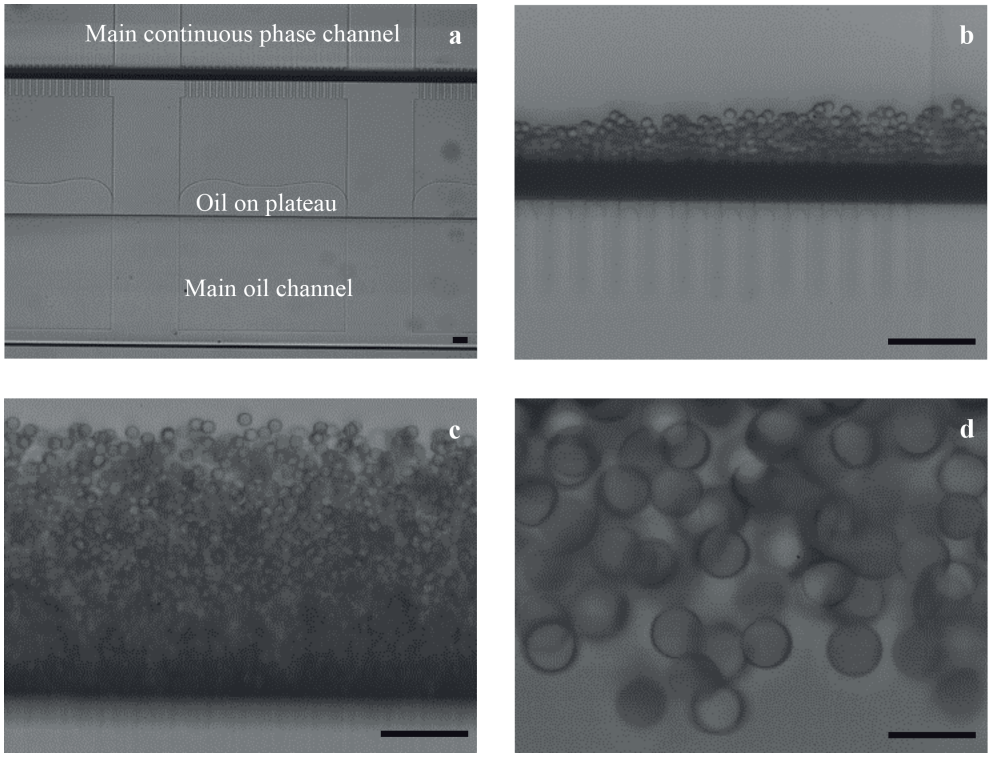

Figure 3.2. The UPE_{10x2} device in operation: start of oil flow over the main plateaus (a), droplet formation at the first DFUs at low pressure (b), production of small monodisperse droplets at maximum productivity (c), production of large monodisperse droplets when using the same chip at higher dispersed phase pressures (d). Scale bars represent 50 μm.

We produced small emulsion droplets in the first pressure regime at the maximum productivity with the UPE_{5x1} and UPE_{10x2} chips, using either 5 wt.% WPI or 2 wt.% Tween 20 in the continuous phase (Figure 3.3 & 3.4, respectively). The droplets were very monodisperse with CVs ranging from 2.7 to 7.8% (discussed in more detail in section 3.3.4). The droplets produced with UPE_{10x2} were almost twice as large as the droplets produced with UPE_{5x1}, for both emulsifiers used (Figure 3.3 & 3.4), which is in line with literature (Kobayashi et al., 2004b; Sugiura et al., 2002; van Dijke et al., 2010c).

Since we were interested in producing several emulsions with droplets of distinct sizes, we used the UPE_{10x2} chip in the second pressure regime to produce larger monodisperse droplets, using 5 wt.% WPI or 2 wt.% Tween 20 (Figure 3.3 & 3.4 respectively). For the UPE_{5x1} chip, a much higher pressure would be required (Equation 3.2) to reach this stage, whereas the droplet sizes remains roughly 1.6-1.8 times the centre-to-centre distance between two DFUs (ten Klooster et al., 2019), which is similar for UPE_{5x1} and UPE_{10x2}. Overall, these larger droplet

sizes are independent of emulsifier used (Figure 3.3 & 3.4), and, as shown previously, of continuous and dispersed phase viscosities (ten Klooster et al., 2019).

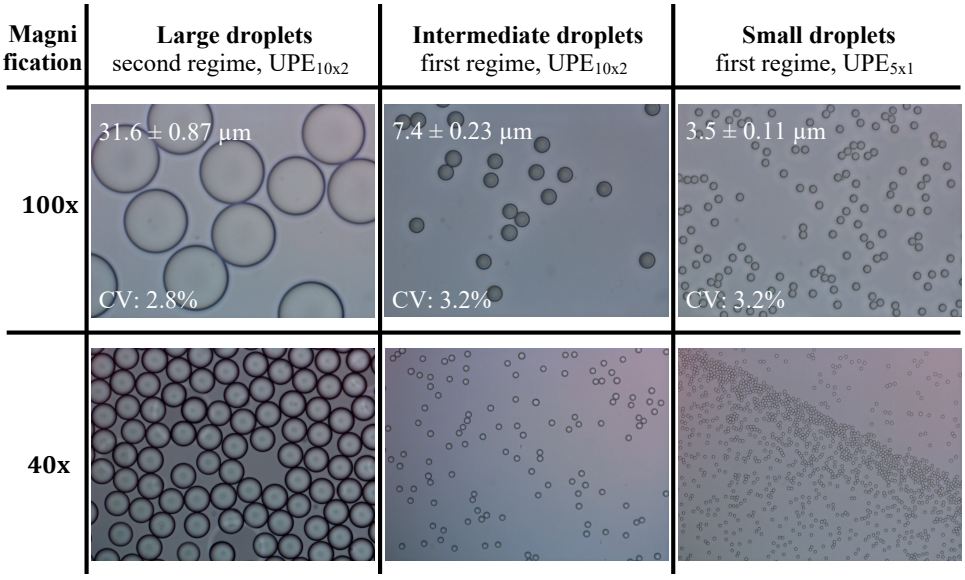

Figure 3.3. Light microscopy images of the produced rapeseed oil droplets at the maximum productivity with 5 wt.% WPI in the continuous phase.

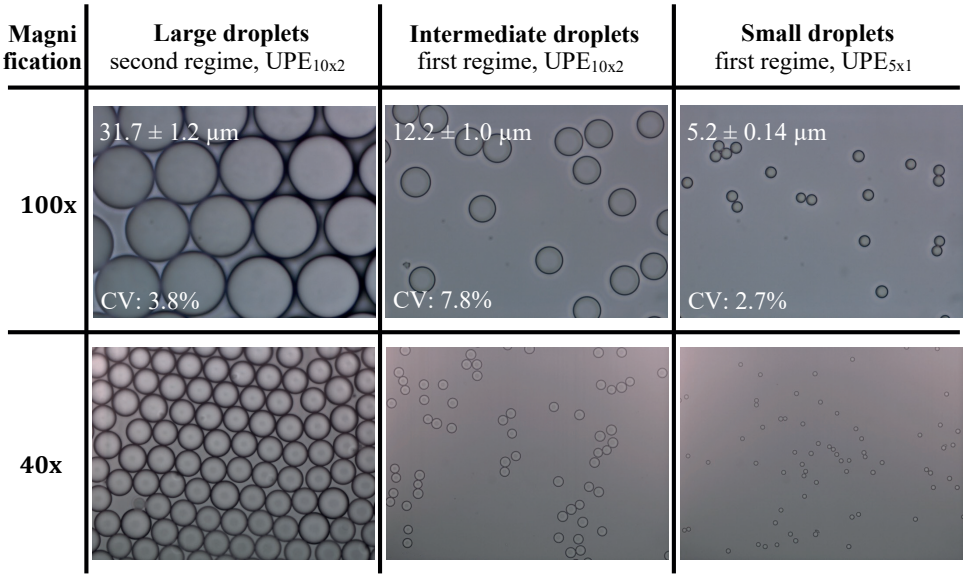

Figure 3.4. Light microscopy images of the produced rapeseed oil droplets at the maximum productivity with 2 wt.% of Tween 20 in the continuous phase.

3.3.2 Droplet formation mechanism

During small droplet formation with UPE, two stages can be distinguished: the down time (filling) and necking time (Deng et al., 2021; ten Klooster et al., 2022c). During the down time, the DFU (re)fills if the applied pressure is higher than the Laplace pressure of the meniscus in the DFU, and this stage finishes when the dispersed phase leaps into the deeper continuous phase channel. This is also the starting point for necking. Necking finishes when the liquid thread, which connects the droplet to the oil in the DFU, breaks due to the interfacial tension force that overcomes the viscous (and inertial) forces (Deng et al., 2021; Sugiura et al., 2001; ten Klooster et al., 2022c).

Effect of emulsifier on droplet formation

For both UPE_{5x1} and UPE_{10x2}, a 3.5-fold higher pressure could be applied in the first pressure regime when comparing WPI with Tween 20 (Table 3.2). Possibly, the interfacial tension at the moment of droplet formation is higher for WPI because of its higher equilibrium interfacial tension (Bos et al., 2001; Deng et al., 2022a; Muijlwijk et al., 2016). An additional explanation could be that WPI changes the contact angle that promotes wetting by the continuous phase upon irreversible protein adsorption at the glass surface, which therewith may increase the pressure stability of the system (Sahin et al., 2016).

Table 3.2. Applied pressures over the different phases for droplet formation at maximum productivities.

Chip	Emulsifier (wt.%)	Breakthrough Pressure (mbar)	Dispersed phase pressure (mbar)	Continuous phase pressure (mbar)	Pressure difference ΔP (mbar)	Theoretical ΔP_{LP} bare O/W meniscus (mbar)
UPE_{5x1}	**5% WPI**	350	2,710	150	2,560	720
UPE_{5x1}	**2% Tween 20**	170	725	25	700	720
UPE_{10x2}	**5% WPI**	175	920	290	630	360
UPE_{10x2}	**2% Tween 20**	90	260	60	200	360

As expected, the value of the blow-up pressure affects the productivity: when switching from 2 wt.% Tween 20 to 5 wt.% WPI, for UPE_{5x1} a 5.2-fold higher production was found; for UPE_{10x2} this was 2.5-fold higher; whereas in literature, a two-fold *lower* productivity was found (Sahin et al., 2016). The difference in these values is most probably the results of differences in device design, and the components used. In the device used by Sahin et al., the Laplace pressure of the *bare* oil-water interface of the meniscus (~ 300 mbar, Equation 3.6) was higher than the maximum pressure that could be applied for both emulsifiers (for Tween 20, 120 mbar and for WPI, 220 mbar) without blow-up occurring.

As a result, emulsifiers have to adsorb before the DFU can refill, which is slower when using WPI than when using Tween 20 (Bos et al., 2001; Deng et al., 2022a; Muijlwijk et al., 2016), leading to lower productivity for their device (Sahin et al., 2016).

Effect of dispersed phase supply channels on droplet formation
The blow-up pressure (ΔP, Table 3.2) is about a 3.5- to 4-fold higher for UPE_{5x1} compared to UPE_{10x2} for both WPI and Tween 20. The blow-up pressure can be deduced as follows: the interfacial tension force during the necking stage can be assumed independent of the chip used. This implies that the maximum viscous force is equal for the chips, which results in an equal flow velocity at blow-up pressure (Stolovicki et al., 2018). This occurs when the necking volumetric flow rate of UPE_{5x1} is a fourfold lower than that of UPE_{10x2} because the DFU area in UPE_{5x1} is four times smaller. The flow resistance of the UPE_{5x1} chip is around a 12.8-fold higher than that of the UPE_{10x2} chip (Equation 3.2, 3.3, 3.4), which implies that the applied pressure has to be a 12.8-fold higher to obtain the same volumetric flow rate (Equation 3.5). The resulting theoretical difference of a 3.2-fold (12.8/4) higher blow-up pressure for the UPE_{5x1} chip compared to the UPE_{10x2} chip is close to the experimental values (3.5-fold for Tween 20 and 4.1-fold for WPI, Table 3.2). This shows that the blow-up pressure can be estimated based on the dimensions of the DFU and dispersed phase supply channels, and that gives a clear handle for productivity enhancement.

3.3.3 Maximum productivities compared to literature
High productivities reported for microfluidic emulsification devices can be encountered in literature; for example 1.5 L/h (Gelin et al., 2020). These productivities are highly subjective to the droplet size and ingredients used. To put the results into perspective, Gelin and co-workers made hexane droplets of 45 μm, with a viscosity that is a two hundredfold (60/0.3) lower than our rapeseed oil. Since productivity scales linearly with viscosity (and in a more complex way with droplet size), it is clear that comparing based on throughput only does not do full justice to the capacity of a system. In the next sections, we discuss how devices presented in literature could be compared and focus on spontaneous devices for their upscaling potential (section 3.1) (Schroën et al., 2015).

The maximum true throughput
The maximum 'true' oil throughput of a device producing an O/W emulsion, in mL/h, can be a way to compare upscaled devices, for example when the goal is to produce monodisperse emulsion samples (Khalid et al., 2015; Krebs et al.,

2012). Especially our 0.30 mL per h for 3.5-µm (CV 3.2%) rapeseed oil droplets, for 5 wt.% WPI, is high compared to literature (Table 3.3 & 3.4). The throughput for 7.4-µm (CV 3.2%) rapeseed oil droplets, using the UPE_{10x2} chip with 5 wt.% WPI, of 0.54 mL oil per h is high when compared to literature for droplets < 10 µm and comparable to the study by Kobayashi et al., who produced 1.5 mL/h of 12-µm (CV 5%) rapeseed oil droplets (Kobayashi et al., 2010), when keeping in mind the larger droplets there. The high throughputs in the current research are also a result of the 100% DFU activation that we achieved, which makes UPE devices stand out from others (Table 3.4).

The true oil throughput of larger droplets (32 µm) in the second pressure regime of ~ 4 mL/h is high, especially since it was achieved with 'only' 8,000 DFUs, showing the potential of this regime for producing larger monodisperse droplets (CVs of 3-4%), although it might be difficult to further upscale this because the droplets need to interact for their formation. Higher true productivities for similar sized droplets have been reported by Kobayashi et al. (23 mL/h of 31-µm rapeseed oil droplets with 211,000 DFUs) (Kobayashi et al., 2005c) and by Vladisavljević et al. (12 mL/h of 27-µm rapeseed oil droplets with 23,000 DFUs) (Vladisavljević et al., 2011) (Table 3.4). The productivity per DFU is similar for these devices, including our UPE (Table 3.4).

Surface area related productivity

Oil droplet productivity of microfluidic emulsification devices is often reported in terms of L/m^2h (Table 3.3 & 3.4). This area-productivity can only be determined if devices in one way or another can be stacked (indicated with the letter 'T' in Table 3.4). An impressive area-productivity has been reported by Vladisavljević and co-workers of 120 L/m^2h for the production of 27-µm rapeseed oil droplets (Table 3.4) (Vladisavljević et al., 2011), and the microfluidic emulsification device called Multi EDGE showed a productivity of 300 L/m^2h for the production of 10-µm hexadecane droplets (ten Klooster et al., 2022c). When correcting for the lower viscosity of hexadecane (3.4 versus 50 mPa s for rapeseed oil (Van Dijke et al., 2010)), denoted as (Productivity*), this would result in 20 L/m^2h for the production of smaller droplets.

It can be useful to calculate a theoretical area-productivity to envision what level of upscaling would be required to reach a specific product flow. For some devices reported in literature, such a theoretical area-productivity has been calculated (Amstad et al., 2016; Sahin et al., 2015), which are indicated in Table 3.4 by the letter 'P'. For the UPE devices presented here and other single-layer upscaled devices reported in literature, we calculated the area-productivity

using the effective area of Multi EDGE (5% (ten Klooster et al., 2022c)) (Table 3.4, letter 'S'), and corrected for the dispersed phase viscosity (productivity*). We compare the productivity for each droplet size based on the actual size in the summary of Table 3.4. The value of 350 L/m^{2}h for UPE$_{5x1}$ when operated with 5 wt.% WPI leading to 3.5-µm droplets compares favourably to the other devices that make small droplets.

3.3.4 Design insights upscaled microfluidic emulsification

The droplet size scales with three to four times the DFU height for constant height/width ratio of the device as shown in section 3.3.1 and in literature (Kobayashi et al., 2005b, 2007; Montessori et al., 2019). The droplet size can be decreased by decreasing the DFU width (Kobayashi et al., 2007; Montessori et al., 2019; ten Klooster et al., 2019), increasing the dispersed phase viscosity, or decreasing the continuous phase viscosity (ten Klooster et al., 2019; Van Dijke et al., 2010; van Dijke et al., 2010c). A minimum DFU height-to-width ratio of ~ 2.5 is required for monodisperse droplet formation (Kobayashi et al., 2004a; Montessori et al., 2019).

Targeting small droplets will be at the expense of productivity per DFU. For example, decreasing the DFU dimensions by a factor of two, will decrease the maximum oil flow during necking by a factor of four (section 3.3.2), thus requiring four times as many DFUs for the same productivity. Since its surface area will be four times smaller, the same total pore area will still lead to the same productivity. So, depending on the practical limitations for the spacing between pores, this might influence the area-productivity. By reducing the smallest dimensions by a factor of two, the Laplace pressure increases by a factor of two (Equation 3.6), which is important when targeting a device with a higher blow-up pressure than the Laplace pressure of the bare oil-water meniscus (see section 3.3.2 and below for the relevance of this). Please note that if the dimensions of all channels are decreased by a factor of two, the flow resistance, and thereby the blow-up pressure, increases by a factor of 16 (Equation 3.2), which may negatively affect the energy efficiency of the device.

Not only the DFU design, but also the sub-structure design leading to the DFUs will influence the overall productivity and pressure stability. When the blow-up pressure is higher than the Laplace pressure of a bare oil-water interface (Equation 3.6) (section 3.3.2) (ten Klooster et al., 2022c), productivity can be greatly enhanced, which also holds for some of our UPE-devices as stated earlier (Table 3.2). By designing the device in such a way, no surfactant adsorption is required for refilling of the DFU to take place, and thus down time is reduced

(section 3.3.2). For example, the productivity of UPE_{10x2} can be improved by increasing its blow-up pressure through increasing the flow resistance of the main dispersed phase supply channels (plateaus, Figure 3.1) (Table 3.2, Equation 3.2-3.5). Please be aware that the blow-up pressure is highly dependent on the type of oil, continuous phase, emulsifier, and on the dimensions of the DFU itself (Sahin et al., 2016; ten Klooster et al., 2019). A high blow-up pressure by a high flow resistance of sub-structures will also have advantages for DFU activation and, above all, for process stability (ten Klooster et al., 2022c). Yet, the blow-up pressure should not be too high to remain energy efficient. In this way, the productivity of many devices reported in literature (Kobayashi et al., 2003, 2007, 2008; ten Klooster et al., 2022c; Vladisavljević et al., 2018) may be improved by increasing substructure resistance as far as technical advances allow (ten Klooster et al., 2022c).

When the dispersed phase flow rate is known, the device can be operated to make a specific oil volume fraction by applying a specific continuous phase flow rate. The required pressure follows from Equations 3.2 & 3.5. If the width and height of the channels are too large, this can hinder regulating the continuous phase flow rate and the gradual fill of droplets into this channel. If they are too small, a significant pressure drop causes distal DFUs to operate close to blow-up, whereas the upstream DFUs run below their maximum production rate. For UPE_{10x2} when using Tween 20 (Table 3.2), the pressure over the continuous phase (60 mbar) was in the range of the pressure applied over the dispersed phase (260 mbar), which may explain the higher CV (7.8%) compared to the other emulsions produced (often 3%) (Figure 3.3 & 3.4).

Away from the droplet size that was discussed earlier, the ingredients used to produce emulsions with such microfluidic chips have a major influence on the productivity. The viscosity of the oil scales inversely with the productivity (Kobayashi et al., 2005a; Van Dijke et al., 2010), and the interfacial tension between water and oil scales directly with the productivity (Kobayashi et al., 2005c, 2005a). Furthermore, productivity decreases with increasing continuous phase viscosity (Kobayashi et al., 2009; Van Dijke et al., 2010). The type and concentration of emulsifier do affect the productivity as well, and its effect can even be dependent on the chip design (section 3.3.2). Generally, the productivity increases with higher (dynamic) interfacial tension (Kobayashi et al., 2005c, 2005a) and with improved device wetting by the continuous phase (Sahin et al., 2016). However, this is not that well-understood yet to allow for a prediction of the productivity based on the emulsifier and its characteristic behaviour both at the oil-water interface and at the surface of the microchip walls.

3.4 Conclusion

We showed that the Upscaled Partitioned EDGE emulsification device (UPE) can produce highly monodisperse rapeseed oil droplets when using Tween 20 and whey proteins as prominent representatives of food-grade surfactant and protein emulsifiers, respectively. Productivities were 0.3 mL/h for 3.5-µm droplets (CV 3.2%) with 11,000 DFUs of 5 × 1 µm; 0.5 mL/h for 7-µm droplets (CV 3.2%) with 8,000 DFUs of 10 × 2 µm; and, with the same chip operated at higher pressures, 4 mL/h for 32-µm droplets (CV 3-4%). These productivities are high compared to other devices presented in literature.

Further optimisation of the chips is possible: the relatively small continuous phase channel dimensions generated a pressure drop over the continuous phase that negatively influences monodisperse droplet productivity, which resulted in a CV of 7% for Tween 20 (instead of 3%). We also show that the pressure at which the DFUs produced larger droplets can be deduced by calculating the flow velocity based on the Hagen-Poiseuille equation. This pressure should be higher than the Laplace pressure of the meniscus inside the DFU without any surfactant adsorbed to generate a fast refill of the DFU. The choice of ingredients influences the emulsion production as well: the productivity is higher when using WPI than when using Tween 20, which could be a result of the higher (dynamic) interfacial tension and/or improved channel wetting by the continuous phase.

The above productivities and design insights will bring us closer to food emulsions products produced with microfluidics. Current productivities are already sufficient to address knotty problems in food research that we address in the next chapters of this thesis, such as the effect of droplet size on chemical and physical stability of emulsions, which was only possible because of these upscaling efforts.

Table 3.3. Overview of upscaled spontaneous microfluidic emulsification devices reported in literature that produce droplets < 80 µm. The main focus was on oil-in-water emulsions, but the bottom seven rows contain water-in-oil emulsion generation devices. Abbreviations: (P)EDGE = (Partitioned) edge-based droplet generation, WP(I)(C) = whey protein (isolate) (concentrate), H_2O = distilled water, SDS = sodium dodecyl sulfate, PVA = polyvinylalcohol, (A)ST = (asymmetric) straight-through, MC = microchannel, PCL = polycaprolactone, PLA = poly(D,L-lactic) acid, DCM = dichloromethane, TGCR = tetraglycerin monolaurate condensed ricinoleic acid esters, PEG = poly(ethylene)glycol, FL = fluorinated, FLo = fluoro. Distilled or ultrapure water was used for all experiments.

Article	Name device	$H \cdot W$ (µm)	Dispersed phase	h_d (mPa s)	Continuous phase	DFUs
This chapter	Upscaled P-EDGE (UPE_5x1)	1 · 5	Stripped rapeseed oil	63.8	H_2O, 2% Tween 20	11,088
This chapter	Upscaled P-EDGE (UPE_5x1)	1 · 5	Stripped rapeseed oil	63.8	H_2O, 5% WPI	11,088
This chapter	Upscaled P-EDGE (UPE_10x2)	2 · 10 (low P)	Stripped rapeseed oil	63.8	H_2O, 2% Tween 20	8,064
This chapter	Upscaled P-EDGE (UPE_10x2)	2 · 10 (low P)	Stripped rapeseed oil	63.8	H_2O, 5% WPI	8,064
This chapter	Upscaled P-EDGE (UPE_10x2)	2 · 10 (high P)	Stripped rapeseed oil	63.8	H_2O, 2% Tween 20	8,064
This chapter	Upscaled P-EDGE (UPE_10x2)	2 · 10 (high P)	Stripped rapeseed oil	63.8	H_2O, 5% WPI	8,064
(van Dijke et al., 2010a)	EDGE-R	1.2 · 500	Sunflower oil	50	H_2O , 6 wt.% WPC	196
(van Dijke et al., 2010a)	EDGE-R	1.2 · 500	Hexadecane	3.4	H_2O , 6 wt.% WPC	196
(Sahin et al., 2015)	P-EDGE	2 · 5 (low P)	Hexadecane	3.4	H_2O, 0.5 wt.% SDS	33
(Sahin et al., 2015)	P-EDGE	2 · 5 (high P)	Hexadecane	3.4	H_2O, 0.5 wt.% SDS	33
(ten Klooster et al., 2022c)	Multi EDGE	2 · 10	Hexadecane	3.4	H_2O, 0.5 wt.% SDS	75,000
(Ofner et al., 2017)	Step	100 · 20	Hexadecane	3.4	H_2O, 2 wt.% PVA	364
(Kobayashi et al., 2003)	ST-MC	9.6 · 48.7	Refined soybean oil	50.4	H_2O 1 wt.% Tween 20	4,300
(Kobayashi et al., 2003)	ST-MC	9.6 · 48.7	Refined soybean oil	50.4	H_2O 1 wt.% SDS	4,300
(Kobayashi et al., 2005b)	AST-MC	11 · 104	Decane	0.87	H_2O 1 wt.% SDS	10,313
(Kobayashi et al., 2005b)	AST-MC	11 · 104	Refined soybean oil	50.4	H_2O 1 wt.% SDS	10,313
(Kobayashi et al., 2007)	MC	0.32 · 3.2	Refined soybean oil	50.4	H_2O 1 wt.% SDS	1,500
(Kobayashi et al., 2007)	MC	0.72 · 3.2	Refined soybean oil	50.4	H_2O 1 wt.% SDS	1,500
(Kobayashi et al., 2007)	MC	1.4 · 3.2	Refined soybean oil	50.4	H_2O 1 wt.% SDS	1,500
(Kobayashi et al., 2001)	MC (SMC-B4)	1.2 · missing	Refined soybean oil	50.4	H_2O, 1.5 wt.% Tween 80	1,200
(Kobayashi et al., 2005c)	ST-MC	6.6 · 26.7	Refined soybean oil	50.4	H_2O ,1wt.% SDS	211,248
(Kobayashi et al., 2005c)	ST-MC	6.6 · 26.7	Silicone oil	48	H_2O ,1wt.% SDS	211,248

(Kobayashi et al., 2010)	MC	2 · 40	Refined soybean oil	50.4	H_2O, 1 wt.% SDS	11,900
(Vladisavljević et al., 2011)	AST-MC	10 · 50	Refined soybean oil	50	H_2O, 2% Tween 20	23,348
(Vladisavljević et al., 2011)	AST-MC	10 · 50	Medium chain triglycerides	20	H_2O, 2% Tween 20	23,348
(Vladisavljević et al., 2011)	AST-MC	10 · 50	Tetradecane	2.7	H_2O, 2% Tween 20	23,348
(Kobayashi et al., 2012)	AST-MC array	17 · 119	Tetradecane	2.7	H_2O, 2 wt.% Tween 20	24,772
(Vladisavljević et al., 2018)	MC (step), DMS6 design 1	5 · 18	2 wt. % PCL (1), 1 wt. % PLA (2) in DCM (3)	0.4	H_2O, 2 wt.% PVA	540
(Vladisavljević et al., 2018)	MC (step), DMS6 design 2	4 · 8	2 wt. % PCL (1), 1 wt. % PLA (2) in DCM (3)	0.4	H_2O, 2 wt.% PVA	1,850
(Kobayashi et al., 2008)	ST-MC, MC TMS 11-2	2.3 · 10	Refined Soybean oil	50.4	H_2O, 1 wt.% SDS	23,548
(Kobayashi et al., 2008)	ST-MC, MC TMS 11-2	2.3 · 10	23.8% H_2O, 1.2% NaCl, 75% glycerol	33.9	3.0 wt.% TGCR(7) in decane	23,548
(Kobayashi et al., 2009)	AST-MC, MC arrays, WMS 1-1	10 · 150	H_2O, 0.86 mol L^{-1} NaCl	1	Decane, 3 wt.% TGCR (7)	6,516
(Stolovicki et al., 2018)	Volcano Step (h=6 µm)	6 · 35	H2O	1	HFE 7500, 1 wt.% FLo-surfactant	384
(Stolovicki et al., 2018)	Volcano Step (h=12 µm)	12 · 70	H2O	1	HFE 7500, 1 wt.% FLo-surfactant	192
(Stolovicki et al., 2018)	Volcano Step (h=20 µm)	20 · 100	H2O	1	HFE 7500, 1 wt.% FLo-surfactant	160
(Amstad et al., 2016)	Millipede (h=20 µm)	20 · 130	H_2O, 10 wt.% PEG (8)	8	FL oil, 1 wt.% FLo-surfactant	550
(Amstad et al., 2016)	Millipede if upscaled (h=20 µm)	20 · 130	H_2O, 10 wt.% PEG (8)	8	FL oil, 1 wt.% FLo-surfactant	550

Table 3.4. Overview of the productivities of upscaled spontaneous microfluidic emulsification devices reported in literature that produce droplets of < 80 µm. The main focus was on oil-in-water emulsions, but the bottom seven rows are about water-in-oil emulsion generation devices. Information on the devices and components used can be found in Table 3.3. *Indicates theoretical productivity when corrected for the dispersed phase viscosity (to 50 mPa s). The letter 'T' in the 'Effective area' or 'Productivity' column indicates a truly upscaled device with multiple rows of DFUs stacked; the letter 'S' indicates that a speculative effective area of 5% was used by us; the letter 'P' that a speculative effective area was mentioned in that publication itself.

Article	Active DFUs (%)	Frequency per DFU (s^{-1})	Productivity (mL / h)	Droplet size (µm)	CV (%)	Effective area	Productivity ($L/(m^2\ h)$)	Productivity* (mL/h)	Productivity* ($L/(m^2\ h)$)
This chapter	100%	19	0.057	5.2	2.7%	5.0% S	51 S	0.073	66 S
This chapter	100%	344	0.30	3.5	3.2%	5.0% S	271 S	0.38	345 S
This chapter	100%	7.8	0.21	12	7.8%	5.0% S	65 S	0.27	83 S
This chapter	100%	89	0.54	7.4	3.2%	5.0% S	167 S	0.69	214 S
This chapter	100%	6.9	3.4	32	3.8%	-	-	4.3	-
This chapter	100%	8.3	4.0	32	2.8%	-	-	5.0	-
(van Dijke et al., 2010a)	100%	150	0.021	7.2	12.1%	5.0% S	9 S	0.021	9 S
(van Dijke et al., 2010a)	100%	2,200	0.34	7.5	11.8%	5.0% S	146 S	0.023	10 S
(Sahin et al., 2015)	100%	1,061	0.053	9.3	4.0%	4.4% P	6,000 P	0.004	408 P
(Sahin et al., 2015)	100%	136	0.19	28	4.5%	4.4% P	25,000 P	0.013	1,700 P
(ten Klooster et al., 2022c)	93%	58	10	11	10%	5.0% T	313 T	0.69	21 T
(Ofner et al., 2017)	100%	70	26	81	2.8%	5.0% S	1,753 S	1.7	119 S
(Kobayashi et al., 2003)	missing	missing	3	39.1	< 3%	1.0% T	30 T	-	30 T
(Kobayashi et al., 2003)	missing	missing	6	38.6	< 3%	1.0% T	60 T	-	60 T
(Kobayashi et al., 2005b)	missing	50	-	40.9	1.3%	5.2% T	-	-	-
(Kobayashi et al., 2005b)	missing	10	-	34.9	1.9%	5.2% T	-	-	-
(Kobayashi et al., 2007)	100%	14.5	0.0001	1.4	16.7%	5.0% S	4 S	0.00011	4 S
(Kobayashi et al., 2007)	100%	missing	-	2.6	9.7%	5.0% S	-	-	-
(Kobayashi et al., 2007)	100%	6.5	0.0008	3.5	8.5%	5.0% S	6 S	0.00079	6 S
(Kobayashi et al., 2001)	50%	3	0.0005	5.2	2.0%	5.0% S	1 S	0.00048	1 S
(Kobayashi et al., 2005c)	60%	3.3	23	31	10%	4.1% T	25 T	24	25 T
(Kobayashi et al., 2005c)	60%	8.5	60	31	10%	4.1% T	66 T	58	63 T
(Kobayashi et al., 2010)	100%	43	1.5	12	5.0%	5.0% S	80 S	1.5	80 S
(Vladisavljević et al., 2011)	97%	14	12	27	(span 0.3)	11.7% T	120 T	12	120 T

(Vladisavljević et al., 2011)	90%	50	60	31.2	(span 0.25	11.7% T	600 T	24	240 T
(Vladisavljević et al., 2011)	50%	250	248	35.6	(span 0.3)	11.7% T	2,700 T	13	146 T
(Kobayashi et al., 2012)	100%	40	1,230	87	2.0%	10.4% T	2,800 T	66	151 T
(Vladisavljević et al., 2018)	92%	2.8	0.045	26	1.6%	5.0% S	46 S	0.0004	0.37 S
(Vladisavljević et al., 2018)	34%	1.5	0.0051	14	4.6%	5.0% S	4 S	0.00004	0.034 S
(Kobayashi et al., 2008)	missing	missing	0.05	6.7	3.9%	2.4% T	2.22 T	0.05	2.2 T
(Kobayashi et al., 2008)	missing	1.1	-	7.1	2.8%	2.4% T	-	-	-
(Kobayashi et al., 2009)	40%	200	87	45	2.5%	9.8% T	1,200 T	1.7	24 T
(Stolovicki et al., 2018)	100%	1,500	29	30	5.2%	5.0% S	18,176 S	0.59	364 S
(Stolovicki et al., 2018)	100%	1,063	51	51	4.8%	5.0% S	15,821 S	1.0	316 S
(Stolovicki et al., 2018)	100%	341	91	96	2.6%	5.0% S	14,217 S	1.8	284 S
(Amstad et al., 2016)	100%	188	100	75	3%	0.6% T	600 T	16.0	96 T
(Amstad et al., 2016)	100%	188	100	75	3%	11% P	11,000 P	16.0	1,760 P

3.5 Appendix

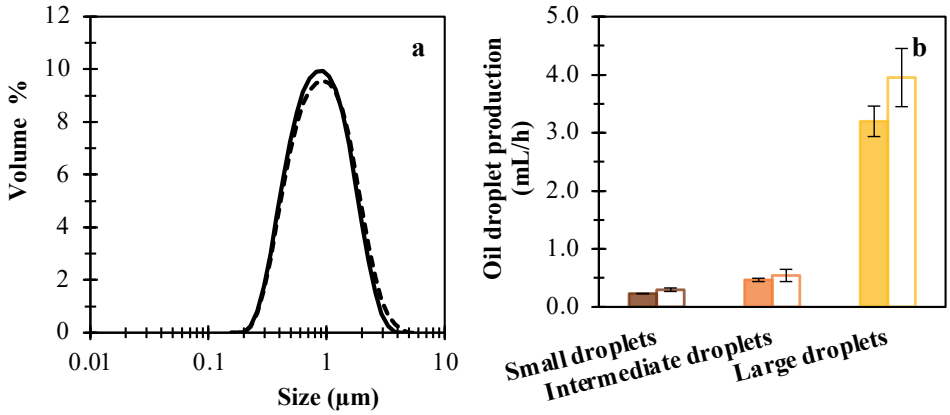

Figure A3.1. Droplet size distributions of sonication-based broken up small droplets (dashed line) and large droplets (solid line) prepared with 2 wt.% Tween 20 (a). The production of oil droplet as measured by image analysis (open bars) and by collecting the emulsion and measuring its oil content (filled bars) (section 3.2.6) when using 5 wt.% WPI in the continuous phase (b).

Table A3.1. The calculated correction factors for the analysis of droplet sizes by the Matlab script, with their standard deviations for the small, intermediate, and large droplets produced with 2 wt.% Tween 20 or 5 wt.% WPI.

	Small	Intermediate	Large
Tween 20	0.906 ± 0.021	0.949 ± 0.012	0.911 ± 0.00024
WPI	0.883 ± 0.0042	0.922 ± 0.019	0.951 ± 0.0039

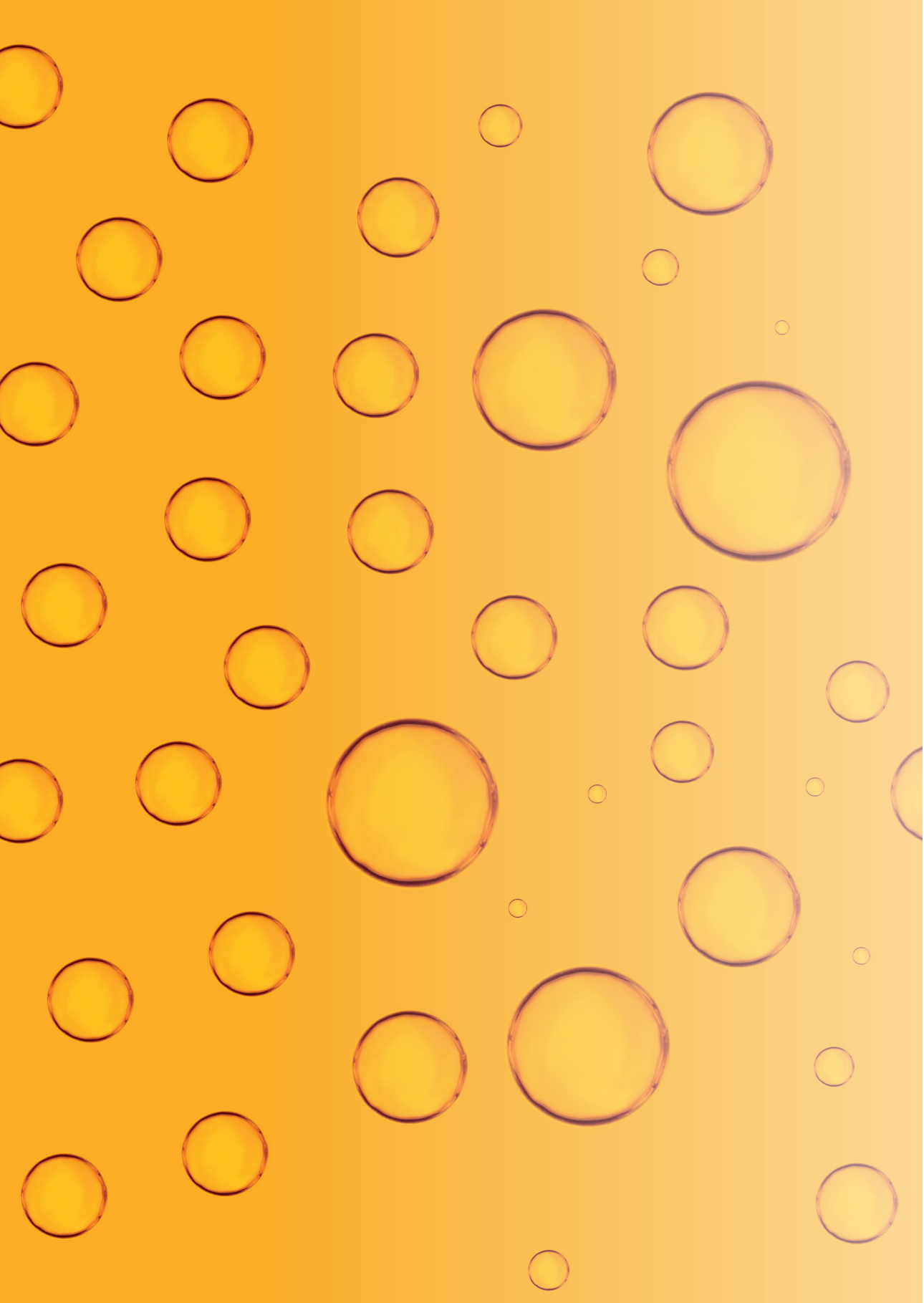

Chapter 4

Unravelling the effect of droplet size on lipid oxidation in emulsions using microfluidics

Manuscript in preparation as:
S. ten Klooster, V. Boerkamp, M. Hennebelle, J. van Duynhoven, K. Schroën, C. Berton-Carabin: *Unravelling the effect of droplet size on lipid oxidation in emulsions using microfluidics*

Abstract

Lipid oxidation deteriorates the sensorial and nutritional quality of emulsions containing polyunsaturated fatty acids. This deleterious reaction is expected to increase with decreasing droplet size, as this increases the specific interfacial area between oil and water, but clear experimental evidence in literature is lacking. Discrepancies in literature can be caused by confounding factors such as the droplet polydispersity inherent to most emulsions, and the effects of components present in the continuous phase.

In this chapter, we used microfluidic emulsification to produce highly monodisperse emulsions with average droplet sizes of 4.7, 9.1, and 26 μm. This allowed us to show, for the first time, that lipid oxidation increases systematically with decreasing droplet size, which is ascribed to the favoured accessibility of the prooxidants present in the continuous phase to the lipids. We further found that co-oxidation of the surfactant used as emulsifier (Tween 20) substantially contributes to the overall oxidative degradation of the systems, especially those containing the fast oxidising smallest droplets. These insights show the importance of the control over droplet size to improve the oxidative stability of emulsion products.

4.1. Introduction

Products containing polyunsaturated fatty acids (PUFAs) have a limited chemical stability due to lipid oxidation, which reduces the shelf life by generating off-flavours and degrading their nutritional quality (Schaich, 2005). Lipid oxidation has become an increasing issue for the food industry given the current trends to promote polyunsaturated fatty acids in the diets for their health benefits, while reducing additives, including synthetic antioxidants, due to consumer preferences and potential health concerns (Berton-Carabin et al., 2014). Lipid oxidation issues are particularly marked in oil-in-water (O/W) emulsions, where the oil–water interface allows contact between the lipid substrate and water-soluble prooxidants, such as metal ions, which initiates lipid oxidation (Berton-Carabin et al., 2014; Laguerre et al., 2009).

Recent publications on lipid oxidation have shed light on spatiotemporal aspects of oxidising emulsions, which has led to hypotheses that would need to be substantiated experimentally, leaving ample room for discoveries (Laguerre et al., 2017, 2020; Villeneuve et al., 2018; Yang et al., 2020). One spatiotemporal aspect that is not well-understood is how the droplet size affects lipid oxidation (Berton-Carabin et al., 2014). A logical hypothesis would be that smaller droplets oxidise faster because they have a larger specific interfacial area, allowing for more initiation reactions. Some results in literature indeed confirm that small droplets oxidise faster (Azuma et al., 2009; Gohtani et al., 1999; Horn et al., 2013; Jacobsen et al., 2000; Kuhn et al., 2012; Lethuaut et al., 2002; Li et al., 2019; Ma et al., 2013; Neves et al., 2017; Rampon et al., 2001; Yang et al., 2020), whereas others indicate that larger droplets oxidise faster (Atarés et al., 2012; Azuma et al., 2009; Horn et al., 2013; Let et al., 2007; Nakaya et al., 2005; Neves et al., 2017; O'Dwyer et al., 2013; Ries et al., 2010), or that droplet size does not influence lipid oxidation (Atarés et al., 2012; Costa et al., 2020; Dimakou et al., 2007; Kiokias et al., 2007; Kuhn et al., 2012; Ma et al., 2013; Neves et al., 2017; Osborn et al., 2004; Yang et al., 2020). How the droplet sizes influences lipid oxidation has been related to the components used (Atarés et al., 2012; Azuma et al., 2009; Horn et al., 2013; Yang et al., 2020) or the applied incubation conditions (Neves et al., 2017).

Part of the confusion about how the droplet size affects lipid oxidation is expected to be related to the difficulty to vary just the droplet size, since other parameters are often changed concurrently, which may affect lipid oxidation as well. For example, the emulsification procedure influences lipid oxidation in emulsions (Horn et al., 2012; Kuhn et al., 2012; Neves et al., 2017). Possible

explanations include the production of free radicals by certain processes that induce cavitation (Berton et al., 2011b), or the modification of the oil-water interfacial composition (Horn et al., 2013; Sørensen et al., 2007). The emulsification procedure and conditions can also modulate the amount of unabsorbed emulsifier and the partitioning of surface-active molecules, such as certain antioxidants (Berton-Carabin et al., 2014). With the inherent variation of multiple parameters when using different emulsification settings and methods, the interpretation of their individual effects on lipid oxidation in emulsions becomes a complex matter.

To advance the current understanding of these aspects, an essential first step is to very precisely control the droplet size. This is not possible using classic emulsification technologies, which motivated us to use upscaled microfluidic devices to make highly monodisperse model emulsions with three distinct droplet sizes that we used at the same oil volume fraction and incubated to monitor lipid oxidation (ten Klooster et al., 2022a). Thus, we systematically varied the droplet size and, accordingly, the total oil-water interfacial area in our lipid oxidation experiments. This led to a better understanding of how lipid oxidation and co-oxidation reactions lead to the overall course of lipid oxidation reactions in emulsions.

4.2. Materials and methods

4.2.1 Materials

Rapeseed oil was kindly provided by Unilever (Wageningen, the Netherlands) and stripped with alumina powder (MP EcoChromet ALUMINA N, Activity: Super I, Biomedicals) to remove surface-active impurities and endogenous antioxidants, in particular tocopherols (Berton et al., 2011a). The fatty acid composition of the rapeseed oil included: 68% oleic, 17% linoleic, 8% linolenic, and 7% saturated fatty acids. Tween 20 (also known as polysorbate 20), ethylenediaminetetraacetic acid calcium disodium salt (EDTA), iron(II) sulfate heptahydrate ($FeSO_4$), sodium phosphate monobasic dihydrate, and sodium phosphate dibasic dihydrate were purchased from Sigma-Aldrich (Zwijndrecht, the Netherlands). For cleaning of the microfluidic chips, we used ethanol (purity 96% v/v, VWR International B.V., Amsterdam, the Netherlands) and piranha solution, which is a 3:1 v/v ratio of 98% sulphuric acid and 35% hydrogen peroxide (both obtained from Sigma-Aldrich, Zwijndrecht, the Netherlands). Ultrapure water (18.2 MΩ) was used for all experiments and prepared using a Milli-Q system (Millipore Corporation, Billerica, MA, USA). The assay reagent for measuring the triglyceride (TAG) content and a TAG standard were purchased

from HUMAN Gesellschaft für Biochemica und Diagnostica mbH (Wiesbaden, Germany). The assay reagent content was: 50 mmol/L PIPES buffer (pH 7.5), 5 mmol/L 4-chlorophenol, 0.25 mmol/L 4-aminoantipyrine, 4.5 mmol/L magnesium ions, 2 mmol/L ATP, 1.3 U/mL lipases, 0.5 U/mL peroxidase, 0.4 U/mL glycerol kinase and 1.5 U/mL glycerol-3-phosphate oxidase. n-Hexane (97%) and 2-propanol (99.8%) were obtained from Actu-All Chemicals (Oss, the Netherlands).

4.2.2 Microfluidic emulsion preparation

Preparation of the continuous phase

The day before emulsion production, Tween 20 (2 wt.%) was dissolved in phosphate buffer (pH 7.0, 10 mM) and stirred for 30 min at room temperature. Both the dispersed phase (stripped rapeseed oil) and the continuous phase (2 wt.% Tween 20 in phosphate buffer) were filtered using a 0.22 µm regenerated cellulose filter (Minisart High-Flow, Sartorius Stedim Biotech GmbH, Goettingen, Germany) prior to use to prevent any dust from entering the microfluidic chip.

Microfluidic chip

To produce highly monodisperse emulsions, microfluidic devices called UPE (Upscaled Partitioned EDGE [Edge-based Droplet Generation]) were used (Figure A4.1) (ten Klooster et al., 2022a). These chips were designed in our lab, made of glass, and produced by deep reactive ion etching by Micronit Microfluidics (Enschede, The Netherlands). To make the smallest droplets (~ 4.5 µm), a chip with 11,088 droplet formation units (DFUs) of 5 × 1 µm (width × height) each were used. To produce the intermediate (~ 9 µm) and largest droplets (~ 26 µm), a chip with 8,064 DFUs of 10 × 2 µm (width × height) each was used. A higher dispersed phase pressure was applied to produce 26 µm droplets. Information about the microfluidic chip characteristics, the principle, and regimes of oil droplet formation can be found in previous work (ten Klooster et al., 2019, 2022a, 2022c).

Microfluidic chip cleaning

The chips were cleaned and operated as described previously (ten Klooster et al., 2022a). In brief, after finishing an experiment, the chip (including the plateaus) was flushed with ethanol, followed by sonication (Branson 1800, Brookfield, CT, USA) in ethanol for 90 min and then in water for 10 min. Next, the chip was placed in an oven at 500 °C for 2 h. The day before an experiment, the chip was sonicated in a glass beaker with piranha for 90 min, which was followed by sonication in ultrapure water for 90 min. It was stored overnight in ultrapure water.

Emulsion preparation by microfluidics
The day of the experiment, the cleaned microfluidic chip was placed in a chip holder from Micronit (Fluidic Connect PRO Chip Holder with 4515 Inserts, Micronit Microfluidics, Enschede, The Netherlands). The channels were first rinsed with ultrapure water and then with the continuous phase. Next, the dispersed phase channel was rinsed with an excess amount of dispersed phase, after which the dispersed phase channel outlet was blocked. The pressure over the dispersed phase was increased to let the dispersed phase flow through the shallow connection between the dispersed and continuous phase channel, the so-called plateau. The plateau ends into many micro-plateaus (Figure A4.1). At the location where the micro-plateaus meet the relatively deep continuous phase channel, oil droplets were generated spontaneously. Increasing the pressure over the dispersed phase increased the droplet formation frequency without changing the droplet sizes. When the pressure was increased beyond the transition pressure, larger monodisperse droplets were formed (see section 4.2.3 for droplet sizes). Based on the production in previous work (ten Klooster et al., 2022a), the continuous phase flow was set such that the resulting oil concentration of the emulsion was > 10 wt.%. The emulsion was collected in a beaker overnight for the small and intermediate droplets and over 3 h for the large droplets. To prevent lipid oxidation and evaporation of the continuous phase as much as possible, the headspace of the collection beaker was flushed with a continuous flow of water-saturated nitrogen gas during production. Finally, the oil content was adjusted to 10 wt.% by addition of continuous phase after the determination of the triglyceride content (section 4.2.3). The emulsions were incubated directly after production as described below.

Incubation and sample taking
As an oxidation initiator, an equimolar mixture of $FeSO_4$ and EDTA was used, which is relevant for food products that contain (traces of) metal ions (Mei et al., 1998). The mixture was prepared by separately dissolving 12 mM $FeSO_4$ and EDTA in a phosphate buffer (pH 7.0, 10 mM). Equivalent volumes of each solution were mixed, and the iron-EDTA complex was allowed to form under moderate stirring in the dark for exactly 1 h.

To 1.5 mL polypropylene tubes (total volume ~ 1.75 mL), either 387.5 µL of emulsion or 387.5 µL of 2-wt.% Tween 20 solution and 12.5 µL of the iron-EDTA complex solution were added. The samples were incubated, in the dark, in heating blocks, at 25 °C, and shaken at 800 rpm to prevent creaming. Samples were taken at carefully selected time points based on the remaining oxygen content in the headspace (section 4.2.4). The samples were covered with a

nitrogen blanket and stored at −80 °C for 48 h to two weeks, before further extraction and lipid oxidation analyses were performed.

4.2.3 Emulsion characterisation

Triglyceride content

The triglyceride (TAG) content was measured using a colorimetric method (Jacobs et al., 1960; Trinder, 1969). In brief, the emulsions were diluted with 2 wt.% Tween 20 to a range of 0.5-4 g oil/L. Next, the droplets were broken up in smaller droplets by sonication with the Branson Sonifier SFX550 (Brookfield, CT, USA), equipped with a 1/8 inch tapered microtip (Branson, Brookfield, CT, USA), at an amplitude of 35% for 15 s. This was done to increase the oil-water interface for effective hydrolysis of triglycerides and thereby to obtain accurate results. The droplet size distribution of the broken droplets was independent of the initial droplet size as shown in the appendix of Chapter 3 (ten Klooster et al., 2022a). Next, about 20 µL of sample were weighed into a 2-mL microtube, and 1 mL of assay reagent was added. The samples were incubated in a heating block, in the dark, and shaken at 800 rpm, at 20 °C, for 20 minutes. The absorbance was measured at a wavelength of 500 nm. The TAG content was determined using a calibration curve of a standard TAG dispersion (0.5-4 g oil/L).

Droplet size

A small volume (3 µL) of sample was taken from the emulsions and observed using a Carl Zeiss Axioscope A1 optical microscope (Carl Zeiss, Breda, the Netherlands) equipped with a camera (AxioCam Mrc5). The droplet size of at least 190 droplets per independently prepared emulsion was measured using a custom-written script in Matlab R2019b (Mathworks, Natick, MA, USA), which is sufficient when droplets are very monodisperse (Deng et al., 2021). The droplet size was expressed as the droplet diameter and was calculated from the droplet circumference. Since the droplet volume scales with the droplet diameter to the power 3, a small systematic error leads to a much larger error in the productivity; therefore, as a check, the centre-to-centre distance of clustered droplets was determined, and with that a correction factor was calculated. This method was shown to be effective in previous work (ten Klooster et al., 2022a).

Unadsorbed surfactant concentration

The amount of excess Tween 20 present in the continuous phase was estimated using a procedure that was based on previous work (Berton-Carabin et al., 2014): first, the number of droplets (N) with a certain droplet radius (r, m) was calculated per kg of oil:

$$N = \frac{1}{\rho_{oil}} \cdot \frac{1}{\frac{4}{3}\pi r^3} \quad (4.1)$$

where ρ_{oil} is the density of the oil (920 kg/m^3). The amount of adsorbed surfactant (S_{ad}, in g per kg oil) was calculated using Equation 4.2:

$$S_{ad} = \frac{N\ 4\ \pi\ r^2\ \Gamma}{1000} \quad (4.2)$$

where Γ (mg/m^2) is the specific adsorbed amount of surfactant at the oil-water interface. Different values for Γ are reported in literature, and we used a relatively high value of 2.3 mg/m^2, which was chosen to estimate what the maximum amount of adsorbed surfactant could be (Berton-Carabin et al., 2014; Berton et al., 2011a). Finally, the excess concentration of Tween 20 in the continuous phase (C_{excess}, g/L) was calculated by:

$$C_{excess} = C_{added} - S_{ad}\ \cdot \phi_{oil}\ \cdot\ \rho_{cont} \quad (4.3)$$

where C_{added} is the concentration of surfactant in the continuous phase (in g/L), ϕ_{oil} the mass ratio of oil to continuous phase (10/90 = 0.111), and ρ_{cont} the continuous phase density, which was assumed to be 1.0 kg/L.

4.2.4 Oxidation experiments

Oxygen measurement

The headspace oxygen content was monitored with a MOCON OpTech-O2 oxygen sensor (Ametek Mocon, Brooklyn Park, MN, USA). The initial amount of total available oxygen was calculated using a 1.35-mL headspace volume with 20.9 % O_2, 46.8 mg/kg oxygen concentration in the oil (Cuvelier et al., 2017), and 8.1 mg/kg oxygen concentration in the continuous phase (Truesdale et al., 1955). The oxygen content was determined in four samples per independently prepared emulsions. Each sample was measured twice daily with three technical replicates, i.e. 12 measurements per timepoint per emulsion.

Oil extraction

The oil was extracted by adding 2.75 mL of 3:1 v/v hexane-isopropanol solvent mixture to 0.4 mL of emulsion (Waraho et al., 2011a). The mixture was thoroughly vortexed and centrifuged (5000×*g*, 20 °C, 20 min), and the upper layer, containing the hexane and extracted lipids, was carefully separated from the bottom layer. The hexane was evaporated under a stream of nitrogen at 25 °C until constant weight, and the remaining oil was frozen at −80 °C and stored for 48 h to three weeks before further measurements were performed.

Lipid oxidation measurements by 1H NMR

Lipid hydroperoxides (primary oxidation products), aldehydes (secondary

oxidation products), and epoxides (secondary oxidation products) were quantified simultaneously by NMR spectroscopy, as previously described (Merkx et al., 2018). In brief, around 570 µL 5:1 $CDCl_3$/DMSO-d_6 were added to a total of 30 µL extracted oil (section above) and transferred to 5-mm NMR tubes (Bruker, Billerica, MA, USA). Samples were measured on an Advance III 600 MHz spectrometer (Bruker BioSpin, Switzerland) equipped with a 5-mm cryo-probe at 295 K. Lipid hydroperoxides and aldehydes were quantified on a molecular substructure level as previously described using a single pulse and a band selective ^{1}H NMR experiment (Merkx et al., 2018).

Epoxides were quantified using ^{1}H-^{13}C heteronuclear single quantum coherence (HSQC) NMR spectroscopy, which was based on previous work (Boerkamp et al., 2022). Here, the protocol was modified to improve the spectral resolution. 2D ^{1}H-^{13}C HSQC spectra with a band-selective ^{13}C REBURB pulse were recorded using the standard "shsqcetgpsisp2.2" Bruker pulse sequence. In the ^{13}C-dimension, a spectral width of 40 ppm with an offset of 58 ppm (δ_C 78 to 38 ppm) was used with 200 increments. In the ^{1}H-dimension, the spectral width was 4 ppm with an off-set of δ 3 ppm (δ_H 5 to 1 ppm) with 1024 increments. Eight scans were collected by using a recycle delay of 0.5 s. For the ^{13}C-dimension, zero-filling up to 1024 points was applied prior to Fourier transformation. The squared cosine (SSB 2) and Gaussian (LB -0.2 Hz, GB 5 Hz) window functions were used for the ^{13}C and ^{1}H-dimensions, respectively. The same phasing was used for all samples. Baseline correction was performed automatically, and the upfield TG backbone peak was calibrated to δ_H 4.13 ppm and δ_C 61.9 ppm. The quantification of epoxides was based on automatic integration of predefined regions as previously reported (Boerkamp et al., 2022).

The spectral processing and integrations for the hydroperoxides, aldehydes, and epoxides was automatically done using MestReNova v14.1 (Mestrelab Research, S.L., Santiago de Compostela, Spain).

4.2.5 Kinetic modelling

The data of lipid oxidation products formed, and oxygen consumed in time were compared with a recently developed kinetic model (Schroën et al., 2022a). This model was used previously to describe lipid oxidation for emulsions that were stabilised by different emulsifiers (Berton et al., 2011b). For the data presented in this chapter, the model was extended to incorporate oxidation of Tween 20, and oxygen diffusion into the tubes. Additional information about the model and how it was used to describe experimental data is described in the appendix (section 4.5.1).

4.2.6 Experimental design

Two emulsions were prepared independently for each droplet size (in total six emulsions). Per timepoint, two aliquots of emulsion were taken, lipids were extracted, and lipid oxidation product were quantified on each aliquot individually. The headspace oxygen concentration was measured as described earlier.

4.3 Results and discussion

4.3.1 Emulsion production

Monodisperse emulsions (10 wt.% oil in 2 wt.% Tween 20) were gently produced with UPE microfluidic emulsification devices. More information can be found in recent publications (ten Klooster et al., 2019, 2022a, 2022c).

Three emulsions were produced in duplicate for the present study. The emulsions with small droplets had an average droplet size of 4.5 and 4.8 μm (coefficient of variation (CV): 7.3 and 6.6%); the emulsions with intermediate droplets had an average droplet size 8.9 and 9.3 μm (CV: 10.8 and 7.8%); the emulsions with large droplets had an average droplet size of 25 and 27 μm (CV: 5.8 and 12%), for the small, intermediate and large droplets, respectively (Figure 4.1, A4.2, & A4.3). The difference in diameter between the smallest and largest droplets was a factor six. The amount of interfacial Tween 20 was estimated to be minor (< 2% of the total Tween 20 used), implying that ~ 98% of the used surfactant remained in excess in the continuous phase (Table A4.1) for all emulsions (Berton-Carabin et al., 2014; Berton et al., 2011b). After emulsification, the hydroperoxide concentration was 1.0 ± 0.4 mmol/kg oil, with no significant difference between the different droplet sizes.

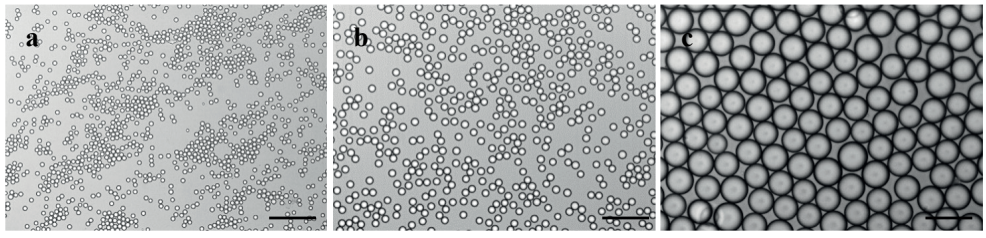

Figure 4.1. Light microscopy images of rapeseed oil droplets in a continuous phase containing 2 wt.% Tween 20, which were prepared with microfluidics. Three different droplet sizes were prepared: small ($D_{1,0}$ = 4.7 μm) (a), intermediate ($D_{1,0}$ = 9.1 μm) (b), and large ($D_{1,0}$ = 26.0 μm) droplets (c). Droplet size distributions are shown in Figure A4.2. Light microscopy images of replicate emulsions are shown in Figure A4.3. Scale bar represents 50 μm.

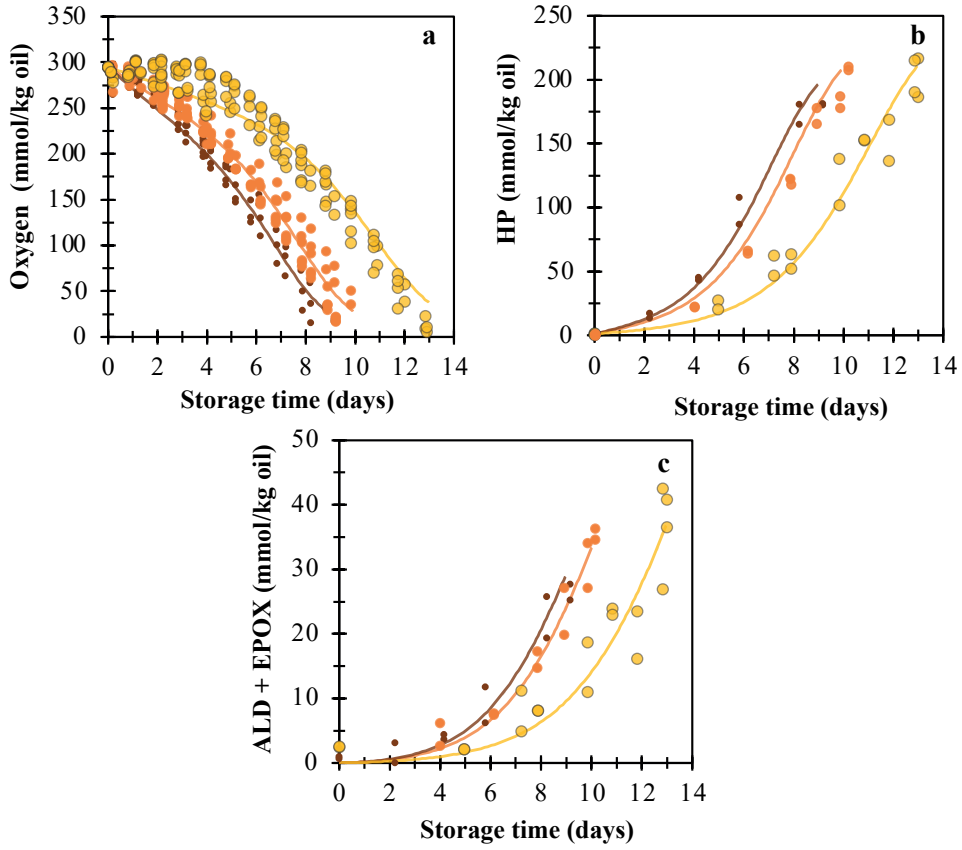

Figure 4.2. Oxygen consumption (a), lipid hydroperoxide formation (b), and secondary oxidation product formation (c) upon incubation of the emulsions. Symbols correspond to emulsions with different droplet sizes: small droplets ($D_{1,0}$ = 4.7 µm) (small, brown circles), intermediate droplets ($D_{1,0}$ = 9.1 µm) (intermediate, orange circles), and large droplets ($D_{1,0}$ = 26.0 µm) (yellow, large circles). The lines are drawn to guide the eye based on the model by (Schroën et al., 2022a) (section 4.2.5 & 4.5.1). Both dependent and independent replicates are shown as individual data points.

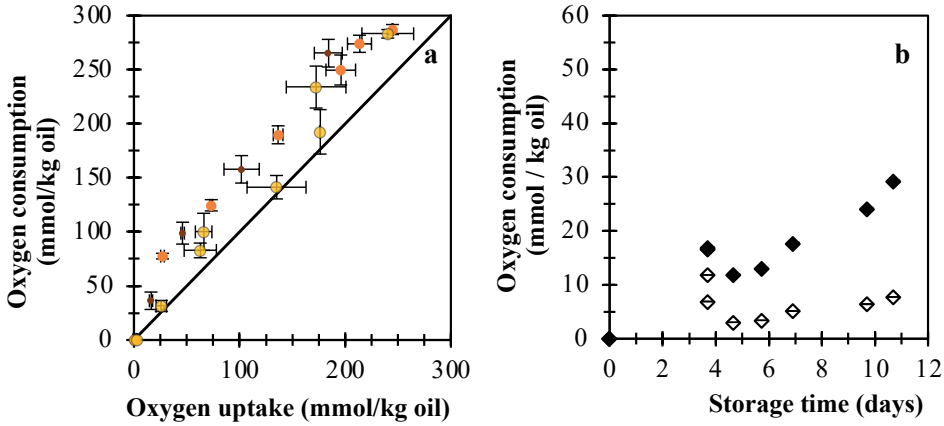

Figure 4.3. (a) Oxygen consumption against oxygen uptake by the formation of lipid oxidation products for emulsions with small droplets ($D_{1,0}$ = 4.7 µm) (small, brown circles), intermediate droplets ($D_{1,0}$ = 9.1 µm) (intermediate, orange, circles), and large droplets ($D_{1,0}$ = 26.0 µm) (yellow, large circles). Oxygen consumption was determined from the oxygen content in the headspace, whereas oxygen uptake was calculated from the detected oxygen-bearing lipid oxidation products (hydroperoxides, aldehydes, and epoxides). The solid line is the line of parity: y = x, and it represents oxygen consumption equals oxygen uptake. (b) Oxygen consumption by a 2-wt.% Tween 20 solution (open diamonds) and by a 2-wt.% Tween 20 solution with 0.19 mM iron-EDTA (filled diamonds). To be consistent with the emulsion systems, the oxygen consumption by Tween 20 is expressed as if there was 10 wt.% of stripped rapeseed oil present. Error bars (sometimes within markers) denote standard deviations of three measurements on three individually incubated samples.

4.3.2 Lipid oxidation in droplets of different sizes

The monodisperse emulsions were incubated at 25 °C in the presence of an iron-EDTA initiator to accelerate lipid oxidation. Under these incubation conditions, samples were physically stable over two weeks (Figure A4.4). Over incubation, all emulsion samples consumed almost all available oxygen in the headspace, and they reached high levels of lipid oxidation products (Figure 4.2a-c). Oxygen consumption and hydroperoxide formation increased with decreasing droplet size (Figure 4.2a & b). In line with that, aldehyde and epoxide formation increased with decreasing droplet size (Figure 4.2c). The ratio of oxidation products from oleic, linoleic, and linolenic acid was independent of the droplet size (Figure A4.5).

Especially at the beginning of incubation, hydroperoxide formation was more rapid for the small droplets compared to the intermediate and large droplets. This result may be ascribed to the increased specific interfacial area that favours contact between the prooxidants in the aqueous phase and the lipid substrate. Hydroperoxide decomposition results in peroxyl and alkoxyl

radicals (Reactions 4.I & 4.II), which can propagate the lipid oxidation reaction (Reaction 4.IV & 4.V). At later stages (few days), the reaction rate was less influenced by the droplet size (Figure 4.2), which could be caused by the limited remaining oxygen impeding further hydroperoxide formation (Reaction 4.V). Similar observations, especially regarding a faster onset of lipid oxidation for small droplets, were previously obtained for fish oil-enriched mayonnaise (Jacobsen et al., 2000). The formation of secondary oxidation products was only moderately faster in the small droplets compared to the intermediate and large droplets. This is most probably the result of the higher hydroperoxide concentration in the emulsion with small droplets, which will increase aldehyde and epoxide formation (Reaction 4.II), rather than effects related to interfacial area. Comparable observations were previously obtained in a modelling study, where the reaction rate constant for aldehyde formation was similar for emulsions that were stabilised by different emulsifiers (Schroën et al., 2022a).

$$LOOH + Fe^{3+} \rightarrow LOO^{\bullet} + H^{+} + Fe^{2+} \quad (4.I)$$

$$LOOH + Fe^{2+} \rightarrow LO^{\bullet} + OH^{-} + Fe^{3+} \quad (4.II)$$

$$LOOH\ (heat/light) \rightarrow LO^{\bullet} + OH^{\bullet} \quad (4.III)$$

$$LO^{\bullet}/LOO^{\bullet} + LH \rightarrow LOH/LOOH + L^{\bullet} \quad (4.IV)$$

$$L^{\bullet} + O_2 \rightarrow LOO^{\bullet} \quad (4.V)$$

$$LOO^{\bullet} + LOO^{\bullet} \rightarrow nonradical\ products \quad (4.VI)$$

4.3.3 Additional effects

We found that the molar amount of oxygen consumed in the headspace exceeded the molar amount of oxygen incorporated as lipid oxidation products (Figure 4.3a), which implies that additional effects take place. This was unexpected, since a closed oxygen balance was previously successfully found for the oxidation of mayonnaise and bulk oil, where the exact same methods to quantify the oxygen consumption and lipid oxidation products were used, as we used here (Boerkamp et al., 2022). The discrepancy that we found in our emulsions might be caused by Tween 20 oxidation (Kerwin, 2008; Nuchi et al., 2001). We incubated the continuous phase without oil (i.e., 2 wt.% Tween 20 with or without 0.19 mM iron-EDTA) and observed an oxygen consumption of 30 mmol (per kg equivalent oil) over 11 days (Figure 4.3b). This was lower than the differences shown in figure 4.3a (maximum difference was ~ 75 mmol O_2/ kg oil), which could suggest that Tween 20 oxidised faster – and to a higher extent – in an oxidising emulsion than when incubated separately. The rationale

behind this could be that relatively high concentrations of radicals were present in oxidising emulsions compared to the Tween 20 solution. Such radicals have been shown to not just abstract hydrogen atoms from other lipids, but also from water (Kim et al., 2014), and possibly they abstract hydrogen atoms from Tween 20 in our emulsions. Once initiated, Tween 20 oxidation might propagate (Reaction 4.IV & 4V). Whether this truly occurs depends on the concentration of the radicals, their diffusion, and their lifetime. Co-oxidation of Tween 20 implies that the lipid substrate has less oxygen available for oxidation, resulting in a decreased formation of lipid hydroperoxides over time. Still, the conclusion that small droplets oxidise faster remains, since oxygen consumption by co-oxidising components was fastest in the emulsions with small droplets (Figure 4.3a) that would have oxidised even faster compared to the large droplets in absence of co-oxidation.

Finally, we also describe another side effect that can play a role, which is diffusion of oxygen into the tubes (Figure A4.6). The oxygen ingress rate depends on the oxygen concentration gradient present (classically described by Fick's law). This does not play a pronounced role early on, but becomes more relevant when the samples have consumed much of the oxygen. We have incorporated the oxygen ingress into the kinetic model based on diffusion rates measured under maximum oxygen gradient (Appendix 4.5.1, Figure A4.6). Also this side-effect did not affect our conclusion that small droplets oxidise faster than large ones because the contribution from oxygen diffusion into the tubes is relatively small, especially at the beginning of incubation, when the effect of droplet size on lipid oxidation rate was most predominant (Figure 4.2).

Please note that effects that occur in concurrence with lipid oxidation may have remained unnoticed in literature, and thus contributed to the confusion in the discussion about the effect of droplet size on lipid oxidation, as discussed in the next section.

4.3.4 Contradicting views from literature put into perspective

In agreement with our results, a number of other studies reported that small droplets oxidise faster than larger ones (Azuma et al., 2009; Gohtani et al., 1999; Horn et al., 2013; Jacobsen et al., 2000; Kuhn et al., 2012; Lethuaut et al., 2002; Li et al., 2019; Ma et al., 2013; Neves et al., 2017; Rampon et al., 2001; Yang et al., 2020) for which multiple hypotheses were suggested. In two of them, the droplet size is just a proxy for the interfacial area that determines the area for (i) influx of oxygen (Ma et al., 2013), (ii) partitioning of emulsifiers and other surface-active molecules (Berton-Carabin et al., 2014), (iii) and reactivity (this

work) (Jacobsen et al., 2000). Hypothesis (i), of a stimulated oxygen diffusion, is unlikely in a continuously mixed system because the diffusion of reactants is much faster in these emulsions than the reaction rate. As shown by Schroën et al., mass transfer greatly exceeds reaction effects when using droplets of up to 100 μm (Damköhler II number 10^{-7}-10^{-5} for droplets of 1 μm) (Schroën et al., 2022a). Hypothesis (ii) can affect lipid oxidation but only when the variation in the amount of interfacial area substantially modifies the concentration of emulsifier present in the continuous phase. An increased amount of such emulsifiers (in particular, proteins) in the continuous phase, promotes their antioxidant effect (Berton et al., 2011b). In our study, the amount of continuous phase Tween 20 was equal for all three emulsions (at least 98% of the Tween 20 was estimated to be unadsorbed) (Table A4.1). In a study by Horn and co-workers, a difference in the amount of unadsorbed emulsifiers could have played a role (Table 4.1) in promoting lipid oxidation for small droplets, compared to large droplets (Horn et al., 2013). (iii) We hypothesise that the faster oxidation of small droplets found in this study is caused by their larger specific interfacial area, which promotes lipid oxidation initiation reactions at the interface.

Other studies have found that larger droplets oxidised faster (Atarés et al., 2012; Azuma et al., 2009; Horn et al., 2013; Let et al., 2007; Nakaya et al., 2005; Neves et al., 2017; O'Dwyer et al., 2013; Ries et al., 2010), or that droplet size did not affect lipid oxidation in emulsions (Atarés et al., 2012; Dimakou et al., 2007; Kiokias et al., 2007; Ma et al., 2013; Osborn et al., 2004; Yang et al., 2020). These contradicting results may have been caused by effects that could obscure the effect of droplet size on lipid oxidation. These effects include, but are probably not limited to: the (i) ratio between prooxidants and interfacial area, (ii) metal-chelating antioxidants, (iii) elevated incubation temperatures, (iv) emulsification method, (v) oil type (vi) (too) small differences in droplet sizes. We will now shortly discuss all these factors.

(i-a) As previously mentioned, we hypothesise that smaller droplets oxidise faster because of the increased contact between the lipids and the prooxidants present in the continuous phase. This is not always expected to be the case: if the ratio of prooxidant to interfacial area is low and if the prooxidants are attracted to the interface (i.e., a negatively charged interface attracts metal cations), then creating more interface is not expected to lead to favoured initiation reactions. (i-b) On the other hand, in systems where initiation of lipid oxidation is very high, termination reactions could possibly become more favoured (Reaction 4.VI), which could obscure any effect of specific interfacial area on the formation of lipid oxidation products. This effect was not expected to be pronounced for

the emulsions that we studied in this chapter.

(ii) As an extension to hypothesis (i), when prooxidants are scavenged by a large excess of metal-binding antioxidants, the initiation of lipid oxidation is not expected to take place at the interface anymore, and non-interfacial-related initiation reactions may become dominant (e.g., Reaction 4.III) (Nakaya et al., 2005).

(iii) If lipid oxidation is initiated at elevated temperature (40-60 °C), Reaction 4.III could start playing a role, which is not related to the specific interfacial area. This also follows from the studies carried out at higher temperature that more often indicate that droplet size does not affect lipid oxidation (or even that larger droplets oxidised faster than smaller droplets) (Table 1).

(iv) If different emulsification methods are used, this can in itself influence lipid oxidation, for example by cavitation, free radical formation will be influenced, and through that the observed formation of lipid oxidation products over time (Berton-Carabin et al., 2014; Serfert et al., 2009). The emulsification method can also alter the interfacial composition (Horn et al., 2013; Let et al., 2007; Sørensen et al., 2007), which has been reported to lead to better oxidative protection for the smaller droplets for specific emulsions (Let et al., 2007; Sørensen et al., 2007). The authors of this work suggested that the interfacial composition is more important than the amount of specific interfacial area (Let et al., 2007). The emulsification procedure also affects the amount of very small droplets (10-200 nm) that are formed (Chapter 5). These very small droplets are hardly detected by standardly used droplet size characterisation methods, but have been shown to be highly reactive. This highlights the importance of prevention of the formation of such droplets, e.g., by using microfluidics.

(v) Finally, an interesting study by Azuma and co-workers showed that with stripped soybean oil, the emulsion with relatively small droplets oxidised faster, whereas with stripped fish oil, the emulsion with relatively large droplets oxidised faster (Azuma et al., 2009). This was ascribed to a different accessibility of the fish oil lipids to prooxidants at the oil-water interface. As can be seen from Table 4.1, in some cases when fish oil was used, indeed the larger droplets oxidised faster (or there was no effect), although there are also studies in which the emulsions with the smaller fish oil droplets oxidised faster (Table 4.1).

(vi) Our results indicate that a large difference in oil droplet sizes is needed to observe an effect of droplet size on lipid oxidation. If the droplet sizes were only

slightly different, as is the case in some studies from literature (Table 4.1), the effect that the specific interfacial area has on lipid oxidation, might be easily obscured by additional effects as described above.

In order to truly differentiate effects, preparation of defined reaction systems is needed. Only due to the highly monodisperse emulsions prepared in this study we could untaintedly observe the effect of droplet size on lipid oxidation.

4.4 Conclusions

We systematically studied the effect of droplet size on lipid oxidation in Tween 20-stabilised monodisperse O/W emulsions, which were prepared with microfluidic emulsification devices. The increased oxidation of smaller droplets was ascribed to their larger amount of oil-water interface, where lipid oxidation was initiated by an iron-based oxidation catalyst. The fast lipid oxidation for small droplets also favoured Tween 20 oxidation. This could be a result of higher concentrations of radicals in small droplets, which may not just propagate lipid oxidation within the droplets, but also Tween 20 oxidation at the interface and possibly even in the continuous phase of the emulsion. These insights show the importance of controlled droplet size to improve our insights in the oxidative stability of emulsion products and, ultimately, to prepare emulsion products with higher oxidative stability.

Table 4.1. Abbreviations: S = small droplets, M = medium/intermediate droplets, L = large droplets, Sp. = stripped, DHA=Docosahexaenoic acid, BN=brominated, WP(I)(C) = whey protein (isolate) (concentrate), PG = polyglycerol, SG = sugar, ML-750 = decaglycerol monolaurate, (Na)Cas = (sodium) caseinate, B-LG = β-lactoglobulin, DG MS = decaglycerin monostearate, TP = tocopherol, SA = Sodium azide, ME=membrane emulsification, RS = Rotor stator, HP = high pressure, '?' means unknown how the weighting for the average droplet size was done. If a emulsion preparation method is stated in brackets, then this method was, or was not, used to make the large and small droplets. If a component is in brackets, than this means that the effect of droplet size on lipid oxidation was performed studied with and without this component.

Article	Oxidation rate	Oil (% of emulsion)	Emulsifier (wt.% of continuous phase)	Other components (wt.% of emulsion)	T (°C)	Method(s)	Droplet sizes (µm)
(Li et al., 2019)	S>L	0.15% Sp. Soybean, 0.05% BN oil	0.14% SDS	0.1% Xanthan	37	RS	2-8, >20
(Gohtani et al., 1999)	S>L	?% DHA	1% DG MS	0.5% Xanthan	25	ME	*D*? 3.4, 6.4
(Lethuaut et al., 2002)	S>M>L	28% Sp. sunflower oil	2% BSA	0.04% SA	47	RS (& HP)	*D*[3,2] 0.4, 1.2, 8.3
(Jacobsen et al., 2000)	S>M>L	16% fish oil, 64% rapeseed oil	20% Egg yolk	Mayo system	37	Combinator (& viscorotor)	*D*[3,2] 2.5, 3.2, 3.3
(Rampon et al., 2001)	S>L	28% Sp. sunflower oil	2% BSA	0.04% SA	37 / 47	RS & HP	*D*[3,2] 0.36, 1.2
(Kuhn et al., 2012)	S>M1=M2>L	27% flaxseed oil	5% WPI	0.02% SA	25	RS & HP	*D*[4,3] Between 0.46 -2.2
(Ma et al., 2013)	S>M>L	1% Methyl α-linolenate	0.15% ML750	0.01% SA	55	RS & ME	*D*[3,2] 1.4, 2.8, 7.4, 31
(Azuma et al., 2009)	S>M>L	0.5% Sp. Soybean oil	0.2% PG / SG FA ester	3 mM AAPH + 20 µM Fe2+	37	MF	*D*? 6.4, 11, 38
(Neves et al., 2017)	S>L	9.2% Fish oil	1% ML750	0.02% SA	5	ME / MF	*D*[3,2] 26.8, 1.2
(Yang et al., 2020)	S>M>L	78% Sp. soybean oil	23% Egg yolk	Mayo system	30	RS	1-4
(Horn et al., 2013)	S>L	10% Fish oil	1% WPI	0.02% SA	20	RS & HP	*D*[3,2] 0.26, 0.71
(Horn et al., 2013)	L>S	10% Fish oil	1% NaCas + B-lac	0.05% SA	20	RS & HP	*D*[3,2] 0.36, 0.55
(Let et al., 2007)	L>M>S	0.5% Fish oil	Cas + WP	-	-	RS & HP	*D*[3,2] 0.70, 0.89, 1.3
(Azuma et al., 2009)	L>M>S	0.5% Sp. Fish oil	0.2% PG FA ester / SG FA ester	3 mM AAPH + 20 µM Fe2+	37	MF	D? 7, 11, 38
(Atarés et al., 2012)	L>S	18% Sp. sunflower oil	1.5% WPI	-	50	RS (& HP)	*D*[3,2] 1.1, 51
(O'Dwyer et al., 2013)	L>S	20% Camelina oil	3% NaCas	0.02% SA	60	HP	*D*? 0.19, 0.29

(Ries et al., 2010)	L>S	10.6% Linoleic acid	0.5, 1, 2, 3, 4, 7, 9.5% WPI / NaCas	0.02% SA	50	RS (& HP)	*D*[3,2] 0.31, 0.65
(Nakaya et al., 2005)	L>M>S	10% Sp. (silica) Soybean / fish oil	0.9% SG lauryl ester / ML750	100 µM EDTA	40	ME / MF	*D*? ~0.8, ~3.3, ~10
(Neves et al., 2017)	L>M=S	9.2% Fish oil	1% ML750	0.02% SA	30	HP	*D*[3,2] 0.09, 0.28, 0.59
(Neves et al., 2017)	L>S	9.2% Fish oil	1% ML750	0.02% SA	30	ME / MF	*D*[3,2] 27, 1.2
(Neves et al., 2017)	L=M=S	9.2% Fish oil	1% ML750	0.02% SA	5	HP	[*D*3,2] 0.09, 0.28, 0.59
(Yang et al., 2020)	S=M=L	78% (Sp.) soybean oil	23% Egg yolk	Mayo system (+ascorbic acid)	30	RS	1-4
(Atarés et al., 2012)	S=L	18% (Sp.) sunflower oil	1.5% WPI	(1 mM Rutin)	50	RS (& HP)	*D*[3,2] ~1, ~50
(Dimakou et al., 2007)	S=M=L	30% Sunflower oil	1% NaCas / Tween 20 / NaCas + Tween 20	-	60	RS & HP	*D*[3,2] 0.67, 0.84, 1.4, 3.2
(Kiokias et al., 2007)	S=M=L	30% Sunflower oil	3% WPC	0.2% SA	35	RS & HP	*D*[3,2] 0.51, 0.63, 1.2, 1.5, 1.9
(Ma et al., 2013)	S=M=L	Methyl linoleate	ML750 (0.15% w/v)	0.01% SA	55	ME	*D*[3,2] 1.5, 2.6, 6.5, 20, 29
(Osborn et al., 2004)	S=L	10/30% Canola oil / caprylic acid	0.5% WPI / SG ester	0.01% SA	50	HP	*D*[3,2] (0.26 & 1.1), (1.5 & 1.1)
(Kuhn et al., 2012)	S>M1=M2>L	27% flaxseed oil	5% WPI	0.02% SA	25	RS & HP	D[4,3] Between 0.46 -2.2
(Costa et al., 2020)	S=L	10% sp. Fish oil	0.5% Tween 80	(0.002% gallic acid)	25 / 35	RS (&HP)	*D*? ± 0.075, ± 0.3

4.5 Appendix

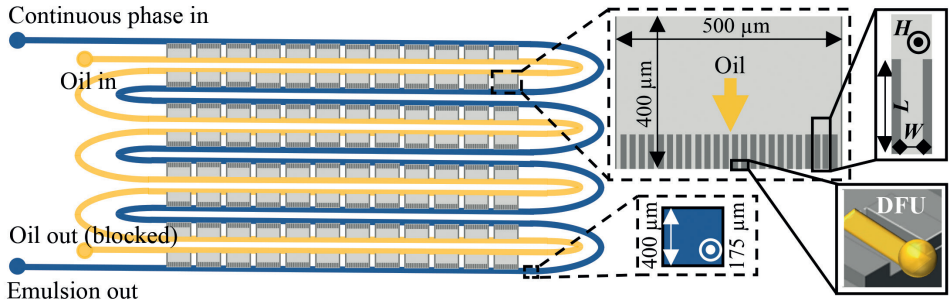

Figure A4.1. Top-view design of the Upscaled Partitioned EDGE chips used in this research. The blue 'twisted road' channel is the continuous phase channel, and the yellow 'twisted road' channel is the to-be-dispersed phase channel. The grey rectangular areas in between these channels are the main plateaus that contain the micro-plateaus with the Droplet Formation Units (DFU). A 3D representation of a DFU is shown in the right lower corner, showing oil – in yellow –, being pushed out of the DFU and forming a droplet ready to detach. This illustration is not to scale, only 12 out of the 42 main plateaus are shown per row.

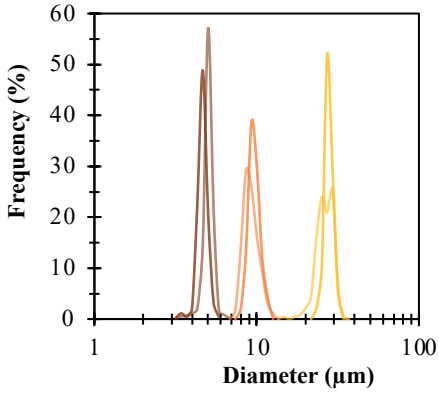

Figure A4.2. Droplet size distributions (volume-based frequency as a function of droplet size) of the six independently prepared emulsions. From left to right, the small (brow), intermediate (orange), and large (yellow) droplets.

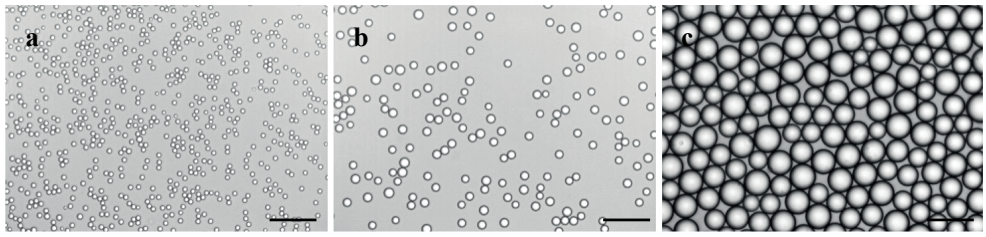

Figure A4.3. Light microscopy images of the rapeseed oil droplets in a continuous phase containing 2 wt.% Tween 20, which were prepared with microfluidics. Three different droplet sizes were prepared: small (a), intermediate (b), and large droplets (c). Droplet size distributions are shown in Figure A2. Light microscopy images of the other replicate emulsions are shown in Figure 4.1.

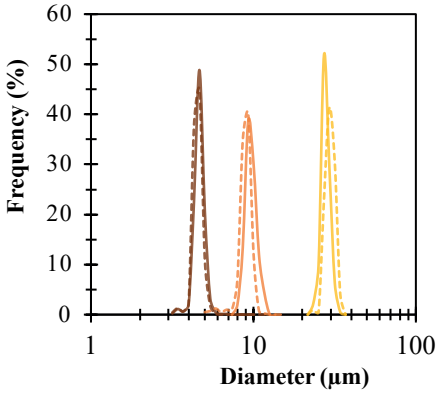

Figure A4.4. Droplet size distributions (volume-based frequency as a function of droplet size) directly after emulsification (solid lines) and after > 7 days of incubation (dashed lines). From left to right, the small (brown), intermediate (orange), and large (yellow) droplets.

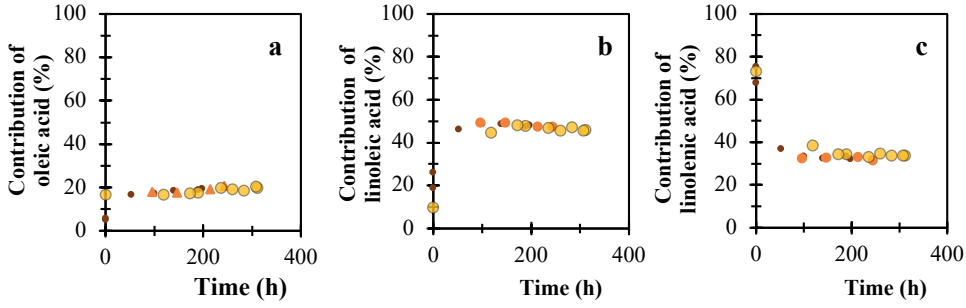

Figure A4.5. The contribution of different unsaturated fatty acid substrates to the total amount of oxidised products: oleate (a), linoleate (b), and linolenate(c). All oxidation products (lipid hydroperoxides, aldehydes, and epoxides) were summed for each fatty acid individually and divided by the total sum of oxidation products. Symbols correspond to emulsions with different droplet sizes: small droplets ($D_{1,0}$ = 4.7 µm) (small, brown circles), intermediate droplets ($D_{1,0}$ = 9.1 µm) (intermediate, orange, circles), and large droplets ($D_{1,0}$ = 26.0 µm) (yellow, large circles).

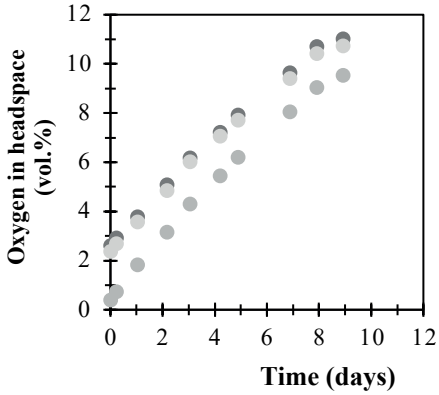

Figure A4.6. Oxygen (vol.%) in the headspace over incubation of 1.5-mL microcentrifuge tubes containing 400 µL of ultrapure water, which were flushed with nitrogen prior to incubation. The incubation was performed in the same way as for emulsion samples (section 4.2.2 'Incubation and sample taking'). Different coloured markers represent independently incubated tubes.

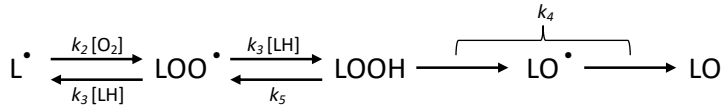

Figure A4.7. Overview of reactions incorporated in the model (Schroën et al., 2022a): L• is a carbon radical, LOO• peroxyl radical, LOOH hydroperoxide (primary oxidation product), LO• alkoxy radical, LO secondary oxidation products, and O_2 oxygen, which was also measured.

4.5.1 Reaction kinetic model

The lines in Figure 4.2 were related to the following lipid oxidation reactions, as proposed in (Schroën et al., 2022a):

$$LH \rightarrow L^{\bullet} \quad \text{(A4.I)}$$

$$L^{\bullet} + O_2 \rightarrow LOO^{\bullet} \quad \text{(A4.II)}$$

$$LOO^{\bullet} + LH \rightarrow LOOH + L^{\bullet} \quad \text{(A4.III)}$$

$$LOOH \rightarrow LO^{\bullet} \rightarrow LO \quad \text{(A4.IV)}$$

$$LOOH \rightarrow LOO^{\bullet} \quad \text{(A4.V)}$$

Based on these reactions, first order reaction rate equations were derived as presented next, and shown in conjunction in Figure A4.7:

$$\frac{d[L^{\bullet}]}{dt} = k_1 \cdot [LH] - k_2 \cdot [L^{\bullet}] \cdot [O_2] + k_3 \cdot [LOO^{\bullet}] \cdot [LH'] \quad \text{(A4.1)}$$

$$\frac{d[LOO^{\bullet}]}{dt} = k_2 \cdot [L^{\bullet}] \cdot [O_2] - k_3 \cdot [LOO^{\bullet}] \cdot [LH'] + k_5 \cdot [LOOH] \quad \text{(A4.2)}$$

$$\frac{d[\mathrm{LOOH}]}{dt} = k_3 \cdot [\mathrm{LOO^{\bullet}}] \cdot [\mathrm{LH'}] - k_5 \cdot [\mathrm{LOOH}] \quad \text{(A4.3)}$$

$$\frac{d[\mathrm{LO}]}{dt} = k_4 \cdot [\mathrm{LOOH}] \quad \text{(A4.4)}$$

In line with the approach, a rate equation for the oxidation of Tween was added:

$$\frac{d[\mathrm{Tween}]}{dt} = k_{Tween} \cdot [\mathrm{Tween}] \cdot [\mathrm{O_2}] \quad \text{(A4.5)}$$

Finally, for oxygen diffusion, Fick's law was used. The measured diffusion coefficient was 2 mmol/hr at maximum oxygen gradient. When adding this term, the rate equation for oxygen becomes:

$$\frac{d[\mathrm{O_2}]}{dt} = -k_{Tween} \cdot [\mathrm{Tween}] \cdot [\mathrm{O_2}] - k_2 \cdot [\mathrm{L^{\bullet}}] \cdot [\mathrm{O_2}] + ([\mathrm{O_2}]_i - [\mathrm{O_2}]_t) \cdot 0.002 \quad \text{(A4.6)}$$

where $[O_2]_i$ and $[O_2]_t$ are the initial molar concentration of oxygen (0.295 mmol/kg oil) and the molar concentration of oxygen at time point *t*, respectively.

The *k*-values used in the model to describe our data points were kept as close as possible to the ones reported previously because some of the applied conditions were similar: we used the same emulsifier (Tween 20), the same incubation temperature (25 °C), and the same concentration of iron-EDTA (oxidation initiator) in the continuous phase (Berton et al., 2011b; Schroën et al., 2022a). There were also experimental differences that are summarised in Table A4.2. Although it is not clear at the moment of writing what the underlying mechanisms are, we have tried to position the model lines as close as possible to the data points based on visual inspection, varying initial radical concentration ($[L^{\bullet}]_{t0}$), k_4 (secondary oxidation product formation), k_5 (radical formation by hydroperoxides), and introduce k_{Tween}. The values are summarised in Table A4.3.

(1) Starting with the largest droplets, we positioned the lines as close as possible to the data points.
   a. $[L^{\bullet}]$ at t_0 was varied for two reasons: (i) the actual value cannot be measured, although the concentrations are expected to be low, and (ii), previously, it was found that within 1-25 µM the model described the data in similar fashion (Schroën et al., 2022a).
   b. The k_4-value was adjusted because previously the hexanal and propanal concentrations were measured (Schroën et al., 2022a), whereas here the total epoxide and aldehyde content was measured.
   c. The k_5-value was allowed to vary between emulsions. It is a reaction between iron and a lipid hydroperoxide, which is expected to increase

with specific interfacial area (Table A4.2) (Schroën et al., 2022a).

d. The Tween oxidation reaction was included in our model because the weight-based ratio of Tween 20 to oil was ~ 15 times higher than in the experiments for which the original model was derived (Table A4.2) (Berton et al., 2011b; Schroën et al., 2022a). Therefore, Tween 20 oxidation was probably negligible compared to lipid oxidation there. That is not the case in our work, and since Tween 20 has been described to be sensitive to oxidation we included this reaction (Equation A4.5) and derived k_{Tween}-values.

(2) Taking the values obtained for the largest droplets as a starting point, the $[L^{\bullet}]_{t0}$, k_5-value, and k_{Tween}-value were changed to position the model lines as close as possible to the data for both the small- and intermediate droplets (Figure 4.2, Table A4.3). There seems to be a connection between the variation of the parameters and the droplet size, which indicates that the effect of droplet size on lipid oxidation is systematic, which is part of follow up research.

Table A4.1. Calculation of the ratio of interfacial Tween 20 to total Tween 20 for the small droplets ($D_{1,0}$ = 4.7 µm).

Diameter smallest droplets (m)	$4.5 \cdot 10^{-6}$
Volume of oil per L emulsion (L)	0.1
Volume of one droplet (m^3)	$4.8 \cdot 10^{-17}$
Number of droplets	$2.1 \cdot 10^{12}$
Interface one droplet (m^2)	$6.4 \cdot 10^{-11}$
Total interface per L emulsion (m^2)	133
Tween 20 interfacial load (mg/m^2)	2.3
Tween 20 at oil droplets interface per L emulsion (g)	0.2
Tween 20 in emulsion (g/L)	18
Fraction of interfacial Tween 20 (compared to total amount)	1.9%

Table A4.2. Differences in kinetic model parameters between our study and the modelling study (Schroën et al., 2022a) (in which the data from (Berton et al., 2011b) was used).

	Tween 20 emulsion in (Schroën et al., 2022)	**This chapter**
Droplet size (µm)	1.4	4.7, 9.1, 26
Tween 20 in continuous phase (g/L)	~ 0.5	~ 20
Tween 20 in emulsion (wt.%)	0.35	1.8
Oil concentration (wt.%)	30	10
Hydroperoxide content t_0 (mmol/kg oil)	~ 10	1
O_2 content initially available (mmol/kg oil)	158	295
LH' content (mmol/kg oil)	4510	3990
Hydroperoxides measured	Conjugated dienes	Total hydroperoxides
Secondary oxidation products measured	Propanal, hexanal	Total aldehydes and epoxides

Table A4.3. Differences in parameters for the kinetic model between our study and the modelling study (Schroën et al., 2022a) (in which the data from (Berton et al., 2011b) was used). '-' indicates that this parameter was not used.

Parameter	(Schroën et al., 2022)	Small droplets	Intermediate droplets	Large droplets
k_1	-	-	-	-
k_2	19.5	19.5	19.5	19.5
k_3	1.95	1.95	1.95	1.95
k_4	$6.0 \cdot 10^{-3}$	$2.0 \cdot 10^{-3}$	$2.0 \cdot 10^{-3}$	$2.0 \cdot 10^{-3}$
k_5	$3.6 \cdot 10^{-3}$	$3.8 \cdot 10^{-4}$	$3.2 \cdot 10^{-4}$	$2.3 \cdot 10^{-4}$
k_{Tween}	-	$5.5 \cdot 10^{-3}$	$3.8 \cdot 10^{-3}$	$2.2 \cdot 10^{-3}$
$[L^{\cdot}]_{t0}$	$1.0 \cdot 10^{-6}$	$3.2 \cdot 10^{-5}$	$2.6 \cdot 10^{-5}$	$1.0 \cdot 10^{-5}$

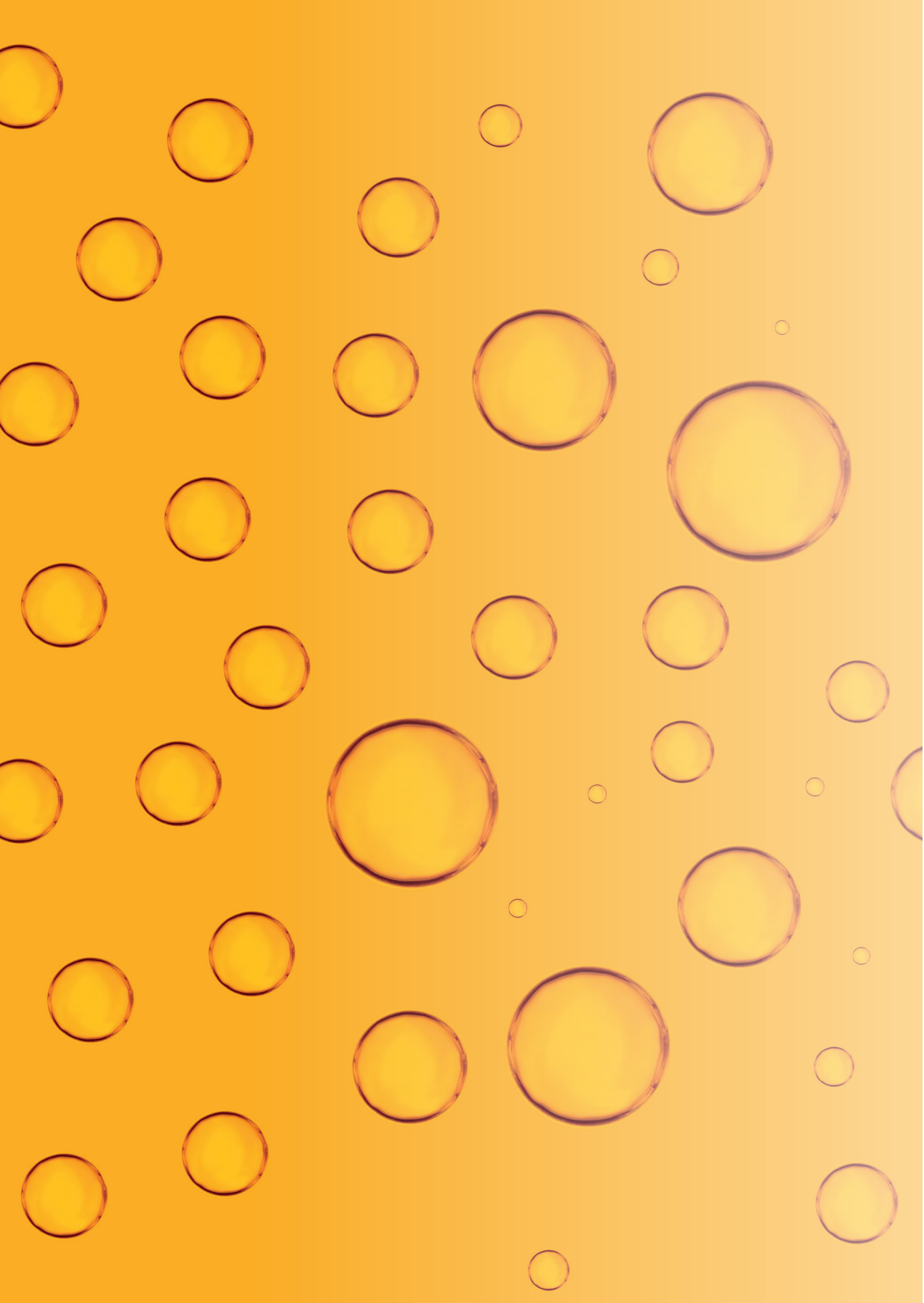

Chapter 5

Tiny, yet impactful: detection and oxidative stability of very small oil droplets in surfactant-stabilised emulsions

This chapter was submitted as:
S. ten Klooster, M. Takeuchi, K. Schroën, R. Tuinier, R. Joosten, H. Friedrich, C. Berton-Carabin: *Tiny, yet impactful: detection and oxidative stability of very small oil droplets in surfactant-stabilised emulsions*

Abstract

The shelf life of multiphase systems, e.g. oil-in-water (O/W) emulsions, is severely limited by physical and/or chemical instabilities, which degrade their texture, macroscopic appearance, sensory and (for edible systems) nutritional quality. One prominent chemical instability is lipid oxidation, which is notoriously complex. The complexity arises from the involvement of many physical structures present at several scales (1–10,000 nm), of which the smallest ones are often overlooked during characterisation.

We used cryogenic transmission electron microscopy (cryo-TEM) to characterise the coexisting colloidal structures at the nanoscale (< 100 nm) in rapeseed oil-based model emulsions stabilised by different concentrations of a nonionic surfactant. We assessed whether the oxidative and physical instabilities of the smallest colloidal structures in such emulsions may be different from those of larger colloidal structures.

By deploying cryo-TEM, we analysed the size of very small oil droplets and of surfactant micelles, which are typically overlooked by dynamic light scattering when larger structures are concomitantly present. Their size and oil content were shown to be stable over incubation, but lipid oxidation products were overrepresented in these very small droplets. These insights highlight the importance of the fraction of “tiny droplets” for the oxidative stability of O/W emulsions.

5.1 Introduction

Oil-in-water (O/W) emulsions can be found in a plethora of industrial products, such as foods, paints, pharma, and cosmetics (Tadros, 2013; Walstra, 2001). These emulsions typically consist of three distinct regions: the core of the oil droplets, the oil-water interface, and the continuous phase, of which the latter often contains a substantial amount of unadsorbed emulsifiers (Berton-Carabin et al., 2014; McClements et al., 2000). Emulsions have a limited shelf life because of physical and/or chemical instabilities (McClements et al., 2000). A prominent phenomenon of chemical instability is lipid oxidation, which is a reaction between oxygen and a labile lipid substrate, such as polyunsaturated fatty acids (PUFAs) (Schaich, 2005). Lipid oxidation leads to: a rancid flavour/odour; possible changes in appearance (e.g., discolouring); or the loss of nutrients and bioactive ingredients (Chen et al., 2013; McClements et al., 2000; Schaich, 2005). The main physical instabilities are: gravitational separation (creaming, sedimentation); coalescence; Ostwald ripening; and flocculation (Leal-Calderon et al., 2007; McClements, 2004). Physical instabilities often lead to a change in texture and/or appearance. These oxidative and physical instabilities are complex, and they are therefore difficult to control. The complexity is caused by the occurrence of the aforementioned phenomena at various time and length scales (Berton-Carabin et al., 2018). Moreover, the physical structure of emulsions affects the oxidative stability and vice versa (Berton-Carabin et al., 2014, 2018).

Emulsions often consist of multiple colloidal structures covering a broad range of sizes, from a few nm to tens of μm (Berton-Carabin et al., 2018). For instance, it is known that small (100–200 nm) and even very small droplets (< 100 nm) can be co-existing with larger ones (Awad et al., 2018). Commonly, three typical systems differing in droplet size are distinguished (Figure 5.1): (i) microemulsions, (ii) nanoemulsions, and (iii) emulsions. We provide a definition for these typical systems in the next lines. (i) In microemulsions or Winsor systems, surfactant micelles (possibly including co-surfactants) contain small amounts of lipids in their hydrophobic core. The curvature of these so-called swollen micelles corresponds to a favourable arrangement of the surfactant molecules, which thereby minimizes the free energy of the system (McClements, 2012). Moreover, the large magnitude of the (configurational) entropy also contributes to the minimisation of the free energy (Vincent, 2010). This results in isotropic and thermodynamically stable systems with droplets of typically 10–50 nm in diameter (Kale et al., 2017). (ii) Nanoemulsions, generally defined as emulsions having droplet sizes below 100 nm, are thermodynamically unstable

(i.e., at most, metastable), which makes them different from microemulsions. A large external energy supply is required for their formation (Kale et al., 2017). (iii) Emulsions, which have droplet sizes above 100 nm, are thermodynamically unstable, and also require an energy input through an *ad hoc* homogenisation procedure. The latter two can be stabilised *kinetically*. In this chapter, we will assess the presence of the structures termed above and intentionally avoid referring to microemulsions, as the term is generally associated to spontaneous emulsification. This is why we will speak about micelles, very small droplets (i.e., swollen micelles and droplets < 100-200 nm) and large droplets, which can all coexist in emulsions encountered in practical systems, such as food matrices (Awad et al., 2018).

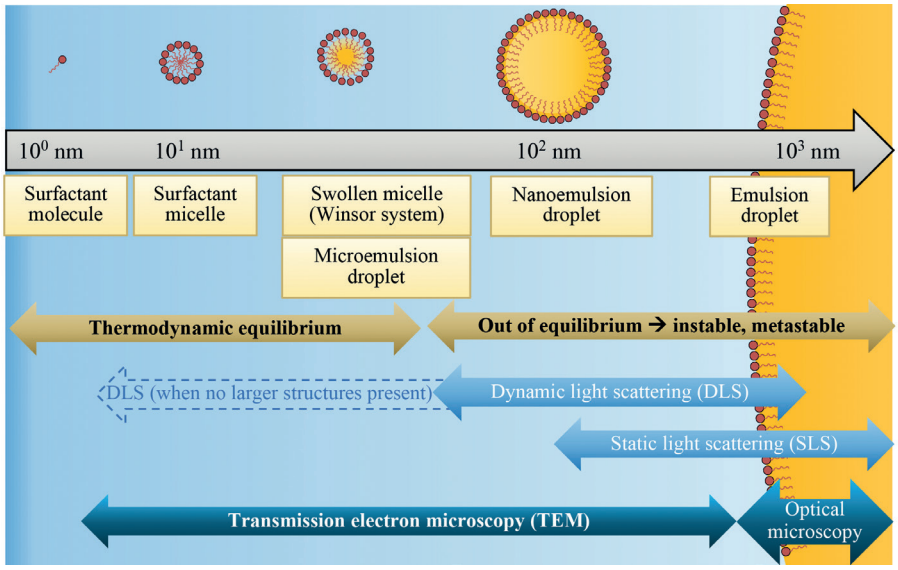

Figure 5.1. Schematics of structures with different sizes that can be present in surfactant-stabilised emulsions. The structures can be distinguished by their terminology and the equipment with which they can be detected.

The effect of the physical structure of emulsions on their oxidative stability has received great interest in literature, but is yet far from being understood (Berton-Carabin et al., 2014; Chen et al., 2011; McClements et al., 2000; Waraho et al., 2011b). For example, small colloidal structures have been postulated to play a decisive role in the lipid oxidation pathways by transferring reactive molecules from one droplet to another (Laguerre et al., 2017, 2020; Villeneuve et al., 2018, 2021), although a recent study from our group has shown that this only occurs for low molar mass and relatively hydrophilic lipid oxidation products (ten Klooster et al., 2022b). Furthermore, as lipid oxidation is presumably initiated

at the oil-water interface, it can be expected to proceed faster if the droplets are smaller due to their larger specific interfacial area (Berton-Carabin et al., 2014). In practice, this effect has not been systematically demonstrated, and contradicting conclusions have been reported (Berton-Carabin et al., 2014). This could be caused by the fact that, when varying homogenisation conditions to alter the interfacial area, other parameters are varied along with that, such as: the amount of emulsifiers present in the continuous phase (Berton-Carabin et al., 2014); the formation of free radicals upon processing (Serfert et al., 2009); and the composition of the oil-water interface (Let et al., 2007; Sørensen et al., 2007). To the best of our knowledge, there are only two studies in which the effect of droplet size on lipid oxidation was studied in one single polydisperse emulsion (Li et al., 2019; Yang et al., 2020), which is advantageous because the continuous phase has the same composition for both size classes. In both studies, lipid oxidation was shown to proceed faster in the small droplets, although the differences were small, and for certain systems no difference was found (Yang et al., 2020).

An important first step to get to an improved understanding of the interrelated physical and oxidative instabilities at play is to characterise the colloidal structures present over the relevant size span. To date, such characterisation is generally conducted by static light scattering (SLS) or dynamic light scattering (DLS). Light scattered by an emulsion scales with the droplet volume squared. Therefore, these techniques are not equipped well to detect very small structures (< 100–200 nm) when they coexist with larger droplets, since the latter largely diminish the contribution of small ones to the measured signal, which scales with the diameter to the power of six (Awad et al., 2018; Patil et al., 2017). The deployment of other characterisation techniques, such as electron microscopy, is therefore needed. Among electron microscopy techniques, cryogenic transmission electron microscopy (cryo-TEM) can be used to gain insights into sub-micrometer structures in liquid emulsions with nm resolution, as samples can be cryogenically fixed and preserved using plunge vitrification (Friedrich et al., 2010).

In this chapter, we characterised the fraction of very small droplets (typically < 200 nm) in rapeseed oil-based model emulsions stabilised by a nonionic surfactant with a versatile range of characterisation techniques: dynamic light scattering (DLS), cryogenic transmission electron microscopy (cryo-TEM), and oil content determination in the relevant fractions. We explored the oxidative and physical stability of this fraction of very small droplets co-present in emulsions and of the emulsions as a whole.

5.2 Materials and methods

5.2.1 Materials

Rapeseed oil was kindly provided by Unilever (Wageningen, Netherlands) and stripped with alumina powder (MP EcoChromet ALUMINA N, Activity: Super I, Biomedicals) to remove impurities and endogenous antioxidants, in particular tocopherols (Berton et al., 2011b). Deuterated chloroform and dimethylsulfoxide ($CDCl_3$ and DMSO-d6) were purchased from Euriso-top (Saint-Aubin, France). n-Hexane and 2-propanol were obtained from Actu-All Chemicals (Oss, the Netherlands). Polysorbate 20 (Tween 20) was purchased from Sigma (Sigma-Aldrich, Zwijndrecht, the Netherlands). Ultrapure water (18.2 MΩ) was used for all experiments and prepared using a Milli-Q system (Millipore Corporation, Billerica, MA, USA). Standard for triacylglycerols and assay reagent (Triglycerides liquicolor mono kit) for a colorimetric quantification method were purchased from HUMAN (HUMAN Gesellschaft für Biochemica und Diagnostica mbH, Wiesbaden, Germany). The assay reagent content was: 50 mmol/L PIPES buffer (pH 7.5), 5 mmol/L 4-chlorophenol, 0.25 mmol/L 4-aminoantipyrine, 4.5 mmol/L magnesium ions, 2 mmol/L ATP, 1.3 U/mL lipases, 0.5 U/mL peroxidase, 0.4 U/mL glycerol kinase and 1.5 U/mL glycerol-3-phosphate oxidase.

5.2.2 Emulsion preparation

Either 0.5 or 2.0 wt.% of Tween 20 were added to 10 mM sodium phosphate buffer (pH=7.0) and stirred for 30 min. For the samples that were used for cryo-TEM analysis and DLS, ultrapure water was used instead of phosphate buffer because the buffer resulted in lower contrast between Tween micelles and the background, and hence this impeded interpretation of cryo-TEM images. Stripped rapeseed oil (10 wt.%) was added to the continuous phase to form a coarse emulsion by high-speed stirring at 11,000 rpm for 1 min with a rotor-stator homogeniser (Ultra-turrax IKA T18 basic, Germany). To produce a somewhat finer emulsion, this coarse emulsion was passed two times through a lab scale colloid mill with gap width of 0.32 mm (IKA Magic Lab, Staufen, Germany), operated for 2 min at 26,000 rpm, and cooled with water at 4 °C. To produce an emulsion with even smaller average droplet size, the coarse emulsion was passed three times through a high-pressure homogeniser (M-110Y Microfluidizer, Microfluidics, Massachusetts, USA) equipped with a F12Y interaction chamber, which was operated at 600 bars and cooled with ice. These emulsions were either incubated, as described below (colloid mill-made emulsions), or used directly for further measurements (all emulsions).

Incubation and sample taking

The 0.5-wt.% Tween 20-based emulsion in buffer made with the colloid mill was incubated as follows: ten milliliters of emulsion were placed into 20-mL headspace vials and incubated at 25 °C while rotating horizontally at 2 rpm in the dark. At selected time points, the content of two headspace vials was pooled into a 50-mL centrifuge tube. Next, 1.5 mL was taken for measurements on the whole emulsion, whereas the rest of the emulsion was centrifuged at 28,000×*g* and 20 °C for 30 min (in duplicate). The phase containing very small droplets (< 200 nm) remained as a subnatant phase below a creamed layer. This subnatant was collected by making a hole at the bottom of the tube. 1.5 mL were taken that were used directly for the physical characterisation measurements. For the extractions and lipid oxidation measurements, the samples were first stored under inert gas at −80 °C for 48 h to 20 days.

5.2.3 Emulsion characterisation

Static light scattering

The oil droplet size (diameter) and size distribution in the emulsions was assessed by static light scattering (SLS) (Malvern Mastersizer 3000, Malvern Instruments Ltd., Malvern, Worcestershire, UK), using a refractive index of 1.47 for the dispersed phase and 1.33 for the dispersant (water); and an absorption index of 0.01.

Dynamic light scattering

The size of the colloidal structures present in the emulsions' subnatant phase (section 5.2.2, 'Incubation and sample taking') was assessed by dynamic light scattering (DLS) (Zetasizer Nano ZS, Malvern Instruments Ltd., Malvern, Worcestershire, UK), using a refractive index of 1.47 for the dispersed phase and 1.33 for the dispersant (water); and an absorption index of 0.01.

Cryogenic transmission electron microscopy

The morphology and size of the colloidal structures present in the emulsions' subnatant phase (section 5.2.2, 'Incubation and sample taking') were measured by cryogenic transmission electron microscopy (cryo-TEM). For cryo-TEM sample preparation, TEM grids with a graphene oxide (GOx) support layer were used during plunge vitrification. This enabled the preparation of mechanically stable TEM samples with a reduced vitrified water layer thickness, which minimizes effects of the embedding medium during imaging, and it enhances the achievable contrast and resolution for nm-sized structures (van de Put et al., 2015). First, the TEM grids were glow-discharged to make the surface of the carbon TEM support film hydrophilic, and 20 µL of GOx aqueous dispersion

were deposited on the top of the TEM grid and dried out. Samples for cryo-TEM were then prepared by applying 3 μL of the emulsion subnatant or of Tween 20 aqueous solution (0.5 wt.%) on the 200 mesh Cu grid with a R2/2 Quantifoil® carbon support film (Quantifoil MicroTools GmbH) covered with graphene oxide (GOx). An automated vitrification robot (Thermo Fisher Scientific Vitrobot™ Mark IV) was used to blot and plunge the samples into liquid ethane. Cryo-TEM imaging was conducted on the TU/e CryoTitan (Thermo Fisher Scientific), which was operated at 300 kV. The TU/e CryoTitan is equipped with a Field-Emission Gun, a post column Gatan Energy Filter (GIF, model 2002), and a post-GIF 2k · 2k Gatan CCD camera (model 794). Cryo-TEM images were acquired at an electron dose rate of 10 e^{-} $Å^{-2}$ s^{-1} with an exposure time of 2 s at a nominal magnification of 24,000×. An in-house Matlab script was used for measuring the diameter of very small droplets from the TEM images (Figure A5.1). For the colloid mill-made emulsion, the total number of small oil droplets analysed for the histogram was 888 (from 14 cryo-TEM images). For the 0.5-wt.% and 2.0-wt.% emulsion prepared with a Microfluidizer, 316 and 448 droplets (from 12 and 7 cryo-images, respectively) were taken for the analysis, respectively.

Oil content determination

The oil content in the subnatant of the centrifuged emulsion samples was quantified using a colorimetric assay for triacylglycerols (Triglycerides Liquicolor Mono kit, HUMAN). In brief, the samples were diluted to a range of 0.4-4 g/L, and about 20 μL of sample were weighed into a 2-mL microtube. Next, 1 mL of assay reagent was added, and the samples were subsequently incubated in a heating block at 800 rpm for 20 minutes at 20 °C. The absorbance was measured at a wavelength of 500 nm, and the concentration was calculated using a calibration curve (0.4-4 g triglycerides/L).

Estimation of unadsorbed surfactant concentration

The amount of excess Tween 20 present in the continuous phase was calculated by the following procedure: first the number of droplets (N, in number per kg oil), with a certain droplet radius (r, in m), were calculated:

$$N = \frac{1}{\rho_{oil}} \Big/ \frac{4}{3}\,\pi\, r^3 \tag{1}$$

where ρ_{oil} is the density of rapeseed oil (920 kg/m^3). The amount of adsorbed surfactant (S_{ad}, in g per kg oil) follows from:

$$S_{ad} = \frac{N\ 4\ \pi\ r^2\ \Gamma}{1000} \tag{2}$$

where Γ (in mg/m^2) is the theoretical mass of adsorbed surfactant per unit of oil-water interface. Since different values for Γ are reported in literature, two different values for Γ were used: 1.5 mg/m^2 (Bos et al., 2001), and 2.3 mg/m^2 (Berton et al., 2011b). Finally, the excess concentration of Tween 20 in the continuous phase (C_{excess}, g/L) can be calculated by:

$$C_{excess} = C_{added} - S_{ad} \quad R_{oil} \quad \rho_{cont} \tag{3}$$

where C_{added} is the concentration of surfactant in the continuous phase (in g/L), R_{oil} the mass ratio of oil to continuous phase (10 / 90 = 0.111) and ρ_{cont} the density of the continuous (aqueous) phase (which is assumed to be 1.0 kg/L here). The amount of adsorbed surfactant was calculated for both the DLS and SLS results (described above), and for each size class, which was weighed by the volume-based presence of that size class. The surface loads obtained from the DLS and SLS results were summed up after weighting them based on the oil content of the subnatant sample (section above); we assume that the oil content of the whole emulsion (SLS result) was one minus that of the subnatant. The average of two measurements (DLS, SLS and oil content) was used for calculating the interfacial area using two independently prepared emulsions per condition.

5.2.4 Lipid oxidation measurements

Lipid extraction

Oil extraction was performed by adding 8 mL hexane-isopropanol (3:1 v/v) to ~ 1.5 mL emulsion and vortexing thoroughly (Waraho et al., 2011a). The mixture was centrifuged at 4,000×g for 20 min and the upper layer, containing the hexane and extracted oil, was carefully separated from the bottom layer. Hexane was evaporated under a stream of nitrogen at 25 °C until constant weight. The remaining oil was stored under inert gas at −80 °C for 48 h to 20 days, before further measurements were performed, which was based on previous research (ten Klooster et al., 2022d).

Lipid oxidation measurements by ^{1}H NMR

Hydroperoxides, aldehydes (primary and secondary oxidation products) and triacylglycerols (reference for total oil amount) were quantified using ^{1}H NMR with an Advance III 600 MHz spectrometer, equipped with a 5 mm cryo-probe at 295 K, following the method described by Merkx *et al*. (2018) (Merkx et al., 2018). In brief, for the whole emulsion samples, 450 µL 5:1 $CDCl_3$/DMSO-d_6 were added to ~ 150 µL extracted oil (as described in 5.2.4) and transferred to 5-mm NMR tubes (Bruker, Billerica, Massachusetts, USA). For the subnatant samples, 580 µL 5:1 $CDCl_3$/DMSO-d_6 were added to ~ 20 µL extracted oil (as described in 5.2.4). From the recorded single pulse experiment, the glycerol

backbone peaks at δ 4.4 pm were used for the quantification of the amount of triacylglycerols. From the band selective pulse the region between δ 13.0 and 8.0 ppm was selectively excited for the quantification of the lipid oxidation products, following Merkx *et al*. (2018) (Merkx et al., 2018). The hydroperoxide signals resonate between δ 11.3 and 10.6 ppm and the aldehydes between δ 9.8 and 9.4 ppm. The calculations, including a factor that accounts for intensity loss during the selective pulse, are described in Merkx *et al.* (2018) (Merkx et al., 2018). The data was processed with Bruker TopSpin 4.0.6 software.

5.2.5 Experimental design

For each measurement, at least two emulsions were prepared independently. Additionally, per data point, two independently incubated samples from the same emulsion were analysed for the performed measurements.

5.3. Results and discussion

5.3.1 Characterisation of Tween 20-stabilised emulsions

The droplet size (diameter) distributions (SLS) of 0.5-wt.% Tween 20-based emulsion prepared with a lab-scale colloid mill and that of 0.5- or 2.0-wt.% Tween 20-based emulsions prepared with a high-pressure homogeniser (Microfluidizer) are shown in Figure 5.2a. As expected, the Microfluidizer produced smaller droplets compared to the colloid mill because of the larger shear rates involved (McClements, 2004; Schroën et al., 2016; Walstra, 1993). For the emulsions prepared with the Microfluidizer, the 2.0-wt.% Tween 20-based emulsion had a slightly smaller average droplet size than the 0.5-wt.% Tween 20-based emulsion. This can be explained by a faster stabilisation of small droplets upon homogenisation when adding a larger amount of surfactant, which could prevent immediate re-coalescence of newly made droplets.

When measuring the droplet size distributions of these whole emulsions by static light scattering (SLS), the diameters of the smallest droplets that could be detected (i.e., at the onset of the peak) were ~ 100 nm for the Microfluidizer-made emulsions and ~ 300 nm for the colloid mill-made emulsion (Figure 5.2a). After centrifugation (28,000×*g*, 30 min) to remove the largest droplets (creamed phase), smaller colloidal structures in the range of 10–200 nm were detected in the subnatant when analysed by dynamic light scattering (DLS) (Figure 5.2b). These small colloidal structures are most likely a heterogenous population consisting of a mixture of ‘swollen micelles’ and ‘nanoemulsion’ droplets, following the terminology defined in section 5.1.

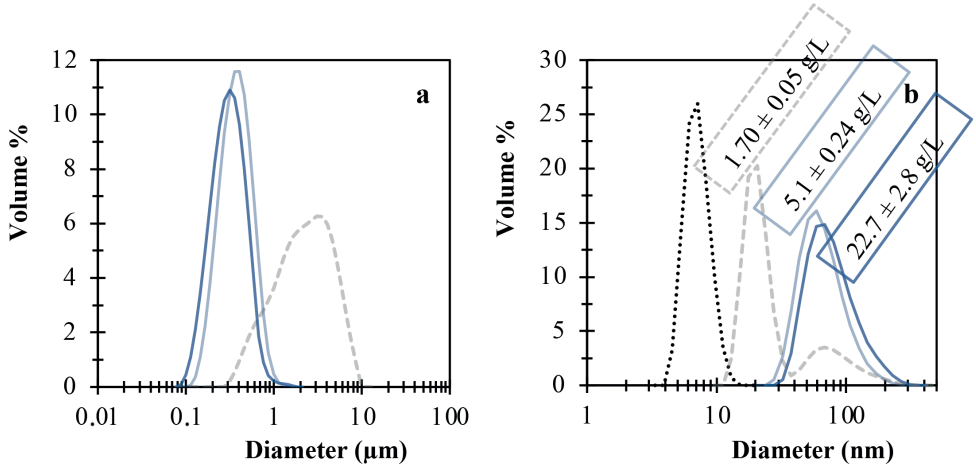

Figure 5.2. The droplet size distributions of: whole emulsion samples measured by SLS (a) and subnatants of centrifuged emulsion samples measured by DLS (b). Different curves represent different emulsion samples: 0.5-wt.% Tween 20 solution as a control (dotted curve, black, only for (b)), 0.5-wt.% Tween 20-based Microfluidizer emulsion (solid curve, light blue), 2.0-wt.% Tween 20-based Microfluidizer emulsion (solid curve, dark blue), and 0.5-wt.% Tween 20-based colloid mill emulsion (dashed curve, grey). The numbers in (b) indicate the triglyceride content of the subnatant samples in g/L (whole emulsion contained 100 g/L triglycerides). The curves and numbers represent averages of two independently prepared samples that were both measured twice.

The droplet size distribution of these 'very small' droplets in the 0.5-wt.% Tween 20-based emulsion made with the colloid mill was bimodal, and it shows a high peak around 20 nm and a lower peak around 80 nm. Surprisingly, from the DLS results, the average diameter of structures present in the subnatant of the 0.5-wt.% Tween 20-based emulsion made with the colloid mill seemed to be smaller than the 0.5-wt.% and 2.0-wt.% Tween 20-based emulsions made with the Microfluidizer. The intensity of light scattered (I_{scat}) by colloidal particles scales as $I_{scat} \sim d^6$, with d the droplet diameter. Moreover, in DLS, the z-averaged size is measured: the d_{65} is highly sensitive to the largest colloids present (Dhont, 1996). At this stage, it is important to recall that DLS is known to be an inappropriate method for the analysis of polydisperse emulsions, since it is highly sensitive to: larger colloids/particles, at the expense of smaller co-existing ones (Awad et al., 2018; Patil et al., 2017); contaminant particles (Ruf, 2002); and issues regarding matching the optical settings with the scattering by the droplets (Awad et al., 2018; Pal et al., 2011).

Cryo-TEM was employed as an alternative strategy to measure the droplet size distributions in the subnatants. Oil droplets appear as dark round objects with diameters of 10–100 nm in the cryo-TEM images of subnatants obtained from

a colloid mill-made emulsion (Figure 5.3a) or from a Microfluidizer-made one (Figure 5.3b & c). The size distributions obtained from image analysis of the cryo-TEM images (Figure 5.4, histograms) are compared with the number-weighted results from DLS (Figure 5.4, superimposed solid curves). The cryo-TEM results proved the presence of very small structures with diameters of 10–30 nm (which most likely correspond to swollen micelles) in the subnatants of Tween 20-based emulsions prepared with a Microfluidizer (for both Tween 20 concentrations) (Figure 5.4b & c), which were not detected by DLS. This highlights the importance of cryo-TEM to assess the presence and size of the tiniest oil containing structures within polydisperse samples, which may be missed by DLS.

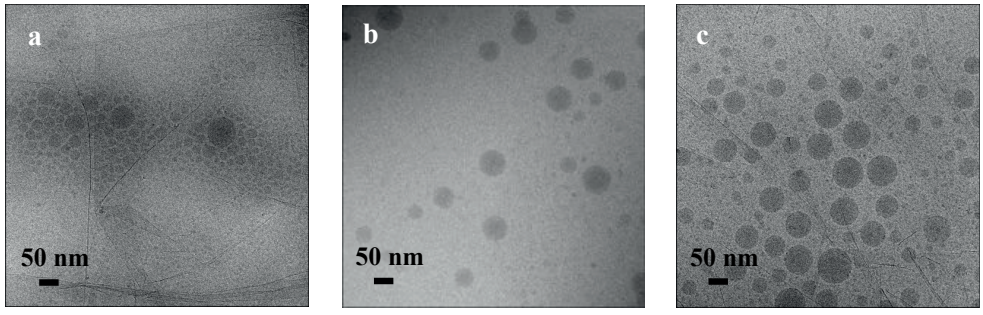

Figure 5.3. Representative cryo-TEM images at 24,000× magnification of emulsion subnatants from a 0.5-wt.% Tween 20-based colloid mill emulsion (a), a 0.5-wt.% Tween 20-based Microfluidizer emulsion (b), and a 2.0-wt.% Tween 20-based Microfluidizer emulsion (c). Applied nominal defocus value was -1.5 µm. Oil droplets are visible as dark spots. Contrast and brightness were adjusted to tune the visibility. Corresponding cryo-TEM images at 6,500× magnification can be found in Figure A5.2.

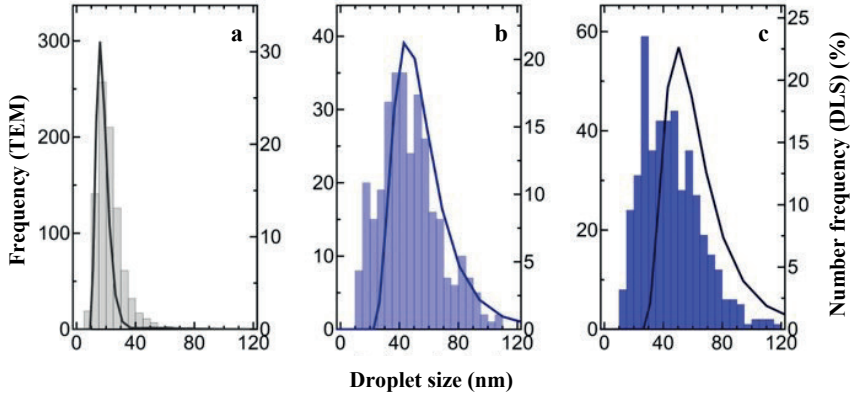

Figure 5.4. The droplet size distributions of oil droplets obtained by using cryo-TEM and DLS (number-weighted hydrodynamic diameter) for subnatant samples from a 0.5-wt.% Tween 20-based colloid mill emulsion (a), a 0.5-wt.% Tween 20-based Microfluidizer emulsion (b), and a 2.0-wt.% Tween 20-based Microfluidizer emulsion (c). Histograms correspond to the size distributions from cryo-TEM data and solid curves correspond to those from DLS data.

The cryo-TEM results confirmed that the diameters of the very small droplets present in the subnatant of a 0.5-wt.% Tween 20-based emulsion made with the colloid mill were, on average, smaller (the major part was 10–30 nm in diameter) compared to those present in the subnatant of the 0.5-wt.% Tween 20-based emulsion prepared with a Microfluidizer (Figure 5.4a & b, respectively). The 0.5-wt.% Tween 20-based emulsion made with the colloid mill was calculated to have 0.29–0.36 wt.% excess Tween 20 in the continuous phase (depending on the theoretical surface load, section 5.2.3), whereas this was only 0.0–0.1 wt.% for the 0.5-wt.% Tween 20-based emulsion made with the Microfluidizer (Table 5.1). This difference in concentration of Tween 20 in the continuous phase may facilitate the formation of swollen micelles. The droplet size distributions of the 0.5- and 2.0-wt.% Tween 20-based Microfluidizer emulsions were very similar (Figure 5.4b & c), which suggests that within the tested concentration range, the surfactant concentration had almost no influence on the size of the generated very small droplets. With cryo-TEM, very small droplets were observed more frequently throughout all imaged samples when the Tween 20 concentration was increased from 0.5 wt.% to 2.0 wt.% (Figure 5.3b & c, respectively). This suggests that more oil becomes dispersed in the very small droplets when more surfactant is present, which was further investigated by measuring the actual oil content of the subnatants. The oil content ranged from 1.7% (± 0.05%) of the total oil fraction in the 0.5-wt.% Tween 20-based emulsion made with the colloid mill, to 5.1% (± 0.24%) in the 0.5-wt.% Tween 20-based emulsion made with the Microfluidizer, and even 22.7% (± 2.8%) in the 2-wt.% Tween 20-based emulsions made with the Microfluidizer (numbers in Figure 5.2b). Therefore, a 4-fold increase in the surfactant concentration lead to an important shift in the oil partitioning towards the fraction of 'very small droplets' (numbers in Figure 5.2b). In contrast, it seems to only moderately change the droplet size distribution of the whole emulsion and of the subnatant (Figure 5.2a & b, comparison of both curves).

As mentioned earlier, surfactant micelles in the aqueous phase of emulsions may have two opposing effects in the oxidative stability of emulsions, either due to their ability to exchange reactive molecules between emulsion droplets (Laguerre et al., 2017, 2020; Li et al., 2020; McClements et al., 1992; Villeneuve et al., 2018, 2021), or due to their protective effect against lipid oxidation (Berton-Carabin et al., 2014; Berton et al., 2011b). Noticeably, micelles could not be detected in the emulsions' subnatants by DLS (Figure 5.2b), even though the theoretical amount of surfactant present in the aqueous phase is much higher than the critical micelle concentration of Tween 20 (0.006 wt.% at 25 °C (Mahmood et al., 2013)) (Table 5.1). This can only be explained by

the concomitant presence of much larger droplets (> 100 nm) that dominate the scattering signal in DLS, as compared to the contribution of the micelles (~ 8-10 nm) (Awad et al., 2018; Law et al., 2012) (Figure 5.2b). To track the potential presence of surfactant micelles in our emulsions, cryo-TEM was used once again. Figure 5.5a & b show cryo-TEM images of a Tween 20 (0.5-wt.%) aqueous solution, without any oil added in which densely packed particles with a diameter of 3–4 nm were observed (indicated with blue arrows in Figure 5.5b). This is smaller than the size of Tween 20 micelles of ~ 8 nm (Figure 5.2b) (Mandal et al., 2013; Pal et al., 2011). Further analysis of the images by fast Fourier transform (FFT) of the zoomed-in regions revealed that there was a periodic pattern with a spacing of about 0.12 nm^{-1} present, which corresponds to a packing distance of ~ 8.3 nm (Figure 5.5c). This suggests that the hydrophobic cores of Tween 20 micelles can only be seen as darker dots of around 3–4 nm in diameter in the cryo-TEM images, and that the average spacing of 8 nm matches the distance between densely packed Tween 20 micelles. Similar features were observed in the emulsion subnatant from a colloid mill-made emulsion (Figure 5.5d – f), which was in line with our expectations due to an excess of Tween 20 being present in the continuous phase (Table 5.1). Awad *et al*. (Awad et al., 2018) also reported the co-existence of micelles and swollen micelles (12–22 nm in diameter) in emulsion systems, which is in line with our findings. In literature, the optically transparent subnatants of such emulsions are sometimes referred to as the continuous phase. For example, a certain amount of hydroperoxides was measured in such a subnatant (centrifugation conditions: 35 min 24,000×*g*), which may lead to various interpretations depending on the type of colloidal structures actually present (Nuchi et al., 2002). In that case, measurements on the size and amount of physical structures in those subnatants was not performed, so the presence of small droplets with a diameter < 100–200 nm may have been overlooked.

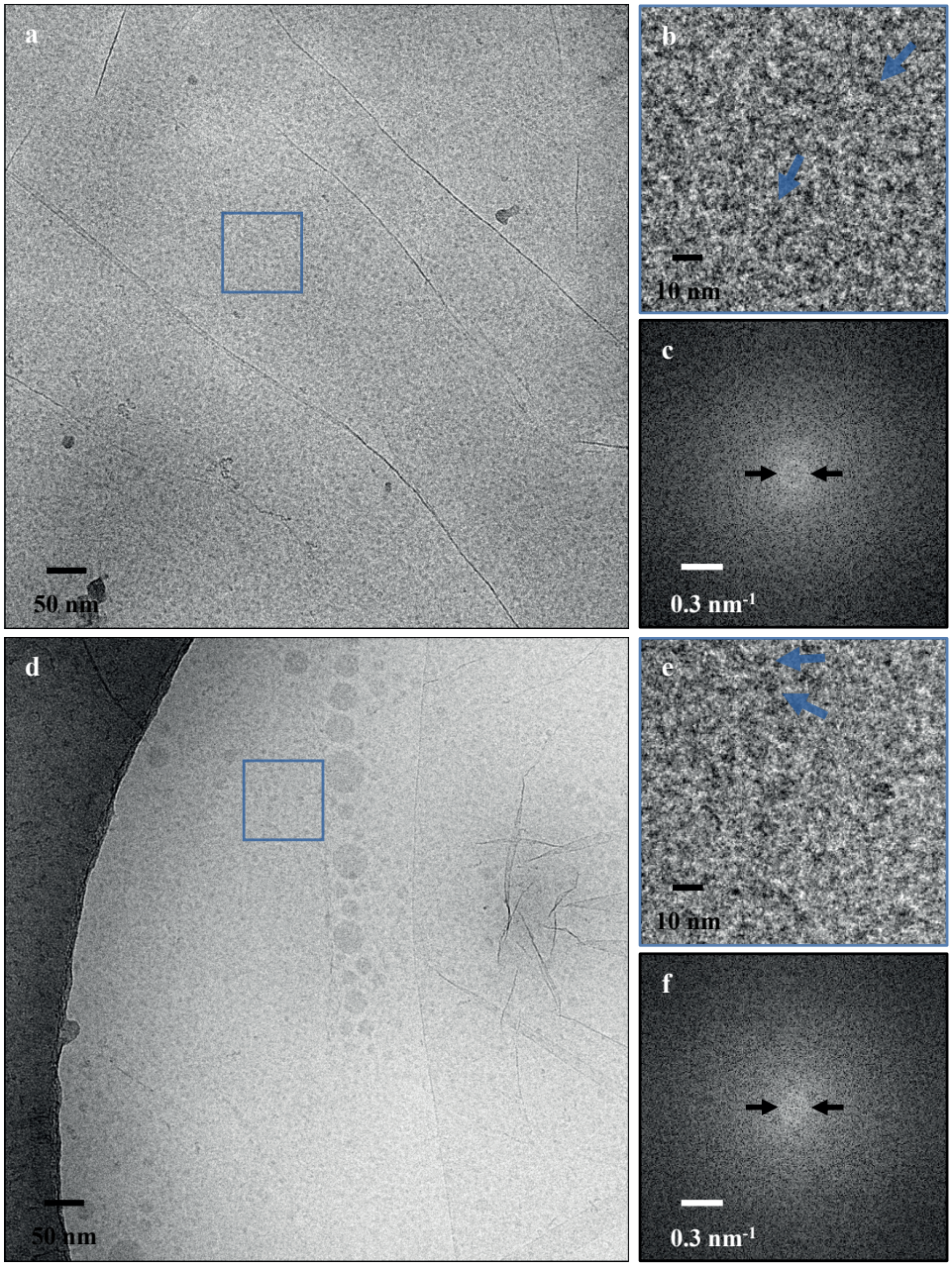

Figure 5.5. (a & b) Representative cryo-TEM images at 24,000× magnification of a 0.5-wt% Tween 20 aqueous solution (a) and the subnatant of 0.5-wt.% Tween 20 emulsion prepared with a colloid mill (b). The applied nominal defocus was -2.5 µm. (b & e) Zoomed-in (blue square) regions of (a) and (d), respectively, where the blue arrows point to areas where micelle cores appear in black (b & e). (c & f) Fast Fourier transform applied to (b) and (e), respectively, where the black arrows indicate a ring, which corresponds to the periodic structure of ~ 8 nm. Contrast and brightness were adjusted for better visibility.

5.3.2 Physical and oxidative stability of the co-existing very small emulsion droplets

Although surfactant micelles have been suggested to play a major role in the oxidative stability of emulsions through exchange of reactive molecules between oil droplets (Laguerre et al., 2017, 2020; Li et al., 2020; McClements et al., 1992; Villeneuve et al., 2018, 2021) or due to their protective effect against lipid oxidation (Berton-Carabin et al., 2014; Berton et al., 2011b), here we are mainly interested in the effect of very small droplets. Upon incubation of the colloid mill-made emulsions at 25 °C, the overall droplet size distribution remained constant over the maximum incubation period tested (17 days, Figure A5.3). Similarly, the droplet size distribution and lipid content of the very small droplet fraction remained unchanged over incubation (Figure 5.6a & b), indicating that these droplets were not subjected to instabilities, such as Oswald ripening and/ or coalescence. Ostwald ripening was not expected to play a role here because the stripped rapeseed oil used as the oil phase consists mostly of triglycerides, which are virtually insoluble in water (Andrikopoulos, 2002).

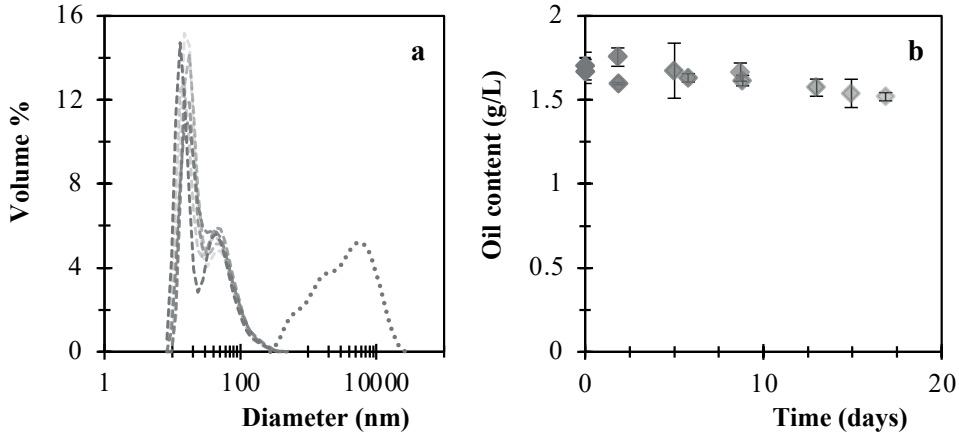

Figure 5.6. (a) The droplet size distributions of colloid mill-made emulsion samples. Different curves represent droplet size distributions of the subnatants collected over incubation of a 0.5-wt.% Tween 20 emulsion prepared with a colloid mill (by DLS) (grey, dashed lines) or the whole emulsion sample (by SLS) (grey, dotted line); the lighter the colour, the later the timepoint (from t_0 [dark grey] to t_2, t_5, t_7, t_9, and finally t_{15} [light grey]. (b) The oil content in these subnatant samples over incubation. The curves in (a) represent averages of two subnatant samples of one independent replicate; for clarity, the outcome of the other independently prepared emulsion is shown in a separate graph in Figure A5.4. In panel (b) the outcomes of the independent replicates are shown as separate data points, and the error bars denote standard deviations of two measurements on two independently incubated samples originating from the same emulsion (total of four measurements per data point).

Lipid oxidation products formed in a more prominent way in the very small droplet fraction (◊ in Figure 5.7) than in the whole emulsion (□, in Figure 5.7), as shown for hydroperoxides (Figure 5.7a) and aldehydes (Figure 5.7b). For some of the data points, the initial amount (t=0) of lipid oxidation products in the very small droplets was already higher than in the corresponding whole emulsion. The increased formation of lipid oxidation products over time could be due to the larger interface-to-volume ratio of these very small droplets, which could promote reactions between aqueous prooxidants (such as metal ions) and polyunsaturated lipids present in the droplets, thereby increasing the lipid oxidation rate (Berton et al., 2011b). In addition, initially higher levels of lipid oxidation products are known to increase subsequent lipid oxidation during storage (Laguerre et al., 2020; Schroën et al., 2022a; Yoshida et al., 1992).

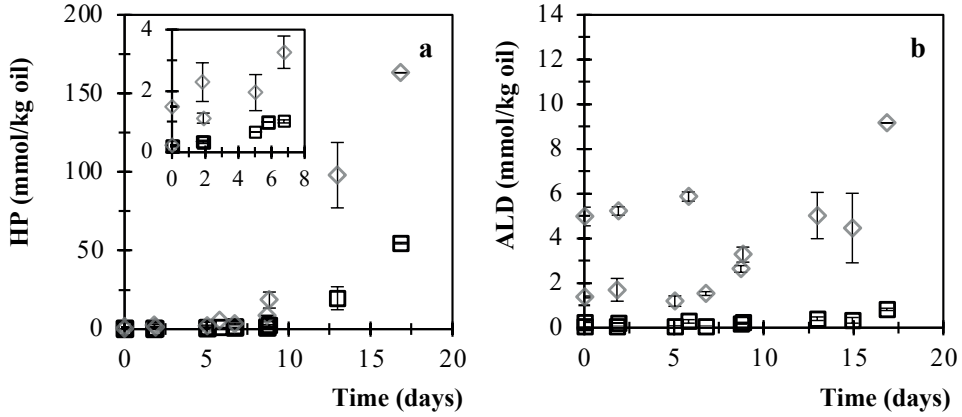

Figure 5.7. Formation of hydroperoxides (a) and aldehydes (b) over incubation of a Tween 20-stabilised emulsion (0.5 wt.% Tween 20, colloid mill). Symbols correspond to a different droplet size from the same emulsion: whole emulsion (□) and very small droplets present in the subnatant phase (◊). For the droplet size distributions of the whole emulsion and very small droplets, see Figure 5.2a. Error bars denote standard deviations of one measurement on two independently incubated emulsion samples originating from the same emulsion, and the outcome of independently prepared emulsions are shown as separate data points.

Investigations on the effect of droplet size on lipid oxidation, where the differently sized droplets originated from the same emulsions, have been reported previously (Li et al., 2019; Yang et al., 2020). A recent publication studied the effect of droplet size on lipid oxidation by monitoring the oxidation of the fluorescent dye BODIPY 665/676 in a surfactant-stabilised emulsion, and faster oxidation was found for the smallest droplets (2-8 μm) compared to the larger droplets (> 20 μm) (Li et al., 2019). Conversely, in another recent study on mayonnaise, using the same dye, the droplet size did not (or barely) influence the lipid oxidation rate. This was ascribed to the small size difference

(1–4 µm) and the possible transfer of the fluorescent dye or oxidation products for long incubation periods (Yang et al., 2020). Only when stripped oil without antioxidants was used, and thus lipid oxidation proceeded quite rapidly, smaller droplets were found to oxidise slightly faster than larger ones (Yang et al., 2020). This highlights that the effect of droplet size on lipid oxidation is often small, if observed at all. In our case, the faster oxidation in small droplets could be highlighted more clearly because the large difference in average size of ~ a factor 70 ($D_{3,2}$-based comparison). These two previous studies were based on fluorescent optical microscopy, which does not allow for detection and consideration of the implication of very small droplets (< 200 nm), whereas especially these seem to have a dramatic effect on lipid oxidation.

When increasing surfactant concentration, more very small droplets are formed (Table 5.1, Figure 5.7), which is expected to increase lipid oxidation because of the larger total interfacial area in the emulsion. In line with this hypothesis, it was found previously that lipid oxidation increased with surfactant concentration (Kargar et al., 2011; Rhee, 1978). In contrast, it is known that excess surfactant in the continuous phase may counteract lipid oxidation, which was shown previously by purposely adding excess surfactant post-emulsification (Berton et al., 2011b). The balance between both effects is probably dependent on the applied conditions and concentrations used, which might explain why in some cases the amount of Tween 20 did not have an effect (Ponginebbi et al., 1999), whereas in other studies lipid oxidation increased with the Tween 20 concentration (Kargar et al., 2011; Rhee, 1978). This, once more, highlights the importance of considering and tracking the very small droplets that can be present in emulsions.

5.4 Conclusions

In this chapter, we investigated the occurrence and effect of very small oil droplets and swollen micelles (< 100 nm) in surfactant-stabilised emulsions, which, so far, have often been overlooked or improperly characterised (Awad et al., 2018). To this end, we combined transmission electron microscopy (TEM) and dynamic light scattering (DLS) techniques. We used cryo-TEM to characterise these very small structures (10–200 nm) and investigated their physical and oxidative stability. Cryo-TEM was shown to be an effective tool to visualise co-existing very small droplets (swollen micelles) and to quantify their size. Additionally, self-assembled empty micelles (~ 8 nm) were detected in the emulsions' subnatants by cryo-TEM, whereas these micelles were not detected using DLS, which was most likely due to the dominance of the scattering signal

by the larger droplets present.

Increasing the surfactant concentration four times (from 0.5 to 2.0 wt.%) led to approximately four times more oil becoming incorporated in the very small droplets (10–200 nm). Increasing the mechanical force used to make the emulsion (from colloid mill to high pressure homogenisation) also increased the fraction of very small droplets three times. Larger shear forces promote droplet elongation during homogenisation, which enhances the formation of small droplets, and the increased surfactant concentration quickly stabilises the newly formed droplets, thereby preventing coalescence during homogenisation.

The amount of oil retained in the very small droplets was stable over the entire incubation time of the emulsions (17 days). However, the lipid oxidation products were – at any time point – overrepresented in the very small droplets. We hypothesize that this is mainly related to their large interface-to-volume ratio compared to the larger droplets present, which favors the contact between prooxidants present in the continuous phase and the unsaturated fatty acids.

This chapter shows that cryo-TEM is a powerful technique to characterise the size of very small lipid-containing structures in emulsions, such as swollen micelles and very small droplets. The obtained insights are pivotal to improve our understanding of the structural and oxidative characteristics of such emulsion systems.

5.5 Appendix

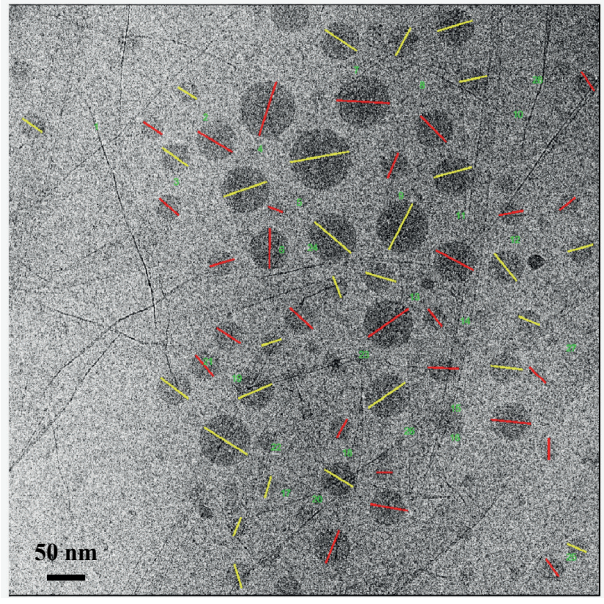

Figure A5.1. Example of droplet diameter analysis with an in-house Matlab script. Cryo-TEM images of the emulsion subnatants at a magnification of 24,000× with nominal defocus of -2.5 µm were used for the analysis. Both yellow and red lines show the assigned droplet diameter during the analysis.

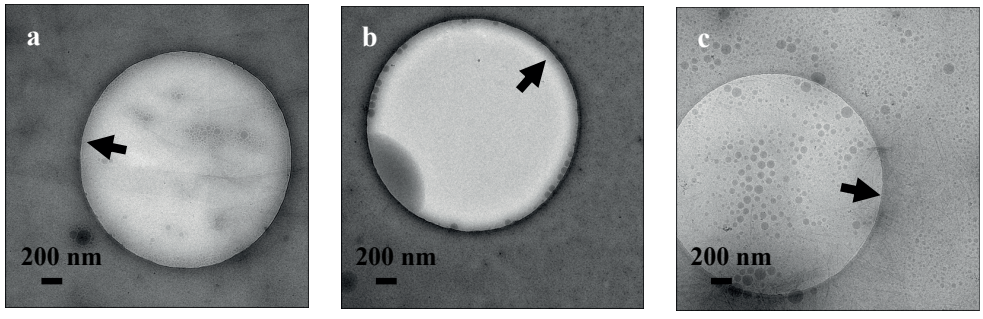

Figure A5.2. Corresponding cryo-TEM images of the emulsion subnatants shown in Figure 5.3 at a magnification of 6,500× of: a 0.5-wt.% Tween 20-based colloid mill-made emulsion (a), a 0.5-wt.% Tween 20-based Microfluidizer-made emulsion (b), and a 2.0-wt.% Tween 20-based Microfluidizer-made emulsion (c). The applied nominal defocus was -20 µm. Black arrows point to the edge of a hole in the carbon film.

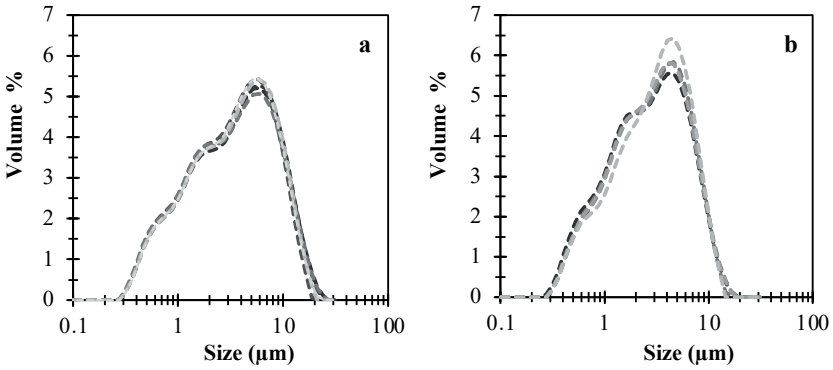

Figure A5.3. Droplet size distributions of two independently prepared (a & b) 0.5-wt.% Tween 20-based emulsion samples prepared with a colloid mill over time. The lighter the colour the later the timepoint (for a: from t_0 [dark grey] to t_1, t_5, t_7, t_9, and finally t_{15} days [light grey], for b: t_0 [dark grey] to t_6, t_9, t_{13}, and finally t_{16} days [light grey]; The lines represent averages of three SLS measurements performed on the same sample.

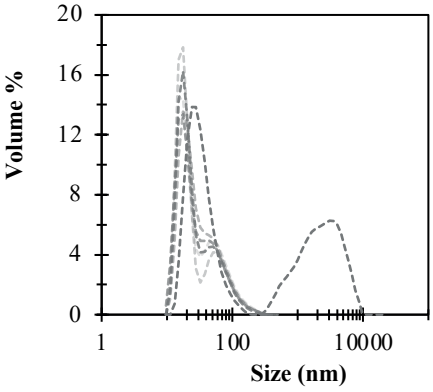

Figure A5.4. Droplet size distributions of the 0.5-wt.% Tween 20-based emulsion samples prepared with a colloid mill. Different lines represent the subnatants collected over incubation via centrifugation (solid lines) or an emulsion sample as such (dashed line), the lighter the colour the later the timepoint (from t_1 [dark grey] to t_2, t_5, t_7, t_9, and finally t_{17} days [light grey]); The lines represent averages of two subnatant samples of one independent replicate; the other replicate is shown in Figure 5.6a.

Table 5.1. Estimated concentrations of excess Tween 20 in the aqueous phase of emulsions. The calculations were performed using theoretical surface loads (Γ) of 1.5 and 2.3 mg/m^2 (Berton et al., 2011b; Bos et al., 2001).

Emulsification device	Total Tween 20 concentration applied in the aqueous phase (wt.%) C_{added}, Eq. 5.3	Theoretical Tween 20 adsorbed (expressed in equivalent wt.% of continuous phase) $S_{ad} \times R_{oil} \times r_{cont}$, Eq. 5.3	Theoretical excess Tween 20 in continuous phase (wt.%) C_{excess}, Eq. 5.3
Colloid mill	0.5	0.14 – 0.21	0.36 – 0.29
Microfluidizer	0.5	0.40 – 0.61*	0.10 – 0*
Microfluidizer	2.0	0.66 – 1.0	1.34 – 0.99

* The calculated value of 0.61 wt.% exceeds the total amount used, indicating that there would be no excess at all. This suggests that the high-boundary theoretical surface load of 2.3 mg/m^2 is too high for the present system in which lower values (closer to the low-boundary value of 1.5 mg/m^2) most likely apply.

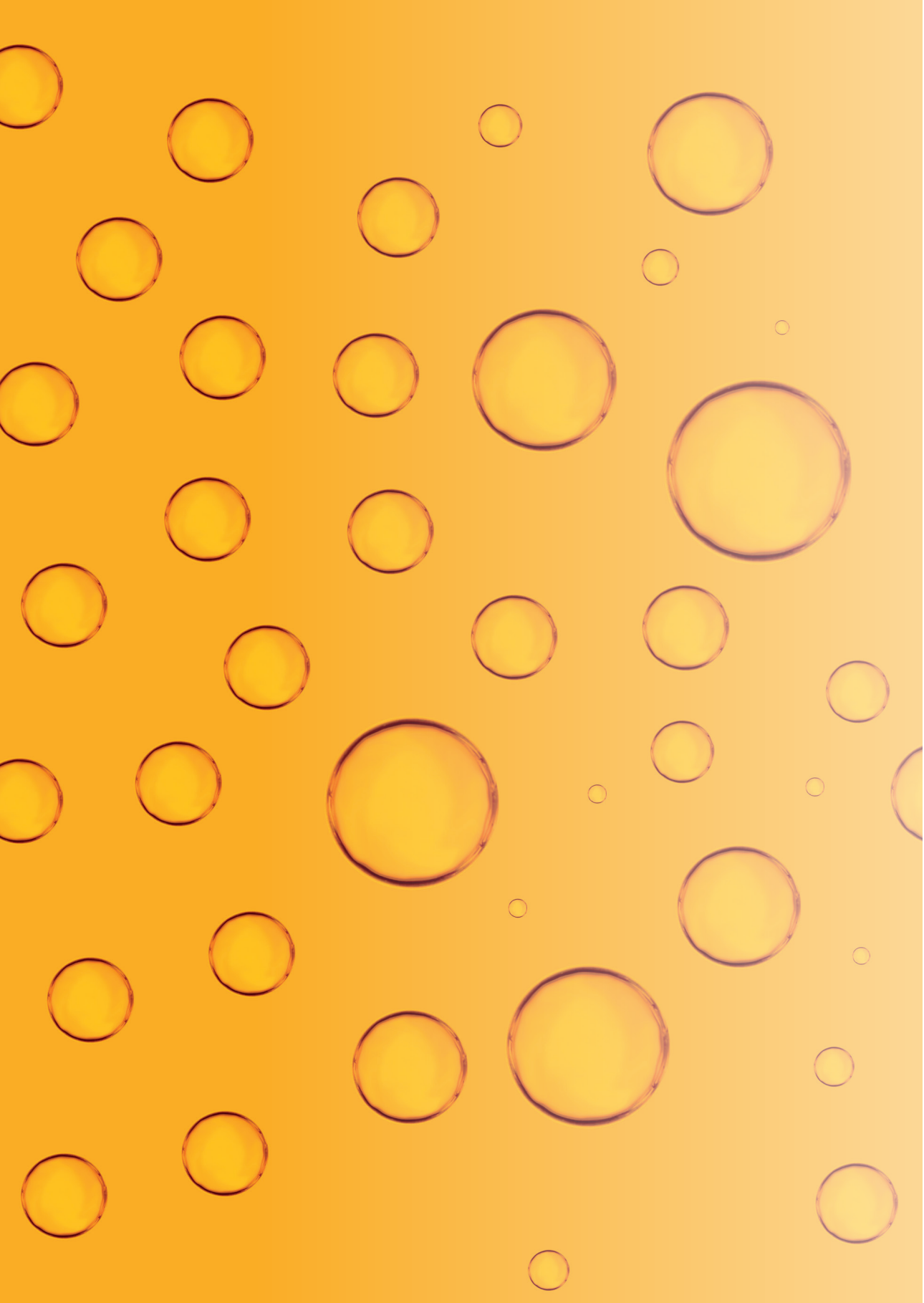

Chapter 6

Droplet size dependency and spatial heterogeneity of lipid oxidation in surfactant- and protein-stabilised emulsions

Manuscript in preparation as:
S. Yang, S. ten Klooster, C. Berton-Carabin, K. Schroën, J. van Duynhoven, J. Hohlbein: *Droplet size dependency and spatial heterogeneity of lipid oxidation in surfactant- and protein-stabilised emulsions*

Abstract

Lipid oxidation is one of the main causes of deterioration in emulsified products containing polyunsaturated fatty acids. In this chapter, we used BODIPY dyes, and fluorescently labelled spin traps (CAMPO-AFDye 647) in emulsions to localise lipid and protein oxidation, respectively.

We found that in a Tween 20-stabilised emulsion, BODIPY 665/676 fluorescence decreased when the formation of lipid oxidation products was still slow, whereas in a WPI-stabilised emulsion the decrease in fluorescence occurred simultaneously with a rapid formation of lipid oxidation products. Image analysis showed that lipid oxidation increased with decreasing droplet size, which supports the hypothesis that in certain conditions, lipid oxidation in emulsions may occur heterogeneously at the level of droplets. For WPI-stabilised monodisperse emulsions, oil droplets of the same size were also found to oxidise in a heterogeneous pattern. This is possibly linked to the observed heterogenous protein oxidation taking place at the interface that is expected to be intertwined with oxidation of lipids. In these emulsions, heterogeneous spots of protein oxidation at the interface were even observed within one droplet. These insights contribute to our understanding of local lipid oxidation events, which may lead to improved oxidative stability of food emulsions.

6.1 Introduction

In foods containing polyunsaturated fatty acids (PUFAs), lipid oxidation causes product deterioration (McClements et al., 2000). Lipid oxidation is often prevented by low temperature storage, modified atmosphere packaging, and the addition of antioxidants (Berton-Carabin et al., 2014). However, these measures cannot completely prevent lipid oxidation (Berton-Carabin et al., 2014), especially when trying to comply with a current health focus to increase the intake of PUFAs, in particular omega-3 fatty acids (Joint, 2010; Vannice et al., 2014). These PUFAs are particularly susceptible to lipid oxidation (Kerr, 1966; Schaich, 2013), which needs to be mitigated. An additional concern is that synthetic antioxidants are tended to be avoided because these additives are becoming less acceptable to consumers, which will make products even more susceptible to lipid oxidation.

All these aspects have rekindled the interest in lipid oxidation, especially for products in which the oil phase is dispersed as droplets in an aqueous phase, forming oil-in-water (O/W) emulsions (e.g., sauces, dressings, soups, and infant milk formula). This structure makes the lipids highly susceptible to oxidation due to the large interfacial area in such products, where prooxidants from the continuous phase can come into contact with lipids (Berton-Carabin et al., 2014; McClements et al., 2000). The complexity of lipid oxidation in O/W emulsions from the perspective of location and time has shifted research focus to these spatiotemporal aspects (Laguerre et al., 2020).

To identify these aspects, confocal laser scanning microscopy (CLSM) has been used to unravel in which droplets lipid oxidation is occurring, and to what extent (Banerjee et al., 2018; Li et al., 2019, 2020; Yang et al., 2020). As a tracer for oxidation, the fluorescent dye BODIPY is often used. BODIPY is excited at a different wavelength depending on whether it is in native state, or in oxidised state (section 6.2.3). A recent paper showed that BODIPY 665/676, when present in medium chain triglyceride (i.e., saturated fatty acids) emulsion droplets, oxidised faster when co-oxidising unsaturated oil droplets were present (Li et al., 2020). This may indicate that lipid oxidation can spread from oxidising droplets to non-oxidised ones, or that oxidising droplets somehow influence each other. For BODIPY 665/676, it was shown that when lipid oxidation is very selectively initiated in one droplet, oxidation does not spread rapidly to neighbouring droplets (Banerjee et al., 2018). From this, it is clear that there is no general consensus about how droplets influence each other, if at all (Banerjee et al., 2018; Raudsepp et al., 2016; Raudsepp, Brüggemann, et al., 2014; ten Klooster

et al., 2022), and that this is contingent on the system's properties (prooxidants, agitation conditions, relative rate of oxidative reactions vs diffusion of reactive molecules). The same dye was used to show that small droplets oxidise faster than larger ones in surfactant-stabilised emulsions (Li et al., 2019), whereas in high internal phase O/W emulsions (mayonnaise), the formulation of the emulsions determines the effect of droplet size on lipid oxidation (Yang et al., 2020). CLSM has also been used to improve our understanding of the simultaneously occurring protein oxidation and lipid oxidation. This has been done by measuring the autofluorescence of oxidised proteins in mayonnaise (Yang et al., 2020) and by combining BODIPY with the CAMPO-AFDye 647, which is a protein oxidation-sensitive, fluorescently labelled spin trap (Yoshida et al., 2003). The main advantage is that multiple markers for co-oxidation can be combined within the same local image and related to different oxidation events. These methodologies can be exploited further to improve our spatiotemporal understanding of local protein and lipid oxidation; for example, to compare the oxidation status of individual droplets/protein layers present within one emulsion system or even present in different emulsion systems.

In this chapter, as a first step, BODIPY fluorescence is correlated to the formation of lipid oxidation products to verify its use as a marker for lipid oxidation. The decrease in BODIPY 665/676 fluorescence is compared with the formation of lipid oxidation products in whey protein isolate- (WPI) and Tween 20-stabilised emulsions. Next, we focus on the spatiotemporal heterogeneity of lipid and protein oxidation in monodisperse emulsions that were prepared with microfluidics, and in polydisperse emulsions that were prepared with a conventional rotor-stator homogeniser.

6.2 Materials and methods

6.2.1 Materials

Soybean oil was kindly supplied by Unilever (Wageningen, the Netherlands). Sodium phosphate dibasic heptahydrate (MW: 268.07 g/mol), sodium phosphate monobasic monohydrate (MW: 137.99 g/mol), and phosphoric acid (85.0-88.0%) were purchased from Sigma-Aldrich (Zwijndrecht, the Netherlands) to make a 10 mM phosphate buffer (pH 3.0). n-Hexane and 2-propanol were obtained from Actu-All Chemicals (Oss, the Netherlands). Deuterated chloroform and dimethylsulfoxide (CDCl3 and DMSO-d6) were purchased from Euriso-top (Saint-Aubin, France). Tween 20 was purchased from Sigma Aldrich (Zwijndrecht, the Netherlands). WPI, purity 97.0–98.4% (BiPro®, Davisco, Switzerland) was used as received. For cleaning the microfluidic chips, we used ethanol, purity 96% v/v

(VWR International B.V., Amsterdam, the Netherlands) and piranha solution, which is a 3:1 v/v ratio of sulphuric acid, purity 96% (Sigma-Aldrich, Zwijndrecht, the Netherlands) and 35 wt.% hydrogen peroxide (Sigma-Aldrich, Zwijndrecht, the Netherlands). The assay reagent for measuring the triacylglycerol (TAG) content and a standard containing TAGs (Triglycerides liquicolor mono kit) were purchased from HUMAN (HUMAN Gesellschaft für Biochemica und Diagnostica mbH, Wiesbaden, Germany). The assay reagent comprised 50 mmol/L PIPES buffer (pH 7.5), 5 mmol/L 4-chlorophenol, 0.25 mmol/L 4-aminoantipyrine, 4.5 mmol/L magnesium ions, 2 mmol/L ATP, 1.3 U/mL lipases, 0.5 U/mL peroxidase, 0.4 U/mL glycerol kinase and 1.5 U/mL glycerol-3-phosphate oxidase. The lipophilic and oxidation sensitive dyes BODIPY 665/676 and BODIPY 581/591 C11 (C11-BODIPY) were purchased from Thermo Fischer (Waltham, MA, USA). CAMPO-AFDye 647 was synthesised by SyMO-Chem B.V. (Eindhoven, the Netherlands). 2,2'-Azobis (2-amidinopropane) dihydrochloride (AAPH) and sodium azide were purchased from Sigma Aldrich (Zwijndrecht, the Netherlands). Ultrapure water (18.2 MΩ) was used for all experiments and prepared using a Milli-Q system (Millipore Corporation, Billerica, MA, USA).

6.2.2 Emulsion preparation

Preparation of oil and continuous phase

Soybean oil was stripped with alumina powder (MP112 EcoChromet ALUMINA N, Activity: Super I, Biomedicals) to remove impurities and endogenous antioxidants (in particular tocopherols) (Berton et al., 2011a). For both emulsification methods used (colloid mill and microfluidics, see below), the oil was filtered using a 0.22-μm filter (Minisart High-Flow, Sartorius Stedim Biotech GmbH, Goettingen, Germany) to remove any small particle that can cause clogging of the microfluidic channels. For the preparation of the continuous phase, either Tween 20 or WPI was dissolved in buffer with a concentration of 2.35 wt.%. Next, the mixture was stirred for 2 h (WPI) or 30 min (Tween 20). To prevent bacterial growth, sodium azide (0.05 wt.%) was added to the emulsions. For lipid oxidation experiments, BODIPY 665/676 was added to the stripped soybean oil (final concentration of 1 or 50 μM in the emulsion). For lipid-protein co-oxidation measurements, C11-BODIPY was added to the emulsions prior to incubation, and CAMPO-AFDye 647 was added after incubation, before the measurements (for details regarding the structure of CAMPO-AFDye 647, see Figure A6.1). The concentration of C11-BODIPY and AFDye 647 in the emulsion was 1 μM.

Colloid mill emulsification

A coarse emulsion was made by adding 15 wt.% of stripped soybean oil (with or without BODIPY 665/676) to the continuous phase, and high-speed stirring

was applied at 11,000 rpm for 1 min with a rotor-stator homogeniser (Ultra-turrax IKA T18 basic, Germany). A fine emulsion was prepared by passing the coarse emulsion through a lab-scale colloid mill with a gap width of 0.32 mm (IKA Magic Lab, Staufen, Germany), operating for 1 min at 26,000 rpm. During operation, the colloid mill was cooled with water at 4 °C.

Microfluidic emulsification
To produce monodisperse emulsions, the microfluidic emulsification chip called UPE_{10x1} (Upscaled Partitioned EDGE [Edge-based Droplet Generation]) was used (Figure A6.2) (ten Klooster et al., 2022). These chips were designed in our lab and produced in glass by deep reactive ion etching (Micronit Microfluidics, Enschede, The Netherlands). A chip with 8,064 droplet formation units (DFUs) of 10 × 1 µm (width × height) each was used. More details about the fabrication, operation, and droplet formation can be found in a previous publication (ten Klooster et al., 2022).

6.2.3 Lipid and protein oxidation

Initial oxygen concentration
The initial amount of oxygen was calculated (mmol/kg oil), using a headspace volume of 1.55 mL headspace with 20.9 % O_2; 46.8 mg/kg oxygen concentration in the oil (Cuvelier et al., 2017); and 8.1 mg/kg oxygen concentration in the continuous phase (Truesdale et al., 1955). The amount of oxygen initially present was ~ 450 mmol/kg oil.

Incubation conditions
To initiate lipid oxidation, 5 mM of 2,2'-azobis (2-amidinopropane) dihydrochloride (AAPH) were added to the emulsion. A volume of 0.2 mL of emulsion was added to 1.5 mL microcentrifuge tubes. The tubes were rotated horizontally at 2 rpm in a dark oven at 25 °C for up to 10 days. At selected time points, two tubes per independently prepared emulsion were taken and either used directly for further measurements (imaging with CLSM) or stored under inert gas at −80 °C for 48 h to 7 days (for lipid extraction and subsequently quantification of lipid oxidation products).

Oil extraction
The extraction of oxidation products was performed by adding 1 mL hexane-isopropanol (3:2 v/v) to ~ 1.5 mL emulsion and vortexing thoroughly, as described previously (Shantha et al., 1994; Srinivasan et al., 1996). The mixture was centrifuged at 4,000×*g* for 20 min and the upper layer, containing the hexane and fat, was carefully separated from the bottom layer. The hexane was

evaporated under a stream of nitrogen at 25 °C until constant weight, and the remaining oil was treated with a nitrogen blanket and frozen at −80 °C for a minimum of 48 h and a maximum of 20 days, until further measurements were performed, which was based on previous research (ten Klooster et al., 2022d).

Lipid oxidation measurements by ^{1}H NMR

Hydroperoxides (primary oxidation products), aldehydes (secondary oxidation products) and triacylglycerols (as a reference for the total amount of oil) were simultaneously quantified using ^{1}H NMR, with an Advance III 600 MHz spectrometer, equipped with a 5-mm cryo-probe at 295 K, following the method described previously (Merkx et al., 2018). In brief, 580 µL of a mixture of $CDCl_3$/DMSO-d6 (5:1 v/v) were added to ~ 20 µl extracted oil (as described in 2.6) and transferred to 5-mm NMR tubes (Bruker, Billerica, Massachusetts, USA). From the recorded single pulse experiment, the glycerol backbone peak at δ 4.4 pm were used for the quantification of the amount of triacylglycerols. With a band selective pulse, the region between δ 13.0 and 8.0 ppm was selectively excited for the quantification of hydroperoxides and aldehydes, following (Merkx et al., 2018). The hydroperoxide signals resonate between δ 11.3 and 10.6 ppm, and the aldehydes resonate between δ 9.8 and 9.4 ppm. The calculations, including a factor that accounts for intensity loss during the selective pulse, are described elsewhere (Merkx et al., 2018). The data were processed with the Bruker TopSpin 4.0.6 software.

Confocal Laser Scanning Microscopy

The emulsion samples were centrifuged for 5 min at 300×*g*, and the cream layer was taken. This procedure was used to prevent the droplets from moving during the CLSM measurement. A silicon gasket was fixed on the cleaned glass, and 2 µL of the cream phase were dripped into a well on a silicon gasket (CultureWell™, GRACEBIO-LABS). The well was then sealed with a glass plate to prevent the evaporation of water from the samples. Fluorescence images were monitored with a confocal laser scanning microscope (CLSM, Leica SP8), equipped with a 63 · NA = 1.2 water immersion objective (HC PLAPO CS2, Leica), and a white-light laser with user-selectable excitation wavelengths. The scanning format was 512 · 512 pixels (62 µm by 62 µm), and the line-scanning speed was set to 100 Hz. For lipid oxidation measurements with BODIPY 665/676, the excitation wavelengths were set to 561 nm and 640 nm to detect oxidised and non-oxidised lipids, respectively. Detection ranges were set from 580 nm to 660 nm and from 660 nm to 750 nm, respectively. For protein oxidation measurements with CAMPO-AFDye 647 (Figure A6.1), the samples were excited at 640 nm with a detection range between 660 nm and 750 nm. C11-BODIPY was excited at 561

nm and 488 nm to detect non-oxidised and oxidised BODIPY, respectively. The emission ranges were set at 580-660 nm and 500-560 nm, respectively.

CLSM imaging data were analysed using StarDist (Schmidt et al., 2018) and MATLAB R2021b (Figure A6.3). First, the raw image data from non-oxidised (ex 640 nm) and oxidised (ex 561 nm) channels were summed up and used for the segmentation of oil droplets in 2D StarDist. In the segmentation steps, the versatile (fluorescence nuclei) model was used for the neural network prediction. We set the percentile low and high values to 1 and 99.8, respectively. The probability/score threshold was set to 0.5 and the overlap threshold was 0.4. After the segmentation steps, the masks were applied to the raw image data for the analysis of the fluorescence intensity changes with MATLAB R2021b. The average intensity and radii were determined for each droplet. The accumulation of CAMPO-AFDye 647 at the interface was obtained by removing the pixels with an intensity lower than 30% of the maximum, which was chosen because it allowed to differentiate the continuous phase from the interface. To quantify protein oxidation at the interface of each individual droplet, the intensity of all pixels was summed up and divided by the circumference. Intensity data were normalised by dividing each data point by the maximum fluorescence intensity in each sample.

6.2.4 Basic characterisation of emulsions

Droplet size measurements

Static light scattering

The oil droplet size of the whole emulsions was measured by static light scattering (SLS) (Malvern Mastersizer 3000, Malvern Instruments Ltd., Malvern, Worcestershire, UK), using a refractive index of 1.465 for the dispersed phase and 1.33 for the dispersant (water); and an absorption index of 0.01.

Dynamic light scattering

The continuous phase and the smallest oil droplets were separated from the larger oil droplets by centrifuging 2 mL of emulsion at 20,000×*g* for 42 min in a 2-mL microcentrifuge tube and collecting ~ 0.3 mL of the subnatant from the bottom of tube. The size of the colloidal structures present in this subnatant was measured by dynamic light scattering (DLS) (Zetasizer Nano ZS, Malvern Instruments Ltd., Malvern, Worcestershire, UK). The refractive index was 1.47 for the dispersed phase, and the absorbance was 0.01.

Combined droplet size distribution

For visualisation purposes, for selected samples, the distributions obtained by DLS and SLS were superimposed on the same graph. For this, the relative intensities from the DLS measurements were adjusted based on the actual oil contents in the subnatant (see below). The relative intensities from the SLS measurements were adjusted based on the assumption that its oil content was one minus the oil content in the subnatant.

CLSM

The droplet sizes of monodisperse emulsions were measured by CLSM. The same segmentation steps (section 6.2.3, 'Confocal laser scanning microscopy') were applied to the raw images. The number of pixels was counted per droplet, and the radius was calculated based on the sum of pixels (Figure A6.3).

Oil content

The amount of lipids corresponding to very small droplets was quantified using a colorimetric method for measuring triacylglycerol content (Triglycerides Liquicolor Mono kit, HUMAN) (Jacobs et al., 1960; Trinder, 1969). In brief, the subnatant samples, obtained as described in the section above, were diluted to a range of 0.4-4 g/L, and about 20 µL of sample were weighed into a 2-mL microcentrifuge tube. Next, 1 mL of assay reagent was added, and the samples were subsequently incubated in a heating block at 800 rpm for 20 minutes at 20 °C. The absorbance was measured at a wavelength of 500 nm, and the concentration was calculated using a calibration curve (0.4-4 g triglycerides/L).

6.2.5 Experimental design

For each measurement, at least two emulsions were prepared independently, except for the measurements with emulsions containing 50 µM of BODIPY 665/676, for which only one emulsion was prepared. Additionally, droplet size measurements and lipid oxidation measurements were performed on two independently incubated samples, which originated from the same emulsion, for each time point.

6.3 Results and discussion

6.3.1 Microstructural characterisation of Tween 20- and WPI-stabilised emulsions

Poly- and monodisperse emulsions were prepared with a lab-scale colloid mill or by microfluidic emulsification, respectively. The droplet size distribution of colloid mill-made emulsions was obtained using DLS and SLS, and the droplet size distribution of microfluidic-made emulsions was obtained using CLSM

microscopy (section 6.2.4). The surface-weighted average droplet diameter (Sauter mean diameter, $D_{3,2}$) of the colloid mill-made emulsion, stabilised by Tween 20, was 1.4 µm (obtained from SLS, section 6.2.4) (Figure 6.1). The difference between the smallest droplets observed (0.018 µm by DLS) and the largest droplets observed (8.7 µm by SLS) was a factor of ~ 500 (Figure 6.1). The Tween 20-based emulsion made with microfluidics had a $D_{3,2}$ of 4.5 µm (obtained from CLSM), which is larger than for the colloid-mill made emulsion, although their size distributions overlap (Figure 6.1). Similarly, the WPI-stabilised emulsion prepared with the colloid mill had a smaller average droplet size ($D_{3,2}$ = 2.3 µm, from SLS) than the WPI-stabilised emulsion prepared with microfluidics ($D_{3,2}$ = 4.5 µm, from CLSM) (Figure 6.1).

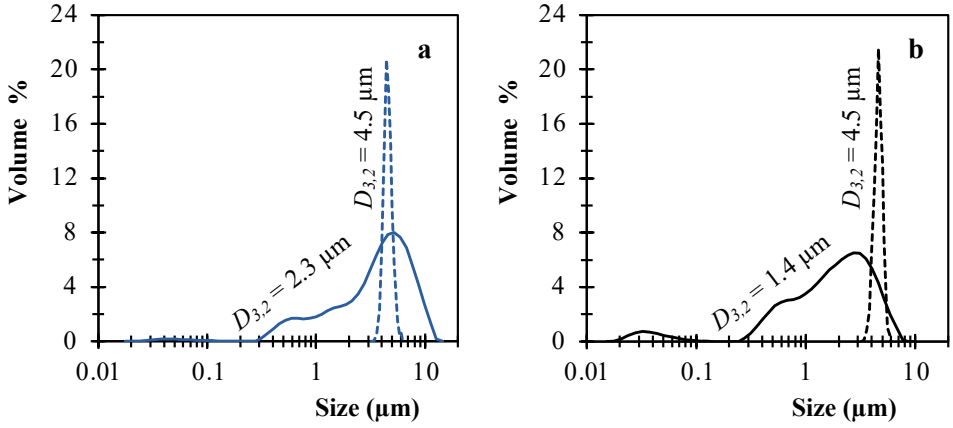

Figure 6.1. Droplet size distributions of the WPI-stabilised (a, blue) and Tween 20-stabilised (b, black) emulsions. Lines represent emulsions prepared with the colloid mill (solid line) or with microfluidics (dashed line). The droplet size distributions for the colloid mill-made emulsion were obtained by combining the SLS results on the whole emulsion sample with the DLS results on the subnatant sample obtained after centrifugation (section 6.2.4, Figure A6.4). The $D_{3,2}$ was obtained from the CLSM results for the microfluidic-made emulsions and from SLS for the colloid mill-made emulsions.

6.3.2 BODIPY 665/676 oxidation

First, we compare BODIPY 665/676 oxidation to the formation of lipid oxidation products. The oxidation of BODIPY 665/676 can be detected by the change in excitation wavelength, which shifts from 640 nm in its native state to 561 nm upon oxidation (Naguib, 2000; Raudsepp et al., 2014). A reaction with peroxyl radicals causes the cleavage of the phenylbutadiene moiety and the formation of an acid group, which can occur at several positions (Figure A6.5) (Drummen et al., 2004; Yoshida et al., 2003). It has been reported that BODIPY 665/676 is more sensitive to react with peroxyl radicals than unsaturated fatty acids

(Raudsepp et al., 2014a). Therefore, this reaction could possibly compete with the propagation of lipid oxidation. To explore this, lipid oxidation was measured in 2 wt.% WPI-stabilised polydisperse emulsions without and with 1 or 50 μM BODIPY 665/676 in the oil (Figure 6.2). The samples containing BODIPY665/676 oxidised less rapidly compared to the sample that did not contain BODIPY 665/676 (Figure 6.2), with the exception of day 6 when the values are closer again. This infers that the reaction between peroxyl radicals and BODIPY 665/676 is competing with the reaction between peroxyl radicals and unsaturated fatty acids, and the concentration of BODIPY needs to be kept as low as possible. A concentration of 1 μM BODIPY 665/676 was used in the other experiments conducted within this chapter.

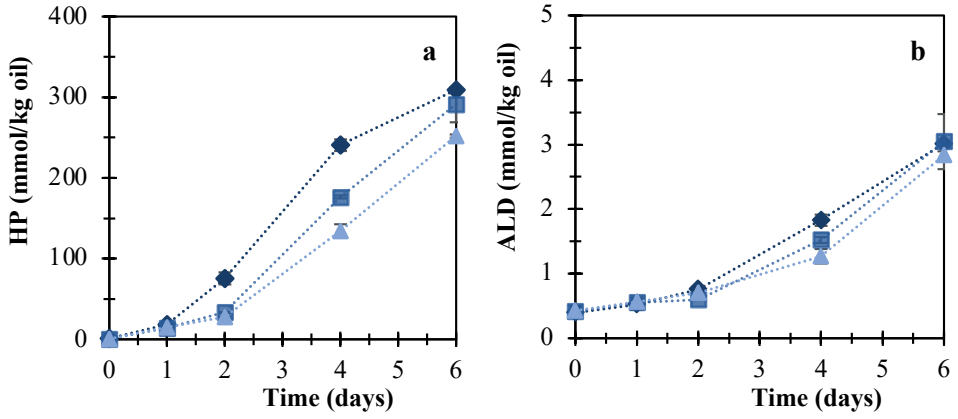

Figure 6.2. Formation of hydroperoxides (HP) (a) and aldehydes (ALD) (b) over incubation in colloid mill-made emulsions stabilised by 2 wt.% WPI. Symbols corresponding to samples containing no BODIPY 665/676 (dark blue, ♦), 1 μM BODIPY 665/676 (blue, ■), and 50 μM BODIPY 665/676 (light blue, ▲). Error bars denote standard deviations of one measurement on two independently incubated samples originating from the same emulsion. The lines between the markers guide the eye.

As a next step, fluorescence needed to be linked to the formation of lipid oxidation products. For monodisperse emulsions this is possible, but for polydisperse emulsion this is not that straightforward. The smallest droplets in which BODIPY 665/676 fluorescence could be quantified were ~ 1 μm. In our polydisperse Tween 20-stabilised emulsion, ~ 28 vol.% of the oil was present in droplets smaller than 1 μm and ~ 4.8 vol.% in droplets smaller than 0.2 μm (resolution limit of this CLSM set-up, Figure A6.3) (Figure 6.1). In Chapter 5, it was shown that the lipid oxidation products were overrepresented in the smallest droplets compared to the whole emulsion, which implies that lipid oxidation would be underestimated if only droplets larger than 1 μm would be analysed.

Furthermore, lipid oxidation markers are standardly expressed in mmol/kg oil. For polydisperse emulsions it is required that the average fluorescence intensity for each droplet is weighted by the volume of that droplet. This is especially important if the droplet size affects lipid oxidation (Chapter 4 & 5), and if there is a wide range of droplet sizes present. For very monodisperse emulsions, prepared with membrane or microfluidic emulsification, the comparison between the formation of lipid oxidation products and the fluorescence intensity by BODIPY 665/676 is rather straightforward. This was one of the motivations to use microfluidic emulsification in this chapter.

Emulsion samples containing 2 wt.% of Tween 20 or 2 wt.% of WPI, prepared with microfluidic emulsification (ten Klooster et al., 2022), were incubated with 5 mM AAPH at 25 °C in the dark. Hydroperoxides and aldehydes were quantified over incubation (Figure 6.3a & b), and the decrease in red fluorescence (BODIPY 665/676) was measured with CLSM (Figure 6.3c). In the monodisperse emulsion stabilised by WPI, the concentration of lipid hydroperoxides increased slightly over the first 4 days and more rapidly between 4 and 6 days of incubation (Figure 6.3a). Similar effects were seen in the fluorescence intensity that showed a minor decrease in red fluorescence in the first 2 days, followed by a more rapid decrease between 4 and 6 days (Figure 6.3c). The rather simultaneous decrease in red fluorescence and increase in hydroperoxides could possibly be explained by an increase in lipid radicals formed in the droplets, which would both increase lipid oxidation and BODIPY 665/676 oxidation (Naguib, 2000; Raudsepp et al., 2014). In future work, a kinetic model could be used to link the estimated formation of peroxyl radicals to BODIPY665/676 oxidation (Schroën et al., 2022a).

For the monodisperse emulsion prepared with Tween 20, the formation of hydroperoxides increased more slowly over 6 days of incubation compared to the WPI-stabilised emulsion (Figure 6.3a), whereas a rapid decrease in red fluorescence was already observed in the first 2 days (Figure 6.3c). This may be caused by the improved solubilisation of BODIPY into the continuous phase when Tween 20 is present (Shao et al., 2015), which could result in a loss of fluorescence intensity from the droplets or in accelerated BODIPY 665/676 oxidation. This indicates that caution is needed when using fluorescence to study lipid oxidation in surfactant-stabilised emulsions.

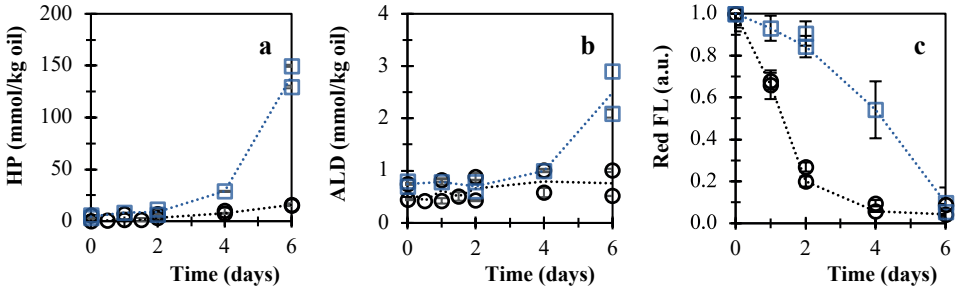

Figure 6.3. Formation of hydroperoxides (HP) (a) and aldehydes (ALD); and decrease of red fluorescence (FL) by BODIPY 665/676 over incubation for microfluidic-made emulsions stabilised by 2 wt.% WPI (□) or 2 wt.% Tween 20 (○). Data shown in (c) was obtained for droplets of 4-5 µm. Error bars (sometimes within marker) denote standard deviations of two measurements on independently incubated samples originating from the same emulsion. The outcomes of independent replicates are shown as separate data points, yet with the same symbols. The lines between the markers guide the eye.

6.3.3 Oxidation in WPI-stabilised emulsions versus Tween 20-stabilised emulsions

The formation of hydroperoxides and aldehydes in the monodisperse WPI-stabilised emulsions was faster than in the monodisperse Tween 20-stabilised emulsions (Figure 6.3a & b). By switching from one emulsifier to another two important factors are varied simultaneously: (i) the type and concentration of emulsifier present in the continuous phase and (ii) the composition of the interface (Berton-Carabin et al., 2014; Genot et al., 2013). Usually, when changing the emulsifier, the droplet size is also affected (Figure 6.1), but the microfluidic emulsification method used here, allowed us to keep the droplet size constant when switching from Tween 20 to WPI. Both Tween 20 and β-lactoglobulin (the main component of WPI) have been described to exert antioxidative effects when present in the continuous phase (Berton et al., 2011b). Another often important effect of emulsifier molecules is that they may be themselves subjected to oxidative reactions, which will reduce the amount of oxygen available for lipid oxidation, and this might mitigate lipid oxidation. On the other hand, such co-oxidation reactions involving emulsifiers may promote lipid oxidation in oil droplets (Berton-Carabin et al., 2014; Genot et al., 2013; Nuchi et al., 2001; Østdal et al., 2002; Salminen et al., 2010). In summary, even though the intrinsic oxidative reactivity of emulsifiers is probably a very important parameter in oxidative stability of emulsions, it is far from understood. When it comes to proteins, recent efforts have been reported to consider this aspect better, which is also covered later in this chapter (Berton-Carabin et al., 2014; Berton et al., 2011b; Yang et al., 2020, 2023).

6.3.4 Oxidation in oil droplets of different sizes

The formation of hydroperoxides and aldehydes in the colloid mill-made emulsions stabilised by Tween 20 proceeded faster than in monodisperse emulsions made with microfluidics (Figure 6.4a & b). We further observed that the decrease in red fluorescence seemed to be slightly faster in small droplets (Figure 6.4c & d). This is in line with the results from Chapters 4 and 5, where we found that small oil droplets oxidise faster than large ones, and that lipid oxidation products are overrepresented in the smallest droplets present in the emulsion. Therefore, the faster lipid oxidation for the colloid mill-made emulsion can be ascribed to its smaller average droplet size (Figure 6.1). For the WPI-stabilised emulsions, the colloid mill-made emulsion also oxidised faster than the microfluidic-made one (Figure 6.5a & b), which we also ascribe to the faster oxidation of smaller droplets (Figure 6.5c & d, Figure 6.1).

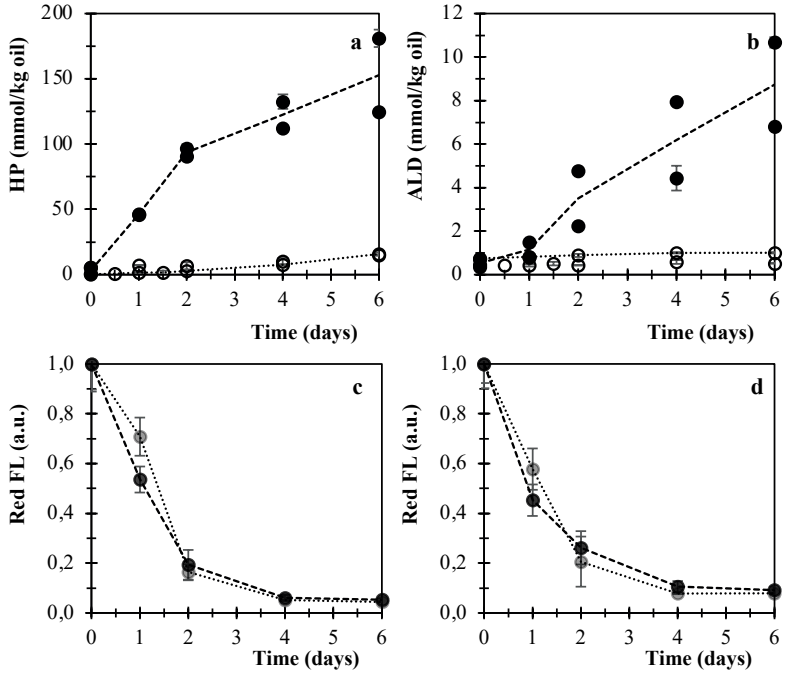

Figure 6.4. Formation of hydroperoxides (HP) (a) and aldehydes (ALD) (b); and decrease of red fluorescence (FL) by BODIPY 665/676 (c & d) over incubation in Tween 20-stabilised emulsions prepared with microfluidics (○) or by colloid mill (●). Symbols in c & d correspond to droplet sizes of: 1-2 µm (grey) and 4-5 µm (black), both from the colloid mill-made emulsion. Error bars (sometimes within the symbol) for a & b denote standard deviations of two measurements on independently incubated samples originating from the same emulsion. The outcome of independent replicates are shown as separate data points (a & b). For c & d, error bars denote standard deviations of many droplets from two independently incubated samples that originated from the same emulsion, and c & d show the results of independently prepared emulsions separately. The lines between the markers guide the eye.

For the Tween 20-stabilised emulsion, the difference in the lipid oxidation course between the emulsions made with the colloid mill or with microfluidics was larger than for the WPI-stabilised emulsions (Figure 6.4a & 6.5a). This is probably caused by the larger difference between droplet sizes for the Tween 20-stabilised emulsions compared to the WPI-stabilised emulsions (Figure 6.1). Moreover, in the Tween 20-stabilised emulsion more very small droplets that oxidise rapidly (Chapter 5) were present than in WPI-stabilised emulsion (Figure 6.1, Figure A6.4). The faster oxidation of smaller droplets is in line with some (Chapter 4 & 5) (Li et al., 2019; Yang et al., 2020), but not all other studies conducted on the effect of droplet size on lipid oxidation (Berton-Carabin et al., 2014), as discussed in detail in Chapter 4. In summary, both the WPI- and Tween 20-stabilised polydisperse emulsions oxidised in a highly heterogeneous way. This is also reflected in the fluorescence signal to some extent, as discussed next.

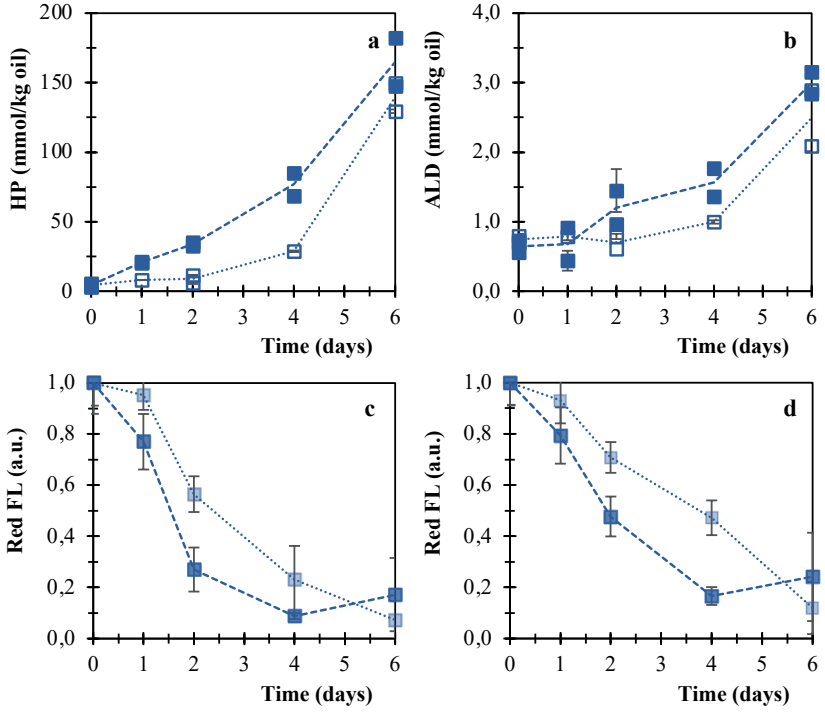

Figure 6.5. Formation of hydroperoxides (HP) (a) and aldehydes (ALD) (b); and decrease of red fluorescence (FL) by BODIPY 665/676 (c) over incubation in WPI-stabilised emulsions, prepared with microfluidics (□) or by colloid mill (■). Symbols in c & d correspond to droplet sizes of: 1-2 µm (light blue) and 4-5 µm (dark blue); both from the colloid mill-made emulsion. Error bars (sometimes within the symbol) for a & b denote standard deviations of two measurements on independently incubated samples originating from the same emulsion. The outcome of independent replicates are shown as separate data points. For c & d, error bars denote standard deviations of many droplets from two independently incubated samples that originated from the same emulsion, and c & d show the results of independently prepared emulsions separately. The lines between the markers guide the eye.

6.3.5 Spatial heterogeneity of lipid oxidation

We observed similar fluorescence intensity in Tween 20-stabilised emulsion droplets of a similar size at every time point (as seen from the error bars of the symbols ○/● in Figure 6.3c & Figure 6.4c & d). For WPI-stabilised emulsions, large differences of BODIPY 665/676 red fluorescence were observed for droplets of a similar size for some timepoints (Figure 6.6, and visualised by error bars of the symbols □/■ in Figure 6.3c & Figure 6.5c & d). This indicates that even when WPI-stabilised droplets have the same size, their oxidation level can differ greatly. This could possibly be linked to protein oxidation because protein and lipid oxidation have been shown to be intertwined previously (Berton et al., 2012). The interplay of lipid and protein oxidation at the interface was further studied with CLSM, and discussed in the next section (section 6.3.6).

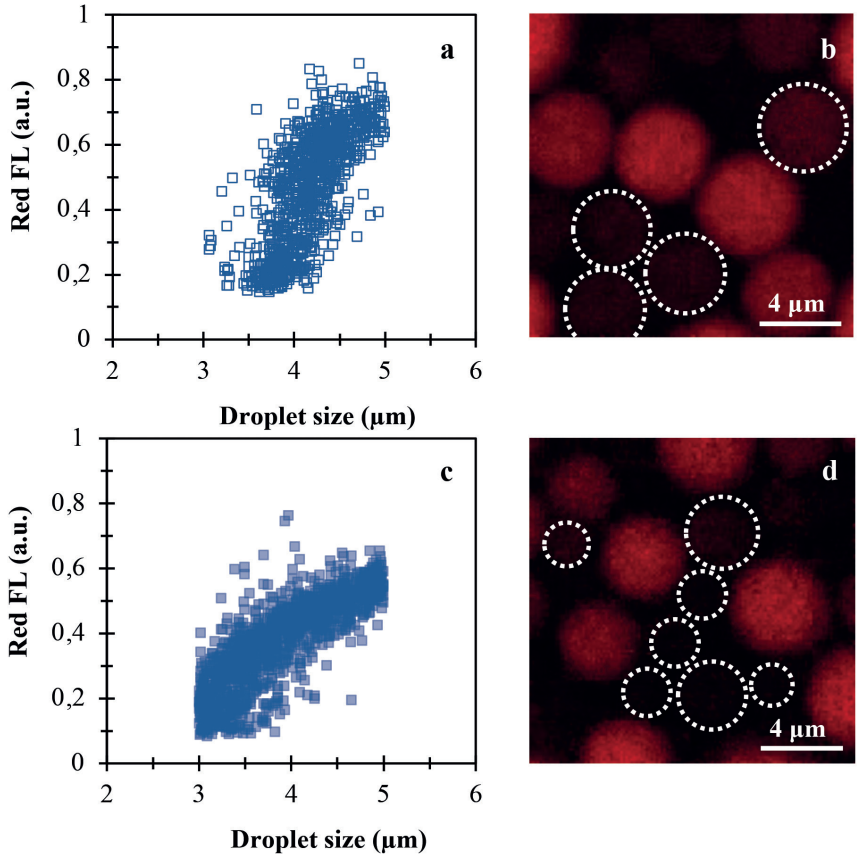

Figure 6.6. (a & c) Red fluorescence (FL) by BODIPY 665/676 against the droplet size (between 3 and 5 µm) for WPI-stabilised emulsions after 4 days of incubation prepared either with microfluidics (a) or with a colloid mill (b). (b & d) CLSM images showing the fluorescence intensity between droplets of similar sizes after 4 days of incubation (d), in a microfluidic-made emulsion (b) and a colloid mill-made emulsion (d).

In a heterogeneously oxidising emulsion, the rapidly oxidising droplets can affect lipid oxidation in slowly oxidising droplets in multiple ways. One of the possibilities is that rapidly oxidising (small) droplets deplete the available oxygen and thereby hinder the hydroperoxide formation in slowly oxidising (larger) droplets. In these experiments, after 6 days the red fluorescence was close to zero for the WPI-stabilised emulsions prepared with microfluidics (Figure 6.3c), whereas only ~ 120 mmol of O_2 per kg oil (out of ~ 450 mmol/kg oil; the maximum amount that may form given the available oxygen in the headspace of the tubes) were consumed by the formation of lipid oxidation products (Figure 6.3a). In principle, a lower amount of oxygen available for the reaction will reduce the reaction rate (Schroën et al., 2022a). However, given the fact that only ~ 25% of the available oxygen was consumed, this is not expected to have been a major factor during the fluorescence experiments. On the other hand, rapidly oxidising (small) droplets have been postulated to promote lipid oxidation in slowly oxidising droplets by the transfer of reactive lipid oxidation products (Laguerre et al., 2017, 2020; Li et al., 2020). Such phenomena were not expected to play a major role in the WPI-stabilised emulsions because lipid oxidation is already initiated effectively by the formation of radicals from AAPH decomposition. In a recent study from our group, we found that only relatively small and hydrophilic lipid oxidation products, such as 4-hydroperoxy-2-nonenal, can transfer between droplets, although they did not systematically increase the formation of lipid oxidation products in other droplets (ten Klooster et al., 2022). Under other conditions, the transfer of reactive lipid oxidation intermediates might result in a faster oxidation in clean droplets. For example, in a study on BODIPY 665/676 oxidation in medium chain triglyceride (MCT) oil droplets, it was found that oxidising rapeseed oil droplets, present in the same emulsion, increased BODIPY 665/676 oxidation in the MCT oil droplets (Li et al., 2020). When combining these findings, it could be that in the study of Li et al., 4-hydroperoxyenals transferred from the oxidising rapeseed oil droplets to the MCT oil droplets, with the former acting as a potential source of peroxyl radicals that led to an increased BODIPY oxidation (Li et al., 2020).

6.3.6 Co-localisation of lipid- and protein oxidation in WPI-stabilised emulsions

It has been reported that proteins at the interface can either counteract or promote lipid oxidation (Berton et al., 2012), but so far, these conclusions have been drawn using data obtained from 'bulk' emulsions, whereas little is known about local effects (Yang et al., 2020, 2023). Here, we used CAMPO-AFDye 647 (Yang et al., 2023) and C11-BODIPY because their emission wavelengths do not overlap, which enables us to co-localise protein and lipid oxidation, respectively. C11-BODIPY has the same core structure as BODIPY 665/676, but contains only

one phenylbutadiene moiety, which probably makes it less sensitive to lipid oxidation (Naguib, 2000; Raudsepp et al., 2014).

To highlight CAMPO-AFDye 647 accumulation at the droplet interface, the raw image data was filtered (section 6.2.3), which results in co-localised images of oxidised lipids, which is indicated by a blue colour, and oxidised proteins, which is indicated by red/pink-coloured spots (Figure 6.7). The images of the colloid mill-made emulsion show heterogeneous spots of CAMPO-AFDye 647 accumulation at the interface. This could indicate that proteins at the interface oxidise in a heterogeneous way, which seems to be the case both between droplets of similar sizes and also on the level of one droplet. For the monodisperse WPI-stabilised emulsions, only little CAMPO-AFDye 647 accumulation took place compared to the polydisperse emulsions (Figure 6.7c). This indicates that in these monodisperse emulsions, little protein oxidation took place at the interface, which might be caused by the lower lipid oxidation of the microfluidic-made emulsions compared to the colloid mill-made emulsions during the first few days of incubation. This may have affected the course of protein oxidation, leading to less CAMPO-AFDye 647 accumulation. Alternatively, the mildness of the microfluidic emulsification could also have played a role.

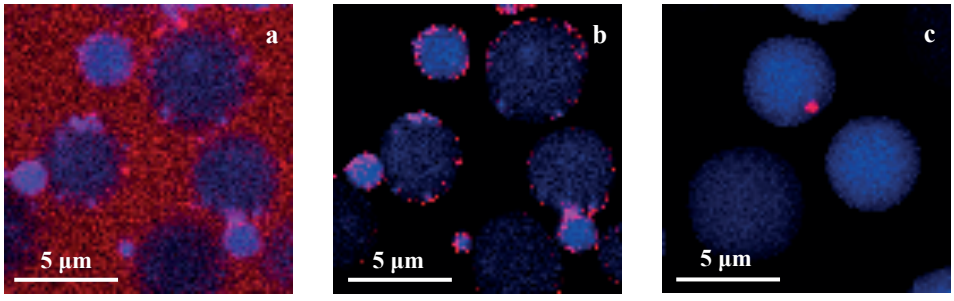

Figure 6.7. (a) Raw image data of colloid mill-made emulsions stabilised by WPI. (b & c) Filtered images of colloid mill- (b) and microfluidic-made emulsions (c). Red indicates CAMPO-AFDye 647 fluorescence, which increases with protein oxidation, and blue C11-BODIPY fluorescence, which increases with BODIPY oxidation.

To investigate the interplay between protein and lipid oxidation, the average fluorescence intensity from C11-BODIPY was determined to quantify lipid oxidation, and the fluorescence by CAMPO-AFDye 647 was summed and next divided by the circumference to quantify protein oxidation. This quantification did not just result in a large variability of lipid oxidation as discussed in the previous section, but also in an extreme variability for protein oxidation due to its heterogeneity. This complicates linking droplet size to protein oxidation and linking protein oxidation to lipid oxidation. Even though this data does not

allow us to draw conclusions on these aspects, it would be logical that for small droplets protein oxidation is highest because: it has been shown that especially proteins at the oil-water interface oxidise (Berton et al., 2012), small droplets oxidise particularly fast (Figure 6.5c & d), and small droplets have a large oil-water interface, where proteins and lipids can interact. What remains is that our data show that both lipid oxidation and protein oxidation proceed in highly heterogeneous fashions in WPI-stabilised emulsions, which cannot be shown with bulk emulsion measurements.

6.4 Conclusions

In this chapter, the decrease in red fluorescence from BODIPY 665/676 oxidation was used to unravel droplet size-dependent spatial heterogeneity of lipid oxidation in Tween 20- and WPI-stabilised emulsions. For highly monodisperse WPI-stabilised emulsions, a rapid increase in hydroperoxides occurred simultaneously with a decrease in red fluorescence. A different trend for Tween 20-stabilised emulsions was observed, where red fluorescence rapidly decreased, whereas the formation of hydroperoxides was slow. How to link these results is not trivial, but this indicates that caution is needed when fluorescence results from different emulsion systems are compared.

For emulsions prepared with Tween 20 and WPI as emulsifiers, lipid oxidation increased with decreasing droplet sizes. This resulted from comparing the formation of lipid oxidation products in monodisperse microfluidic-made emulsions with polydisperse colloid mill-made emulsions and when comparing droplets present within the same emulsion, as shown by BODIPY 665/676 oxidation. For WPI-stabilised emulsions, also a major difference in oxidation status, as indicated by red fluorescence, between droplets of the same size was observed. This could either be a result of coincidence that in one droplet more lipid oxidation was initiated or due to heterogeneity of protein oxidation at the interfacial layer, which is known to be intertwined with lipid oxidation. Heterogeneous protein oxidation was shown to occur by the heterogeneous accumulation of CAMPO-AFDye 647 at the interface. This heterogeneity was not just observed at the level of droplets, but also at the level of the same interface of individual droplets. The intrinsic reactivity of emulsifiers (both proteins and surfactants) is probably of importance for the oxidative stability of emulsions, but it is far from completely understood.

These insights contribute to our understanding of locally proceeding oxidation events, which may lead to improved oxidative stability of ‘bulk’ emulsions.

6.5 Appendix

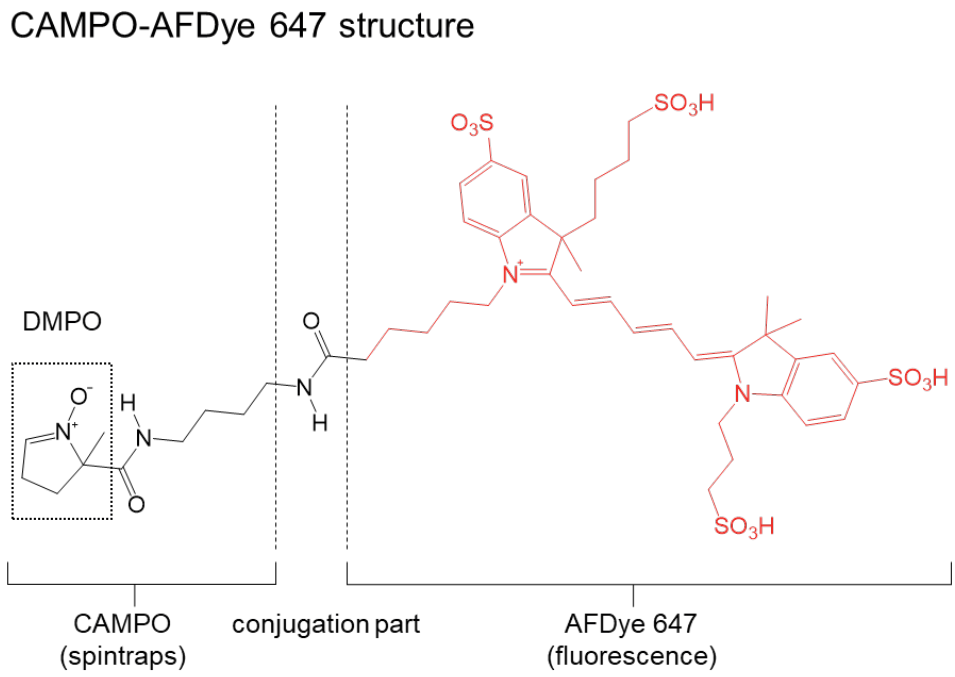

Figure A6.1. The chemical structure of the fluorescently labelled spin trap (CAMPO-AFDye 647). CAMPO, which is a derivate of DMPO, is conjugated with the fluorescent dye, AFDye 647.

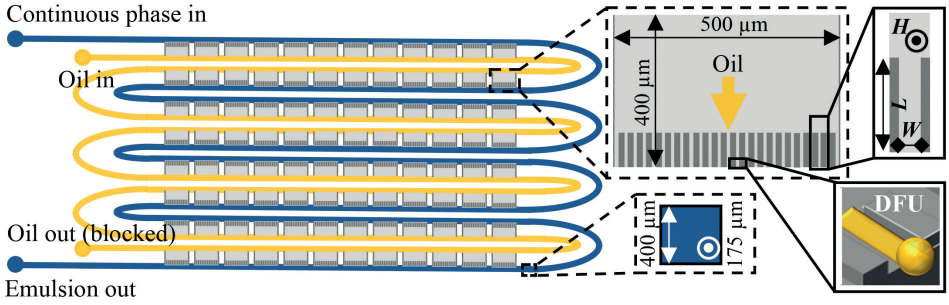

Figure A6.2. Top-view design of the Upscaled Partitioned EDGE chips used in this research. The blue 'twisted road' channel is the continuous phase channel, and the yellow 'twisted road' channel is the to-be-dispersed phase channel. The grey rectangular areas in between these channels are the main plateaus that contain the micro-plateaus with the Droplet Formation Units (DFU). A 3D representation of a DFU is shown in the right lower corner, showing oil – in yellow –, being pushed out of the DFU and forming a droplet ready to detach. This illustration is not to scale, only 12 out of the 42 main plateaus are shown per row.

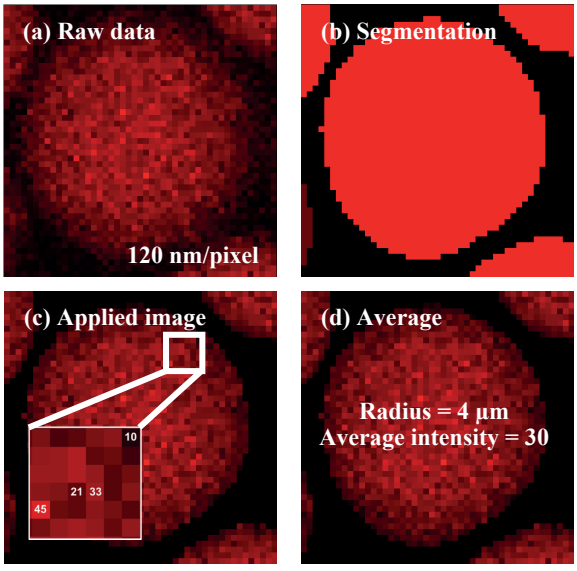

(e) Final data

Droplet	Diameter (µm)	Average Intensity (a.u.)
1	3	23
2	3.2	25
3	2.5	20
-	-	-
1300	4.0	25

Figure A6.3. (a) Raw image data were acquired using CLSM as described in the main text (section 6.2.3 & 6.2.4). The pixel size was 120 nm (512 · 512 pixels for 61.63 · 61.63 um). Images of two channels (ex 640 nm and ex 561 nm) were first summed and subsequently used for the segmentation. (b) The masks of oil droplets were acquired by applying 2D StarDist to the summed images (ex 561 + ex 640 nm). (c) Next, masks and raw data were multiplied using MATLAB R2021b. (d) The average intensity in the droplet was used for further analyses, and the size of the droplets was calculated from the counts of pixel numbers. (e) Final data was obtained as a list of droplet numbers and radii with the average intensity. For comparing the data obtained under different conditions, the initial intensity was set to 1 and all data points were divided by the maximum intensity to obtain a normalised intensity.

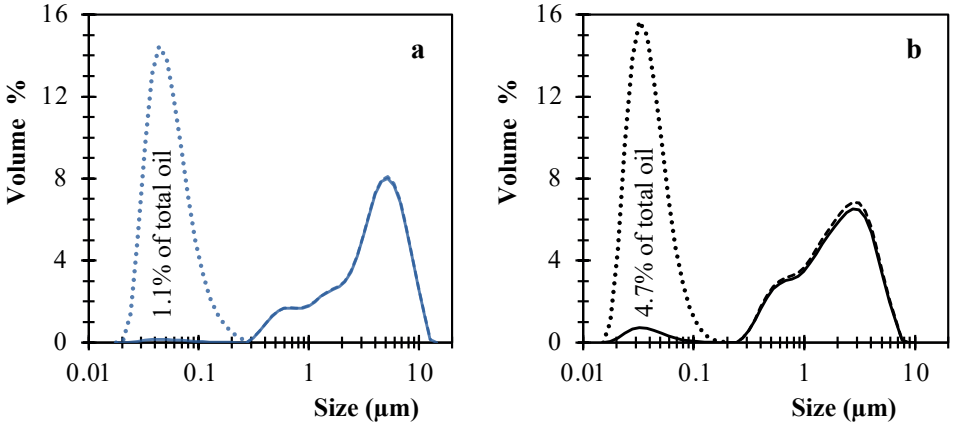

Figure A6.4. Droplet size distributions of the colloid mill-made emulsions with WPI (a, blue) or with Tween 20 (b, black). Lines represent different samples and measurement techniques: DLS on the subnatant samples (dotted line), SLS on whole emulsion sample (dashed line), and the combination of those measurements (solid line), which was based on the oil content in the subnatant (text in the graphs) (section 6.2.4).

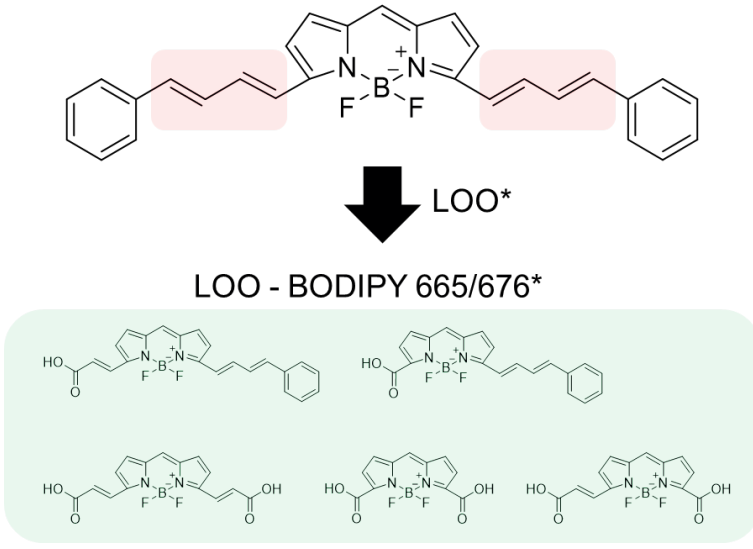

Figure A6.5. The native structure of BODIPY 665/676 and its possible modified structures upon oxidation.

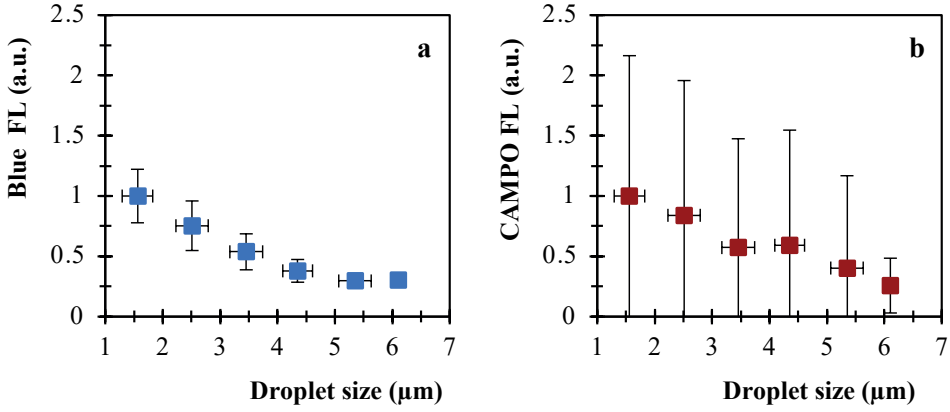

Figure A6.6. Blue fluorescence (a) from C11-BODIPY and CAMPO-AFDye 647 fluorescence (b) against droplet size. The higher the fluorescence, the higher the BODIPY (lipid) (a) or CAMPO (protein (b) oxidation. Error bars denote standard deviations. Data from one independently prepared emulsion is shown.

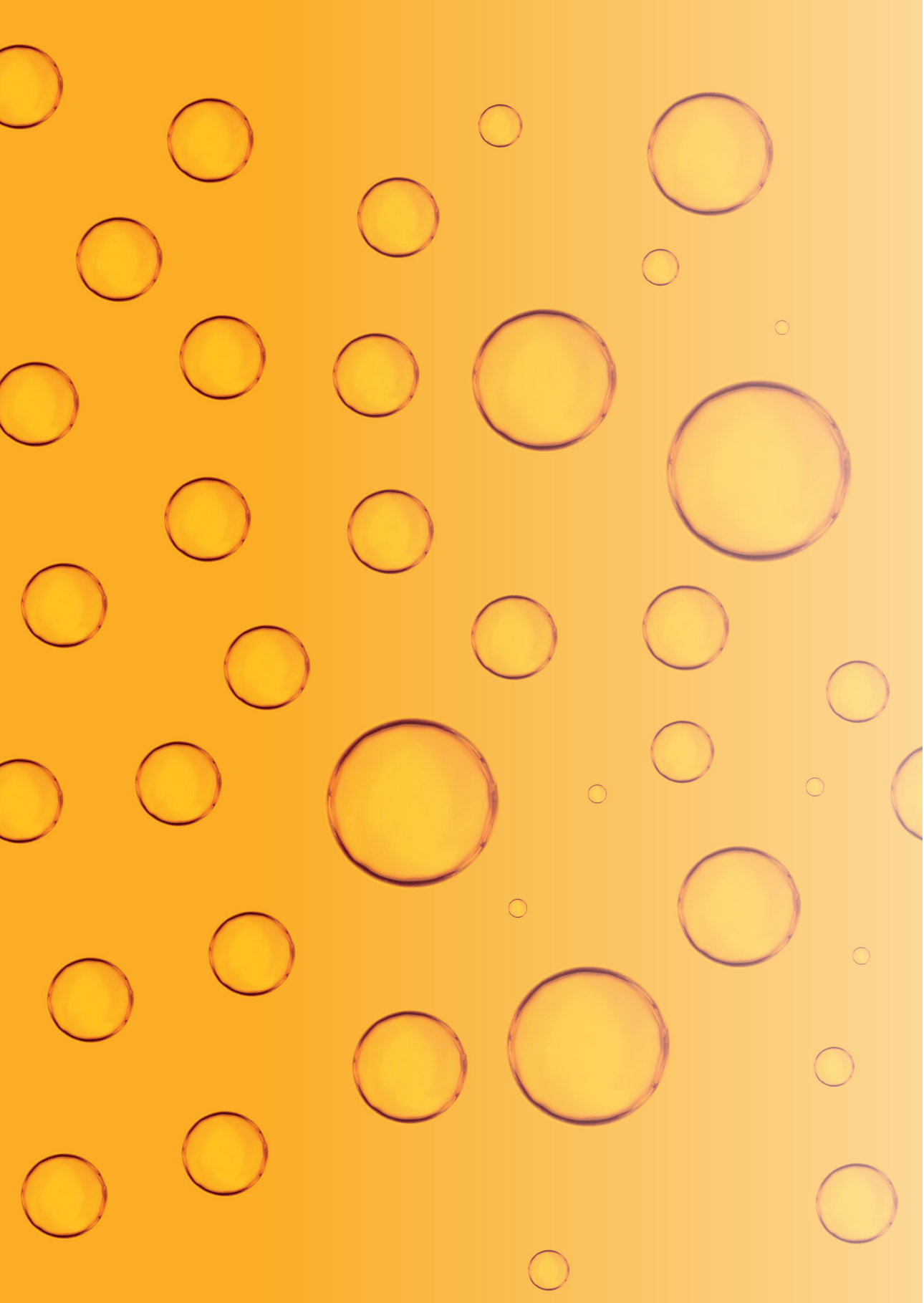

Chapter 7

Lipid oxidation products in model food emulsions: do they stay in or leave droplets, that's the question

This chapter was published as:
S. ten Klooster, K. Schroën, C. Berton-Carabin: *Lipid oxidation products in model food emulsions: do they stay in or leave droplets, that's the question*, Food Chemistry 405 (2023), 134992.

Abstract

Lipid oxidation is a major factor limiting the shelf life of food and other emulsion products. In this chapter, we explore which lipid oxidation products may transfer between oil droplets in model food emulsions stabilised by excess amounts of surfactant, and whether this affects the overall reaction. No significant differences in concentrations of triglyceride-bound hydroperoxides were found before and after mixing 'clean' oil droplets with pre-oxidised ones. Shorter and more hydrophilic lipid oxidation products, such as 4-hydroperoxy-2-nonenal and 2,4-decadienal, were found to equilibrate between oil droplets within 30 minutes. Adding exogenous 4-hydroperoxy-2-nonenal to an emulsion led to overall higher lipid oxidation values, although this effect was not systematic nor instantaneous. Therefore, it may be questioned whether transfer and subsequent initiation are always relevant for oxidising emulsion systems. In future research, this question should be addressed for complex emulsions that are closer to real-life food products.

Introduction

Food or biobased products containing polyunsaturated fatty acids (PUFAs) are prone to lipid oxidation, which has a negative impact on the quality of the products (Schaich, 2005). This is particularly marked in oil-in-water (O/W) emulsions, where the large amount of oil-water interface allows contact between PUFAs and water-soluble prooxidants, such as metal ions (Berton-Carabin et al., 2014). Lipid oxidation is not only considered the main factor in determining the shelf life of food emulsions (e.g., mayonnaise), but can also be problematic in other biobased systems (pharmaceuticals [for example mRNA vaccines (Schoenmaker et al., 2021)], cosmetics, etc.). Accordingly, lipid oxidation in emulsions has received a lot of attention in the last two decades.

Besides the chemically complex cascade of reactions that occur during lipid oxidation, it has been proposed that the overall course of the reaction could be affected by transfer of lipid oxidation products between oil droplets, which could be facilitated through surfactant micelles (Laguerre et al., 2017). A well-known mechanism that may point in the direction of such a transfer is compositional ripening; in emulsions containing droplets made of different pure alkanes, complete exchange of the droplets' core materials usually takes place within days. This phenomenon has been reported for emulsions stabilised with surfactants or proteins, which are usually present in excess (McClements et al., 1992; Samtlebe et al., 2012; Villeneuve et al., 2021). The exchange of other lipid or lipophilic components between oil droplets has also been studied, as summarised in Table 7.1. If such a transfer happens in oxidising food emulsions, this may cause 'clean' (i.e., non-oxidised) oil droplets to become contaminated by lipid oxidation intermediate products from neighbouring oxidising droplets (Laguerre et al., 2020).

Lipid oxidation intermediates such as hydroperoxides can react with metal ions at the oil-water interface, forming reactive peroxyl ($LOO^{\bullet}$) and alkoxyl ($LO^{\bullet}$) radicals that rapidly re-initiate the lipid oxidation radical chain reaction (Reaction 7.I – 7.IV) (Schaich, 2005). A recent hypothesis suggests that such transfer and 'secondary initiation' pathways are the main mechanisms for propagation of lipid oxidation (Laguerre et al., 2017, 2020).

$$LOOH + Fe^{3+} \rightarrow LOO^{\bullet} + H^{+} + Fe^{2+} \quad (7.I)$$

$$LOOH + Fe^{2+} \rightarrow LO^{\bullet} + OH^{-} + Fe^{3+} \quad (7.II)$$

$$LO^{\bullet}/LOO^{\bullet} + LH \rightarrow LOH/LOOH + L^{\bullet} \quad (7.III)$$

$$L^{\bullet} + O_2 \rightarrow LOO^{\bullet} \quad (7.IV)$$

Another recent paper showed that a lipophilic fluorescent dye (BODIPY 665/676), present in medium chain triglyceride (MCT) emulsion droplets, oxidises faster when oxidising vegetable oil droplets are present in the same emulsion (Li et al., 2020). This may suggest that lipid oxidation can spread from oxidising droplets to initially clean ones. It is, however, unclear which components would be responsible for this, and whether the kinetics of the cascaded reaction may cause such an effect.

In this chapter, we aim to unravel which lipid oxidation products may transfer between oil droplets in a model food emulsion, and whether transferred molecules would substantially promote lipid oxidation. To do so, an emulsion prepared with high-density, pre-oxidised oil was mixed with an emulsion made with regular, (low-density) clean oil. Both emulsions were mixed and incubated. Over time, the droplets that were made with oxidised oil were physically separated from the droplets that were made with clean oil, which was owed to the density difference between both starting oils. Next, a range of lipid oxidation products were quantified with nuclear magnetic resonance (^{1}H NMR) in the initially clean droplets. In addition, the potential lipid oxidation-initiating effect of the oxidation product 4-hydroperoxy-2-nonenal was investigated.

Table 7.1. Overview of studies in which the exchange of one or multiple lipid or lipophilic molecules between oil droplets was investigated.

Article	Studied molecule(s) for transfer (% of oil phase)	Oil phase (% of total emulsion)	Continuous phase (% of continuous phase)	Results as interpreted in the papers.
(Nuchi et al., 2002)	4 wt.% peroxidised linoleic acid / methyl linoleate / trilinolein	10% oil (96 wt.% corn oil, 4 wt.% peroxidised lipids)	1 wt.% Brij 76, 0.1 mM EDTA	All three types of lipid hydroperoxides were solubilised out of the lipid droplets into the continuous phase containing Brij 76 micelles, in the order of linolenic acid > methyl linoleate ~ trilinolein.
(Li et al., 2020)	1 wt.% 2,4-decadienal	0.2 wt.% oil (33% brominated vegetable oil, 66% MCT oil)	0.14 wt.% SDS	This aldehyde equilibrated within 10 minutes between MCT oil droplets even without surfactant micelles (SDS concentration was 0.5 mM, CMC of SDS is 8 mM).
(Cui et al., 2019)	Hydroperoxides of stripped walnut oil	5 wt.% walnut oil	0.25 wt.% SDS, with 0 / 0.3 / 0.6 wt.% NaCl	Initially, ± 15% of the hydroperoxides were solubilised by SDS micelles into the aqueous phase, and this increased to 35% upon increasing the NaCl concentration to 0.3 wt.%.
(Raudsepp et al., 2014c)	Medium chain triglyceride oil	82 wt.% linseed oil / MCT oil	egg yolk (12 wt.%), mustard (2 wt.%), vinegar (2 wt.%), lemon juice (2 wt.%)	No mixing of the droplets' contents occurred over 2 days of incubation.

(McClements et al., 1992)	Hexadecane / octadecane	10 wt.% hexadecane / octadecane	2 wt.% Tween 20	Complete transfer of the oils (all droplets containing 50% of both oils) in the droplets took over 7 days. The rate of exchange increased with additional surfactant.
(McClements et al., 1993)	Hexadecane / octadecane	10 wt.% hexadecane / octadecane	0.5 / 2.5 wt.% whey protein isolate / casein	Oil exchange occurred with both proteins and increased with protein concentration, but was incomplete after 29 days.
(Samtlebe et al., 2012)	Tetradecane / eicosane	10 wt.% oil	1 / 2 wt.% Tween 20	The mass transfer of n-tetradecane to n-eicosane occurred over the course of several hours. The rate of dissolution increased with the tetradecane droplet to eicosane emulsion ratio and with surfactant concentration.
	Tetradecane / eicosane	10 wt.% oil	1 / 2 wt.% sodium caseinate	There was some change in the alkane melting peak shape, but no evidence of substantial mass transfer in the time allowed regardless of the concentration of caseinate used.
	Caprylic/capric triacylglycerol / palm stearin	10 wt.% oil	1 wt.% sodium caseinate	The rate of mass transfer was slower in this triacylglycerol system (after 24 days still no equilibration) than for the hydrocarbon system (see above).
(Richards et al., 2002)	Propyl gallate / tertiary butyl-hydroquinone / butylated hydroxytoluene	5 wt.% hexadecane / olive oil / salmon oil	0.1 mM EDTA, 0.5-3 wt.% Brij 700	The nonpolar antioxidant butylated hydroxytoluene was solubilised less than the more polar antioxidants tertiary butylhydroquinone and propyl gallate. Solubilisation increased with added Brij 700 (after emulsification).
(Keller et al., 2016)	Vanillic acid	30 wt.% oil (not emulsified)	2 mmol vanillic acid/kg water, either with or without Tween 40 (0.9 / 3.6 wt.%)	3/4 of the vanillic acid partitioned in the aqueous phase and 1/4 in the oil phase for the two-phase non-emulsified system without Tween 40. In the presence of Tween 40, the major part of vanillic acid (90%) was found in the aqueous phase.
(Raudsepp et al., 2016)	5.7 μM DTBP (di-tert-butyl peroxide)	30 wt.% stripped sunflower / MCT oil	0.72 wt.% Tween 20, sodium acetate-acetic acid buffer (pH = 4.65)	DTBP radical life-times were short; thus, the radical chain reactions progressed only up to ~60 μm from the initiation site. The radical reactions were not able to cross the interfaces and progress to neighbouring oil droplets. The propagation and diffusion of radicals was dependent on the degree of unsaturation of the oil, and the viscosity of the lipid medium.
(Raudsepp et al., 2014b)	13 mM AMVN (2,2′-azobis(2,4-dimethyl) valeronitrile)	30 wt.% stripped sunflower / MCT oil	0.72 wt.% Tween 20, sodium acetate-acetic acid buffer (pH = 4.65). Sodium acetate buffer (pH 4.65)	Radicals can be transferred between oil droplets and lipid autoxidation can spread between neighbouring oil droplets.
(Banerjee et al., 2018)	Propagation of lipid oxidation rection	70 wt.% cod liver oil	4.7 wt.% sodium caseinate	Oxidation reactions readily propagate through the interior of the oil droplet. The oxidation of one droplet does not appear to spread to an adjacent and neighbouring droplet.

7.2 Materials and methods

7.2.1 Materials

Rapeseed oil (kindly supplied by Unilever, Wageningen, the Netherlands) and a mixture of brominated oil (Spectrum Chemical, Gardena, USA) and n-hexane (Actu-All Chemicals, Oss, the Netherlands) (5:1 v/v) were stripped with alumina powder (MP112 EcoChromet ALUMINA N, Activity: Super I, Biomedicals) to remove impurities and endogenous antioxidants (in particular tocopherols) (Berton et al., 2011a); n-hexane was then evaporated from the brominated oil by a continuous flow of nitrogen, while the mixture was stirred at 40 °C, until constant weight was reached. Sodium phosphate monobasic dihydrate and sodium phosphate dibasic dihydrate (Sigma-Aldrich, Zwijndrecht, the Netherlands) were used to make the phosphate buffer (pH 7.0). 2-propanol was obtained from Actu-All Chemicals (Oss, the Netherlands). Deuterated chloroform and dimethylsulfoxide ($CDCl_3$ and DMSO-d6) were purchased from Euriso-top (Saint-Aubin, France). Ethylenediaminetetraacetic acid calcium disodium salt (EDTA) and Tween 20 were purchased from Sigma Aldrich (Sigma-Aldrich, Zwijndrecht, the Netherlands). 4-Hydroperoxy 2-nonenal (purity ≥ 95%) was obtained from Cayman Chemical (Ann Arbor, USA), and *trans*,*trans*-2,4-decadienal (purity ≥ 97%) was obtained from Fisher Scientific (Roskilde, Denmark). Ultrapure water (18.2 MΩ) was used for all experiments and prepared using a Milli-Q system (Millipore Corporation, Billerica, MA, USA).

7.2.2 Emulsion preparation

Preparation of the oil

50 g of stripped rapeseed oil were incubated in a 250-mL bottle with the lid loosely put on the bottle in an oven at 40 °C and stirred for 7 days at 100 rpm. After 7 days, the oxidation level was measured (see section 7.2.5). If the oxidation level was lower than desired (< 60 mmol hydroperoxides/kg oil), the incubation was extended, until the desired level was reached. Afterwards, the oxidised oil was collected and stored with a nitrogen blanket at −80 °C until further use. For the independent replicates, the same batch of pre-oxidised oil was used. For the experiments with 0.5 and 2 wt.% Tween 20, a different batch of pre-oxidised oil was used. The pre-oxidised rapeseed oil was mixed with stripped brominated oil in a 65:35 ratio (w/w).

Emulsion preparation, incubation and sample taking

Transfer experiment with pre-oxidised oil

Either 0.5 or 2 wt.% of Tween 20 was dissolved in a 10-mM phosphate buffer (pH 7.0) and stirred for 15 min at 300 rpm. Next, EDTA (75 mg/kg continuous

phase) was added, and the solution was stirred for 15 min. A coarse emulsion was made by adding 10 wt.% of either the stripped rapeseed oil (for the clean emulsion) or the mixture of pre-oxidised oil and brominated oil (for the pre-oxidised emulsion) (see section above) to the continuous phase, and high-speed stirring was applied at 11,000 rpm for 1 min with a rotor-stator homogeniser (Ultra-turrax IKA T18 basic, Germany) (Figure 7.1a & b). To obtain the final emulsion, the coarse emulsions were homogenised by passing them three times through a high pressure M-110Y Microfluidizer (Microfluidics, Massachusetts, USA), equipped with a Y-shaped interaction chamber (F12Y; minimum internal dimension: 75 µm), at 600 bars. The clean emulsion was mixed with the pre-oxidised emulsion in a 1:1 ratio (w/w) (Figure 7.1c). Finally, 12 mL of mixed emulsion were added to 20-mL headspace vials, which were treated with a nitrogen blanket to minimize further oxidation. The tubes were rotated horizontally at 2 rpm in a dark oven at 25 °C for up to 14 days.

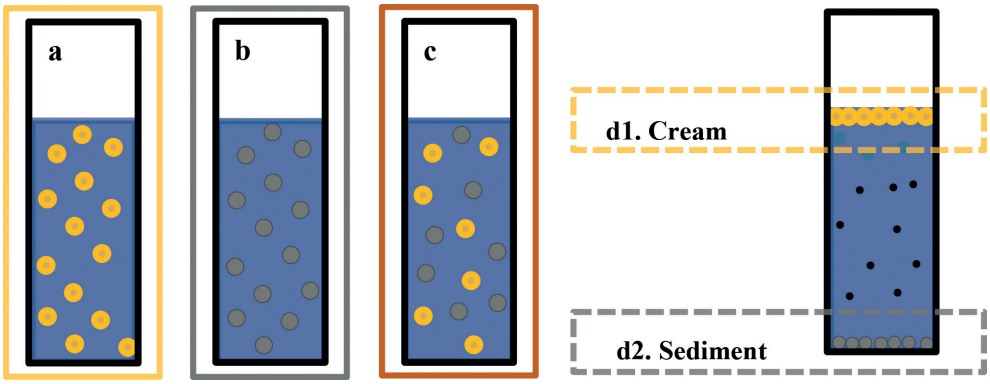

Figure 7.1. Schematic representation of the samples that were prepared and analysed for this research: emulsion prepared with clean oil (a), emulsion prepared with pre-oxidised oil (or spiked with exogenously added aldehydes) (b), and a 1:1 ratio (w/w) emulsion of a and b that was incubated (c). Over time, samples were taken from emulsion a and c, and emulsion c was centrifuged to collect the cream (d1) containing the initially clean droplets and sediment (d2) containing the pre-oxidised droplets.

Transfer of exogenously added aldehydes

Tween 20 (2 wt.%) was dissolved in a 10-mM phosphate buffer (pH 7.0) and stirred for 15 min at 300 rpm. Next, EDTA (75 mg / kg continuous phase) was added, and the solution was stirred for 15 min. For this set of emulsions, the used oil was either the stripped rapeseed oil for the 'clean' droplets, or for the 'supplemented' droplets, a mix of stripped rapeseed oil (65 wt.%) and stripped brominated oil (35 wt.%) with 0.2 mmol 4-hydroperoxy-2-nonenal or 2,4-decadienal per kg oil (commercial aldehydes, added exogenously to the oil). The emulsion was prepared as described in section above. The clean emulsion

was mixed with the emulsion containing the exogenous aldehyde in a 1:1 ratio (w/w). Sample taking was performed immediately after carefully mixing the two emulsions, and this was done as described in the section below.

Sample taking procedure for transfer experiments
Samples from the mixed emulsion were taken at carefully selected time points, and the initially clean droplets were separated from the initially oxidised droplets by centrifuging 20 mL of emulsion in 50-mL tubes at 28,000×g for 30 min at 4 °C, which was based on previous research (Li et al., 2020). The liquid in between the thick cream and thick sediment was discarded, and a small amount (~ 0.2 g) of cream or sediment was transferred with a spatula into 15-mL centrifuge tubes and redispersed in 1.5 mL ultrapure water (Figure 7.1d). Next, the samples were treated with a nitrogen blanket and stored at −80 °C until further use (minimally 48 h, maximally 20 days) (Merkx et al., 2018; ten Klooster et al., 2022d).

Effect of exogenously added 4-hydroperoxy-2-nonenal on lipid oxidation
Tween 20 (0.5 wt.%) was dissolved in ultrapure water and stirred for 30 min at 300 rpm. Stripped rapeseed oil was added with or without 0.2 mmol 4-hydroperoxy-2-nonenal/kg oil. A coarse emulsion was then made by mixing the oil (10 wt.% of final emulsion) and aqueous phases with a high-speed stirrer at 11,000 rpm for 1 min with a rotor-stator homogeniser (Ultra-turrax IKA T18 basic, Germany). The fine emulsion was prepared by passing the coarse emulsion through a lab scale colloid mill with gap width of 0.32 mm (IKA Magic Lab, Staufen, Germany), operating for 1.5 min at 26,000 rpm, and the colloid mill was cooled with water at 4 °C. Headspace vials (20 mL) containing 2 mL emulsion were rotated horizontally at 2 rpm in a dark oven at 25 °C for up to 14 days. Samples were taken at selected time points, treated with a nitrogen blanket, and stored at −80 °C until further use (minimally 48 h, maximally 20 days) (Merkx et al., 2018; ten Klooster et al., 2022d).

7.2.4 Droplet size measurements
The oil droplet size of the emulsions was measured by static light scattering (SLS) (Malvern Mastersizer 3000, Malvern Instruments Ltd., Malvern, Worcestershire, UK), using a refractive index of 1.465 for the dispersed phase and 1.33 for the dispersant (water); and an absorption index of 0.01. The droplet sizes for all the prepared emulsions remained constant over an incubation period of 14 days (Figure A7.1). The droplet size distributions in the creamed layers were always very similar to the droplet size distributions of the clean emulsions (prior to mixing), which confirms that the clean droplets can be effectively isolated from

the mixed system (Figure A7.2 & A7.3).

The continuous phase and the smallest oil droplets were separated from the larger oil droplets by centrifuging 2 mL of emulsion at 20,000×*g* for 60 min in a 2-mL Eppendorf tube and collecting ~ 0.3 mL of the subnatant. The size of the colloidal structures present in this subnatant were measured by dynamic light scattering (DLS) (Zetasizer Nano ZS, Malvern Instruments Ltd., Malvern, Worcestershire, UK). The refractive index was 1.47 for the dispersed phase, and the absorbance was 0.01.

7.2.5 Lipid oxidation measurements

Lipid extraction

The extraction was performed by adding 8 mL hexane-isopropanol (3:1 v/v) to ± 1.5 mL emulsion and vortexing thoroughly, as previously described (Waraho et al., 2011a). The mixture was centrifuged at 4,000×*g* for 20 min and the upper layer, containing the hexane and fat, was carefully separated from the bottom layer. The hexane was evaporated under a stream of nitrogen at 25 °C until constant weight, and the remaining oil was treated with a nitrogen blanket and frozen at −80 °C for a minimum of 48 h and a maximum of 20 days until further measurements, which was based on previous research (ten Klooster et al., 2022d).

Lipid oxidation measurements by ^{1}H NMR

Hydroperoxides (primary oxidation products), aldehydes (secondary oxidation products) and triacylglycerols (as a reference for the total amount of oil) were simultaneously quantified using ^{1}H NMR, with an Advance III 600 MHz spectrometer, equipped with a 5-mm cryo-probe at 295 K, following the method described by Merkx et al. (Merkx et al., 2018). In brief, extracted oil (as described above) and a mixture of $CDCl_3$/DMSO-d6 (5:1 v/v) were mixed in a ratio of 1:3 (v/v) and transferred to 5-mm NMR tubes (Bruker, Billerica, Massachusetts, USA). From the recorded single pulse experiment, the glycerol backbone peaks at δ 4.4 pm were used for the quantification of the amount of triacylglycerols. From the band selective pulse, the region between δ 13.0 and 8.0 ppm was selectively excited for the quantification of the lipid oxidation products, following Merkx et al. (Merkx et al., 2018). The hydroperoxide signals resonate between δ 11.3 and 10.6 ppm, and the aldehydes resonate between δ 9.8 and 9.4 ppm. The calculations, including a factor that accounts for intensity loss during the selective pulse, are described in (Merkx et al., 2018). The data were processed with the Bruker TopSpin 4.0.6 software.

7.2.6 Experimental design

For each measurement, at least two emulsions were prepared independently. For the experiment on the effect of 4-hydroperoxy-2-nonenal on lipid oxidation, four emulsions were prepared independently per condition investigated. Additionally, per time point, two independently incubated samples from the same emulsion were analysed for droplet size and lipid oxidation products. Statistical analysis of variance (F-test and T-test) (Microsoft Office Excel 2016) was carried out on experimental lipid oxidation values between different samples. Differences at $p < 0.05$ were considered significant.

7.3 Results and discussion

7.3.1 Colloidal structures in the emulsions

The emulsion droplets containing the clean oil, the pre-oxidised oil, and the 1:1 w/w mixture of both had sizes around 0.1-0.8 μm as measured by SLS (Figure A7.2), and the emulsions were physically stable over incubation (Figure A7.1). We also detected small association colloids, with sizes of around 25-100 nm, in the subnatant of a centrifuged emulsion (Figure 7.2).

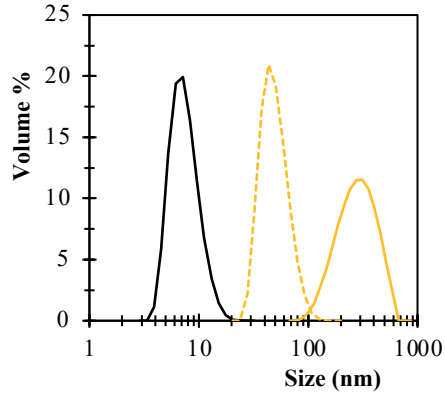

Figure 7.2. Droplet size distributions in (from left to right): a 0.25-wt.% Tween 20 solution (by DLS) (black solid line); the subnatant collected after centrifugation of an emulsion made with clean rapeseed oil and with 2 wt.% Tween 20 (by DLS) (yellow dashed line); and the whole clean emulsion made with 2 wt.% Tween 20 (by SLS) (solid yellow line).

Empty surfactant micelles (i.e., with sizes corresponding to the black line in Figure 7.2) could not be detected in the emulsions' subnatants by DLS, but cryo-TEM did allow us to highlight their presence (Chapter 5). This is in agreement with other studies in which it was shown that empty micelles (and very small oil droplets) could not be detected by DLS due to the presence of larger droplets,

which very largely dominate the scattering signal; yet, NMR investigations confirmed the presence of such smaller structures (Awad et al., 2018; Law et al., 2012). It was previously reported that the subnatant (centrifugation conditions: 35 min 24,000×*g*), referred to as: the continuous phase, contained hydroperoxides (Nuchi et al., 2002). Since physical characterisation of the subnatant was not reported in this previous study, this may also have been small droplets with a diameter ~ 100 nm, instead of oil-free micelles (Nuchi et al., 2002).

7.3.2 Triglyceride-bound hydroperoxides

Directly after mixing the clean- and oxidised droplets, the clean droplets were isolated by collecting a sample of the creamed phase after centrifugation (Figure 7.1). The level of TAG-bound hydroperoxides of the clean emulsion droplets isolated from the mix was found to be unaffected by the mixing ($p > 0.05$) (Figure A7.4). This is an indication that: (1) we can properly separate the droplets initially made with clean oil from the mixed emulsion, and (2) that transfer of TAG-bound hydroperoxides is not immediate (or below the detection threshold). For the emulsions prepared with 2.0 wt.% Tween 20, some cream samples had a higher hydroperoxide content than the non-mixed clean emulsion, but this slight difference was not statistically significant ($p > 0.05$) (Figure A7.4). This may have been caused by the presence of very small pre-oxidised droplets (Figure 7.2) that cannot be removed effectively by centrifugation, which results in a relatively large variability in hydroperoxide concentrations (Figure A7.4, right panel).

The lipid hydroperoxide content in the mixed emulsion was measured over time for emulsions prepared with 0.5 and 2 wt.% Tween 20 (Figure 7.3a & b, respectively). The hydroperoxide content in the mixed emulsion and in the pre-oxidised droplets seems to be relatively constant over time, which is due to the incubation conducted in the presence of EDTA and under low amounts of oxygen (headspace contains ~ 0.3 vol.% O_2 after applying the nitrogen blanket). The hydroperoxide content in the initially clean droplets remained close to zero over the incubation for about 10 days, for both the emulsions prepared with 0.5 wt.% Tween 20 and with 2 wt.% Tween 20 (Figure 7.3a & b, respectively). This indicates that barely any hydroperoxides (if any at all) transferred from the pre-oxidised droplets to the clean droplets in the presence of an excess amount of surfactant and under rotation (i.e., no concentration gradients in the samples). Similar conclusions of barely any transfer (if any) of lipid molecules between O/W emulsion droplets were reported for medium chain triglycerides (Raudsepp et al., 2014c). Our results show that the presence of one or multiple

hydroperoxide groups on a triglyceride molecule does not make it more prone to transfer either via collision of droplets or through transfer via the continuous phase, which are two mechanisms that were theoretically proposed (Laguerre et al., 2017).

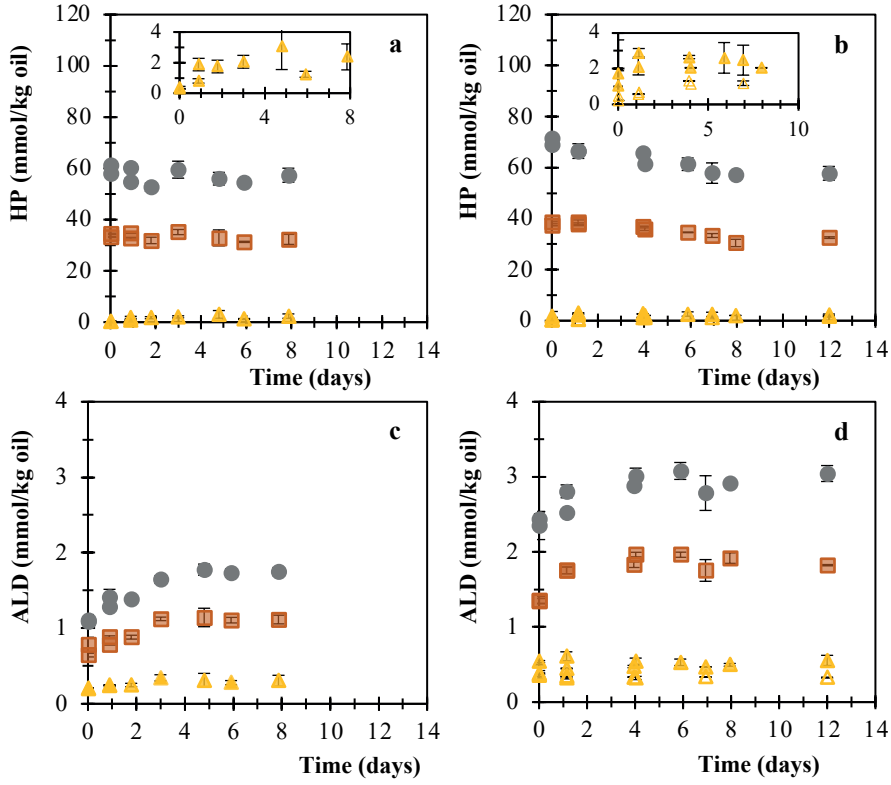

Figure 7.3. Hydroperoxide (a & b) and aldehyde (c & d) content over incubation. Symbols correspond to: the (homogeneous) mix of clean and pre-oxidised emulsion droplets (■), the pre-oxidised droplets isolated from the mix (●), the clean droplets isolated from the mix (▲), and the clean emulsion incubated separately under the same conditions (△, only b & d). For (a) & (c) emulsions were prepared with 0.5 wt.% Tween 20 and (b) & (d) with 2 wt.% Tween 20. Error bars (sometimes within the marker) denote standard deviations of two measurements on two independently incubated samples originating from the same emulsion. The outcomes of the independent replicates are shown as separate datapoints.

In contrast, for emulsions containing alkenes, a complete equilibration occurred within 3-6 days (McClements et al., 1992). There is obviously a great difference in solubility in the continuous phase of alkenes compared to long-chain triglycerides. As the latter have almost zero-solubility in water (Wooster et al., 2008), this most likely hampers any related transfer via solubilisation in the continuous phase. Alternatively, transfer may take place through surfactant micelles, although this possibility is largely contingent on the type of lipid

(Villeneuve et al., 2021). For instance, the large size of triglycerides (~3.4 nm) compared to the micelle core (~2 nm) (Villeneuve et al., 2021) may be the reason that these molecules cannot be as easily included in surfactant micelles as, for example, n-hexadecane molecules (~ 1.8 nm) (Coupland et al., 1996). You and co-workers suggested that the reduction of transfer can also be caused by increased hydrophobic interactions between the oil and the targeted molecule (You et al., 2012), which they based on a finding that by increasing the hydrophobic chain length of the surfactant from 4 to 8 groups, the transfer of the surfactant was ~ 600 times slower. Such hydrophobic interactions between triglycerides could also prevent triglycerides (bearing a hydroperoxide group) from transferring to other droplets.

If we zoom in on the hydroperoxide levels in the clean droplets over time (inserts Figure 7.3a & b), they increased by ~ 1-3 mmol/kg oil over the first day of incubation, and then remained constant. There are two possible explanations for this result: (1) a transfer of hydroperoxides from the oxidised droplets to the initially clean ones, or (2) *in situ* oxidation of the oil droplets collected in the cream. If this minor increase were due to transfer, we would expect the hydroperoxide content to increase further from 1-12 days, but this did not occur. When the clean emulsion droplets were incubated independently (i.e., without being mixed with pre-oxidised ones), under the same conditions, the hydroperoxide content also increased slightly to ~ 1.5 mmol/kg oil (Figure 7.3b), which is similar ($p > 0.05$) to the concentration in the cream at $t = 7$ days and $t = 12$ days. Moreover, we cannot exclude that the clean droplets in the mixed system oxidise faster than the clean droplets that were incubated separately, which is further addressed in section 7.3.4.

7.3.3 Can certain aldehydes transfer to other droplets?

Similarly to hydroperoxides, the aldehyde content was measured in the mixed emulsion, in the initially clean droplets separated from the mixed emulsion, and in the pre-oxidised droplets separated from the mixed emulsion (Figure 7.3c & d, respectively). Please note that the initial aldehyde content was slightly different between the samples made with 0.5 and 2 wt.% Tween 20 because a different batch of oxidised oil was used. As was the case for hydroperoxides, the aldehyde content in the initially clean droplets in the mixed emulsion did not seem to increase over incubation time (Figure 7.3c & d). The aldehyde content in the mix and in the oxidised droplets from the mix increased slightly over the incubation period, most probably as a result of radicals formed during homogenisation that keep propagating the reaction (Serfert et al., 2009). It was expected that EDTA would prevent secondary oxidation product formation

since it chelates prooxidant metal ions, which is why it is recognized as a strong antioxidant (McClements et al., 2000).

The ^{1}H NMR method allows us to quantify specific secondary oxidation molecules, such as 4-hydro(pero)xyenals and 2-alkenals, with very low quantification thresholds (Guillén et al., 2004; Merkx et al., 2018). These aldehydes constitute the main part of the total aldehydes in the pre-oxidised oil (Figure A7.5). With the ^{1}H NMR method, next to aldehydes, such as hexanal, propanal, hexenal, etc., also aldehyde groups that are still attached to a triglyceride (TAG), called oxo-2.5 glycerides, are measured (Hollebrands et al., 2017). The level of 4-hydro(pero) xyenals and 2-alkenals in the clean emulsion at t_0, in the oxidised emulsion droplets at t_0, and in the clean droplets isolated from the mix at t_0 and t = 1 days are shown in Figure 7.4a & b for the emulsions made with 2 wt.% Tween 20 and in Figure A7.6 for the emulsions made with 0.5 wt.% Tween 20. These results indicate that small amounts of 4-hydro(pero)xyenals and 2-alkenals can transfer from the oxidised droplets to the clean ones and do so relatively rapidly (< 30 min). We performed a similar experiment, but then with pure exogenous commercial aldehydes 4-hydroperoxy-2-nonenal and 2,4-decadienal. These components almost totally equilibrate over the emulsion droplets (Figure 7.4c & d), which was in agreement with the publication by Li et al., where it was shown that 2,4-decadienal could rapidly transfer between MCT oil droplets (Li et al., 2020). This indicates that from the pre-oxidised oil, only the low molecular weight oxidation products are expected to transfer, whereas oxo-2.5 glycerides could not transfer, which was also the case for the TAG-bound hydroperoxides (section 7.3.2) (Figure 7.4). This finding can probably be explained by the higher water solubility of the low molecular weight oxidation products (Wooster et al., 2008). Alternative explanations are that the latter would fit inside the micelle core (~ 2 nm) (Villeneuve et al., 2021), or that they have weaker hydrophobic interactions with the oil (You et al., 2012). Lipid oxidation was not shown to progress to neighbouring droplets previously (Banerjee et al., 2018; Raudsepp et al., 2016), which could be clarified by our finding that only very low amounts of lipid oxidation transfer from oxidised to clean oil droplets (Figure 7.4). In contrast, it has been shown to quickly progress within one droplet itself (Banerjee et al., 2018). Yet, there is also experimental evidence that in certain conditions lipid oxidation does progress to neighbouring droplets (Li et al., 2020; Raudsepp et al., 2014b). Li and co-workers hypothesized that low amounts of low molecular weight aldehydes may be a possible source of initiation of oxidation (Li et al., 2020), which is discussed in the next section.

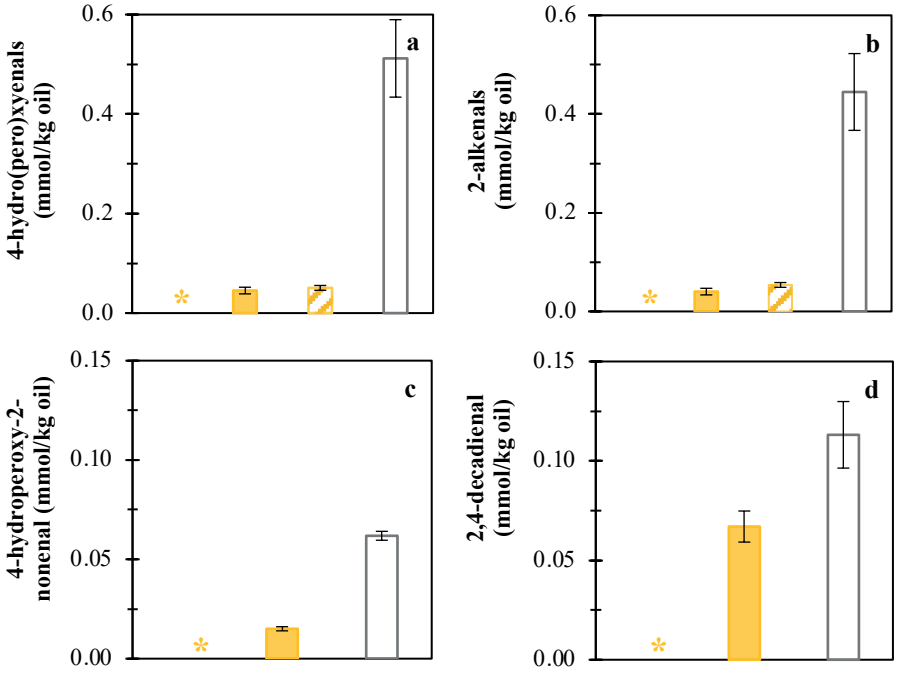

Figure 7.4. Specific secondary oxidation product content in emulsion samples produced with 2 wt.% Tween 20, where (a) & (b) are about the transfer of endogenous oxidation products and (c) & (d) about commercial exogenously added aldehydes. The bars with different colours correspond to different emulsion samples: from left to right: the clean emulsion immediately after homogenisation (yellow), the clean droplets re-isolated from the mix immediately after gently mixing (t_0) (filled yellow) and after 1 day of incubation (striped yellow), and the pre-oxidised emulsion sample immediately after homogenisation (open grey). * indicates below detection threshold. Error bars denote standard deviations of two independent replicates that are both measured twice.

7.3.4 Oxidation re-initiation by lipid oxidation products

Emulsions containing 0.2 mmol commercial 4-hydroperoxy-2-nonenal/kg oil (added exogenously to the oil prior to emulsification) and blank emulsions were incubated and analysed for hydroperoxide concentrations (Figure 7.5). As a general trend, the blank emulsions show lower hydroperoxide levels (significantly different at t = 2 days, but insignificant at the other time points, which can be explained by rather large differences between the replicates). Thus, the lipid oxidation-initiating effect that 4-hydroperoxy-2-nonenal may cause does not seem highly systematic, or at least, reproducible. This can be explained by the fact that lipid oxidation is a radical chain reaction, which implies that *if* lipid oxidation is initiated (e.g., by 4-hydroperoxy-2-nonenal), hydroperoxides keep being formed in a cascaded manner (Reaction 7.I – 7.IV). It may, however, take a few days before the effect on the formation of hydroperoxides becomes

pronounced, as also argued in a recently published article (Schroën et al., 2022a). Therefore, it is questionable whether the transfer of lipid oxidation reactive products and subsequent initiation does substantially contribute to propagation of lipid oxidation in emulsions, or whether it is subordinate to the already oxidising droplets that oxidise further at high rates. This would be in line with experimental findings that lipid oxidation does not progress to neighbouring droplets (Banerjee et al., 2018; Raudsepp et al., 2016). It has also been suggested that certain radicals can transfer between oil droplets and thereby spread lipid oxidation (Raudsepp et al., 2014b). This could speed up spreading of lipid oxidation because these radicals (unlike e.g. 4-hydroperoxy-2-nonenal), can directly propagate lipid oxidation in relatively clean oil droplets without having to be formed into a radical first. Whether a radical present in an oxidising oil droplet can transfer and initiate lipid oxidation in a clean oil droplet is highly dependent on its lifetime, the time required to transfer from one droplet to another (Laguerre et al., 2017), the degree of unsaturation of the oil and the viscosity of the lipid phase (Raudsepp et al., 2016). Still, whether transfer plays a significant role in overall lipid oxidation is expected to be sample and condition dependent: prooxidant effect of (transferred) lipid oxidation products, storage temperature, O_2 availability, oil content, prooxidant (metal ion) availability, etc.

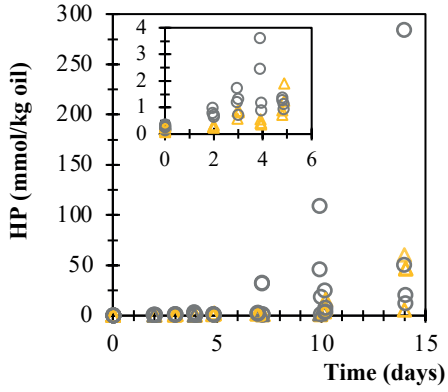

Figure 7.5. Hydroperoxide concentration over incubation. Symbol correspond to samples with 0.2 mmol of 4-hydroperoxy-2-nonenal/kg oil (added to the oil prior to emulsification) (○) or without 4-hydroperoxy-2-nonenal (blank) (△). The outcomes of the dependent and independent replicates are both shown as separate points.

7.4 Conclusion

Starting from a previously published hypothesis that one oil droplet can contaminate neighbouring droplets with lipid oxidation, and thereby propagate this undesired reaction in emulsions (Laguerre et al., 2017, 2020; Villeneuve et al., 2018), we investigated in this chapter which molecules could play a role in such a scenario. This was done by mixing an emulsion made with pre-oxidised rapeseed oil with an emulsion made with clean rapeseed oil. To the best of our knowledge, we are the first to show that barely any TAG-bound hydroperoxides transfer from one droplet to another (under the applied conditions), if they do at all, even though an excess amount of surfactant was present in the continuous phase, and even though the emulsions were rotated over incubation. It was shown previously that alkadienals can transfer from one MCT oil droplet to another (Li et al., 2020), and our work confirms that such relatively short and hydrophilic molecules, such as 2-alkenals, alkadienals and 4-hydroperoxy-2-alkenals, can equilibrate rapidly (< 30 min) over the rapeseed emulsion droplets, although the effect on lipid oxidation is not instantaneous. Therefore, it may be questioned whether the transfer and subsequent initiation are always relevant for oxidising emulsion systems. It is clear that this highly depends on the emulsion system of interest and on the applied conditions, so more research is required to elucidate this further.

7.5 Appendix

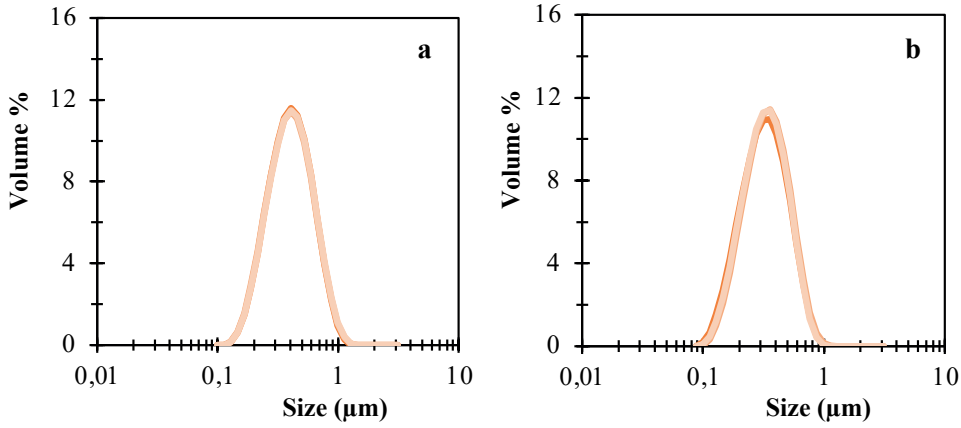

Figure A7.1. The droplet size distributions of the mixed emulsions (with the pre-oxidised and clean droplets) prepared with: 0.5 wt.% Tween 20 (a) and 2 wt.% Tween 20 (b). Lines correspond to different time points: t_0 (the dark orange line), an intermediate time point (t_4 or t_5) (the orange line) and the last time point (t_8 or t_{12}) (the light orange line). Lines are an average of three measurements on the same sample. The graph of one independent replicate is shown, the other replicates gave very similar results.

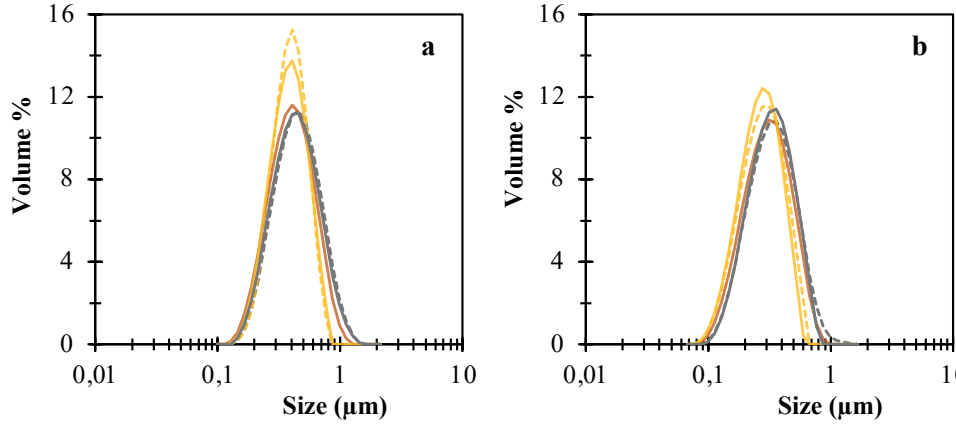

Figure A7.2. The droplet size distributions of emulsions at t_0. Lines correspond to: emulsions made with pre-oxidised oil at t_0 (grey dotted), emulsions made with clean stripped oil at t_0 (yellow dotted), the 1:1 (w/w) mix at t_0 (orange dotted) and the clean (solid yellow) and pre-oxidised (solid grey) emulsion droplets that were re-isolated from the mixed emulsion, for the emulsions prepared with: 0.5 wt.% of Tween 20 (a) and 2 wt.% Tween 20 (b). The graphs of one independent replicate is shown, the other replicates gave very similar results.

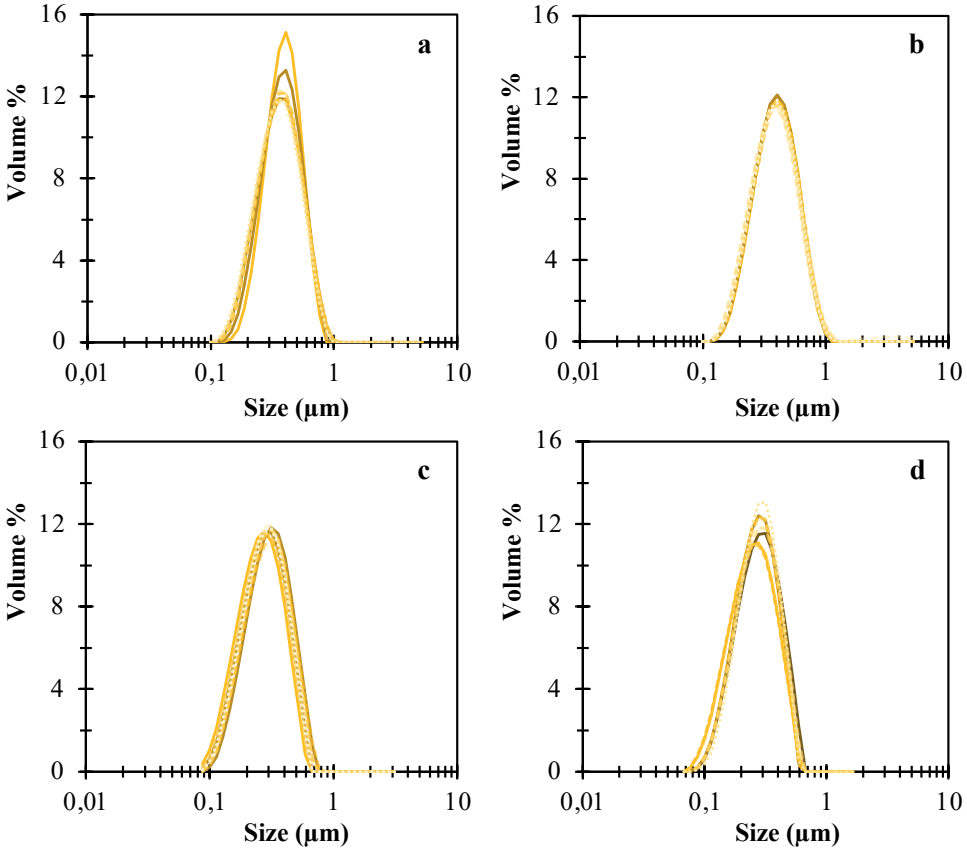

Figure A7.3. The droplet size distributions of the clean emulsion (at t_0) and the clean emulsion droplets isolated from the mixed emulsions, for emulsions containing: 0.5 wt.% Tween 20 (a & b) and 2 wt.% Tween 20 (c & d). Lines correspond to samples either prior to or after mixing with the pre-oxidised droplets, at different time points: the clean emulsion at t_0 before mixing (yellow solid) and all the creams (dotted/dashed) with the lighter and more dotted the line, the later the time point. Duplicates (taken at the same time from a different tube of which the sample originated from the same independently prepared emulsion) are shown by dashed lines with the same colour. Independent replicates are shown in the separate graphs (a / b and c / d).

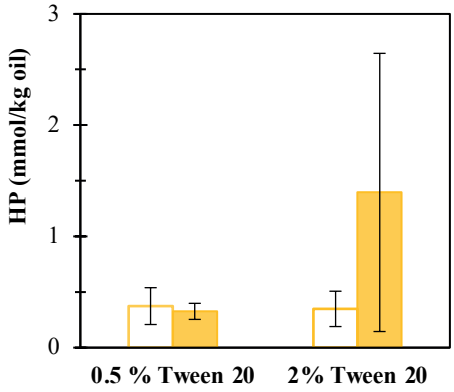

Figure A7.4. The hydroperoxide content of the clean emulsion directly after homogenisation (open yellow bars) and in the clean droplets that were re-isolated after gently mixing with the pre-oxidised emulsion (filled yellow bars). Error bars denote standard deviations of two independent replicates from which two samples were taken that were measured (total of four measurements per data point).

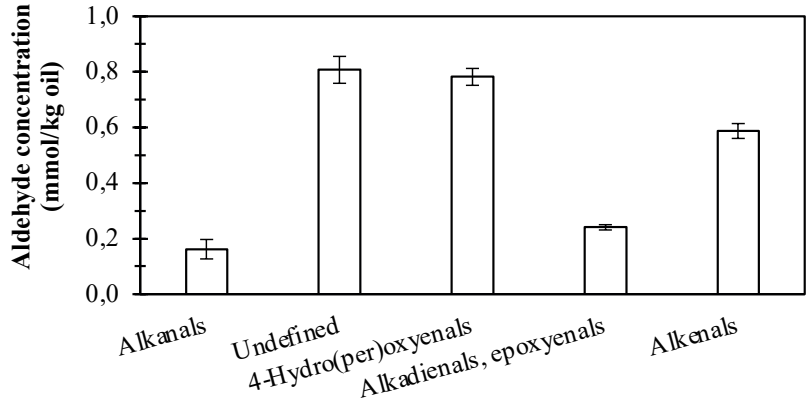

Figure A7.5. The concentration of different types of aldehydes in the pre-oxidised oil with a total aldehyde content of 2.6 ± 0.15 mmol/kg oil.

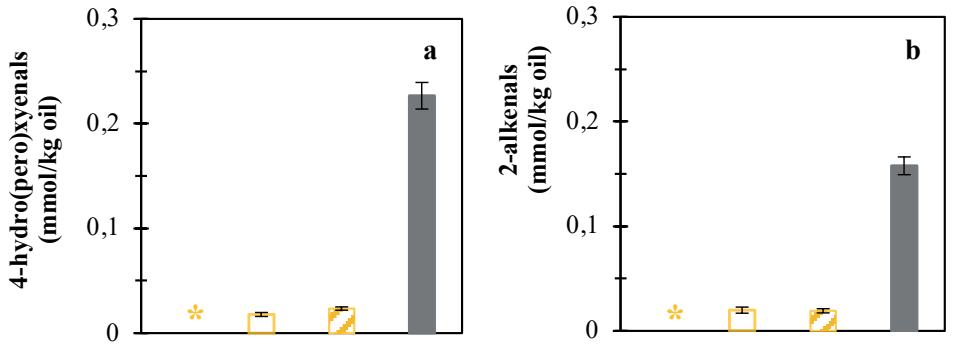

Figure A7.6. 4-hydro(pero)xyenal (a) and 2-alkenal (b) content in emulsions produced with 0.5 wt.% Tween 20. The bars with different colours correspond to different emulsion samples: from left to right: the clean emulsion immediately after homogenisation (open yellow), the clean droplets re-isolated from the mix immediately after gently mixing (t_0) (filled yellow) and after 1 day of incubation (striped yellow), and the pre-oxidised emulsion sample immediately after homogenisation (filled grey). * indicates below detection threshold. Error bars denote standard deviations of two independent replicates that are both measured twice.

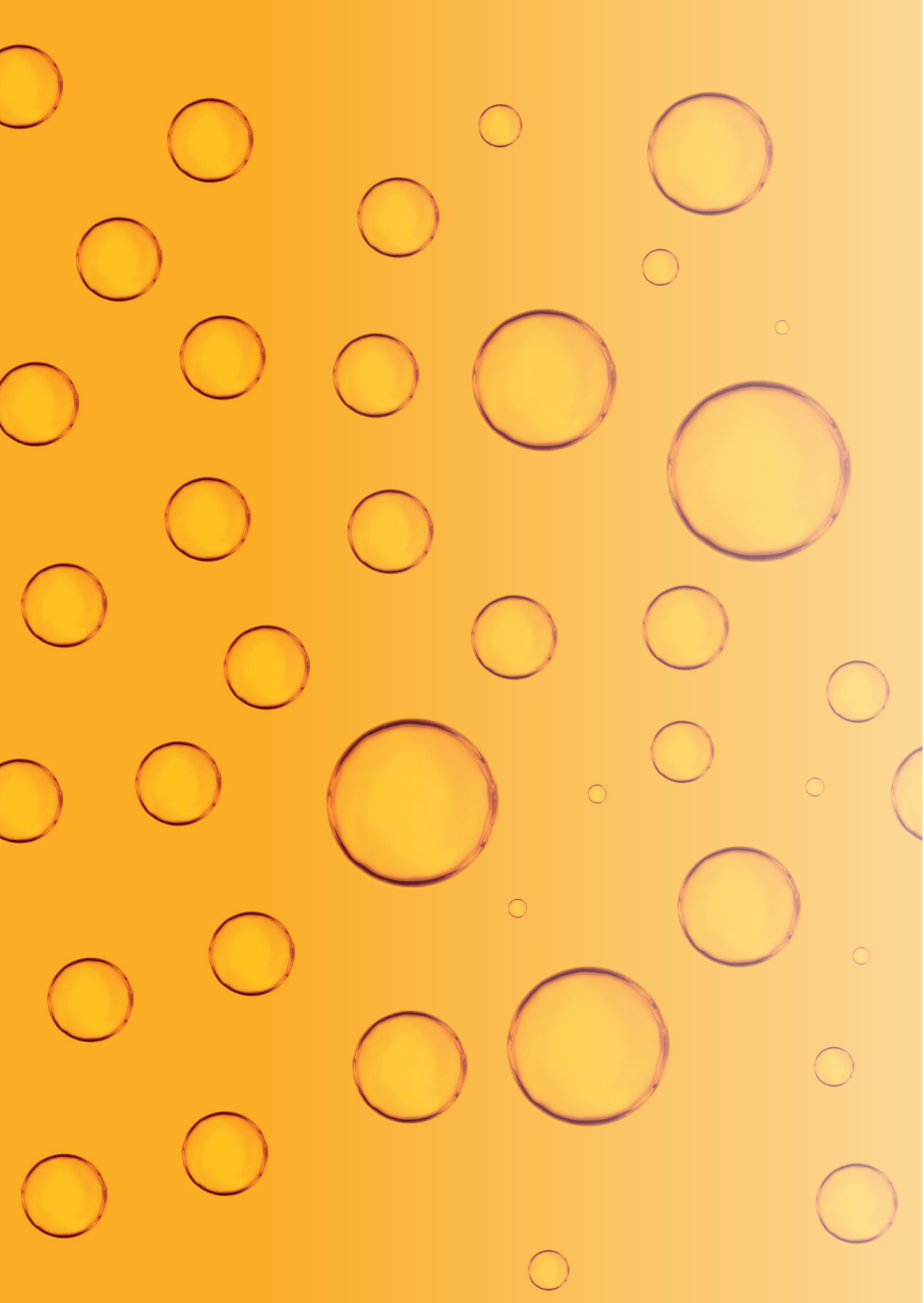

Chapter 8

Alkyl chain length modulates antioxidant activity of gallic acid esters in spray-dried emulsions

This chapter was published as:
S. ten Klooster, P. Villeneuve, C. Bourlieu-Lacanal, E. Durand, K. Schroën, C. Berton-Carabin: *Alkyl chain length modulates antioxidant activity of gallic acid esters in spray-dried emulsions*, Food Chemistry 387 (2022), 132880.

Abstract

Lipid oxidation is a well-recognized issue in dried food emulsions, such as infant milk formula. Antioxidants can be used to mitigate this issue; however, their efficiency in such complex systems is far from understood. In this chapter, antioxidant polarity is varied through the alkyl chain length of gallic acid esters (0 to 16 carbon atoms) incorporated to O/W emulsions that are subsequently spray-dried. During processing and subsequent storage of the samples, antioxidants with more than eight carbon atoms are effective. Both for encapsulated fat and surface free fat, we observe a slight cut-off effect, which means that beyond eight alkyl groups, a more nonpolar antioxidant is slightly less effective. Depending on the antioxidant polarity, lipid oxidation is faster either in the encapsulated or in the surface free fat. The insights obtained contribute to understanding lipid oxidation in low moisture food emulsions, and thus lead to effective antioxidant strategies.

8.1. Introduction

Many food products consist of several immiscible phases, with one phase dispersed in the other as droplets, which are stabilised by an emulsifier (e.g., proteins). When such oil-in-water (O/W) emulsions contain polyunsaturated fatty acids, lipid oxidation can readily occur, which has a negative impact on the sensorial and nutritional quality of the products (Schaich, 2005). Lipid oxidation has become a renewed challenge in the current context of enrichment of targeted food products with the long-chain polyunsaturated fatty acids eicosapentaenoic acid (EPA) and docosahexaenoic acid (DHA) because of their positive impact on human health (Ganesan et al., 2014). The Food and Agriculture Organisation (FAO) recently even set regulations for minimum amounts of EPA and DHA in infant formula products. It is now well-known that EPA and DHA improve immune responses, cognition functions, and visual acuity when sufficiently consumed in early life (Joint, 2010; Lien et al., 2018).

In bulk oils and wet O/W emulsions, lipid oxidation pathways have been studied extensively, which has led to insights in the activity of various antioxidants (Shahidi et al., 2010). In bulk oils, polar antioxidants are generally more effective in delaying lipid oxidation compared to relatively nonpolar ones, as described in pioneering work more than 40 years ago (Porter et al., 1989). It was argued that if lipid oxidation is initiated at the air-oil interface, more polar antioxidants with interfacial activity would be more effective because of their accumulation at this site (Frankel et al., 1994). Later, the effect of antioxidant polarity in bulk oils was assessed by systematically incrementing the length of the alkyl chain grafted on phenolic acids with which so-called 'phenolipids' are formed. It was found that also extrinsic factors, such as traces of water, influence lipid oxidation greatly (Laguerre et al., 2011, 2015). The theory that the air-oil interface is the main site of oxidation was later argued to be unlikely, and it was shown that association colloids in bulk oils can act as prooxidants (Homma et al., 2015). Thus, antioxidant effectiveness in bulk oils seems to be dependent on both intrinsic factors (such as antioxidant hydrophobicity) and extrinsic factors (Laguerre et al., 2015; Phonsatta et al., 2017).

Opposite to bulk oils, in wet O/W emulsions, the most nonpolar antioxidants were initially reported to be the most effective, which was termed as 'the polar paradox' (Porter et al., 1989). In such wet emulsions, the antioxidant polarity was also systematically varied, and the antioxidants with an intermediate alkyl chain length were the most effective. This gave further nuance to the polar paradox, and this finding is known as the 'cut-off effect' (Laguerre et al., 2009,

2015). The most likely explanation for this effect is the tendency of amphiphilic molecules to accumulate near the oil-water interface, which is postulated to be the site of lipid oxidation initiation in an emulsion (Laguerre et al., 2015, 2017; Phonsatta et al., 2017). However, this effect seems to be dependent on extrinsic factors as well; it was found that antioxidant effectiveness in emulsions also depends on the phase to which it was added (oil or water phase), on the emulsifier, and on the polarity of the oxidation initiator (da Silveira et al., 2021; Phonsatta et al., 2017; Stöckmann et al., 2000).

Infant milk formulas are generally sold as powders, which have to be reconstituted by dispersion in water before consumption. In these powders, oil is either entrapped as droplets in a dry matrix or present as free fat on the surface (Figure 8.1) (Vignolles et al., 2007). This structural difference from wet O/W emulsions is expected to affect lipid oxidation, but insights in the oxidation behaviour in low moisture food emulsions are still lacking (Barden et al., 2016; Velasco et al., 2003). Some studies interpret the data of a simultaneous degradation of antioxidants and formation of lipid oxidation products in encapsulated fat as an evidence for a different lipid oxidation status between the droplets (Morales et al., 2015; Velasco et al., 2006). In contrast, the oxidation of surface free fat is reported to start with the degradation of antioxidants, during which the formation of lipid oxidation products is suppressed, followed by a rapid increase in lipid oxidation products, which is comparable to the situation in bulk oils (Morales et al., 2015; Velasco et al., 2006). In dried emulsions, it is expected that the oil-solid matrix interface, which surrounds the encapsulated fat droplets, has an effect on lipid oxidation that largely differs from the role of the oil-water interface in wet emulsions. Velasco and co-workers recently tested different gallic acid alkyl esters in such products, and found that the most nonpolar one that they tested (lauryl gallate) was the most effective at delaying lipid oxidation in both the free and encapsulated fat (Velasco et al., 2009). If oxidation of surface free fat would proceed in a similar manner as in bulk fat, it may be expected that polar antioxidants would be the most effective, but that was not the case (Velasco et al., 2009).

To assess whether an optimal alkyl chain length also applies in dried systems, a next step would be to use a broader range of phenolipids with increasing alkyl chain length up to nonpolar ones. We assume that phenolipids with a medium chain length are especially of great interest for application in dried emulsions given the combined protective effects found in both wet emulsions and in bulk oils. Furthermore, these antioxidants may be instrumental in preventing lipid oxidation in wet emulsions (the starting material for the powders) and

preventing early oxidation events, which has been shown to be detrimental to the subsequent oxidative stability of the dry product (Sánchez et al., 2016).

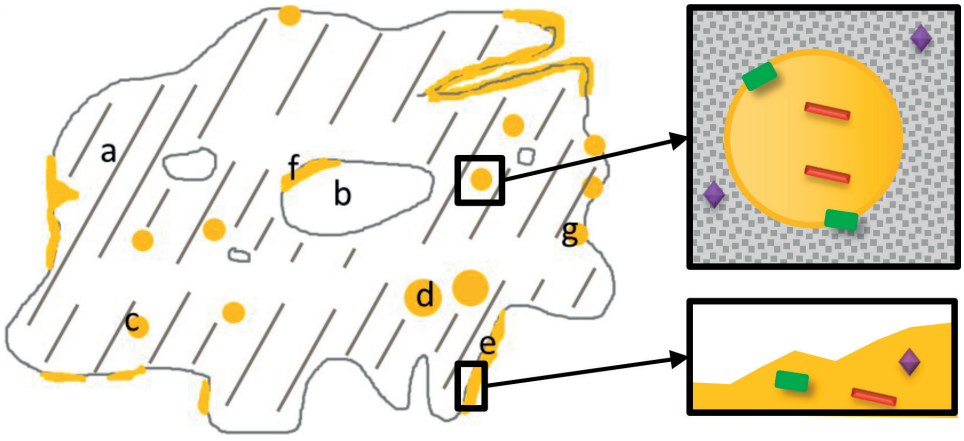

Figure 8.1. (left) Schematic structure of a (dried) emulsion powder particle with fat (in yellow), and matrix material (grey stripes), which is generally present in a glassy state. The particle contains multiple compartments: matrix of sugars and proteins (a), vacuole (b), encapsulated fat (c), coalesced encapsulated fat (d), surface free fat (e), inner free fat (f), and surface globular fat (g). (right) The purple diamonds, green rectangles, and orange rods depict the possible locations of relatively polar, amphiphilic, and nonpolar antioxidants, in either encapsulated (top panel) or surface fat (bottom panel), respectively.

In this chapter, we aimed to unravel the effect of phenolipid chain length on lipid oxidation in the free and encapsulated fat fractions of dried emulsions. For this, the polarity of the antioxidant gallic acid was systematically varied by grafting alkyl chains of increasing length (gallic acid [G0], propyl [G3], octyl [G8], lauryl [G12], and hexadecyl gallate [G16]), and these gallates were incorporated in O/W emulsions that were subsequently spray-dried. The obtained powders were incubated at 40 °C under relative humidity of 50%, and lipid oxidation was measured over time with nuclear magnetic resonance (^{1}H NMR), which allowed for measuring a range of oxidation markers simultaneously (Merkx et al., 2018). We compared initial formation of lipid oxidation products using a curve fit procedure, which allowed us to chart differences on a quantitative- and objective basis.

8.2. Material and methods

8.2.1 Materials

Whey protein isolate (WPI), with purity 97.0–98.4% (BiPro®, Davisco, Switzerland), and sodium caseinate (SC), with purity 97% (Excellion™, Sodium

Caseinate S, Friesland Campina, the Netherlands), were used as dairy protein sources. Maltodextrin with a dextrose equivalent of 21 was kindly provided by Nutricia, Danone (Utrecht, Netherlands). Sunflower oil was obtained from a local supermarket, mixed with fish oil (3 wt.% of total oil) (MEG-3, DSM Nutritional Products, Canada), and stripped with alumina powder (MP EcoChromet ALUMINA N, Activity: Super I, Biomedicals) to remove impurities and endogenous antioxidants, in particular tocopherols (Berton et al., 2011a). n-Hexane and 2-propanol were obtained from Actu-All Chemicals (Oss, the Netherlands). Deuterated chloroform and dimethylsulfoxide ($CDCl_3$ and DMSO-d6) were purchased from Euriso-top (Saint-Aubin, France). Ultrapure water (18.2 MΩ) was used for all experiments and prepared using a Milli-Q system (Millipore Corporation, Billerica, MA, USA).

8.2.2 Emulsion preparation

Synthesis of gallic acid esters

The synthesis of gallic acid alkyl esters was performed according to an established procedure (Durand et al., 2019). In brief, gallic acid (850.6 mg, 5 mmol) and its corresponding alcohol (15 mmol) were dissolved in dry *p*-dioxane (10 mL) in a 50-mL round bottom flask. Next, concentrated sulfuric acid (5 mmol, 273 µL) was added, the mixture was refluxed for 8 hours, and the reaction's progress was monitored by thin layer chromatography. The solvent was removed under vacuum and the alkyl gallates were separated through column chromatography (20% ethyl acetate in methylene chloride). The purity was measured with ^{1}H and ^{13}C NMR, using a Bruker AVIII-HD-500 at 500 MHz and 126 MHz, respectively, in DMSO-d6 (section 8.5.1). For all gallates the purity was > 99%.

Preparation of the aqueous phase

The day before the emulsions were made, all glassware was cleaned with detergent and rinsed with ultrapure water to ensure that it was free of possible contaminants that might influence oxidation. First, WPI (1.22 wt.% of final emulsion) was dissolved in ultrapure water for 30 min at room temperature by gentle stirring. Next, sodium caseinate (4.87 wt. %) was added, and the mixture was stirred for 2 h at 50 °C. Finally, maltodextrin DE 21 (27.9 wt. %) was added, and the solution was stirred for an additional 30 min.

Preparation of the emulsions

Emulsions containing the different antioxidants (gallic acid [G0], propyl [G3], octyl [G8], lauryl [G12], and hexadecyl gallate [G16]) were prepared (total mass of each emulsion was 246 g). The antioxidants were first dissolved in methanol in such concentrations that adding 100 µL methanolic solution to the oil leaded

to a concentration of 600 μmol of antioxidant/kg oil (equivalent to 100 mg/kg for gallic acid). Methanol was next evaporated by placing the mixture under a flow of nitrogen. Stripped oil (14.8 wt.% sunflower oil and 0.46 wt.% fish oil), with or without antioxidant was added to the previously prepared continuous phase to form the emulsion. First, a coarse emulsion was made by high-speed stirring at 11,000 rpm for 1 min with a rotor-stator homogeniser (Ultra-turrax IKA T18 basic, Germany). The coarse emulsion was then passed two times through a lab scale colloid mill, with gap width of 0.32 mm (IKA Magic Lab, Staufen, Germany), operated for 1.5 min at 26,000 rpm.

Spray drying of the emulsions

The emulsions were spray-dried using a Büchi B-290 laboratory spray dryer (Büchi Labortechnik AG, Flawil Switzerland). The inlet air temperature was set to 180 °C and the flow rate was between 35 and 45% to obtain an outlet air temperature of 100 °C. The aspirator was set to 90%. The amount of powder obtained was about 20 g with an average particle size of 46 ± 8 μm and an average moisture content of 3.0 ± 0.4 wt.%. The powder yield was ~ 16 wt.% of the initial dry matter, which was relatively high compared to other values reported in literature for high-oil emulsions using lab-scale spray dryers (Langrish et al., 2006).

Sample incubation

Aliquots of powder (1.5 g) were distributed in 50-mL plastic cups without lids, which were incubated in a climate chamber (Memmert, Büchenbach, Germany) at 40 °C and 50% relative humidity in the dark. At regular time intervals, samples from two aliquots were taken for further measurements.

8.2.3 Emulsion characterisation

Oil droplet size

The oil droplet size in the emulsion was measured by static light scattering (Malvern Mastersizer 3000, Malvern Instruments Ltd., Malvern, Worcestershire, UK). The refractive index was 1.465 for the dispersed phase (mix of stripped sunflower and fish oil) and 1.33 for the dispersant (water). The absorption index was 0.01. The average droplet size ($D_{3,2}$) of the emulsions was 0.9 ± 0.04 μm (Figure A8.1).

Powder particle size

The powder particle size was measured with light microscopy imaging (Malvern Morphology 4, Malvern instruments Ltd., Malvern, Worcestershire, UK). The powder was spread over the microscope glass slide by the automatic powder

dispenser with an applied air pressure of 3 bar.

Sorption isotherm
The sorption isotherms of one sample containing G8 and one sample containing G12 were determined with a dynamic vapor sorption elevated temperature analyser (Surface Measurement System, London, UK) at a temperature of 40 °C. For the measurement, 10 ± 1 mg of sample was used. The relative humidity was varied between 0% and 90% with steps of 10% and the sample weight was equilibrated at each step. Equilibration was considered completed when the change in mass was less than 0.001 mg/min. The temperature, humidity and mass were recorded every min.

8.2.4 Lipid oxidation measurements

Free and encapsulated fat extraction
Surface free fat and encapsulated fat were extracted using the methods described by Kim et al. and Sánchez et. al., with small adjustments (Kim et al., 2005; Sánchez et al., 2016). In brief, 1.5 g powder was washed three times with 6 mL hexane. For each washing step, the hexane and powder mixture were rotated vertically for 10 min at 20 rpm. Prior to filtration, the powder was allowed to sediment to the bottom of the tube (~ 5 min), and next the hexane phase was filtered two times (No. 4, Whatman, Maidstone, Kent, UK). Hexane was then evaporated under a stream of nitrogen at 25 °C until constant weight, and the remaining oil was frozen at −80 °C and stored for 48 h to three weeks before further measurements were performed.

To extract the encapsulated fat, the powder (collected after extraction of surface free fat) was reconstituted by adding 1 mL of ultrapure water to 0.25 g of powder at 50 °C and by vortexing two times 1 min. The extraction was then performed by adding 8 mL hexane-isopropanol (3:1 v/v) to 1.5 mL reconstituted emulsion. The mixture was centrifuged at 5000×*g* for 20 min and the upper layer, containing the hexane and extracted lipids, was carefully separated from the bottom layer. The hexane then was evaporated in the same way as for the surface free fat.

Lipid oxidation measurements by ^{1}H NMR
Hydroperoxides (primary oxidation products), aldehydes (secondary oxidation products), gallates (antioxidants) and triacylglycerols (as a reference for the total amount of oil) were simultaneously quantified by ^{1}H NMR using an Advance III 600 MHz spectrometer, equipped with a 5 mm cryo-probe at 295 K, following the method described by (Merkx et al., 2018). In brief, 550 µL 5:1

$CDCl_3$/DMSO-d6 were added to a total of 30-60 µL extracted oil (as described in 2.4) and transferred to 5-mm NMR tubes (Bruker, Billerica, MA, USA). From the recorded single pulse experiment, the glycerol backbone peaks at δ 4.4 pm were used for the quantification of the amount of triacylglycerols, and the gallate peak at 7.1 for the quantification of the amounts of gallates. From the band selective pulse, the region between δ 13.0 and 8.0 ppm was selectively excited, for the quantification of the lipid oxidation products. The hydroperoxide signals resonate between δ 11.3 and 10.6 ppm and the aldehydes between δ 9.8 and 9.4 ppm. The calculations, including a factor that accounts for intensity loss during the selective pulse, were described in (Merkx et al., 2018). The data was processed with the Bruker TopSpin 4.0.6 software.

8.2.5 Experimental design and data fitting procedure

Two spray-dried emulsions were prepared independently for each gallate used. Per time point, two aliquots of powder were taken, the free- and encapsulated fat fractions were extracted, and further measurements were performed. We considered various standard equations to fit the experimental hydroperoxide concentration data and found that an exponential equation (Equation 8.1) was best suited based on the Akaike criterion that encompasses agreement of fit and number of parameters used. Furthermore, we systematically checked the distribution of the residuals.

$$y = y_0 e^{kt} \tag{8.1}$$

where y is the hydroperoxide concentration (mmol/kg oil), y_0 the hydroperoxide concentration just after spray drying (mmol/kg oil), k is indicative for hydroperoxide formation rate (d^{-1}) and t the time (d). Please note that k should not be interpreted as an actual reaction rate, since it does not capture the full complexity of the cascaded reactions involved in lipid oxidation. Yet, it is useful to compare our samples in a quantitative, objective manner.

Both y_0 and k were used as fitting parameters, and the residual sum of squares was minimized based on relative differences with the measured data. In this way, all data points were equally weighed in the determination of the parameters that otherwise would be completely dominated by the highest values measured. The estimated y_0 value was compared with the measured initial hydroperoxide concentration. The 95% confidence intervals for k and y_0 were calculated using the Student's T-distribution formula in Excel (Microsoft Office, 2016) with a sample size of 2 (two emulsions were produced and incubated independently).

8.3 Results and discussion

Regarding the general properties of the powder that we prepared, it had an average moisture content of 3.0 ± 0.4 wt.% after spray drying; the sorption isotherms (moisture content against water activity) at 40 °C are shown in Figure A8.2 and were identical for both antioxidants used, which was expected. The powder had an average surface free fat content of 2.3 ± 0.3 wt.% (compared to the total mass of powder, this represented around 7.6 wt.% of the total lipids) and an average particle size of 46 ± 8 μm.

8.3.1 Oxidation in encapsulated fat

Lipid oxidation was measured with ^{1}H NMR spectroscopy, which allows for measuring a range of hydroperoxides and a range of aldehydes simultaneously; more information about this method can be found in the work of Merkx and co-workers (Merkx et al., 2018). The amounts of hydroperoxides and aldehydes formed over time in the encapsulated fat are shown in Figure 8.2a and b, respectively. High levels of oxidation products were formed after a few days for the blank system that did not contain any antioxidant. The amounts of hydroperoxides and aldehydes were only slightly lower when gallic acid was present, and the antioxidant effectiveness increased with the alkyl chain length. The gallates with a medium to long alkyl chain (G8, G12 and G16) were all able to delay the formation of high amounts of lipid oxidation products by around 15 days.

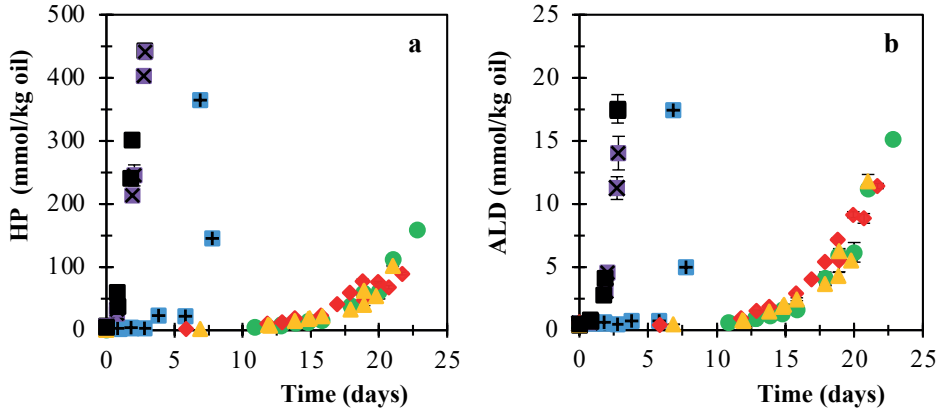

Figure 8.2. Formation of: hydroperoxides (a) and aldehydes (b) in the encapsulated fat of the spray-dried emulsions over incubation. Symbols correspond to the systems containing gallates with different alkyl chain length: gallic acid (G0) (X), propyl gallate (G3) (+), octyl gallate (G8) (●), dodecyl gallate (G12) (▲), and hexadecyl gallate (G16) (♦); and to the blank (no antioxidant) (■). Error bars denote standard deviations of one measurement on two independently incubated samples originating from the same emulsion. The outcomes of the independent replicates are shown as separate points.

Although we added all gallates to the oil phase before making the emulsion and spray drying it, they can be expected to rapidly partition between the dispersed phase, the interface, and the continuous phase. The actual partitioning coefficients (log [p_w^o]) between a vegetable oil and citric acid buffer are negative for gallic acid (~ -1) and increases linearly with the gallates alkyl chain lengths up to G4 (Freiría-Gándara et al., 2018). This indicates that especially G0 would preferably locate in the polar water phase, and thus likely end up to a large extent in the glassy matrix after spray drying, where it has a very limited mobility making it ineffective. Furthermore, it has been reported that gallic acid (G0) can form non-covalent bonds with both caseinate and whey proteins (at pH 6.0 and 7.0 respectively), which could cause it to be even less effective (Cao et al., 2017; Zhan et al., 2020). Based on the effectiveness of caffeic acid esters in fish oil-enriched milk (Alemán et al., 2015), one could expect G3 to be relatively effective compared to G8-G16, but this was clearly not the case (Figure 8.2). G3 has been reported to partition mainly to the oil-water interface in wet (surfactant-based) emulsions (Losada Barreiro et al., 2013). Part of this interface may become glassy, therewith reducing the accessibility of G3 to the oxidising lipids. We can also not exclude that during drying the partitioning of G3 may be shifted to the surrounding glassy matrix. To summarise, based on the results of Freiría-Gándara and co-workers, the gallates with alkyl chain lengths ≥ G8 were expected to end up in the encapsulated oil at higher concentrations compared to G0 and G3, with little differences between G8, G12, and G16. We think that this can explain, for a large part, the reported results in effectiveness to prevent lipid oxidation.

In the work of Velasco and co-workers on freeze-dried emulsions, it was concluded that their most hydrophobic gallate (G12), was the most effective in the encapsulated fat (Velasco et al., 2009), which is not completely in line with our results because we do not see a distinct difference between G8, G12 and G16 (Figure 8.2). Our results are in line with another study about roasted peanuts (which can be regarded as a low-moisture system with dispersed lipids) in which hydrophobic antioxidants (in this case, G8 and G12) were also found to be the most effective (Phonsatta et al., 2017). The suggested rational was that polar antioxidants were not readily present in the oil phase, which made them less effective than more nonpolar ones. In wet O/W emulsions, gallates with an intermediate polarity (~ G3) were generally the most effective (Losada Barreiro et al., 2013; Stöckmann et al., 2000), although this has been shown to be dependent on the type of emulsifier or oxidation initiator as well (da Silveira et al., 2021; Phonsatta et al., 2017; Stöckmann et al., 2000). Also for fish oil-enriched milk, which is a wet emulsion system that can be compared

with our model dairy emulsions, the caffeic acid esters with intermediate alkyl chain lengths (G1-G4) were the most effective (Alemán et al., 2015). Since the interface is often regarded as the actual site where lipid oxidation occurs in a wet emulsion (Berton-Carabin et al., 2014; Laguerre et al., 2020), this suggests that the antioxidant has to be close to this site to be effective. Romsted and Bravo-Diaz have developed a pseudophase kinetic model to determine the partitioning of chain-breaking antioxidants in surfactant-stabilised emulsions (Romsted et al., 2013, 2002). With this method, they showed that the effectiveness of gallates with an intermediate polarity (~ G3) could be linked to their partitioning in high concentrations at the interface (Losada Barreiro et al., 2013). Yet, it is questionable to which extent this pseudophase kinetic model can be used for our system for two reasons: (1) we worked with a protein-stabilised emulsion consisting of different protein types, which has not been covered using with the pseudophase model, and (2) the matrix surrounding the droplets is in the glassy state, which can influence diffusivity greatly compared to the situation for which the pseudophase model was derived (fully liquid surfactant-stabilised emulsions). Therefore, in a spray-dried emulsion, it is still unknown whether the oil-matrix interface is also the location of lipid oxidation initiation.

Another aspect that we considered, is that during spray drying a fraction of the gallates might be chemically degraded. Therefore, we measured the concentrations of gallates by NMR and found no marked differences in the concentrations of the relatively nonpolar gallates (G8, G12 and G16) (G0 cannot be measured), compared to the amounts in the emulsion or in the oil (Figure A8.3). A recent study on the thermal stability of gallic acid showed that this phenolic compound is hardly degraded in aqueous solution when subjected to a temperature of 100 °C for half an hour (Volf et al., 2014). All this suggests that in our systems, the gallates were hardly affected by the sample preparation procedure, if at all.

We did find differences in the initial amounts of lipid oxidation products in the different powders, and that is why we have traced their formation throughout the production process. The concentration of hydroperoxides in the oil (prior to emulsification), in the wet emulsions and directly after spray drying in the encapsulated fat is shown in Figure 8.3. None of the antioxidants totally prevented an onset of lipid oxidation during processing, which is in line with the study of Sánchez and co-workers (Sánchez et al., 2016). A slight increase in hydroperoxides can be observed for the blank during emulsification, which is in line with studies on homogenisation of milk protein-stabilised emulsions (Horn et al., 2012, 2013). The subsequent spray drying had a more pronounced

effect in that respect, probably due to the high temperatures (~ 100 °C) used in the process (Baik et al., 2004). When comparing the effectiveness of the gallates during processing and storage, we generally observed that the antioxidants that are the most effective during storage were also the most effective during the processing (Figure 8.3). One exception was propyl gallate (G3), which was relatively effective during processing, but not that much during storage. This can be related to previous studies showing that in wet emulsions, moderately amphiphilic gallates, such as G3, can be effective, which is often related to their partitioning at the interface (Losada Barreiro et al., 2013; Stöckmann et al., 2000). Yet, this is not the case in the powders, probably due to its partitioning as described above. Clearly, positive effects obtained in wet emulsions (prior to spray drying) are not always indicative for effects occurring during storage of the powders, which we already concluded when we compared our results to fish oil-enriched milk (Alemán et al., 2015). Although the amounts of lipid oxidation products that are formed prior to drying are very limited, it is thought that they can still play a significant role in the development of oxidation later on (Sánchez et al., 2016), which may also explain variations between outcomes reported in literature (Drusch et al., 2007).

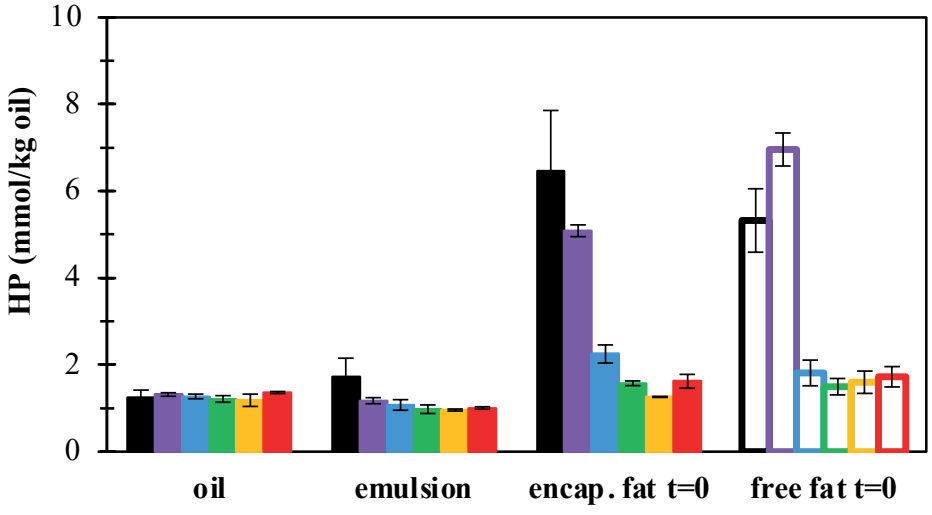

Figure 8.3. Formation of hydroperoxides during processing. The bars with different colours correspond to systems with no antioxidant (blank) or gallates with various alkyl chain lengths. From left to right: Blank (black), G0 (purple), G3 (blue), G8 (green), G12 (yellow), and G16 (red). Error bars denote standard deviations of two independent experiments that are both measured twice.

To wrap up, phenolipids have to be relatively nonpolar to optimally protect the encapsulated fat in dried emulsions, compared to wet emulsions. For

wet emulsions, there are three possible explanations for the fact that more nonpolar antioxidants are less effective: (i) reduced mobility of the antioxidant molecule at longer alkyl chain length, (ii) self-aggregation of the antioxidant, therewith lowering mobility, and (iii) localisation of the antioxidant away from the interface (Laguerre et al., 2015; Phonsatta et al., 2017). Since increasing the alkyl chain length of the gallates from G8 to G12 to G16 did not greatly influence oxidation in the encapsulated fat, these effects do not play major roles in the encapsulated fat of dried emulsions. However, especially explanation (i) and (ii) could (together with the similar p_w^o for G8-G16 (Freiría-Gándara et al., 2018)) explain why our most hydrophobic antioxidant (G16) is not necessarily the most effective antioxidant in the encapsulated fat. In addition, it has been reported previously that the complexity of real food emulsions (such as milk and mayonnaise) can contribute to a less obvious effect of the alkyl chain length of antioxidants on their effectiveness compared to model O/W emulsions (Alemán et al., 2015; Laguerre et al., 2009).

8.3.2 Oxidation in surface free fat

In a similar manner as done for the encapsulated fat, we now discuss how lipid oxidation in surface free fat is affected by antioxidant polarity. In the next section, we use a fitting procedure to compare both fat fractions, and the respective effects that antioxidants (at 600 μmol/kg oil) have on the overall course of hydroperoxide formation. For surface free fat, we observed similarities with the trends observed for the encapsulated fat: compared to the blank without antioxidant, gallic acid slightly decreased the concentration of lipid oxidation products, but the G8, G12 and G16 gallates delayed lipid oxidation much more effectively during processing and subsequent storage (Figure 8.3, Figure 8.4). For surface free fat, the formation of hydroperoxides seemed to be a function of the alkyl chain length amongst the three longest carbon chain antioxidants tested. In fact, G8 seemed to be more effective than G12, which in turn was more effective than G16, and this was visible in the formation of both primary and secondary lipid oxidation products (whether these differences are statistically significant is further discussed in section 8.3.3). In wet emulsions, this is known as the cut-off effect (Laguerre et al., 2009). This cut-off effect was not found for dried emulsion by Velasco and co-workers, who concluded that hydrophobic gallates are more effective for the free fat fraction compared to more hydrophilic antioxidants (Velasco et al., 2009). Yet, a possible cut-off effect for dried emulsions could probably not be studied because only G0, G3, and G12 gallates were used. From a structural point of view, it has been proposed that free fat has similarities with bulk oil (i.e., a limited air-oil interface, and a potentially important role of dispersed colloidal structures based on polar lipids) (Laguerre

et al., 2015; Morales et al., 2015; Velasco et al., 2006). Regarding the pathways of lipid oxidation in bulk oil, the so-called polar paradox was formulated, which implies that the most hydrophilic antioxidants are the most effective (Porter et al., 1989; Velasco et al., 2006), as exemplified for a homologous series of gallates (Phonsatta et al., 2017). For our dried emulsions, this relation was clearly not found: the antioxidant has to be hydrophobic enough to partition into the oil phase of the wet emulsion (which is probably not the case for G0 and G3 as described above). When increasing the alkyl chain length further, the antioxidants seemed to become less effective, although the actual differences are small (Figure 8.4) (section 8.3.3). Such a slightly better performance of the G8 antioxidant, compared to G16, might be due to a higher affinity for an interface, which can be an asset when prooxidant colloidal structures are involved (Frankel et al., 1994; Laguerre et al., 2015).

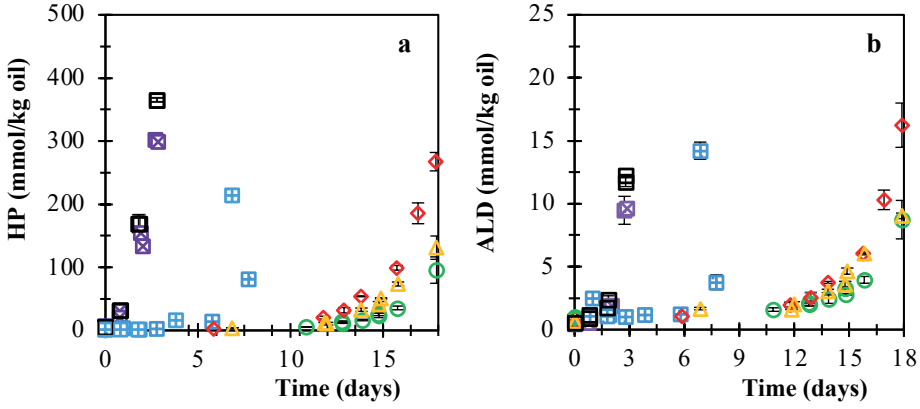

Figure 8.4. Formation of hydroperoxides (a) and aldehydes (b) in the free fat of the powders over time. Symbols correspond to the systems containing gallates with a varied alkyl chain length: gallic acid (G0) (X), propyl gallate (G3) (+), octyl gallate (G8) (●), dodecyl gallate (G12) (▲), and hexadecyl gallate (G16) (♦); and to the blank (no antioxidant) (■). Error bars denote standard deviations of one measurement on two independently incubated samples originating from the same emulsion. The outcomes of the independent replicates are shown as separate points. For clarity, the data until 18 days are shown.

8.3.3 Initial hydroperoxide formation

The dry powders were stored under conditions where the oxygen concentration was constant, and thus the oxygen concentration was non-limiting. Here, we only considered the initial stages of oxidation (when typically < 10% of the oxidisable bonds have reacted, which corresponds to hydroperoxide concentrations below 50 mmol/kg oil (Figure A8.6)), so we can assume that the concentration of oxidisable bonds did not largely change compared to the initial concentration.

The data were fitted by nonlinear regression using Equation 8.1, and k and y_0 were both used as fitting parameters (for motivation of the choices made, see section 8.2.5). In general, the accuracy of the fit that we found is high for all curves tested, and also the residuals were distributed evenly, which is a requirement for any fitting equation (the outcomes of the fit are shown together with the data points < 50 mmol/kg oil in Figure A8.6, and the residual plot is shown in Figure A8.7). In this manner, we compare the effect of the different gallates on the course of the hydroperoxide formation in the dried emulsions. The values found for y_0 were compared with the actual measured values at t = 0 (triangles, Figure 8.5b), and these were found to be in very good agreement. The values for k and y_0 are plotted against the alkyl chain length of the gallates in Figure 8.5a and b, respectively.

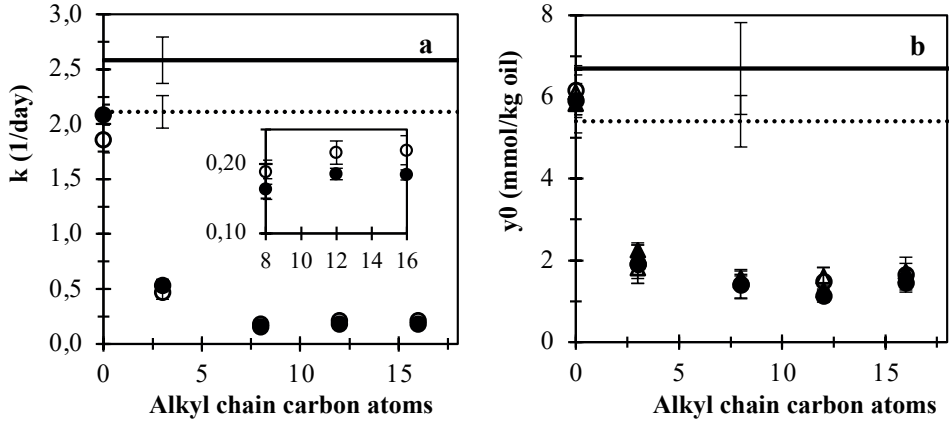

Figure 8.5. The fitting parameters k (indicative for hydroperoxide formation (d^{-1})) (a) and y_0 (concentration of hydroperoxides in the dried emulsion at t = 0) (b) against the alkyl chain length of the gallates for free fat (○) and encapsulated fat (●). The dashed and solid lines denote the values for the free and encapsulated fat in emulsions without antioxidant, respectively. The triangles (Δ) in (b) denote the experimentally measured values. Error bars represent 95% confidence intervals, some being within the marker points. The insert in panel (a) is a magnification of the right part of the graph with k for G8 to G16.

When considering both k and y_0, we can confirm that in both the encapsulated and surface free fat the relatively nonpolar antioxidants (G8, G12 and G16) were by far more effective at delaying lipid oxidation, both initially (y_0) and during incubation (k), than their shorter counterparts, of which G3 was still more effective compared to gallic acid. The data, which have proved to be very reproducible (as revealed by the low standard deviations), also allow us for establishing comparisons in the performance of antioxidants, even when differences are very small.

When using no antioxidant or a relatively polar antioxidant, lipid oxidation was slightly faster in the encapsulated fat than in the surface free fat, but this trend switched when increasing the alkyl chain length (Figure 8.5 and Figure A8.4 & A8.5). An obvious difference between the free and encapsulated fat that may explain this crossover is the nature of the interface to which it is exposed, either air, or the solid matrix. This may imply that the differences in antioxidant effectiveness are related to the affinity of the antioxidant for interfaces. Especially for the surface free fat, the antioxidant effectiveness seemed to be reduced beyond G8 (Figure 8.4a). This effect seemed less marked for the encapsulated fat, and this led to this switchover (Figure 8.5a) around G8. Since the 95% confidence intervals overlap slightly for G8, G12, and G16 (error bars in Figure 8.5a, insert), the significance of this effect is subject to discussion.

When we did not use any antioxidant, we observe that encapsulated fat oxidised faster than free fat, although the differences were rather small. In literature, it has been reported frequently that surface free fat oxidises faster (Morales et al., 2015; Velasco et al., 2006), which is mostly ascribed to a better oxygen availability for this fraction (Velasco et al., 2003, 2009). On the other hand, it is well-known that oxygen is able to diffuse through glassy matrices, although the diffusion rate is rather low and affected by the matrix components present (Drusch et al., 2009). For example, low molecular weight carbohydrates (i.e., high dextrose equivalent) tend to decrease the oxygen diffusivity (Drusch et al., 2007), which was relevant for our model system, containing maltodextrin (dextrose equivalent of 21). On the other hand, our model system contained relatively high amounts of proteins, which has shown to increase the free volume of the matrix material and, therewith, the accessibility of oxygen to oil (Drusch et al., 2009). Recently, Linke et al. showed that the so-called internal oxygen (oxygen in oil and powder particle) only has a minor influence on oxidation of spray-dried emulsions (Linke et al., 2020). They concluded that the transfer rate of oxygen through the matrix determines oxidation of encapsulated fat, and that this transfer rate can be relatively high compared to the reaction rate. Since we found hardly any difference between free and encapsulated fat, we expect that oxygen mass transfer limitations in the matrix did not apply in the systems that we studied.

8.4 Conclusion

In this chapter, we varied the alkyl chain length of gallic acid alkyl esters and measured lipid oxidation in the surface free fat and in the encapsulated fat of a spray-dried emulsion. For both fat fractions, we have shown that the alkyl chain

length has to be relatively long (so, the antioxidant molecule should not be too polar) in order to be effective at delaying lipid oxidation. Gallates with an alkyl chain length of ≥ G8 are expected to mainly partition into the lipid phase, where they can actively counteract lipid oxidation. The oil-matrix interface probably does not play such an essential role at controlling lipid oxidation in powder compared to wet O/W emulsions. In fact, for wet emulsions, the oil-water interface is a critical locus, which results in amphiphilic antioxidants usually being more effective than hydrophobic ones. In the present chapter, a slight cut-off effect seems to be observed especially for the surface free fat, even though the corresponding differences in antioxidant effectiveness ≥ G8 are very small.

The lipid oxidation events that take place during processing can have a major influence on the subsequent lipid oxidation during storage, and it is therefore important to include this in the evaluation of antioxidants. The relatively nonpolar antioxidants are the most effective in preventing lipid oxidation during processing, which makes us conclude that differences in initial amounts are an important parameter to consider. A limitation here may be the detection/quantification thresholds of the available analytical methods because relevant concentrations may be rather low.

According to our findings, the patterns of the lipid oxidation reaction in the free fat and in the encapsulated fat fractions are always very close. Yet, we highlight a moderate but consistent switchover effect. Encapsulated fat oxidised faster than surface free fat when using no antioxidant or the polar gallates, whereas the opposite trend was highlighted when using relatively nonpolar gallates. This switchover is probably caused by the most nonpolar gallates used that are less effective in the surface free fat, whereas they are still relatively effective in the encapsulated fat.

All the insights obtained through this chapter do not just improve our basic understanding of lipid oxidation in low moisture food emulsions, but also paves the way for more effective antioxidant strategies in related food products.

8.5 Appendix

^{1}H and ^{13}C NMR settings

NMR data were acquired using a Bruker AVIII-HD-500 at 500 MHz and 126 MHz, respectively, in DMSO-d6.

Propyl gallate, C3GA: 1H NMR (500 MHz, DMSO-d6) δ 9.26 (s, 2H), 8.93 (s, 1H), 6.95 (s, 2H), 4.17 (t, J = 6.5 Hz, 2H), 1.70 – 1.57 (m, 2H), 0.93 (t, J = 7.4 Hz, 3H). 13C NMR (126 MHz, DMSO-d6) δ 166.31, 146.00, 138.79, 120.02, 108.90, 64.13, 30.81, 14.36.

Octyl gallate, C8GA: 1H NMR (500 MHz, DMSO-d6) δ 9.25 (s, 2H), 8.93 (s, 1H), 6.95 (s, 2H), 4.15 (t, J = 6.5 Hz, 2H), 1.70 – 1.60 (m, 2H), 1.44 – 1.16 (m, 10H), 0.86 (t, J = 6.9 Hz, 3H). 13C NMR (126 MHz, DMSO) δ 166.30, 146.00, 138.79, 120.02, 108.90, 64.41, 40.49, 40.33, 40.16, 39.99, 39.83, 39.66, 39.49, 31.69, 29.12, 29.10, 28.75, 26.01, 22.54, 14.42.

Dodecyl gallate, C12GA: 1H NMR (500 MHz, DMSO-d6) δ 9.26 (s, 2H), 8.94 (s, 1H), 6.94 (s, 2H), 4.15 (t, J = 6.5 Hz, 2H), 1.69 – 1.60 (m, 2H), 1.40 – 1.34 (m, 2H), 1.32 – 1.22 (m, 16H), 0.85 (t, J = 6.8 Hz, 3H). 13C NMR (126 MHz, DMSO-d6) δ 166.30, 145.99, 138.79, 119.99, 108.88, 64.41, 31.77, 29.51, 29.49, 29.47, 29.45, 29.19, 29.15, 28.74, 25.99, 22.57, 14.44.

Hexadecyl gallate, C16GA: 1H NMR (500 MHz, DMSO-d6) δ 9.24 (s, 2H), 8.92 (s, 1H), 6.94 (s, 2H), 4.15 (t, J = 6.5 Hz, 2H), 1.68 – 1.60 (m, 2H), 1.42 – 1.22 (m, 26H), 0.88 – 0.83 (m, 3H). 13C NMR (126 MHz, DMSO-d6) δ 166.30, 146.00, 138.79, 120.00, 108.90, 64.41, 40.48, 40.40, 40.31, 40.15, 39.98, 39.81, 39.65, 39.48, 31.76, 29.50, 29.48, 29.45, 29.18, 29.16, 28.75, 26.00, 22.57, 14.43.

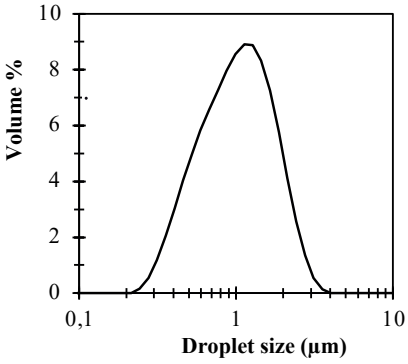

Figure A8.1. Droplet size distribution (volume-based frequency [%] as a function of droplet size [µm]) of the emulsion.

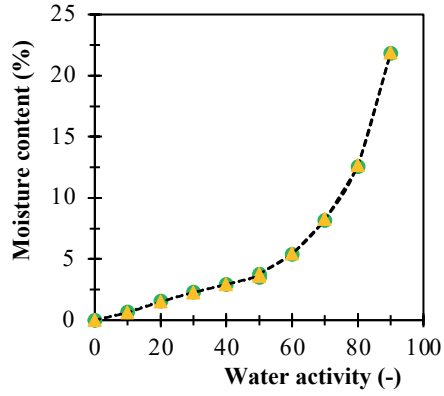

Figure A8.2. Sorption isotherms of spray dried samples containing G8 (●) and G12 (▲) at 40 °C.

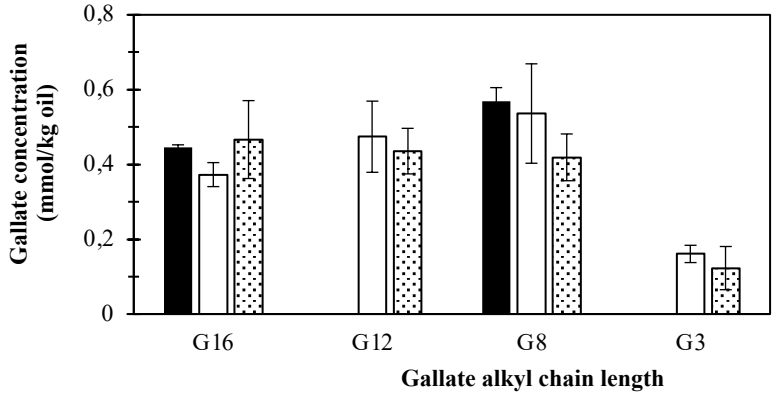

Figure A8.3. The concentrations of gallates as measured by NMR in the oil (filled bar), emulsion (empty bar), and encapsulated fat (dotted bar). The error bars denote standard deviation of two independent experiments that are both measured twice.

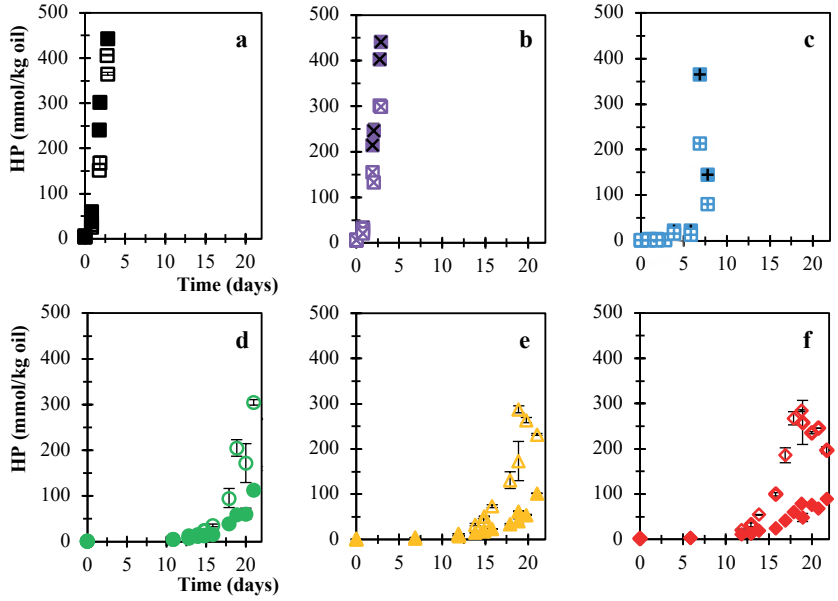

Figure A8.4. Formation of hydroperoxides over time for the blank (a, ■), G0 (b, X), G3 (c, +), G8 (d, ●), G12 (e, ▲), and G16 (f, ♦). Open symbols denote free fat and closed symbols encapsulated fat. Error bars denote standard deviations of one measurement on two independently incubated samples originating from the same emulsion. The outcomes of the independent replicates are shown as separate points.

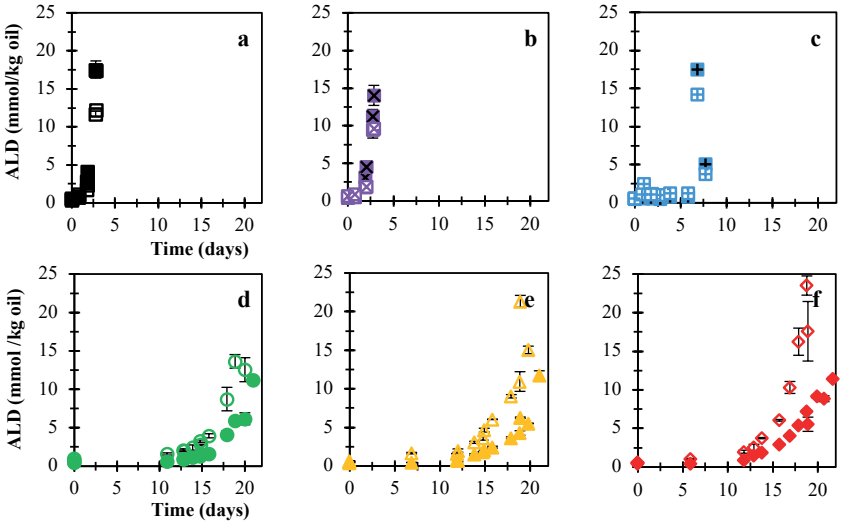

Figure A8.5. Formation of aldehydes over time for the blank (a, ■), G0 (b, X), G3 (c, +), G8 (d, ●), G12 (e, ▲), and G16 (f, ♦). Open symbols denote free fat and closed symbols encapsulated fat. Error bars denote standard deviations of one measurement on two independently incubated samples originating from the same emulsion. The outcomes of the independent replicates are shown as separate points.

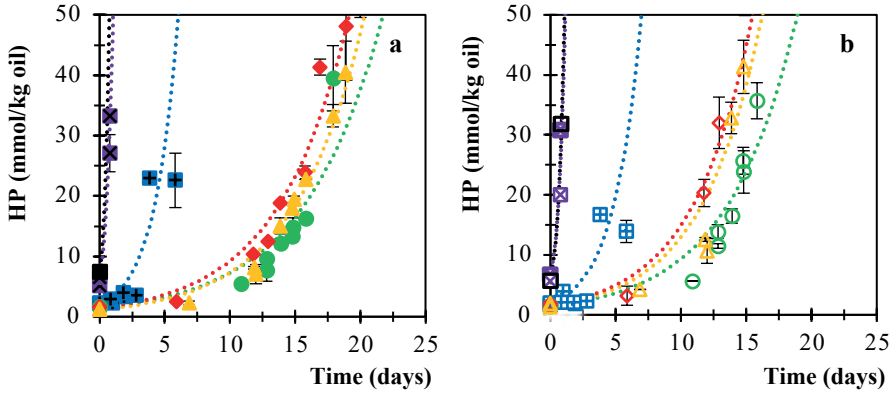

Figure A8.6. Formation of hydroperoxides in the encapsulated fat (a) and in the free fat (b) of the powders over time, showing values until 50 mmol/kg oil. Symbols correspond to the systems containing gallates with different alkyl chain length: gallic acid (G0) (**X**), propyl gallate (G3) (**+**), octyl gallate (G8) (●), dodecyl gallate (G12) (▲), and hexadecyl gallate (G16) (♦); and to the blank (no antioxidant) (■). The dotted lines correspond to the outcome of fitting the data of the two repeats simultaneously to Equation 8.1. Error bars denote standard deviations of one measurement on two independently incubated samples originating from the same emulsion. The outcomes of the independent replicates are shown as separate points.

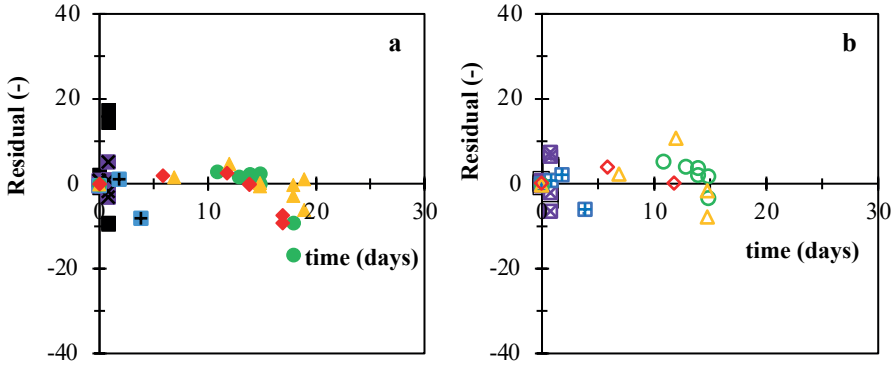

Figure A8.7. Residual plots obtained through fitting the data of two independently prepared emulsions simultaneously to Equation 8.1 for the free fat (a) and the embedded fat (b) of the powders. Symbols correspond to the systems containing gallates with different alkyl chain length: gallic acid (G0) (**X**), propyl gallate (G3) (**+**), octyl gallate (G8) (●), dodecyl gallate (G12) (▲), and hexadecyl gallate (G16) (♦); and to the blank (no antioxidant) (■).

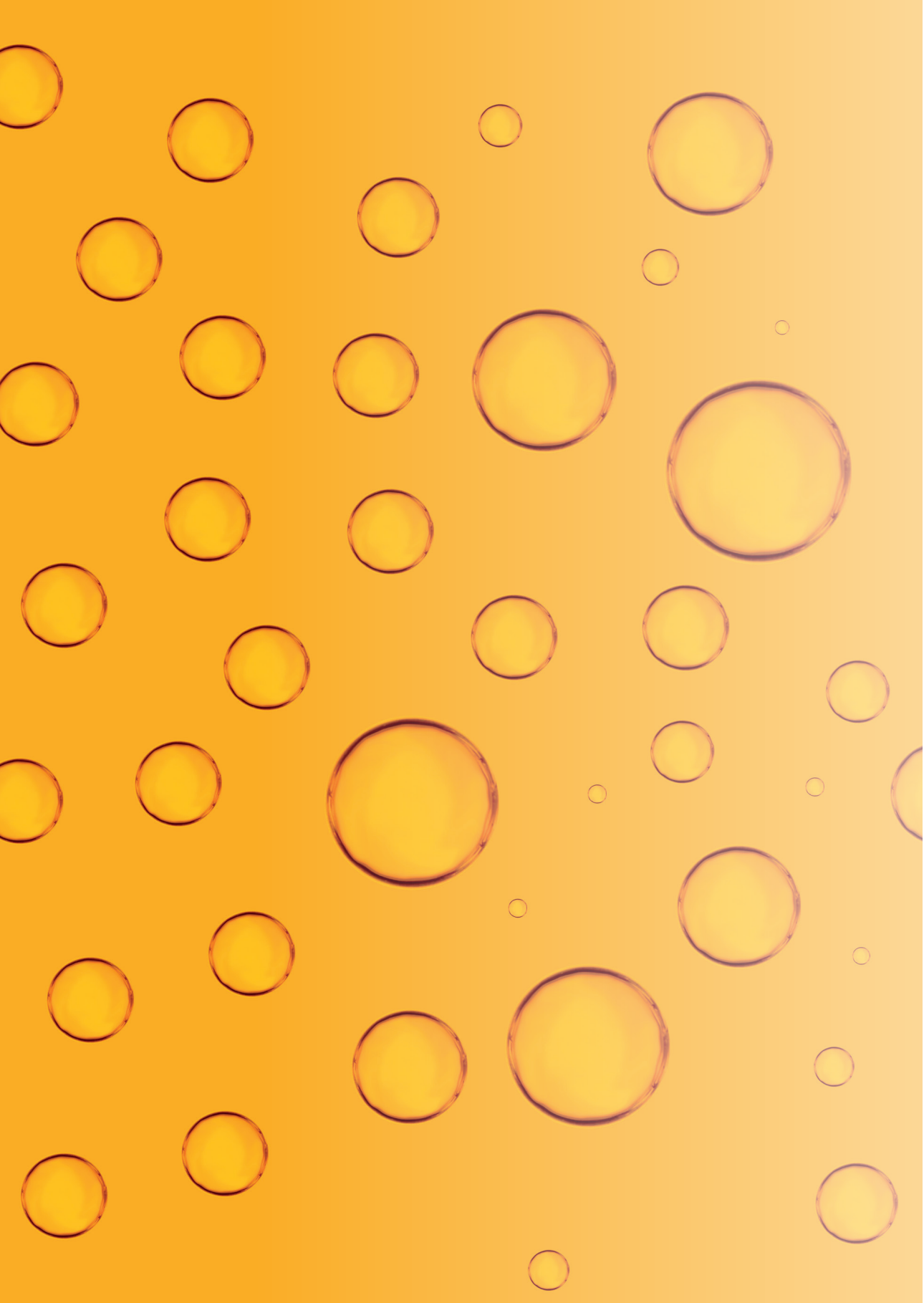

Chapter 9

General discussion

9.1 Introduction

Ever since the serendipitous preparation of the 'Mahonaisse', in 1756, obtaining stable emulsion systems out of incompatible components has remained challenging, not just from a physical point of view, but also from a chemical point of view. The aim of this project was to understand on a fundamental level how emulsion products become oxidised with a specific focus on the role of the structures present in emulsions at a wide range of length scales.

As a first step, control over emulsion preparation needed to be improved greatly compared to conventional techniques that don't really allow tight control over droplet size. To do so, we upscaled microfluidic emulsification devices that are known to generate monodisperse droplets. The design of these devices was based on the identified droplet formation mechanisms. With these devices, we showed to be able to produce monodisperse emulsions, with contrasted droplets sizes, at high enough productivities (**Chapter 2 & 3**) to conduct lipid oxidation experiments.

Using those monodisperse emulsions, lipid oxidation was shown to systematically increase with decreasing droplet size, which we ascribed to favoured lipid oxidation initiation reactions at the oil-water interface, where prooxidants come into contact with the lipids (**Chapter 4**). The surfactants used as emulsifiers were found to be subjected to oxidation as well, which was most pronounced in the fastest oxidising emulsion with the smallest droplets. This is important to consider from a mechanistic perspective, and when molar balances of oxidative reactions are made. Opposing to emulsions made with microfluidics, the smallest droplets present in classical emulsions are as small as a few tens of nanometres, which we showed by deploying cryo-transmission electron microscopy (**Chapter 5**). These small droplets are often overlooked with standard measurements that are used to determine droplet size distributions. In these tiny droplets, lipid oxidation products were found to be overrepresented compared to the emulsion as a whole. Accordingly, lipid oxidation is expected to be highly heterogeneous in 'classical' emulsions because droplet sizes can range over three orders of magnitude. This was further investigated in **Chapter 6**, where we tracked the lipid and protein oxidation status of individual droplets with confocal laser scanning microscopy. We, again, found that small droplets oxidised faster than their larger counterparts. However, we showed that even in monodisperse protein-stabilised emulsions, lipid and protein oxidation can be heterogeneous to some extent. We hypothesise that this may be due to the oxidative state of proteins that co-determines lipid oxidation and vice versa.

The heterogeneity of lipid oxidation can cause transfer of small secondary lipid oxidation products, as shown in **Chapter 7**. The consequences of this transfer greatly depends on the concentration of the oxidation products, their reactivity, their diffusivity, and on the reactivity of the components already present (**Chapter 6 & 7**). Next to wet emulsions, we also considered spray-dried emulsions in which the diffusivity of components through the glassy continuous phase is, in essence, very limited. In that case, we found that antioxidants have to be nonpolar to locate in the oil, where they can effectively counteract lipid oxidation (**Chapter 8**).

In this thesis, we first needed to put considerable effort into designing upscaled microfluidic emulsification devices, which were then used to deconvolute these complicating factors that play a role in lipid oxidation. In this ultimate chapter, we first highlight our findings and remaining challenges regarding emulsion preparation with conventional (section 9.2.1) and microfluidic emulsification devices (section 9.2.2). Next, we discuss how the integral length scale approach of this thesis has improved our understanding of lipid oxidation in emulsions, and which knowledge gaps still exist (section 9.3). Improving the stability of emulsion remains challenging, and this may be improved by using microfluidics to produce emulsions at a large scale. Therefore, in the final section of this chapter (section 9.4), we provide an answer to the compelling question: 'Is microfluidic emulsification only a powerful analytical tool, or can it also be a means to produce stable emulsions on larger scale?'

9.2 Dynamics of droplet formation across length scales

The Mahonaisse, first served in 1756, was probably produced by hand, using a whisk-like tool. Although this preparation method is still common practice in our kitchens, industrial emulsions are produced quite differently, using so-called homogenisers. By applying shear, homogenisers (machine itself ~ several m) produce the emulsions droplets (~ 0.01-100 μm) containing molecules (~ 1 nm) that provide the (off)taste of a product. This implies that a wide length scale plays a role in emulsion production. In this section, we first focus on the important aspects of droplet formation in conventional and microfluidic emulsification devices, which implies addressing the length scales mentioned earlier.

9.2.1 Very small droplet formation in homogenisers

In high pressure homogenisers, coarse droplets are pushed under high pressure through narrow constrictions, which generates long wisps of oil that break-up

into smaller droplets due to instabilities (Roos et al., 2016; Walstra, 1993). Since the formation and possible rapid recoalescence of droplets is highly uncontrolled in such devices, it is not surprising that the resulting emulsions are highly polydisperse, with differences between the largest (~ 10^1 µm) and the smallest droplet (~ 10^1 nm) that ranges over three orders of magnitude (Chapter 5). These smallest droplets have been given special attention in this thesis.

Also in subtle emulsification techniques, such as shear-based microfluidic emulsification devices (T-junction), simultaneous satellite droplet formation was observed (Sun et al., 2018), with diameters of 1-2 µm, when forming a mother droplet of ~ 60 µm (Figure 9.1). The formation of satellites during droplet break-up in microfluidics tickles our imagination, but it cannot be translated directly to homogenisers because in such devices droplet formation occurs in a much more chaotic manner (Roos et al., 2016).

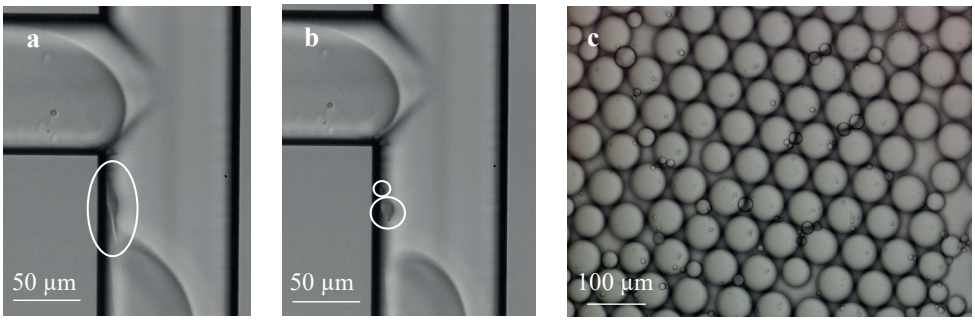

Figure 9.1. (a-b) The co-formation of satellite droplets during the formation of a mother droplet (of ~ 60 µm) in a microfluidic T-junction emulsification device. The dispersed phase was a 50/50 (wt. ratio) mix of decane and stripped rapeseed oil, and the continuous phase contained 0.5 wt.% SDS. The formation of the satellite droplets is highlighted in white circles. (c) The prepared oil droplets together with the satellite droplets outside the chip.

In Chapter 5, these very small droplets (10^1 nm) were separated from the larger ones by centrifugation. Cryo-TEM showed to be capable of capturing the fingerprint of the very small structures co-present. Dynamic light scattering may be standardly used to obtain droplet size distributions, but this technique is not capable of analysing small structures in the presence of large ones (Chapter 5) (Awad et al., 2018). This is due to the signal generated by large droplets that greatly exceeds the signal of small structures. Furthermore, cryo-TEM also allows to distinguish empty micelles from small droplets, which is an additional benefit.

We could show that the amount of very small droplets that were formed in surfactant-stabilised emulsions increases with the shear force, which was varied by using a colloid mill as a more gentle emulsification method compared to a high pressure homogeniser. Even though the surfactant concentration only had little effect on the average size of the larger droplets (0.5-20 µm), the formation of very small droplets increased with the surfactant concentration. The very small droplets of 10-100 nm were also found both in whey protein- and caseinate-stabilised emulsions prepared either with a lab-scale colloid mill or with a high-pressure homogeniser (Figure 9.2, Table 9.1) (Chapter 5 & 6). This makes us conclude that droplet formation and stabilisation are thus fast in both techniques that very small droplet formation does occur.

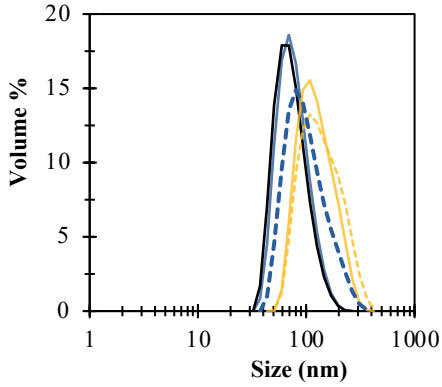

Figure 9.2. Droplet size distributions (DLS) of subnatant emulsion samples obtained after centrifugation (28,000×*g*, 30 min). Line colours correspond to emulsions made with different emulsifiers: 2 wt.% Tween 20 (black), 1 wt.% sodium caseinate (SC) (yellow), or 1 wt.% whey protein isolate (WPI) (blue). The line style corresponds to emulsification technique used to prepare the emulsion: Microfluidizer (solid line) or colloid mill (dotted line).

Table 9.1. TAG content of the subnatant samples of centrifuged emulsions.

Equipment	Emulsifier (wt.%)	Oil content in very small droplets (wt.% of total oil)
Colloid mill	1% WPI	0.6 ± 0.006
Colloid mill	1% SC	1.0 ± 0.010
Colloid mill	2% Tween 20	8.0 ± 0.037
Microfluidizer	1% WPI	20.3 ± 0.000
Microfluidizer	1% SC	21.4 ± 0.23
Microfluidizer	2% Tween 20	23.3 ± 1.4

9.2.2 Droplet formation in microfluidic emulsification devices

The production of Mahonaisse-like products has evolved from using whisk-like tools to using large scale homogenisers, and this evolution is still ongoing with the aim to create highly uniform droplet size distributions. On the other hand, extensive research into microfluidics has created the possibility to produce very monodisperse emulsions at a scale of mL/h (and even L/h depending on the desired droplet size) (Chapter 2 & 3), which enables e.g., lipid oxidation experiments that would not have been possible with classically prepared emulsions. In this thesis, one major challenge was to produce monodisperse emulsions with droplet sizes relevant to the food industry, and at high enough productivities to perform lipid oxidation experiments. It is not a surprise that this has been such a challenge when realising that the chip area of Multi EDGE (Chapter 2) is 1 cm^2 and the volume just 0.4 cm^3.

By diving into the droplet formation mechanisms, we realised that increasing the productivity could not just be achieved by numbering up droplet formation units, but also by improving the design of the microfluidic emulsification devices. This was most notably possible by the design of the channels that supply the dispersed phase to the droplet formation units. With this approach, we achieved an emulsification productivity of 0.4 mL/h rapeseed oil for the production of 3.5-µm droplets in 5 wt.% WPI (Chapter 3), which is impressive for such small droplets. The most important aspects for upscaling microfluidic emulsification, given the target set in this thesis, are described below.

Dispersed phase supply channels

The pressure needed to supply oil to the DFUs scales inversely with the flow resistance that can be calculated by the Hagen-Poiseuille equation with the dimensions of the dispersed phase supply channels. A low flow resistance (wide or short supply channels) or a high pressure results in a high oil flow velocity. Consequently, the viscous force in the neck of the forming droplet will become thus high that the interfacial tension force cannot exceed it. The droplets then keep growing without pinch-off, until another force causes an instability, which we call blow-up.

In Chapter 3, we found that the blow-up pressure can be estimated if the maximum flow velocity of the dispersed phase and the dimensions of the dispersed phase supply channels are known. In earlier work, it was shown that the maximum flow velocity scales inversely with the viscosity of the dispersed phase (Kobayashi et al., 2005a; ten Klooster et al., 2019; Van Dijke et al., 2010) and directly with the interfacial tension (Kobayashi et al., 2005c, 2005a). The emulsifier can also be

used to vary the interfacial tension (Chapter 3) (Sahin et al., 2016). The interfacial tension is highly dynamic during droplet formation, which implies that it is dependent on the droplet formation rate (Deng et al., 2022b). In addition, the blow-up pressure is dependent on the contact angle between the continuous phase and the glass wall, which is difficult to estimate (Sahin et al., 2016; ten Klooster et al., 2022c). In Chapter 3, we found that when substituting a continuous phase containing 2 wt.% Tween 20 with a continuous phase containing 5 wt.% WPI, a 3.5 times higher blow-up pressure was found for two different chip designs, and this obviously influences the overall productivity that can be reached. It remains difficult to disentangle the effects of the dynamic interfacial tension and the contact angle that is co-determined by the oil-water interfacial tension. This complicates estimating the maximum flow velocity of the dispersed phase (and the blow-up pressure) depending on the ingredients used.

In general, it would be favourable for the operation of the chips if the maximum dispersed phase flow velocity could be deduced (e.g., by design of the micro-structures on the main plateau). When the maximum dispersed phase flow velocity is known, the chip can be designed to have a higher blow-up pressure than the Laplace pressure of the meniscus inside the DFU; if that is the case, surfactant adsorption is not required to kick-off the refilling-event, which speeds up the refill and therewith the droplet formation process (Chapter 2). In turn, this increases the overall productivity of the device.

Droplet sizes

In EDGE-like devices, the droplet size scales with 3-4 times the height of the droplet formation unit (DFU) in the spontaneous droplet formation regime for constant height/width ratio of the device, as shown in Chapter 3 and in literature (Kobayashi et al., 2005b, 2007; Montessori et al., 2019). The droplet size can also be decreased by decreasing the DFU width (Kobayashi et al., 2007; Montessori et al., 2019; ten Klooster et al., 2019), which would leave emulsion formulation unaffected. Alternatively, smaller droplets can be obtained by increasing the dispersed phase viscosity or by the decreasing the continuous phase viscosity, which will have an effect of product specifications (ten Klooster et al., 2019; Van Dijke et al., 2010; van Dijke et al., 2010c). A minimum DFU height-to-width ratio of ~ 2.5 is required for monodisperse droplet formation (Kobayashi et al., 2004a; Montessori et al., 2019).

Larger monodisperse droplets can be formed above the blow-up pressure, based on the cascaded mechanism of physical push by a neighbouring droplet (ten Klooster et al., 2019). The droplet size scales with ~ 1.7 times the centre-

to-centre distance between the DFUs (Chapter 3). This droplet formation mechanism could be an interesting option for scale-up, although the droplets need to be in close proximity thus facilitating droplet contact (Chapter 3), which means that in sieve-type of devices this droplet formation mechanism is much harder to achieve given construction limitations, and it has not been observed yet, to the best of our knowledge (Chapter 2).

Ingredient use

As described earlier, in EDGE devices the maximum productivity and oil droplet sizes are dependent on the ingredients used, but there are other ingredient properties that should be considered as well. For example, low concentrations of WPI (1 wt.%) or 5 wt.% of pea protein isolate (PPI) led to coalescence of previously formed droplets with the oil meniscus that is about to form the next droplet (Figure 9.3a), which is detrimental to droplet monodispersity (Deng et al., 2021, 2022c).

Besides, PPI made the droplets flocculate, which led to the formation of a string of droplets moving downstream the continuous phase channel (Figure 9.3b). It is known that PPI contains relatively large proteins that cannot stabilise the droplets as fast as their smaller counterparts (Hinderink et al., 2021).

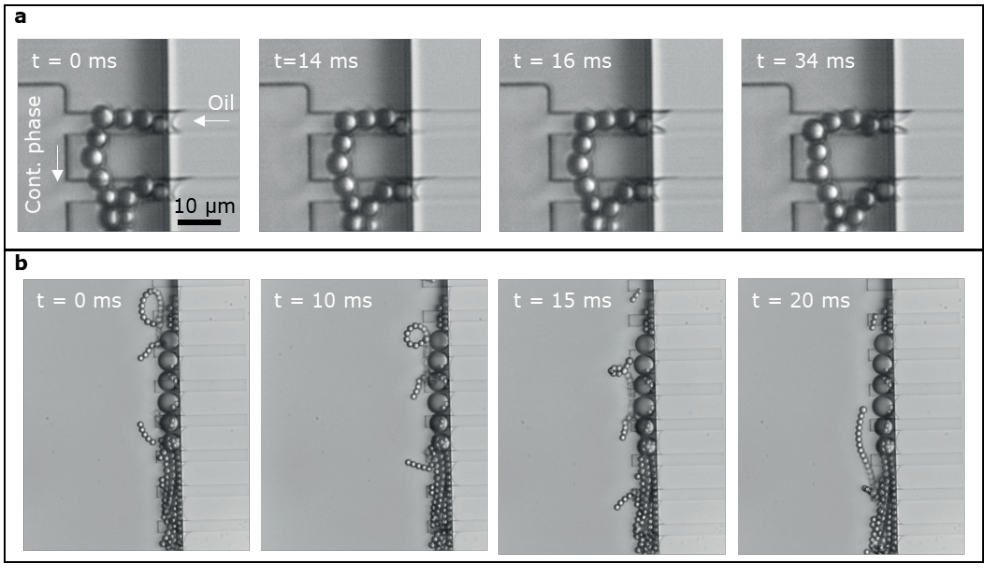

Figure 9.3. Droplet formation in Partitioned EDGE devices with rapeseed oil as the dispersed phase and 5 wt.% of PPI in the continuous phase. (a) The oil-water meniscus coalesces with the previously formed droplet between t = 3 and t = 4 ms. At t = 16 ms a new droplet is formed that pushes its successor away. (b) A flocculated string of droplets flows downstream (flow from top to bottom).

Furthermore, it can be expected that due to their more hydrophobic nature, PPI proteins would interact differently with the chip material, thus influencing the contact angle in a different way, which affects the droplet formation process. Finally, it is known that PPI contains polar lipids, which may affect the interfacial tension and interfacial properties, and thus the physical (in)stability of the droplets. From this it is clear that there are limitations in ingredient choice when using microfluidics to prepare emulsions, although this also holds for conventional emulsification techniques.

Continuous phase channels
The continuous phase channels are an unjustifiably disregarded aspect of spontaneous microfluidic emulsification device design. When the continuous phase channel is too large, the droplets produced near the channel walls will be hardly carried away because of the lower continuous phase flow at this location (Chapter 2). Conversely, continuous phase channels with small dimensions require a higher pressure to make the continuous phase flow, which also has consequences. The applied pressure will drop along the continuous phase channel, which causes that for the first DFUs the continuous phase 'presses back' against the oil flow, but this is not the case for the last DFUs. As a result, the first DFUs run below their maximum productivity, whereas the last DFUs run close to blow-up, which leads to a lower maximum productivity and/or a decreased monodispersity (Chapter 3). Therefore, it is recommended to design the continuous phase channel dimensions based on the desired productivity and oil content.

In general, the length of the continuous phase channel is equal to the space needed for the DFUs, and the width and height of the channel should allow for a controlled flow of droplets without creating a large pressure drop over the dispersed phase channels. To the best of our knowledge, this aspect has not been studied systematically. Therefore, a logical next step towards application of microfluidic emulsification would be to study how a gradual flow of emulsion with desired oil concentrations can be obtained without droplet coalescence or droplet formation issues.

9.2.3 Prototype upscaled microfluidic emulsification devices
To be able to provide an answer to the question: 'is microfluidic emulsification a tool or an end?' we discuss upscaling towards industrial scale, which will also shed light on other challenges. The scaling relations found in Chapter 2 and 3 are used for a first estimation of the design of the prototype. This prototype should be considered as a case study on what would be required to upscale

a microfluidic emulsification device rather than as a perfect device that can directly be fabricated.

The calculations presented next relate to a productivity of 10 m^3/h emulsion containing 10 wt.% rapeseed oil with droplets of 1 µm as an illustration of an emulsion product relevant to the food industry. An overview of the design parameters, and the dimensions of the upscaled devices, are shown in Table 9.2 and Figure 9.4. The device is designed based on the productivities of UPE_{5x1}, presented in Chapter 3, for the 3.5-µm rapeseed oil droplets with 5 wt.% WPI in the continuous phase. Since we found that the droplet size directly scales with the DFU width and height, we will reduce the width and height four times (for simplicity) to produce droplets of 0.9 µm. The productivity per DFU is then expected to be $4^2 = 16$ times smaller, so 16 times as many DFUs will be required to reach the same productivity as for the 3.5-µm rapeseed oil droplets. Since the area of one DFU will be 16 times smaller (0.25 · 0.25), the required porous area does not change (ignoring possible fabrication limitations). All the required $4.8 \cdot 10^{11}$ DFUs of 1.25 · 0.25 µm together require a space of 0.15 m^2. Assuming that the same porosity (total DFU area divided by total chip area) of 5% can be obtained as for Multi EDGE, the total area will be 3.0 m^2 (0.15/0.05) for the required productivity. Although this is a large surface for a microfluidic device, it is within the possibilities of what is currently technically feasible.

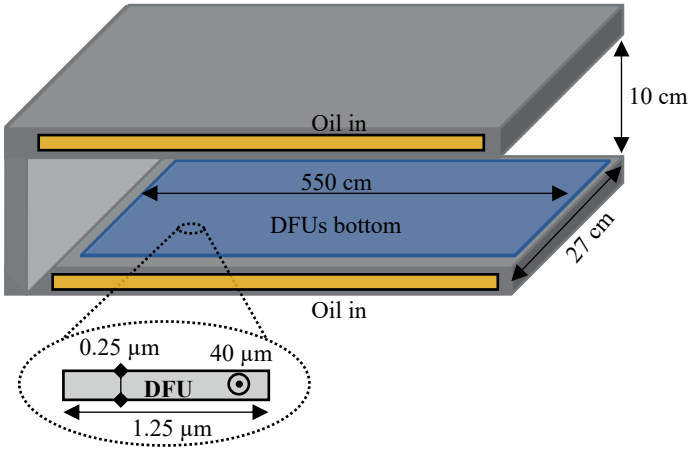

Figure 9.4. Schematic representation of the design of the prototype upscaled microfluidic emulsification device. Representation is not to scale.

Table 9.2. Overview of important parameter of the prototype upscaled microfluidic emulsification device.

Input for design of prototype	**UPE_{5x1} (Chapter 3)**	**Prototype**	**Ratio (Prototype/ UPE_{5x1})**
Oil	rapeseed oil	rapeseed oil	-
Continuous phase	5 wt.% WPI	5 wt% WPI	-
Droplet size (μm)	3.5	0.88	0.25
Total (desired) oil throughput	0.38 mL/h	1 m^3/h	$2.6 \cdot 10^{6}$
Effective area	-	5%	-
DFUs			
Area (w · h, μm)	5 · 1	1.25 · 0.25	0.063
Oil throughput per DFU (mL/s)	$9.0 \cdot 10^{-9}$	$5.6 \cdot 10^{-10}$	0.063
Droplet formation time (ms)	2.9	0.6	0.21
Droplet formation rate per DFU (s^{-1})	$3.4 \cdot 10^{2}$	$1.7 \cdot 10^{3}$	5
DFUs	11,088	$4.9 \cdot 10^{11}$	$4.4 \cdot 10^{7}$
Droplet formation rate total device (s^{-1})	$3.8 \cdot 10^{6}$	$8.33 \cdot 10^{14}$	$2.2 \cdot 10^{8}$
Continuous phase			
Space DFUs together (m^2)	$5.5 \cdot 10^{-8}$	0.15	$2.7 \cdot 10^{6}$
Space DFUs including uneffective area (m^2)	-	3.0	-
Continuous phase channel dimensions (w · h · l, cm)	0.04 · 0.018 · 30	550 · 10 · 27	-
Continuous phase flow (m/s)	0.014	0.045	3.3
Continuous phase distance during 1 droplet (μm)	41	27	0.66
DFU substructures			
Laplace pressure bare oil-water interface (bar)	0.72	2.9	4.0
(Desired) Blow-up pressure (bar)	2.7	10	3.7
DFU substructures (w · h · l, μm)	5 · 1 · 50	1.25 · 0.25 · 40	-
*Substructures flow resistance (per DFU) (*Pa s m^{-3}*)*	$2.8 \cdot 10^{19}$	$1.8 \cdot 10^{21}$	65

The device is designed as a sieve-type of device, and the continuous phase channel will be a shallow and wide slit (Figure 9.4). Ideally, DFUs are placed in both the top and bottom plate and form droplets actively. For a non-stacked layout, both the top and bottom plates (containing the DFUs) have total dimensions of 0.27 · 5.5 m, which should be subdivided into smaller plates. The height of the continuous phase slit would be 10 cm. For the chosen productivity, this results in a laminar continuous phase flow with a velocity of 0.045 m/s (Re ≈ 900). At this flow velocity, the interfacial tension force was expected to be at least ten times higher than the drag force by the continuous phase, which ensures that the droplet formation mechanism is still spontaneous (see calculation below).

Viscous drag force versus interfacial tension force

The viscous force by the continuous phase flow around an impermeable oil droplet, neglecting lubrication effects, can be estimated using the Stokes drag, as: $F_v = 6\pi\eta a v$, where η is the continuous phase viscosity (~ 1.5 mPa s), a the diameter of the droplet (1 μm) and v the continuous phase flow (0.045 m/s on

average, assumed to be 0.01 m/s at 1 μm from the channel wall). Using these relatively high values, this generates a $F_v \sim 3 \cdot 10^{-10}$.

The interfacial tension force can be estimated by $F_i = \gamma x$, where γ is the interfacial tension (~ 20 mN/m) and x the typical length scale (half the height of the DFU, 0.125 μm). Using these relatively low values generates a F_i of $\sim 3 \cdot 10^{-9}$. Therefore, the interfacial tension force is expected to be the dominant force during droplet formation mechanism in this case study for upscaling microfluidic emulsification (Table 9.2).

The substructures of the DFUs have a major impact on the productivity. Here, the Laplace pressure of the bare oil-water meniscus inside the DFU will be ~ 2.9 bar. Ideally, we would have a blow-up pressure of around 10 bar to allow for immediate forward motion of the meniscus (so, without the need for surfactant adsorption), which makes refilling of the DFU quick (Chapter 2). In addition, having a higher blow-up pressure than the Laplace pressure of the bare oil-water meniscus will promote DFU activation (Chapter 2 & 3). Based on this blow-up pressure of 10 bar and the 16 times lower flow per DFU of this device compared to UPE_{5x1} (Chapter 3), the flow resistance, expressed per DFU, would have to be $1.7 \cdot 10^{21}$ Pa s m^{-3} when using rapeseed oil. To reach this, a DFU with a width, height, and length of 1.25, 0.25, and 40 μm is sufficient ($1.8 \cdot 10^{21}$ Pa s m^{-3}) (Figure 9.4). The main plateau can be higher (e.g., 1 μm), which will still allow for gradual supply of oil to the DFUs without generating an unnecessarily high blow-up pressure. The DFUs should be connected to multiple main plateaus to ensure a gradual oil supply to all the DFUs. As an alternative for the design suggested here (Figure 9.4), the continuous phase could flow around a hollow tube in which the oil flows and which contains the DFUS.

It is interesting to hypothesise what the situation would when using the droplet formation mechanism based on the physical push by a neighbouring droplet for upscaling the production of 1-μm droplets. To achieve this, the centre-to-centre distance between the DFUs should be 0.6 μm (1/1.7) (Chapter 3), although it has not been explored whether this droplet formation mechanism is still applicable at that scale. Droplet productivity will be less limited by the interfacial tension force, and therefore a higher maximum productivity is in principle possible (Chapter 3). This droplet formation mechanism only works well if droplets interact, which is relatively easy to achieve in the small devices used in this thesis due to the confinement generated by a top plate (Chapter 3). It may be harder to achieve this droplet formation mechanism in a free-standing sieve-type of device. To the best of our knowledge, it has not been observed in

sieve-type devices (Chapter 2), and this is part of follow-up projects.

Device material
For the production of oil droplets, the DFU walls need to be wetted well by the continuous phase to promote droplet formation (Maan et al., 2013b; Sahin et al., 2016; Van Dijke et al., 2008). Besides, the material must be robust for the duration of the production run, and, if the device is used repeatedly, it should be robust to chemicals used to clean the device. Glass and silicon chips have shown their worth in proof-of-concept studies (Chapter 2, 3). However, even though glass is very robust, and (if clean) very hydrophilic, the major disadvantage of glass and silicon is that these materials are brittle. This may lead to contamination of the products without being able to trace the shards in the final food product. Therefore, it is not desirable to use process equipment of glass in food or pharma production. It is very challenging to make devices out of other materials because structures as small as a few μm, and preferably even smaller than 1 μm, have to be made. Besides, the channel walls have to be either very hydrophilic for the preparation of O/W emulsions or hydrophobic for the preparation of W/O emulsions. It is not trivial that these wall properties remain their hydrophilicity given the reported interactions with ingredients (Sahin et al., 2016).

Other microfluidic device materials than glass or silicon as channel walls have been used. Maan and co-workers, used metal-coated surfaces for the production of O/W emulsions (Maan et al., 2013a). The main factors that were of influence on the productivity were presumably the surface roughness and the surface wettability. Productivities and droplet sizes measured for copper-nickel devices were similar to those determined for silicon devices. More specifically for lipid oxidation, the use of copper might be unfavourable because it is known to be a prooxidant. The use of microfluidics (to date mainly in science) has grown steadily in the last decades, and nowadays there is also a major interest in manufacturing devices in all types of materials, such as: hydrogels (Nie et al., 2020), polymers (Niculescu et al., 2021) and paper (Li et al., 2012). In addition, 3D printing of the devices is named as a promising technology for fabrication of the devices (Bhattacharjee et al., 2016). It is good to see all these opportunities arising, and it is expected that the dimensions that can be prepared will come closer to the ones described here. For now, this is still a challenge, as are the properties of the materials (often rather hydrophobic) in relation to the wettability needed for oil-in-water emulsification. In that sense, the in-air-microfluidic technology could be an interesting option because droplet formation takes place in flight (Schroën et al., 2022b; Visser et al., 2018), which is described as the manipulation of microfluidic streams in the air, so without

the use of a microfluidic chip. One disadvantage of this technology is that numbering-up DFUs is not that easily achieved because the flow of each DFU has to be regulated very precisely.

Companies already using microfluidic emulsification
Based on all of the above, it is not surprising that start-up companies have aimed to upscale microfluidic emulsification to industrial scale. [1-4] Here, we give a short overview of current efforts. The information used here is obtained from the websites of those companies.

The materials used to fabricate the devices were, for example, glass[2] or ceramics[1]. The production of specific medicines using microfluidics is currently already under development.[2] The advantages of using microfluidics according to these companies are: to improve medicines regarding the accurate and extended-acting release of bioactive molecules;[1-4] improved active beauty with superior appearance;[2] and enhanced aromatic experience by minimizing bitterness yet creating a new level of taste[2]. Also in-air microfluidics is being upscaled.[4] The advantage of this technology is that there is no need for the use of a microfluidic chip.

[1] https://www.nanomi.com/
[2] https://www.microcaps.ch/
[3] https://www.emultech.nl/
[4] https://iamfluidics.com/

9.2.4 Intermediate conclusions: dynamics of droplet formation across length scales

Producing emulsions with conventional emulsification techniques results in wide droplet size distributions that cover ranges of up to three orders of magnitude. These distributions include droplets that are as small as 10^1 nm, even when the emulsions are stabilised by proteins. It remains challenging to detect these very small droplets, and here we used cryo-TEM to probe their sizes. With microfluidics, emulsions with very narrow droplet size distributions can be prepared, which do not contain very small droplets. Within this thesis, we established scaling relations for the design of upscaled spontaneous emulsification devices. This resulted in the ability to generate droplet sizes between 3.5-30 μm at production rates that allowed for lipid oxidation experiments outside the chip.

When considering microfluidics in the light of producing a 10-wt.% rapeseed

oil-based emulsion with droplets of < 1 μm at a productivity of 10 m^3/h, we concluded that this may be possible in the future, although challenges remain: (i) the choice of appropriate construction materials for such devices (integrity, inertness, wettability), (ii) control over droplet filling in the continuous phase channels, (iii) improved understanding of maximum productivity for different ingredients, without imposing coalescence and/or other instabilities, (iv) the possible use of the second droplet formation regime that is reliant on physical droplet interactions.

The fact that multiple start-ups are working on upscaling microfluidic emulsification may hint at production of monodisperse emulsions becoming feasible at industrial-relevant scale. However, the incentives to actually apply it at this scale will greatly depend on the need to replace current technologies that have an impressive track record. Only if additional benefits start playing a role, such as the considerable reduction in energy, this will drive innovation for bulk products with relatively low added-value. For their high-added value counterparts that generally can be produced at much smaller scale, benefits related to the ultimate control of size (relevant to controlled delivery products) may push innovation. This seems to be the case in the start-ups that we noted.
Away from upscaling, the microfluidic emulsification devices that we developed have shown their worth to improve our fundamental understanding of lipid oxidation in emulsions. This is further described in the next section.

9.3 Dynamics of lipid oxidation in emulsions across length scales

The Mahonaisse, first served in 1756, would have lost its appreciation due to lipid oxidation in just a few days because at the time probably no antioxidants were used (at least not for that purpose). In addition, a fridge did not yet exist, which could have counteracted both oxidation and microbial growth. Even now, more than 250 years later, the industry still struggles with counteracting lipid oxidation. In this thesis, we have focused on many different length scales that are involved in lipid oxidation: from the tube in which samples were incubated (several cm), to spray-dried emulsion powder particles (a few hundreds of μm), to oil droplets (100-0.01 μm), to interfaces (a few nm), to continuous phase components (a few nm), and, finally, all the way down to the formation of molecules that can result in an undesired taste (< 1 nm). In this section, the findings in this thesis across these length scales will be discussed from large (incubation tube) to small (single molecules), with a specific focus on the asset of microfluidic emulsification devices to improve our fundamental understanding of lipid oxidation in emulsions.

9.3.1 Emulsion as a whole

Incubation tubes (10-1 cm) used, set the maximum concentration of lipid oxidation that can take place. Through mass balances for oxygen, this can be checked, but this is often not considered (Schroën et al., 2022a). For bulk oil and mayonnaise, it has been shown successfully that by summing up the hydroperoxides, aldehydes, and epoxides, the mass balance of oxygen can be covered (Boerkamp et al., 2022). In Chapter 4, the oxygen consumption was faster than the total amount of lipid oxidation products formed, which was probably due to co-oxidation of Tween 20. Even when only part of the oxygen is consumed by other reactions, this will limit the formation of peroxyl radicals because the its formation rate is determined by a reaction rate constant multiplied by the substrate concentrations (including O_2; appendix Chapter 4) (Schroën et al., 2022a).

In static systems, the concentration of oxygen available for the reaction will be the saturation concentration in oil (~ 1.4 mmol/kg oil at 25 °C (Cuvelier et al., 2017)). As soon as oxidation reactions start taking place, the oxygen concentration in the oil will reduce, but it can be supplemented by the oxygen present in the headspace. Oxygen diffusion can be rather slow, which leads to an oxygen gradient over the height of the tube. For a standing tube, the diffusion of oxygen from the headspace to 10 cm into the oil will typically take hundreds of hours (Schroën et al., 2022a). Precaution is also needed regarding opening of tubes during incubation because this implies that the headspace will be replenished with oxygen, which will reboot the oxidation reaction. This also occurs in practice if consumers reopen the package after partial use. Finally, if the incubation tube is not properly sealed, oxygen can leak into the tube. This can cause both faster oxidation and a higher total amount of oxidation products formed. In practice, oxygen leakage in test tubes is hardly ever considered.

Powder particles (500-10 µm) characteristics have been postulated to have a major impact on lipid oxidation in (spray-)dried emulsions, where the oil is either 'encapsulated' in the matrix or spread over the surface of the powder particle. In literature, many studies ascribe the faster oxidation of surface free oil to its enhanced oxygen accessibility compared to encapsulated oil droplets (Hardas et al., 2002; Morales et al., 2015; Velasco et al., 2003, 2006, 2009). It has been argued that the more dense the matrix, the better it protects against the oxygen accessibility (Drusch et al., 2007, 2012; Hogan et al., 2003; Imagi et al., 1992; Orlien et al., 2000). This only holds for matrixes free of defects, which would be quite a challenge to meet in practice.

In our study on spray-dried emulsions, we found that for both the encapsulated and surface free oil, the relatively hydrophobic antioxidants were most effective (Chapter 8). We ascribed this result to the partitioning of nonpolar antioxidants to the oil where they can effectively counteract lipid oxidation. The encapsulated oil oxidised faster when the oil contained no antioxidant or a relatively polar antioxidant, whereas the surface free oil oxidised faster in the presence of an effective (relatively hydrophobic) antioxidant. In other words, for both types of oil, lipid oxidation seemed to increase slightly when the alkyl chain length of the antioxidant was increased from 8 to 16 alkyl groups, and this seemed to be a little bit more pronounced for the surface free oil than for the encapsulated oil. This indicates that the accessibility of oxygen to the oil is not the only factor that determines the sensitivity of lipid oxidation in spray-dried emulsions. If the limited oxygen accessibility of encapsulated oil would be the reason for lower oxidation compared to the surface free oil, then especially the maximum rate of hydroperoxide formation should be lower, and that is not what we found. Others have shown that the increase in lipid oxidation products in surface free oil often just starts earlier compared to in the encapsulated oil (Morales et al., 2015; Velasco et al., 2006). This can be an indication of a lower concentration of oxygen present in the encapsulated oil, but also of a higher concentration of radicals in the surface free oil, which will also affect the course of the reaction later on. Higher concentrations of radicals will increase the formation of hydroperoxides, which also is a substrate for new radical generation (Chapter 4, Reaction 4.I & 4.II). On the other hand, the concentration of radicals can be suppressed by antioxidants, if they are present at the right location. In literature, it has been shown that hydrophilic prooxidants are not active in spray-dried emulsions (Orlien et al., 2000), which indicates that the initiation of lipid oxidation in spray-dried emulsions most probably starts either in the oil itself, or at the oil-matrix interface.

9.3.2. Oil droplets of different sizes

Oil droplets (100-0.01 μm) emulsified in a continuous phase generally oxidise earlier and faster compared to bulk oils (Berton-Carabin et al., 2014; McClements et al., 2000; Van Ruth et al., 1999). This is postulated to be due to promoted contact between unsaturated lipids in droplets and prooxidants dissolved in the continuous phase. This would also suggest that smaller droplets oxidise faster because of their increased interfacial area, but clear evidence for this was lacking (Berton-Carabin et al., 2014). As pointed out in this thesis, it is impossible to study this systematically in classically prepared emulsions, since their droplet sizes can span up to three orders of magnitude. Therefore, droplet size distributions necessarily overlap substantially.

As pointed out previously, microfluidic emulsification devices allowed us to produce monodisperse emulsions and vary the droplet size very systematically between 3.5 and 30 μm (Chapter 2 & 3). Using these emulsions, we showed for the first time a systematic increase of lipid oxidation with decreasing droplet size. We ascribed this result to enhanced lipid oxidation initiation reactions, presumably due to the increased interfacial area, where the prooxidant iron-EDTA complex could react with the lipids. How the reaction rate constant for initiation of lipid oxidation scales with the interfacial area most probably has to do with the partitioning of prooxidants. To quantitively relate the oil droplet size to the cascaded lipid oxidation reaction, it is favourable that no side-reactions that consume oxygen occur because this influences the course of the lipid oxidation reaction. This may even enable estimating the concentrations of radicals present.

In an actual food emulsion, the effect of droplet size on lipid oxidation may become even more complex when interfacial components exert an anti-, or prooxidant effect. Smaller droplets are expected to be exposed to both components more frequently, which may either reduce or improve their oxidative stability. The next step is to go to classically prepared emulsions, although for such emulsions it is important to follow the leads supplied in this thesis to still be able to distinguish droplet size effects from other effects.

In the smallest droplets present in emulsions (10-200 nm), lipid oxidation products were overrepresented, which is in line with the droplet size effect described in the previous section. Although the droplets of 10-200 nm only contained ~ 1.6 wt.% of the total oil, these tiny droplets did make up for ~ 50% of the total interfacial area. We, therefore, ascribe the fast oxidation of these very small droplets to their large interfacial area. This was substantiated by the higher concentration of 4-hydroxy-2-nonenal to 4-hydroperoxy-2-nonenal in the very small droplets compared to the whole emulsion (Figure 9.5). This points at increased hydroperoxide decomposition in these very small droplets leading to enhanced initiation. In turn, this leads to increased propagation of the lipid oxidation reaction.

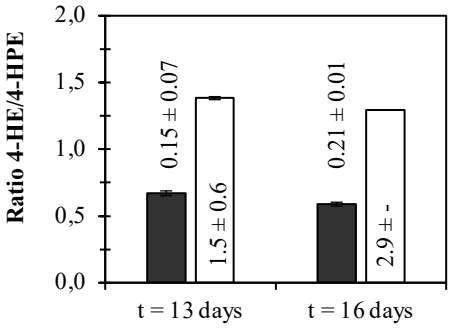

Figure 9.5. Approximation of the ratio of 4-hydroxy-enals (4-HE) to 4-hydroperoxy-enals (4-HPE) in the whole emulsion (filled bar) and in very small droplets obtained by centrifugation (open bar). Numbers indicate total amount of 4-hydro(pero)xy-enals in mmol/kg oil with their standard deviations (one measurement on one/two independently incubated emulsions originating from the same emulsion). Samples contained 0.5 wt.% Tween 20 in the continuous phase, 10 wt.% rapeseed oil, and were made with a lab-scale colloid mill (see section 5.2, Chapter 5).

In a polydisperse emulsion, containing 10^9-10^{15} droplets per mL dispersed oil, the three orders of magnitude difference in size between the largest and the smallest droplets implies that oxidation can occur in a highly heterogeneous fashion depending on droplet size. This heterogeneity was quantified and visualised by confocal laser scanning microscopy (Chapter 6). In protein-stabilised emulsions, droplets of the same size also oxidised in a heterogeneous way. Also using CLSM, we observed highly heterogenous protein oxidation, which is known to be intertangled with lipid oxidation. This heterogeneous protein oxidation is, therefore, expected to play a role in the observed heterogeneity of lipid oxidation.

Even though we did not observed this under the conditions studied, the fast oxidation of the tiny droplets might decrease the oxidation rate in other droplets due to the depletion of oxygen under specific conditions. This will especially be the case if the oxygen content in the tube is low, and/or if there is a large difference in oxidation rate between the droplets. To explain this a bit further, we can focus on hydroperoxide (LOOH) formation. For this component to form, the alkyl radical ($L^{\bullet}$) first has to react with oxygen (O_2) to form a peroxyl radical ($LOO^{\bullet}$). Next, the $LOO^{\bullet}$ has to abstract a hydrogen atom from another component (e.g., unsaturated fatty acid (LH')) to form a LOOH. These reactions are dependent on a reaction rate constant (k_2, k_3) and on the substrate concentrations (for k_2: [$L^{\bullet}$] and [O_2]; for k_3: [$LOO^{\bullet}$] and [LH']) (Schroën et al., 2022a). This cascaded reaction complicates estimating the effect of oxygen depletion on the reaction rate because the limiting step would need to be identified, before the effect of a

decrease in [O_2] can be identified (Schroën et al., 2022a).

In literature, various effects have been reported that possibly relate to the existence of these tiny droplets, and there thus is a clear need for better consideration and characterisation of these smallest droplets for many reasons. For micron-scale droplets, the interfacial volume is negligible (McClements et al., 2000). In contrast, this is not the case for droplets < 200 nm of which the interfacial is > 13 vol.% of the total droplet (when using an interfacial thickness of 5 nm) (McClements et al., 2000). Please keep in mind that the amount of oil in the very small droplets could be as low as 1.7 wt.% (Chapter 5), so the total interfacial volume is still small compared to the oil volume in such an emulsion. On the other hand, the very small droplets are important to consider when interfacial phenomena are under scrutiny because the very small droplets can generate half of the total oil-water interface of the emulsion (Chapter 5). If they are not considered, this may lead to misinterpretations such as a 'continuous phase' containing lipid hydroperoxides, which probably were actually present in the very small droplets (Nuchi et al., 2002). The fast-oxidising very small droplets could not be included in the measurement of lipid oxidation by confocal microscopy (Chapter 7). Therefore, with confocal microscopy, a major part of lipid oxidation will be missed when applied to polydisperse emulsions (Chapter 7). The very small droplets also complicate surface load determination, which has been based on excess emulsifier concentration in the subnatant (that probably contained very small droplets) (Berton et al., 2011a; Bos et al., 2001; Faraji et al., 2004; Ye, 2008). In this regard, spontaneous microfluidic emulsification might be the way forward to investigate emulsions because they produce very monodisperse that are free of very small droplets.

9.3.3 Continuous phase

Continuous phase components (~ 0.1-10 nm) such as proteins and surfactants have been related to pro- and/or antioxidative effects (Berton-Carabin et al., 2014). In addition to this, **lipid oxidation products (~ 0.1-3 nm)** that were formed in the oil droplets can also transfer to the continuous phase (Jacobsen et al., 1999; Vandemoortele et al., 2020) or to other droplets (Chapter 7) (Li et al., 2020). We found that short and hydrophilic lipid oxidation products, such as 4-hydroperoxy-2-nonenal (solubility in water over 60 g/L), can be rapidly transferred between droplets (Chapter 7), although it is good to keep in mind that the actual concentrations of such oxidation products are low. This implies that the actually measured values of such oxidation products may be lower than the total amount that was formed, for example, in a very small droplet. Triglycerides (TAGs) bearing a hydroperoxide group did not exchange between

droplets, which was most probably due to their extremely poor solubility in water. In order to predict the transfer behaviour of oxidation products, the molecular structure and properties (size, hydrophilicity) would need to be compared, but TAGs and 4-hydroperoxy-2-nonenal are two extremes. Where the transition takes place from transferring to non- or slowly transferring component cannot be predicted to date. Measuring partitioning behaviour in non-reacting two phase systems could be a way to go. Alternatively, systematically adjusting the properties of the component of interest by changing an alkyl chain length (as done in chapter 8 for antioxidants) could improve our understanding of transferring components in emulsions. Other suggestions from literature that can be taken into account are: (i) hydrophobic interactions of components with the oil (You et al., 2012) and (ii) component-specific transfer through surfactant micelles (Villeneuve et al., 2021).

The transfer of reactive lipid oxidation products to the continuous phase, possibly increased Tween 20 oxidation in Chapter 4. In line with this, it has been shown that 4-hydroxy-2-nonenal can be degraded by (oxidation) reactions in a Tween 20 solution (Vandemoortele et al., 2020). Such reactions might even be more pronounced for 4-hydroperoxy-2-nonenal because it bears an even more reactive hydroperoxide group instead of a hydroxide group. These findings shed light on how intertangled the oxidation of continuous and dispersed phase components may be. For example, it has been found previously that lipid oxidation products can bind covalently and noncovalently to proteins, which especially occurs at the interface (Berton et al., 2012). In addition, this may also occur to lipid oxidation products that enter the continuous phase (Vandemoortele et al., 2020). Besides, emulsifiers have been shown to ignite lipid oxidation and *vice versa* (Berton-Carabin et al., 2014; Nuchi et al., 2001; Østdal et al., 2002), but one often ignored aspect is that co-oxidation of components will consume oxygen that is then not available for lipid oxidation (Chapter 4). If experiments were conducted in closed containers, this may provoke the conclusion that the component of interest exerts an antioxidant effect, whereas it rather exerts an 'oxygen-snatching effect'.

Regarding the transfer of lipid oxidation products to other droplets, we found that the addition of 4-hydroperoxy-2-nonenal (0.2 mmol/kg oil) to vegetable oil droplets further devoid of this component, can promote subsequent lipid oxidation; yet, this occurred with substantial variability regarding the course of the reaction among independent replicates. Whether such oxidation products ignite oxidation in the 'fresh' droplets, will depend on how easily that droplet would oxidise without that sensitive component. In the case of BODIPY

665/676 present in medium chain triglyceride oil droplets, transferred sensitive components probably subsequently ignite oxidation via propagation reactions (H abstraction) (Li et al., 2020). On the other hand, if the 'fresh' droplet already contains molecules that are sensitive to initiation reactions, the provision of other sensitive molecules is most probably not going to have a marked impact as seemed to be the case in the emulsions studied in this thesis.

Finally, the main role that lipid oxidation products play in lipid oxidation, is that they provide an undesired flavour to food and other biobased products. Off-flavour perception has been shown to be a complex subject because of multiple reasons: (i) there is a very wide range of lipid oxidation products, and the products formed are dependent on oxidative pathways (Hoppenreijs et al., 2021; Merkx et al., 2018; Schaich, 2005), which in turn are dependent on many aspects related to the incubation conditions and on the emulsion system itself (Berton-Carabin et al., 2014), (ii) different individual molecules provide a different off-flavour perception (Venkateshwarlu et al., 2004), (iii) synergistic and compensatory effects have been shown between oxidation products (Jacobsen, 1999; Venkateshwarlu et al., 2004), and maybe even most interestingly, (iv) oxidation products present in the continuous phase have been described to have a major contribution to off-flavour perception (Jacobsen, 1999).

All these findings highlight the importance of an improved understanding of the dependency of lipid oxidation on the droplet size, the transfer of lipid oxidation products through the continuous phase, and the intertangled nature of (co-) oxidation of lipids and components present in the continuous phase, to which this thesis has already made valuable contributions.

9.3.4 Intermediate conclusions: dynamics of lipid oxidation in emulsions across length scales

The complexity of lipid oxidation in emulsions arises from many dynamic processes that occur across wide length scales. In this thesis, we did shed light on multiple dynamic aspects of lipid oxidation in emulsions. This was done by using microfluidics as a tool to prepare monodisperse emulsions with different droplet sizes (section 9.2.2) and by using advanced analytical techniques, such as: NMR spectroscopy, confocal microscopy, and cryo-TEM, for the characterisation of the oxidising emulsions. This allowed us, for example, to show very systematically that increasing the specific surface area of an emulsion also increases lipid oxidation, most probably because this favours catalysis-based reactions that initiate oxidation. The use of kinetic modelling

enabled us to get an idea of how such reactions affect the course of the lipid oxidation reaction.

For polydisperse emulsions, cryo-TEM allowed us to map the droplet size distribution of the tiniest droplets present. This led to the discovery that the large difference in droplet sizes is also reflected in the oxidation rates, making emulsions very heterogeneous reacting systems. The droplet size-dependent heterogeneity of lipid oxidation was also quantified and visualised with CLSM. In protein-stabilised emulsions, droplets of the same size also oxidised in a heterogeneous way. It is expected that (co-)oxidation of the protein plays a role in these differences. Under specific conditions, quickly oxidising droplets may affect overall oxidation in other parts of the emulsions in two ways: (i) depletion of oxygen and therewith reduced lipid oxidation in other droplets, and, (ii) transfer of reactive lipid oxidation intermediates, such as 4-hydroperoxy-enals, to other droplets, where lipid oxidation can then be initiated under the condition that the transferred molecule is (much) more sensitive to reactions that initiate oxidation than the substrate already present. Besides, co-oxidising components will affect the course of oxidation reactions, and this may be mistaken for an antioxidant effect imposed by such components.

9.4 Conclusions: dynamics of lipid oxidation and droplet formation across length scales

Throughout this chapter, we have shown that to understand lipid oxidation, we have to consider different dynamic processes across a wide length scale. To disentangle these dynamic processes, microfluidics can be used as an ultimate tool to produce emulsions with well-controlled droplet sizes. Microfluidic-made emulsions allow for improving our understanding regarding radical formation in emulsions, which enables describing of the course of the lipid oxidation reaction using modelling. These lipid oxidation reactions are intertwined with the oxidation of continuous phase components, which is an aspect that is still poorly understood. We could improve our understanding of this aspect if we could measure: the type, concentration, and chemical status of these continuous phase components, but that has been challenging due to the presence of tiny droplets. Also this challenge can be tackled by using microfluidic-made emulsions, since tiny droplets are not present in such samples, and since we can systematically vary the amount of oil-water interface. To extent the findings obtained for microfluidic-made emulsions to classic emulsions, we have to consider that classic emulsions contain droplets of many different sizes, all with

different oxidation statuses. In addition, we have to consider how the oxidation in the droplets of many sizes is intertwined with the wide variety of components present at the interface and in the continuous phase, which are either 'naturally' present there or that have moved there after being formed by lipid oxidation reactions occurring inside oil droplets.

It is incredible how much we have learned about emulsions ever since the first production of the 'Mahonaisse' in 1756 to which this thesis has made a valuable contribution. We can still learn more, especially regarding: radical concentrations, reaction kinetics, transfer effects, and co-oxidising species. This will bring us in a much better position to predict ánd extend the oxidative shelf life of both wet and spray-dried emulsion products. For products like mayonnaise and infant milk formula, lipid oxidation is the main deterioration factor, but for other products, microbial and physical stability have to be considered as well. Over the past centuries, such knowledge has contributed to enormous improvements in emulsion product stability, which started from a 'stability' of probably a few days, to products that are stable for over one year now. This is partly due to the evolution in emulsification processes, which have evolved from the use of hand-whisk tools to homogenisers, and this evolution is still ongoing. Producing emulsion products by microfluidics at industrial scale may sounds like a futuristic tale. However, it might lay within reach already, as indicated by the upscaled prototype microfluidic device presented in this chapter and by the emerging start-up companies that are working on upscaling this technology. This might lead to the next revolution in terms of improved shelf life and added functionality by controlled release of active compounds, either for food or pharmaceutical applications. Until then, we will definitely continue to explore the use of microfluidic tools for an improved understanding of emulsion stability.

References

Abrahamse, A. J., Van Lierop, R., Van der Sman, R. G. M., Van der Padt, A., & Boom, R. M. (2002). Analysis of droplet formation and interactions during cross-flow membrane emulsification. *Journal of Membrane Science*, *204*(1–2), 125–137.

Alemán, M., Bou, R., Guardiola, F., Durand, E., Villeneuve, P., Jacobsen, C., & Sørensen, A.-D. M. (2015). Antioxidative effect of lipophilized caffeic acid in fish oil enriched mayonnaise and milk. *Food Chemistry*, *167*, 236–244.

Amstad, E., Chemama, M., Eggersdorfer, M., Arriaga, L. R., Brenner, M. P., & Weitz, D. A. (2016). Robust scalable high throughput production of monodisperse drops. *Lab on a Chip*, *16*(21), 4163–4172.

Andrikopoulos, N. K. (2002). Triglyceride species compositions of common edible vegetable oils and methods used for their identification and quantification. *Food Reviews International*, *18*(1), 71–102.

Atarés, L., Marshall, L. J., Akhtar, M., & Murray, B. S. (2012). Structure and oxidative stability of oil in water emulsions as affected by rutin and homogenization procedure. *Food Chemistry*, *134*(3), 1418–1424.

Awad, T. S., Asker, D., & Romsted, L. S. (2018). Evidence of coexisting microemulsion droplets in oil-in-water emulsions revealed by 2D DOSY 1H NMR. *Journal of Colloid and Interface Science*, *514*, 83–92.

Azuma, G., Kimura, N., Hosokawa, M., & Miyashita, K. (2009). Effect of droplet size on the oxidative stability of soybean oil TAG and fish oil TAG in oil-in-water emulsion. *Journal of Oleo Science*, *58*(6), 329–338.

Baik, M., Suhendro, E. L., Nawar, W. W., McClements, D. J., Decker, E. A., & Chinachoti, P. (2004). Effects of antioxidants and humidity on the oxidative stability of microencapsulated fish oil. *Journal of the American Oil Chemists' Society*, *81*(4), 355–360.

Banerjee, C., Breitenbach, T., & Ogilby, P. R. (2018). Spatially resolved experiments to monitor the singlet oxygen initiated oxidation of lipid droplets in emulsions. *ChemPhotoChem*, *2*(7), 586–595.

Barden, L., & Decker, E. A. (2016). Lipid oxidation in low-moisture food: a review. *Critical Reviews in Food Science and Nutrition*, *56*(15), 2467–2482.

Berton-Carabin, C. C., Ropers, M. H., & Genot, C. (2014). Lipid Oxidation in Oil-in-Water Emulsions: Involvement of the Interfacial Layer. *Comprehensive Reviews in Food Science and Food Safety*, *13*(5), 945–977.

Berton-Carabin, C. C., Sagis, L., & Schroën, K. (2018). Formation, Structure, and Functionality of Interfacial Layers in Food Emulsions. *Annual Review of Food Science and Technology*, *9*(1), 551–587.

Berton, C., Genot, C., & Ropers, M.-H. (2011a). Quantification of unadsorbed protein and surfactant emulsifiers in oil-in-water emulsions. *Journal of Colloid and Interface Science*, *354*(2), 739–748.

Berton, C., Ropers, M.-H., Guibert, D., Solé, V., & Genot, C. (2012). Modifications of interfacial proteins in oil-in-water emulsions prior to and during lipid oxidation. *Journal of Agricultural and Food Chemistry*, *60*(35), 8659–8671.

Berton, C., Ropers, M.-H., Viau, M., & Genot, C. (2011b). Contribution of the interfacial layer to the protection of emulsified lipids against oxidation. *Journal of Agricultural and Food Chemistry*, *59*(9), 5052–5061.

Bhattacharjee, N., Urrios, A., Kang, S., & Folch, A. (2016). The upcoming 3D-printing revolution in microfluidics. *Lab on a Chip*, *16*(10), 1720–1742.

Boerkamp, V. J. P., Merkx, D. W. H., Wang, J., Vincken, J.-P., Hennebelle, M., & van Duynhoven, J. P. M. (2022). Quantitative assessment of epoxide formation in oil and mayonnaise by 1H-13C HSQC NMR spectroscopy. *Food Chemistry*, *390*, 133145.

Bolland, J. L. (1946). Kinetic studies in the chemistry of rubber and related materials. I. The thermal oxidation of ethyl linoleate. *Proceedings of the Royal Society of London. Series A. Mathematical and Physical Sciences*, *186*(1005), 218–236.

Bos, M. A., & Van Vliet, T. (2001). Interfacial rheological properties of adsorbed protein layers and surfactants: a review. *Advances in Colloid and Interface Science*, *91*(3), 437–471.

Botti, T. C., Hutin, A., Quintella, E., & Carvalho, M. S. (2022). Effect of interfacial rheology on drop coalescence in water–oil emulsion. *Soft Matter*, *18*(7), 1423–1434.

Cao, Y., & Xiong, Y. L. (2017). Interaction of whey proteins with phenolic derivatives under neutral and acidic pH conditions. *Journal of Food Science*, *82*(2), 409–419.

Charcosset, C., Limayem, I., & Fessi, H. (2004). The membrane emulsification process—a review. *Journal of Chemical Technology and Biotechnology*, *79*(3), 209–218.

Chen, B., McClements, D. J., & Decker, E. A. (2011). Minor components in food oils: a critical review of their roles on lipid oxidation chemistry in bulk oils and emulsions. *Critical Reviews in Food Science and Nutrition*, *51*(10), 901–916.

Chen, B., McClements, D. J., & Decker, E. A. (2013). Design of foods with bioactive lipids for improved health. *Annu. Rev. Food Sci. Technol*, *4*(1), 35–56.

Conchouso, D., Castro, D., Khan, S. A., & Foulds, I. G. (2014). Three-dimensional parallelization of microfluidic droplet generators for a litre per hour volume production of single emulsions. *Lab on a Chip*, *14*(16), 3011–3020.

Costa, M., Freiría-Gándara, J., Losada-Barreiro, S., Paiva-Martins, F., & Bravo-Díaz, C. (2020). Effects of droplet size on the interfacial concentrations of antioxidants in fish and olive oil-in-water emulsions and nanoemulsions and on their oxidative stability. *Journal of Colloid and Interface Science*, *562*, 352–362.

Coupland, J. N., Zhu, Z., Wan, H., McClements, D. J., Nawar, W. W., & Chinachoti, P. (1996). Droplet composition affects the rate of oxidation of emulsified ethyl linoleate. *Journal of the American Oil Chemists' Society*, *73*(6), 795–901.

Cui, L., Shen, P., Gao, Z., Yi, J., & Chen, B. (2019). New insights into the impact of sodium chloride on the lipid oxidation of oil-in-water emulsions. *Journal of Agricultural and Food Chemistry*, *67*(15), 4321–4327.

Cuvelier, M.-E., Soto, P., Courtois, F., Broyart, B., & Bonazzi, C. (2017). Oxygen solubility measured in aqueous or oily media by a method using a non-invasive sensor. *Food Control*, *73*, 1466–1473.

da Silveira, T. F. F., Laguerre, M., Bourlieu-Lacanal, C., Lecomte, J., Durand, E., Figueroa-Espinoza, M. C., Baréa, B., Barouh, N., Castro, I. A., & Villeneuve, P. (2021). Impact of surfactant concentration and antioxidant mode of incorporation on the oxidative stability of oil-in-water nanoemulsions. *LWT*, *141*, 110892.

Dangla, R., Fradet, E., Lopez, Y., & Baroud, C. N. (2013). The physical mechanisms of step emulsification. *Journal of Physics D: Applied Physics*, *46*(11), 114003.

Deng, B., Schroën, K., & de Ruiter, J. (2021). Effects of dynamic adsorption on bubble formation and coalescence in partitioned-EDGE devices. *Journal of Colloid and Interface Science*, *602*, 316–324.

Deng, B., Schroën, K., & de Ruiter, J. (2022a). Dynamics of bubble formation in spontaneous microfluidic devices: Controlling dynamic adsorption via liquid phase properties. *Journal of Colloid and Interface Science*, *622*, 218–227.

Deng, B., Schroën, K., Steegmans, M., & de Ruiter, J. (2022b). Capillary pressure-based measurement of dynamic interfacial tension in a spontaneous microfluidic sensor. *Lab on a Chip*, *22*(20), 3860–3868.

Deng, B., Wijnen, D., Schroën, K., & de Ruiter, J. (2022c). Onsite coalescence behaviour of whey protein-stabilized bubbles generated at parallel microscale pores: Role of pore geometry and liquid phase properties. *Food Hydrocolloids*, 108435.

Dhont, J. K. G. (1996). Chapter 3 Light scattering. In J. K. G. Dhont (Ed.), *Studies in Interface Science* (Vol. 2, Issue C, pp. 107–170). Elsevier.

Dimakou, C. P., Kiokias, S. N., Tsaprouni, I. V, & Oreopoulou, V. (2007). Effect of processing and storage parameters on the oxidative deterioration of oil-in-water emulsions. *Food Biophysics*, *2*(1), 38–45.

Drummen, G. P. C., Gadella, B. M., Post, J. A., & Brouwers, J. F. (2004). Mass spectrometric characterization of the oxidation of the fluorescent lipid peroxidation reporter molecule C11-BODIPY581/591. *Free Radical Biology and Medicine*, *36*(12), 1635–1644.

Drusch, S., Rätzke, K., Shaikh, M. Q., Serfert, Y., Steckel, H., Scampicchio, M., Voigt, I., Schwarz, K., & Mannino, S. (2009). Differences in free volume elements of the carrier matrix affect the stability of microencapsulated lipophilic food ingredients. *Food Biophysics*, *4*(1), 42–48.

Drusch, S., Serfert, Y., Berger, A., Shaikh, M. Q., Rätzke, K., Zaporojtchenko, V., & Schwarz, K. (2012). New insights into the microencapsulation properties of sodium caseinate and hydrolyzed casein. *Food Hydrocolloids*, *27*(2), 332–338.

Drusch, S., Serfert, Y., Scampicchio, M., Schmidt-Hansberg, B., & Schwarz, K. (2007). Impact of physicochemical characteristics on the oxidative stability of fish oil microencapsulated by spray-drying. *Journal of Agricultural and Food Chemistry*, *55*(26), 11044–11051.

Durand, E., Zhao, Y., Ruesgas-Ramón, M., Figueroa-Espinoza, M. C., Lamy, S., Coupland, J. N., Elias, R. J., & Villeneuve, P. (2019). Evaluation of antioxidant activity and interaction with radical species using the vesicle conjugated autoxidizable triene (VesiCAT) assay. *European Journal of Lipid Science and Technology*, *121*(5), 1800419.

Eggersdorfer, M. L., Seybold, H., Ofner, A., Weitz, D. A., & Studart, A. R. (2018). Wetting controls of droplet formation in step emulsification. *Proceedings of the National Academy of Sciences*, *115*(38), 9479–9484.

Faraji, H., McClements, D. J., & Decker, E. A. (2004). Role of continuous phase protein on the oxidative stability of fish oil-in-water emulsions. *Journal of Agricultural and Food Chemistry*, *52*(14), 4558–4564.

Forney, L. J., Reddy, C. A., Tien, M., & Aust, S. D. (1982). The involvement of hydroxyl radical derived from hydrogen peroxide in lignin degradation by the white rot fungus Phanerochaete chrysosporium. *Journal of Biological Chemistry*, *257*(19), 11455–11462.

Frankel, E. N., Huang, S.-W., Kanner, J., & German, J. B. (1994). Interfacial phenomena in the evaluation of antioxidants: bulk oils vs emulsions. *Journal of Agricultural and Food Chemistry*, *42*(5), 1054–1059.

Freiría-Gándara, J., Losada-Barreiro, S., Paiva-Martins, F., & Bravo-Díaz, C. (2018). Differential partitioning of bioantioxidants in edible oil–water and octanol–water systems: linear free energy relationships. *Journal of Chemical & Engineering Data*, *63*(8), 2999–3007.

Friedrich, H., Frederik, P. M., De With, G., & Sommerdijk, N. A. J. M. (2010). Imaging of self-assembled structures: Interpretation of TEM and Cryo-TEM images. *Angewandte Chemie - International Edition*, *49*(43), 7850–7858.

Galvis, E., Yarusevych, S., & Culham, J. R. (2012). Incompressible laminar developing flow in microchannels. *Journal of Fluids Engineering*, *134*(1), 14503.

Ganesan, B., Brothersen, C., & McMahon, D. J. (2014). Fortification of foods with omega-3 polyunsaturated fatty acids. *Critical Reviews in Food Science and Nutrition*, *54*(1), 98–114.

Genot, C., Berton, C., & Ropers, M.-H. (2013). The role of the interfacial layer and emulsifying proteins in the oxidation in oil-in-water emulsions. In *Lipid Oxidation* (pp. 177–210). Elsevier.

Gijsbertsen-Abrahamse, A. J., van der Padt, A., & Boom, R. M. (2004). Status of cross-flow membrane emulsification and outlook for industrial application. *Journal of Membrane Science*, *230*(1), 149–159.

Gohtani, S., Sirendi, M., Yamamoto, N., Kajikawa, K., & Yamano, Y. (1999). Effect of droplet size on oxidation of docosahexaenoic acid in emulsion system. *Journal of Dispersion Science and Technology*, *20*(5), 1319–1325.

Guillén, M. D., & Ruiz, A. (2004). Formation of hydroperoxy-and hydroxyalkenals during thermal oxidative degradation of sesame oil monitored by proton NMR. *European Journal of Lipid Science and Technology*, *106*(10), 680–687.

Gumus, C. E., & Decker, E. A. (2021). Oxidation in Low Moisture Foods as a Function of Surface Lipids and Fat Content. *Foods*, *10*(4), 860.

Guo, X., Chen, M., Li, Y., Dai, T., Shuai, X., Chen, J., & Liu, C. (2020). Modification of food macromolecules using dynamic high pressure microfluidization: A review. *Trends in Food Science & Technology*.

Hardas, N., Danvirivakul, S., Foley, J. L., Nawar, W. W., & Chinachoti, P. (2002). Effect of relative humidity on the oxidative and physical stability of encapsulated milk fat. *Journal of the American Oil Chemists' Society*, *79*(2), 151–158.

Hinderink, E. B. A., de Ruiter, J., de Leeuw, J., Schroën, K., Sagis, L. M. C., & Berton-Carabin, C. C. (2021). Early film formation in protein-stabilised emulsions: Insights from a microfluidic approach. *Food Hydrocolloids*, *118*, 106785.

Hogan, S. A., O'riordan, E. D., & O'sullivan, M. (2003). Microencapsulation and oxidative stability of spray-dried fish oil emulsions. *Journal of Microencapsulation*, *20*(5), 675–688.

Hollebrands, B., & Janssen, H.-G. (2017). Liquid chromatography-atmospheric pressure photo ionization-mass spectrometry analysis of the nonvolatile precursors of rancid smell in mayonnaise. *LC GC Europe*, *30*.

Homma, R., Suzuki, K., Cui, L., McClements, D. J., & Decker, E. A. (2015). Impact of association colloids on lipid oxidation in triacylglycerols and fatty acid ethyl esters. *Journal of Agricultural and Food Chemistry*, *63*(46), 10161–10169.

Hoppenreijs, L. J. G., Berton-Carabin, C. C., Dubbelboer, A., & Hennebelle, M. (2021). Evaluation of oxygen partial pressure, temperature and stripping of antioxidants for accelerated shelf-life testing of oil blends using 1H NMR. *Food Research International*, *147*, 110555.

Horn, A. F., Barouh, N., Nielsen, N. S., Baron, C. P., & Jacobsen, C. (2013). Homogenization pressure and temperature affect protein partitioning and oxidative stability of emulsions. *Journal of the American Oil Chemists' Society*, *90*(10), 1541–1550.

Horn, A. F., Nielsen, N. S., Jensen, L. S., Horsewell, A., & Jacobsen, C. (2012). The choice of homogenisation equipment affects lipid oxidation in emulsions. *Food Chemistry*, *134*(2), 803–810.

Imagi, J., Muraya, K., Yamashita, D., Adachi, S., & Matsuno, R. (1992). Retarded oxidation of liquid lipids entrapped in matrixes of saccharides or proteins. *Bioscience, Biotechnology, and Biochemistry*, *56*(8), 1236–1240.

Jacobs, N. J., & Vandenmark, P. J. (1960). Colorimetric method for determination of triglycsrides. *Arch Biochem. Biophys*, *88*, 250–255.

Jacobsen, C. (1999). Sensory impact of lipid oxidation in complex food systems. *Lipid/Fett*, *101*(12), 484–492.

Jacobsen, C., Hartvigsen, K., Lund, P., Thomsen, M. K., Skibsted, L. H., Adler-Nissen, J., Hølmer, G., & Meyer, A. S. (2000). Oxidation in fish oil-enriched mayonnaise3. Assessment of the influence of the emulsion structure on oxidation by discriminant partial least squares regression analysis. *European Food Research and Technology*, *211*(2), 86–98.

Jacobsen, C., Meyer, A. S., & Adler-Nissen, J. (1999). Oxidation mechanisms in real food emulsions: oil-water partition coefficients of selected volatile off-flavor compounds in mayonnaise. *Zeitschrift Für Lebensmitteluntersuchung Und-Forschung A*, *208*, 317–327.

Joint, F. A. O. (2010). *Fats and fatty acids in human nutrition. Report of an expert consultation, 10-14 November 2008, Geneva*.

Kale, S. N., & Deore, S. L. (2017). Emulsion micro emulsion and nano emulsion: a review. *Systematic Reviews in Pharmacy*, *8*(1), 39.

Kargar, M., Spyropoulos, F., & Norton, I. T. (2011). The effect of interfacial microstructure on the lipid oxidation stability of oil-in-water emulsions. *Journal of Colloid and Interface Science*, *357*(2), 527–533.

Kawakatsu, T., Kikuchi, Y., & Nakajima, M. (1997). Regular-sized cell creation in microchannel emulsification by visual microprocessing method. *Journal of the American Oil Chemists' Society*, *74*(3), 317–321.

Keller, S., Locquet, N., & Cuvelier, M.-E. (2016). Partitioning of vanillic acid in oil-in-water emulsions: Impact of the Tween® 40 emulsifier. *Food Research International*, *88*, 61–69.

Kerr, J. A. (1966). Bond dissociation energies by kinetic methods. *Chemical Reviews*, *66*(5), 465–500.

Kerwin, B. A. (2008). Polysorbates 20 and 80 used in the formulation of protein biotherapeutics: structure and degradation pathways. *Journal of Pharmaceutical Sciences*, *97*(8), 2924–2935.

Khalid, N., Kobayashi, I., Neves, M. A., Uemura, K., Nakajima, M., & Nabetani, H. (2014). Monodisperse W/O/W emulsions encapsulating l-ascorbic acid: insights on their formulation using microchannel emulsification and stability studies. *Colloids and Surfaces A: Physicochemical and Engineering Aspects*, *458*, 69–77.

Khalid, N., Kobayashi, I., Wang, Z., Neves, M. A., Uemura, K., Nakajima, M., & Nabetani, H. (2015). Formulation of monodisperse oil-in-water emulsions loaded with ergocalciferol and cholecalciferol by microchannel emulsification: insights of production characteristics and stability. *International Journal of Food Science & Technology*, *50*(8), 1807–1814.

Khalid, N., Shu, G., Kobayashi, I., Nakajima, M., & Barrow, C. J. (2017). Formulation and characterization of monodisperse O/W emulsions encapsulating astaxanthin extracts using microchannel emulsification: Insights of formulation and stability evaluation. *Colloids and Surfaces B: Biointerfaces*, *157*, 355–365.

Kim, E. H.-J., Chen, X. D., & Pearce, D. (2005). Melting characteristics of fat present on the surface of industrial spray-dried dairy powders. *Colloids and Surfaces B: Biointerfaces*, *42*(1), 1–8.

Kim, J. Y., Kim, M.-J., & Lee, J. (2014). Role of moisture on the lipid oxidation determined by D2O in a linoleic acid model system. *Food Chemistry*, *146*, 134–140.

Kiokias, S., Dimakou, C., & Oreopoulou, V. (2007). Effect of heat treatment and droplet size on the oxidative stability of whey protein emulsions. *Food Chemistry*, *105*(1), 94–100.

Kobayashi, I., Mukataka, S., & Nakajima, M. (2004a). CFD simulation and analysis of emulsion droplet formation from straight-through microchannels. *Langmuir*, *20*(22), 9868–9877.

Kobayashi, I., Mukataka, S., & Nakajima, M. (2004b). Effect of slot aspect ratio on droplet formation from silicon straight-through microchannels. *Journal of Colloid and Interface Science*, *279*(1), 277–280.

Kobayashi, I., Mukataka, S., & Nakajima, M. (2005a). Effects of type and physical properties of oil phase on oil-in-water emulsion droplet formation in straight-through microchannel emulsification, experimental and CFD studies. *Langmuir*, *21*(13), 5722–5730.

Kobayashi, I., Mukataka, S., & Nakajima, M. (2005b). Novel asymmetric through-hole array microfabricated on a silicon plate for formulating monodisperse emulsions. *Langmuir : The ACS Journal of Surfaces and Colloids*, *21*(17), 7629–7632.

Kobayashi, I., Mukataka, S., & Nakajima, M. (2005c). Production of monodisperse oil-in-water emulsions using a large silicon straight-through microchannel plate. *Industrial & Engineering Chemistry Research*, *44*(15), 5852–5856.

Kobayashi, I., Murayama, Y., Kuroiwa, T., Uemura, K., & Nakajima, M. (2009). Production of monodisperse water-in-oil emulsions consisting of highly uniform droplets using asymmetric straight-through microchannel arrays. *Microfluidics and Nanofluidics*, *7*(1), 107.

Kobayashi, I., Nakajima, M., & Mukataka, S. (2003). Preparation characteristics of oil-in-water emulsions using differently charged surfactants in straight-through microchannel emulsification. *Colloids and Surfaces A: Physicochemical and Engineering Aspects*, *229*(1–3), 33–41.

Kobayashi, I., Nakajima, M., Nabetani, H., Kikuchi, Y., Shohno, A., & Satoh, K. (2001). Preparation of micron-scale monodisperse oil-in-water microspheres by microchannel emulsification. *Journal of the American Oil Chemists' Society*, *78*(8), 797–802.

Kobayashi, I., Neves, M. A., Wada, Y., Uemura, K., & Nakajima, M. (2012). Large microchannel emulsification device for mass producing uniformly sized droplets on a liter per hour scale. *Green Processing and Synthesis*, *1*(4), 353–362.

Kobayashi, I., Takano, T., Maeda, R., Wada, Y., Uemura, K., & Nakajima, M. (2008). Straight-through microchannel devices for generating monodisperse emulsion droplets several microns in size. *Microfluidics and Nanofluidics*, *4*(3), 167–177.

Kobayashi, I., Uemura, K., & Nakajima, M. (2007). Formulation of monodisperse emulsions using submicron-channel arrays. *Colloids and Surfaces A: Physicochemical and Engineering Aspects*, *296*(1–3), 285–289.

Kobayashi, I., Wada, Y., Uemura, K., & Nakajima, M. (2010). Microchannel emulsification for mass production of uniform fine droplets: integration of microchannel arrays on a chip. *Microfluidics and Nanofluidics*, *8*(2), 255–262.

Krebs, T., Schroën, K., & Boom, R. (2012). Coalescence dynamics of surfactant-stabilized emulsions studied with microfluidics. *Soft Matter*, *8*(41), 10650–10657.

Kuhn, K. R., & Cunha, R. L. (2012). Flaxseed oil–whey protein isolate emulsions: effect of high pressure homogenization. *Journal of Food Engineering*, *111*(2), 449–457.

Laguerre, M., Bayrasy, C., Panya, A., Weiss, J., McClements, D. J., Lecomte, J., Decker, E. A., & Villeneuve, P. (2015). What makes good antioxidants in lipid-based systems? The next theories beyond the polar paradox. *Critical Reviews in Food Science and Nutrition*, *55*(2), 183–201.

Laguerre, M., Bily, A., Roller, M., & Birtić, S. (2017). Mass Transport Phenomena in Lipid Oxidation and Antioxidation. *Annual Review of Food Science and Technology*, *8*(1), 391–411.

Laguerre, M., Chen, B., Lecomte, J., Villeneuve, P., McClements, D. J., & Decker, E. A. (2011). Antioxidant properties of chlorogenic acid and its alkyl esters in stripped corn oil in combination with phospholipids and/or water. *Journal of Agricultural and Food Chemistry*, *59*(18), 10361–10366.

Laguerre, M., López Giraldo, L. J., Lecomte, J., Figueroa-Espinoza, M.-C., Baréa, B., Weiss, J., Decker, E. A., & Villeneuve, P. (2009). Chain Length Affects Antioxidant Properties of Chlorogenate Esters in Emulsion: The Cutoff Theory Behind the Polar Paradox. *Journal of Agricultural and Food Chemistry*, *57*(23), 11335–11342.

Laguerre, M., Tenon, M., Bily, A., & Birtić, S. (2020). Toward a Spatiotemporal Model of Oxidation in Lipid Dispersions: a Hypothesis-Driven Review. *European Journal of Lipid Science and Technology*, *122*(3), 1900209.

Langrish, T. A. G., Marquez, N., & Kota, K. (2006). An investigation and quantitative assessment of particle shape in milk powders from a laboratory-scale spray dryer. *Drying Technology*, *24*(12), 1619–1630.

Law, S. J., & Britton, M. M. (2012). Sizing of reverse micelles in microemulsions using NMR measurements of diffusion. *Langmuir*, *28*(32), 11699–11706.

Leal-Calderon, F., Schmitt, V., & Bibette, J. (2007). *Emulsion science: basic principles*. Springer Science & Business Media.

Let, M. B., Jacobsen, C., Sørensen, A.-D. M., & Meyer, A. S. (2007). Homogenization conditions affect the oxidative stability of fish oil enriched milk emulsions: lipid oxidation. *Journal of Agricultural and Food Chemistry*, *55*(5), 1773–1780.

Lethuaut, L., Métro, F., & Genot, C. (2002). Effect of droplet size on lipid oxidation rates of oil-in-water emulsions stabilized by protein. *Journal of the American Oil Chemists' Society*, *79*(5), 425–430.

Li, P., McClements, D. J., & Decker, E. A. (2019). Application of flow cytometry as novel technology in studying the effect of droplet size on lipid oxidation in oil-in-water emulsions. *Journal of Agricultural and Food Chemistry*, *68*(2), 567–573.

Li, P., McClements, D. J., & Decker, E. A. (2020). Application of flow cytometry as novel technology in studying lipid oxidation and mass transport phenomena in oil-in-water emulsions. *Food Chemistry*, *315*, 126225.

Li, X., Ballerini, D. R., & Shen, W. (2012). A perspective on paper-based microfluidics: Current status and future trends. *Biomicrofluidics*, *6*(1), 11301.

Lien, E. L., Richard, C., & Hoffman, D. R. (2018). DHA and ARA addition to infant formula: current status and future research directions. *Prostaglandins, Leukotrienes and Essential Fatty Acids*, *128*, 26–40.

Linke, A., Linke, T., & Kohlus, R. (2020). Contribution of the internal and external oxygen to the oxidation of microencapsulated fish oil. *European Journal of Lipid Science and Technology*, *122*(8), 1900381.

Losada Barreiro, S., Bravo-Díaz, C., Paiva-Martins, F., & Romsted, L. S. (2013). Maxima in antioxidant distributions and efficiencies with increasing hydrophobicity of gallic acid and its alkyl esters. The pseudophase model interpretation of the "cutoff effect." *Journal of Agricultural and Food Chemistry*, *61*(26), 6533–6543.

Ma, T., Kobayashi, T., & Adachi, S. (2013). Effect of droplet size on autoxidation rates of methyl linoleate and α-linolenate in an oil-in-water emulsion. *Journal of Oleo Science*, *62*(12), 1003–1008.

Maan, A. A., Boom, R., & Schroën, K. (2013a). Preparation of monodispersed oil-in-water emulsions through semi-metal microfluidic EDGE systems. *Microfluidics and Nanofluidics*, *14*(5), 775–784.

Maan, A. A., Sahin, S., Mujawar, L. H., Boom, R., & Schroën, K. (2013b). Effect of surface wettability on microfluidic EDGE emulsification. *Journal of Colloid and Interface Science*, *403*, 157–159.

Mahmood, M. E., & Al-koofee, D. a F. (2013). Effect of Temperature Changes on Critical Micelle Concentration for Tween Series Surfactant. *Global Journal of Science Frontier Research Chemistry*, *13*(4), 1–7.

Mandal, S., Banerjee, C., Ghosh, S., Kuchlyan, J., & Sarkar, N. (2013). Modulation of the photophysical properties of curcumin in nonionic surfactant (Tween-20) forming micelles and niosomes: a comparative study of different microenvironments. *The Journal of Physical Chemistry B*, *117*(23), 6957–6968.

McClements, D. J. (2004). *Food emulsions: principles, practices, and techniques*. CRC press.

McClements, D. J. (2012). Nanoemulsions versus microemulsions: terminology, differences, and similarities. *Soft Matter*, *8*(6), 1719–1729.

McClements, D. J., & Decker, E. A. (2000). Lipid Oxidation in Oil-in-Water Emulsions: Impact of Molecular Environment on Chemical Reactions in Heterogeneous Food Systems. *Journal of Food Science*, *65*(8), 1270–1282.

McClements, D. J., Dungan, S. R., German, J. B., & Kinsella, J. E. (1992). Oil exchange between oil-in-water emulsion droplets stabilised with a non-ionic surfactant. *Food Hydrocolloids*, *6*(5), 415–422.

McClements, D. J., Dungan, S. R., German, J. B., & Kinsella, J. E. (1993). Evidence of oil exchange between oil-in-water emulsion droplets stabilized by milk proteins. *Journal of Colloid and Interface Science*, *156*(2), 425–429.

Mei, L., McClements, D. J., Wu, J., & Decker, E. A. (1998). Iron-catalyzed lipid oxidation in emulsion as affected by surfactant, pH and NaCl. *Food Chemistry*, *61*(3), 307–312.

Merkx, D. W. H., Hong, G. T. S., Ermacora, A., & Van Duynhoven, J. P. M. (2018). Rapid quantitative profiling of lipid oxidation products in a food emulsion by 1H NMR. *Analytical Chemistry*, *90*(7), 4863–4870.

Montessori, A., Lauricella, M., Stolovicki, E., Weitz, D. A., & Succi, S. (2019). Jetting to dripping transition: Critical aspect ratio in step emulsifiers. *Physics of Fluids*, *31*(2), 21703.

Montessori, A., Lauricella, M., Succi, S., Stolovicki, E., & Weitz, D. (2018). Elucidating the mechanism of step emulsification. *Physical Review Fluids*, *3*(7), 72202.

Morales, A., Marmesat, S., Ruiz-Méndez, M. V., Márquez-Ruiz, G., & Velasco, J. (2015). New analytical evidence of discontinuous oxidation in dried microencapsulated lipids. *Journal of the American Oil Chemists' Society*, *92*(11–12), 1601–1607.

Muijlwijk, K., Colijn, I., Harsono, H., Krebs, T., Berton-Carabin, C., & Schroën, K. (2017). Coalescence of protein-stabilised emulsions studied with microfluidics. *Food Hydrocolloids*, *70*, 96–104.

Muijlwijk, K., Hinderink, E., Ershov, D., Berton-Carabin, C., & Schroën, K. (2016). Interfacial tension measured at high expansion rates and within milliseconds using microfluidics. *Journal of Colloid and Interface Science*, *470*, 71–79.

Naguib, Y. M. A. (2000). Antioxidant activities of astaxanthin and related carotenoids. *Journal of Agricultural and Food Chemistry*, *48*(4), 1150–1154.

Nakashima, T. (1991). Membrane emulsification by microporous glass. *Key Eng. Mater.*, *61*, 513–516.

Nakaya, K., Ushio, H., Matsukawa, S., Shimizu, M., & Ohshima, T. (2005). Effects of droplet size on the oxidative stability of oil-in-water emulsions. *Lipids*, *40*(5), 501–507.

Neves, M. A., Wang, Z., Kobayashi, I., & Nakajima, M. (2017). Assessment of Oxidative Stability in Fish Oil-in-Water Emulsions: Effect of Emulsification Process, Droplet Size and Storage Temperature. *Journal of Food Process Engineering*, *40*(1), e12316.

Niculescu, A.-G., Chircov, C., Bîrcă, A. C., & Grumezescu, A. M. (2021). Fabrication and applications of microfluidic devices: A review. *International Journal of Molecular Sciences*, *22*(4), 2011.

Nie, J., Fu, J., & He, Y. (2020). Hydrogels: the next generation body materials for microfluidic chips? *Small*, *16*(46), 2003797.

Nuchi, C. D., Hernandez, P., McClements, D. J., & Decker, E. A. (2002). Ability of lipid hydroperoxides to partition into surfactant micelles and alter lipid oxidation rates in emulsions. *Journal of Agricultural and Food Chemistry*, *50*(19), 5445–5449.

Nuchi, C. D., McClements, D. J., & Decker, E. A. (2001). Impact of Tween 20 hydroperoxides and iron on the oxidation of methyl linoleate and salmon oil dispersions. *Journal of Agricultural and Food Chemistry*, *49*(10), 4912–4916.

O'Dwyer, S. P., O'Beirne, D., Eidhin, D. N., & O'Kennedy, B. T. (2013). Effects of sodium caseinate concentration and storage conditions on the oxidative stability of oil-in-water emulsions. *Food Chemistry*, *138*(2–3), 1145–1152.

Ofner, A., Moore, D. G., Rühs, P. A., Schwendimann, P., Eggersdorfer, M., Amstad, E., Weitz, D. A., & Studart, A. R. (2017). High-Throughput Step Emulsification for the Production of Functional Materials Using a Glass Microfluidic Device. *Macromolecular Chemistry and Physics*, *218*(2).

Orlien, V., Andersen, A. B., Sinkko, T., & Skibsted, L. H. (2000). Hydroperoxide formation in rapeseed oil encapsulated in a glassy food model as influenced by hydrophilic and lipophilic radicals. *Food Chemistry*, *68*(2), 191–199.

Osborn, H. T., & Akoh, C. C. (2004). Effect of emulsifier type, droplet size, and oil concentration on lipid oxidation in structured lipid-based oil-in-water emulsions. *Food Chemistry*, *84*(3), 451–456.

Østdal, H., Davies, M. J., & Andersen, H. J. (2002). Reaction between protein radicals and other biomolecules. *Free Radical Biology and Medicine*, *33*(2), 201–209.

Pal, N., Verma, S. D., Singh, M. K., & Sen, S. (2011). Fluorescence correlation spectroscopy: an efficient tool for measuring size, size-distribution and polydispersity of microemulsion droplets in solution. *Analytical Chemistry*, *83*(20), 7736–7744.

Patil, S. M., Keire, D. A., & Chen, K. (2017). Comparison of NMR and dynamic light scattering for measuring diffusion coefficients of formulated insulin: implications for particle size distribution measurements in drug products. *The AAPS Journal*, *19*(6), 1760–1766.

Persson, K. H., Blute, I. A., Mira, I. C., & Gustafsson, J. (2014). Creation of well-defined particle stabilized oil-in-water nanoemulsions. *Colloids and Surfaces A: Physicochemical and Engineering Aspects*, *459*, 48–57.

Phonsatta, N., Deetae, P., Luangpituksa, P., Grajeda-Iglesias, C., Figueroa-Espinoza, M. C., Le Comte, J., Villeneuve, P., Decker, E. A., Visessanguan, W., & Panya, A. (2017). Comparison of antioxidant evaluation assays for investigating antioxidative activity of gallic acid and its alkyl esters in different food matrices. *Journal of Agricultural and Food Chemistry*, *65*(34), 7509–7518.

Ponginebbi, L., Nawar, W. W., & Chinachoti, P. (1999). Oxidation of linoleic acid in emulsions: Effect of substrate, emulsifier, and sugar concentration. *Journal of the American Oil Chemists' Society*, *76*(1), 131.

Porter, W. L., Black, E. D., & Drolet, A. M. (1989). Use of polyamide oxidative fluorescence test on lipid emulsions: contrast in relative effectiveness of antioxidants in bulk versus dispersed systems. *Journal of Agricultural and Food Chemistry*, *37*(3), 615–624.

Rampon, V., Lethuaut, L., Mouhous-Riou, N., & Genot, C. (2001). Interface characterization and aging of bovine serum albumin stabilized oil-in-water emulsions as revealed by front-surface fluorescence. *Journal of Agricultural and Food Chemistry*, *49*(8), 4046–4051.

Raudsepp, P., Brüggemann, D. A., & Andersen, M. L. (2014a). Detection of radicals in single droplets of oil-in-water emulsions with the lipophilic fluorescent probe BODIPY665/676 and confocal laser scanning microscopy. *Free Radical Biology and Medicine*, *70*, 233–240.

Raudsepp, P., Brüggemann, D. A., & Andersen, M. L. (2014b). Evidence for transfer of radicals between oil-in-water emulsion droplets as detected by the probe (E, E)-3, 5-bis (4-phenyl-1, 3-butadienyl)-4, 4-difluoro-4-bora-3a, 4a-diaza-s-indacene, BODIPY665/676. *Journal of Agricultural and Food Chemistry*, *62*(51), 12428–12435.

Raudsepp, P., Brüggemann, D. A., Knudsen, J. C., & Andersen, M. L. (2016). Localized lipid autoxidation initiated by two-photon irradiation within single oil droplets in oil-in-water emulsions. *Food Chemistry*, *199*, 760–767.

Raudsepp, P., Brüggemann, D. A., Lenferink, A., Otto, C., & Andersen, M. L. (2014c). Oxidative stabilization of mixed mayonnaises made with linseed oil and saturated medium-chain triglyceride oil. *Food Chemistry*, *152*, 378–385.

Rhee, K. I. S. (1978). Factors affecting oxygen uptake in model systems used for investigating lipid peroxidation in meat. *Journal of Food Science*, *43*(1), 6–9.

Richards, M. P., Chaiyasit, W., McClements, D. J., & Decker, E. A. (2002). Ability of surfactant micelles to alter the partitioning of phenolic antioxidants in oil-in-water emulsions. *Journal of Agricultural and Food Chemistry*, *50*(5), 1254–1259.

Ries, D., Ye, A., Haisman, D., & Singh, H. (2010). Antioxidant properties of caseins and whey proteins in model oil-in-water emulsions. *International Dairy Journal*, *20*(2), 72–78.

Romsted, L. S., & Bravo-Díaz, C. (2013). Modeling chemical reactivity in emulsions. *Current Opinion in Colloid & Interface Science*, *18*(1), 3–14.

Romsted, L. S., & Zhang, J. (2002). Kinetic method for determining antioxidant distributions in model food emulsions: distribution constants of t-butylhydroquinone in mixtures of octane, water, and a nonionic emulsifier. *Journal of Agricultural and Food Chemistry*, *50*(11), 3328–3336.

Roos, Y. H., Fryer, P. J., Knorr, D., Schuchmann, H. P., Schroën, K., Schutyser, M. A. I., Trystram, G., & Windhab, E. J. (2016). Food engineering at multiple scales: Case studies, challenges and the future—A European perspective. *Food Engineering Reviews*, *8*(2), 91–115.

Ruf, H. (2002). Treatment of contributions of dust to dynamic light scattering data. *Langmuir*, *18*(10), 3804–3814.

Şahin, S. (2016). *Upscaling microstructured emulsification devices*. Wageningen University and Research.

Sahin, S., Bliznyuk, O., Cordova, A. R., & Schroën, K. (2016). Microfluidic EDGE emulsification: the importance of interface interactions on droplet formation and pressure stability. *Scientific Reports*, *6*, 26407.

Sahin, S., & Schroën, K. (2015). Partitioned EDGE devices for high throughput production of monodisperse emulsion droplets with two distinct sizes. *Lab on a Chip*, *15*(11), 2486–2495.

Saito, M., Yin, L.-J., Kobayashi, I., & Nakajima, M. (2006). Comparison of stability of bovine serum albumin-stabilized emulsions prepared by microchannel emulsification and homogenization. *Food Hydrocolloids*, *20*(7), 1020–1028.

Salminen, H., Heinonen, M., & Decker, E. A. (2010). Antioxidant effects of berry phenolics incorporated in oil-in-water emulsions with continuous phase β-lactoglobulin. *Journal of the American Oil Chemists' Society*, *87*(4), 419–428.

Samtlebe, M., Yucel, U., Weiss, J., & Coupland, J. N. (2012). Stability of solid lipid nanoparticles in the presence of liquid oil emulsions. *Journal of the American Oil Chemists' Society*, *89*(4), 609–617.

Sánchez, M. del R. H., Cuvelier, M.-E., & Turchiuli, C. (2016). Effect of α-tocopherol on oxidative stability of oil during spray drying and storage of dried emulsions. *Food Research International*, *88*, 32–41.

Schaich, K. M. (1992). Metals and lipid oxidation. Contemporary issues. *Lipids*, *27*(3), 209–218.

Schaich, K. M. (2005). Lipid oxidation: theoretical aspects. *Bailey's Industrial Oil and Fat Products*.

Schaich, K. M. (2013). Challenges in elucidating lipid oxidation mechanisms: When, where, and how do products arise? In *Lipid oxidation* (pp. 1–52). Elsevier.

Schmidt, U., Weigert, M., Broaddus, C., & Myers, G. (2018). Cell detection with star-convex polygons. In *Lecture Notes in Computer Science (including subseries Lecture Notes in Artificial Intelligence and Lecture Notes in Bioinformatics): Vol. 11071 LNCS*.

Schoenmaker, L., Witzigmann, D., Kulkarni, J. A., Verbeke, R., Kersten, G., Jiskoot, W., & Crommelin, D. J. A. (2021). mRNA-lipid nanoparticle COVID-19 vaccines: Structure and stability. *International Journal of Pharmaceutics*, *601*, 120586.

Schroën, K., & Berton-Carabin, C. C. (2016). Emulsification: Established and Future Technologies. In H. G. Merkus & G. M. H. Meesters (Eds.), *Production, Handling and Characterization of Particulate Materials* (pp. 257–289). Springer International Publishing.

Schroën, K., & Berton-Carabin, C. C. (2022a). A unifying approach to lipid oxidation in emulsions: Modelling and experimental validation. *Food Research International*, 111621.

Schroën, K., Berton-Carabin, C., Renard, D., Marquis, M., Boire, A., Cochereau, R., Amine, C., & Marze, S. (2021). Droplet microfluidics for food and nutrition applications. *Micromachines*, *12*(8), 863.

Schroën, K., Bliznyuk, O., Muijlwijk, K., Sahin, S., & Berton-Carabin, C. C. (2015). Microfluidic emulsification devices: from micrometer insights to large-scale food emulsion production. *Current Opinion in Food Science*, *3*, 33–40.

Schroën, K., Wu, L., & Corstens, M. (2022b). Food-grade microgel capsules tailored for anti-obesity strategies through microfluidic preparation. *Current Opinion in Food Science*, *45*, 100816.

Serfert, Y., Drusch, S., & Schwarz, K. (2009). Chemical stabilisation of oils rich in long-chain polyunsaturated fatty acids during homogenisation, microencapsulation and storage. *Food Chemistry*, *113*(4), 1106–1112.

Shahidi, F., & Zhong, Y. (2010). Lipid oxidation and improving the oxidative stability. *Chemical Society Reviews*, *39*(11), 4067–4079.

Shang, L., Cheng, Y., & Zhao, Y. (2017). Emerging droplet microfluidics. *Chemical Reviews*, *117*(12), 7964–8040.

Shantha, N. C., & Decker, E. A. (1994). Rapid, sensitive, iron-based spectrophotometric methods for determination of peroxide values of food lipids. *Journal of AOAC International*, *77*(2), 421–424.

Shao, X., Kang, R., Zhang, Y., Huang, Z., Peng, F., Zhang, J., Wang, Y., Pan, F., Zhang, W., & Zhao, W. (2015). Highly selective and sensitive 1-amino BODIPY-based red fluorescent probe for thiophenols with high off-to-on contrast ratio. *Analytical Chemistry*, *87*(1), 399–405.

Shen, B., Ricouvier, J., Malloggi, F., & Tabeling, P. (2016). Designing colloidal molecules with microfluidics. *Advanced Science*, *3*(6).

Sørensen, A.-D. M., Baron, C. P., Let, M. B., Brüggemann, D. A., Pedersen, L. R. L., & Jacobsen, C. (2007). Homogenization conditions affect the oxidative stability of fish oil enriched milk emulsions: Oxidation linked to changes in protein composition at the oil– water interface. *Journal of Agricultural and Food Chemistry*, *55*(5), 1781–1789.

Srinivasan, S., Xiong, Y. L., & Decker, E. A. (1996). Inhibition of protein and lipid oxidation in beef heart surimi-like material by antioxidants and combinations of pH, NaCl, and buffer type in the washing media. *Journal of Agricultural and Food Chemistry*, *44*(1), 119–125.

Stöckmann, H., Schwarz, K., & Huynh-Ba, T. (2000). The influence of various emulsifiers on the partitioning and antioxidant activity of hydroxybenzoic acids and their derivatives in oil-in-water emulsions. *Journal of the American Oil Chemists' Society*, *77*(5), 535–542.

Stolovicki, E., Ziblat, R., & Weitz, D. A. (2018). Throughput enhancement of parallel step emulsifier devices by shear-free and efficient nozzle clearance. *Lab on a Chip*, *18*(1), 132–138.

Sugiura, S., Nakajima, M., Iwamoto, S., & Seki, M. (2001). Interfacial tension driven monodispersed droplet formation from microfabricated channel array. *Langmuir*, *17*(18), 5562–5566.

Sugiura, S., Nakajima, M., Kumazawa, N., Iwamoto, S., & Seki, M. (2002). Characterization of Spontaneous Transformation-Based Droplet Formation during Microchannel Emulsification. *The Journal of Physical Chemistry B*, *106*(36), 9405–9409.

Sun, X., Zhu, C., Fu, T., Ma, Y., & Li, H. Z. (2018). Dynamics of droplet breakup and formation of satellite droplets in a microfluidic T-junction. *Chemical Engineering Science*, *188*, 158–169.

Tadros, T. F. (2013). Emulsion Formation, Stability, and Rheology. In T. F. Tadros (Ed.), *Emulsion Formation and Stability* (pp. 1–75). John Wiley & Sons, Ltd.

Teh, S.-Y., Lin, R., Hung, L.-H., & Lee, A. P. (2008). Droplet microfluidics. *Lab on a Chip*, *8*(2), 198–220.

ten Klooster, S., Berton-Carabin, C., & Schroën, K. (2022a). Design insights for upscaling spontaneous microfluidic emulsification devices based on behavior of the Upscaled Partitioned EDGE device. *Food Research International*, 112365.

ten Klooster, S., Schroën, K., & Berton-Carabin, C. (2022b). Lipid oxidation products in model food emulsions: do they stay in or leave droplets, that's the question. *Food Chemistry*, 134992.

ten Klooster, S., van den Berg, J., Berton-Carabin, C., de Ruiter, J., & Schroën, K. (2022c). Upscaling microfluidic emulsification: the importance of sub-structure design in EDGE devices. *Chemical Engineering Science*, 117993.

ten Klooster, S., Villeneuve, P., Bourlieu-Lacanal, C., Durand, E., Schroën, K., & Berton-Carabin, C. (2022d). Alkyl chain length modulates antioxidant activity of gallic acid esters in spray-dried emulsions. *Food Chemistry*, *387*, 132880.

ten Klooster, Sahin, S., & Schroën, K. (2019). Monodisperse droplet formation by spontaneous and interaction based mechanisms in partitioned EDGE microfluidic device. *Scientific Reports*, *9*(1), 1–12.

Theberge, A. B., Courtois, F., Schaerli, Y., Fischlechner, M., Abell, C., Hollfelder, F., & Huck, W. T. S. (2010). Microdroplets in microfluidics: an evolving platform for discoveries in chemistry and biology. *Angewandte Chemie International Edition*, *49*(34), 5846–5868.

Trinder, P. (1969). Quantitative determination of triglyceride using GPO-PAP method. *Ann Biochem*, *6*, 24–27.

Truesdale, G. A., Downing, A. L., & Lowden, G. F. (1955). The solubility of oxygen in pure water and sea-water. *Journal of Applied Chemistry*, *5*(2), 53–62.

van de Put, M. W. P., Patterson, J. P., Bomans, P. H. H., Wilson, N. R., Friedrich, H., Van Benthem, R. A. T. M., De With, G., O'Reilly, R. K., & Sommerdijk, N. A. J. M. (2015). Graphene oxide single sheets as substrates for high resolution cryoTEM. *Soft Matter*, *11*(7), 1265–1270.

Van Dijke, K. C., Schroën, K. C., & Boom, R. M. (2008). Microchannel emulsification: from computational fluid dynamics to predictive analytical model. *Langmuir*, *24*(18), 10107–10115.

van Dijke, K. C., Schroën, K., van der Padt, A., & Boom, R. (2010a). EDGE emulsification for food-grade dispersions. *Journal of Food Engineering*, *97*(3), 348–354.

van Dijke, K. C., Veldhuis, G., Schroën, K., & Boom, R. M. (2010b). Simultaneous formation of many droplets in a single microfluidic droplet formation unit. *AIChE Journal*, *56*(3), 833–836.

van Dijke, K., de Ruiter, R., Schroën, K., & Boom, R. (2010c). The mechanism of droplet formation in microfluidic EDGE systems. *Soft Matter*, *6*(2), 321–330.

van Dijke, K., Veldhuis, G., Schroën, K., & Boom, R. (2009). Parallelized edge-based droplet generation (EDGE) devices. *Lab on a Chip*, *9*(19), 2824–2830.

Van Dijke, Kobayashi, I., Schroën, K., Uemura, K., Nakajima, M., & Boom, R. (2010). Effect of viscosities of dispersed and continuous phases in microchannel oil-in-water emulsification. *Microfluidics and Nanofluidics*, *9*(1), 77–85.

Van Ruth, S. M., Roozen, J. P., & Jansen, F. (1999). Release of odour active compounds from oxidised sunflower oil and its oil-in-water emulsion. *Proceedings Weurman 99 Flavour Research Symposium: Freising, Germany, 22-25 June 1999*, 22.

Vandemoortele, A., Simon, M., Claes, A., & De Meulenaer, B. (2020). Behavior of Hexanal,(E)-Hex-2-enal, 4-Hydroxyhex-2-enal, and 4-Hydroxynon-2-enal in Oil-in-Water Emulsions. *Journal of Agricultural and Food Chemistry*, *68*(41), 11568–11577.

Vannice, G., & Rasmussen, H. (2014). Position of the academy of nutrition and dietetics: dietary fatty acids for healthy adults. *Journal of the Academy of Nutrition and Dietetics*, *114*(1), 136–153.

Velasco, J., Dobarganes, C., & Márquez-Ruiz, G. (2003). Variables affecting lipid oxidation in dried microencapsulated oils. *Grasas y Aceites*, *54*(3), 304–314.

Velasco, J., Holgado, F., Dobarganes, C., & Márquez-Ruiz, G. (2009). Antioxidant activity of added phenolic compounds in freeze-dried microencapsulated sunflower oil. *Journal of the American Oil Chemists' Society*, *86*(5), 445–452.

Velasco, J., Marmesat, S., Dobarganes, C., & Márquez-Ruiz, G. (2006). Heterogeneous aspects of lipid oxidation in dried microencapsulated oils. *Journal of Agricultural and Food Chemistry*, *54*(5), 1722–1729.

Venkateshwarlu, G., Let, M. B., Meyer, A. S., & Jacobsen, C. (2004). Modeling the sensory impact of defined combinations of volatile lipid oxidation products on fishy and metallic off-flavors. *Journal of Agricultural and Food Chemistry*, *52*(6), 1635–1641.

Vignolles, M.-L., Jeantet, R., Lopez, C., & Schuck, P. (2007). Free fat, surface fat and dairy powders: interactions between process and product. A review. *Le Lait*, *87*(3), 187–236.

Villeneuve, P., Bourlieu-Lacanal, C., Durand, E., Lecomte, J., McClements, D. J., & Decker, E. A. (2021). Lipid oxidation in emulsions and bulk oils: a review of the importance of micelles. *Critical Reviews in Food Science and Nutrition*, 1–41.

Villeneuve, P., Durand, E., & Decker, E. A. (2018). The Need for a New Step in the Study of Lipid Oxidation in Heterophasic Systems. *Journal of Agricultural and Food Chemistry*, *66*(32), 8433–8434.

Vincent, B. (2010). Emulsions. In T. Cosgrove (Ed.), *Colloid Science - Principles, Methods and Applications* (2nd ed., pp. 117–133). John Wiley & Sons.

Visser, C. W., Kamperman, T., Karbaat, L. P., Lohse, D., & Karperien, M. (2018). In-air microfluidics enables rapid fabrication of emulsions, suspensions, and 3D modular (bio) materials. *Science Advances*, *4*(1), eaao1175.

Vladisavljević, G. T., Ekanem, E. E., Zhang, Z., Khalid, N., Kobayashi, I., & Nakajima, M. (2018). Long-term stability of droplet production by microchannel (step) emulsification in microfluidic silicon chips with large number of terraced microchannels. *Chemical Engineering Journal*, *333*(Supplement C), 380–391.

Vladisavljević, G. T., Kobayashi, I., & Nakajima, M. (2011). Effect of dispersed phase viscosity on maximum droplet generation frequency in microchannel emulsification using asymmetric straight-through channels. *Microfluidics and Nanofluidics*, *10*(6), 1199–1209.

Vladisavljević, G. T., Kobayashi, I., & Nakajima, M. (2012). Production of uniform droplets using membrane, microchannel and microfluidic emulsification devices. *Microfluidics and Nanofluidics*, *13*(1), 151–178.

Volf, I., Ignat, I., Neamtu, M., & Popa, V. I. (2014). Thermal stability, antioxidant activity, and photo-oxidation of natural polyphenols. *Chemical Papers*, *68*(1), 121–129.

Walstra, P. (1993). Principles of emulsion formation. *Chemical Engineering Science*, *48*(2), 333–349.

Walstra, P. (2001). Introduction. In P. Walstra (Ed.), *Physical Chemistry of Foods* (1st ed., pp. 1–8). CRC press.

Waraho, T., McClements, D. J., & Decker, E. A. (2011a). Impact of free fatty acid concentration and structure on lipid oxidation in oil-in-water emulsions. *Food Chemistry*, *129*(3), 854–859.

Waraho, T., McClements, D. J., & Decker, E. A. (2011b). Mechanisms of lipid oxidation in food dispersions. *Trends in Food Science & Technology*, *22*(1), 3–13.

Weiss, J., Canceliere, C., & McClements, D. J. (2000). Mass transport phenomena in oil-in-water emulsions containing surfactant micelles: Ostwald ripening. *Langmuir*, *16*(17), 6833–6838.

Wooster, T. J., Golding, M., & Sanguansri, P. (2008). Impact of oil type on nanoemulsion formation and Ostwald ripening stability. *Langmuir*, *24*(22), 12758–12765.

Yang, S., Takeuchi, M., Friedrich, H., van Duynhoven, J. P. M., & Hohlbein, J. (2023). Unravelling mechanisms of protein and lipid oxidation in mayonnaise at multiple length scales. *Food Chemistry*, *402*(March 2022), 134417.

Yang, S., Verhoeff, A. A., Merkx, D. W. H., van Duynhoven, J. P. M., & Hohlbein, J. (2020). Quantitative spatiotemporal mapping of lipid and protein oxidation in mayonnaise. *Antioxidants*, *9*(12), 1278.

Ye, A. (2008). Interfacial composition and stability of emulsions made with mixtures of commercial sodium caseinate and whey protein concentrate. *Food Chemistry*, *110*(4), 946–952.

Yoshida, Y., & Niki, E. (1992). Oxidation of methyl linoleate in aqueous dispersions induced by copper and iron. *Archives of Biochemistry and Biophysics*, *295*(1), 107–114.

Yoshida, Y., Shimakawa, S., Itoh, N., & Niki, E. (2003). Action of DCFH and BODIPY as a probe for radical oxidation in hydrophilic and lipophilic domain. *Free Radical Research*, *37*(8), 861–872.

You, Y., Bloomfield, A., Liu, J., Fu, L., Herzon, S. B., & Yan, E. C. Y. (2012). Real-time kinetics of surfactant molecule transfer between emulsion particles probed by in situ second harmonic generation spectroscopy. *Journal of the American Chemical Society*, *134*(9), 4264–4268.

Zhan, F., Hu, J., He, C., Sun, J., Li, J., & Li, B. (2020). Complexation between sodium caseinate and gallic acid: Effects on foam properties and interfacial properties of foam. *Food Hydrocolloids*, *99*, 105365.

Zhang, Y., Kobayashi, I., Neves, M. A., Uemura, K., & Nakajima, M. (2015). Effects of surface treatment and storage conditions of silicon microchannel emulsification plates on their surface hydrophilicity and preparation of soybean oil-in-water emulsion droplets. *Journal of Food Engineering*, *167*, 106–113.

Zhu, P., & Wang, L. (2017). Passive and active droplet generation with microfluidics: a review. *Lab on a Chip*, *17*(1), 34–75.

Summary

An early 'experiment' on food emulsion production dates back to 1756, when a sauce called 'Mahonaisse' was produced. This product was received well, but it was probably not very stable. As is generally known now, the stability of emulsion products is highly influenced by their ingredients and by the preparation process used; yet, suppressing both physical and lipid oxidation instabilities in emulsion products remains challenging because the dynamic processes involved are not that well-understood. This thesis is dedicated to shed light on how dynamic processes that occur at scales ranging from the molecular to the macroscopic scale contribute to lipid oxidation. To achieve this, we used innovative analysis methods that are at the very edge of what is currently possible, and we developed experimental set-ups that enabled, for example, the production of monodisperse emulsions.

As a first step, we tried to get a better control over the oil droplet size using microfluidic techniques, since conventional emulsification techniques have a very limited control over droplet size distributions. The oil throughput with microfluidic emulsification devices is typically < 100 μL/h for the production of vegetable oil-based emulsions with droplets < 10 μm. This throughput was not enough to perform lipid oxidation experiments; therefore, in the first chapters (**Chapter 2 & 3**), we addressed upscaling options for the production of relatively small droplets (< 10 μm) as well as for larger droplets (10-50 μm) that are formed through different mechanisms.

An upscaled microfluidic emulsification chip containing 75,000 droplet formation units is presented in **Chapter 2**. Using this chip, we showed in a proof-of-concept study that productivity can be improved greatly if the flow resistance is high enough to allow for a maximum pressure applied over the dispersed phase that exceeds the Laplace pressure of the bare oil-water interface inside the droplet formation unit. This reduces the time needed for refilling the droplet formation unit, and thus increases the productivity. These insights were used to design the UPE (Upscaled Partitioned EDGE) chip, which is presented in **Chapter 3**. With this chip, we were able to make highly monodisperse droplets of different sizes between 3.5 and 30 μm by using either the interfacial tension-based droplet formation mechanism or a relatively new mechanism based on a cascaded physical push by neighbouring droplets. This led to design guidelines at various levels for upscaled microfluidic emulsion production: (i) droplet formation unit design for the desired droplet size, (ii) dispersed phase supply channels design for high productivity, and, (iii) continuous phase channel

design for targeted oil concentration in the emulsion. Furthermore, the effect of ingredients on droplet size and productivity was reported.

The highly monodisperse droplets produced with the microfluidic chips from Chapter 3 enabled studying the effect of droplet size on lipid oxidation in a surfactant-stabilised model emulsion, as reported in **Chapter 4**. We found a systematic increase of lipid oxidation with decreasing droplet size, which was ascribed to a favoured contact between the prooxidant iron-EDTA complex and the lipids. The results in this chapter also show that Tween 20 co-oxidation took place, and that this may be initiated by lipid oxidation, which is a phenomenon that has hardly been considered so far. Unlike monodisperse microfluidic droplets, the size difference between the smallest and the largest droplets in 'classically produced' emulsions can be in the order of a factor 1000, and this is expected to play a considerable role in oxidation. This was investigated in dept in **Chapter 5**, where advanced cryo-transmission electron microscopy was used to show that 'very small' droplets (10-100 nm) exist in these emulsions; the lower end of this range is close to the size of surfactant micelles (~ 10 nm). We found that both primary and secondary lipid oxidation products were overrepresented in these very small droplets, which was again ascribed to favoured lipid oxidation initiation due to the larger interfacial area and subsequent reaction propagation. This latter effect was substantiated by the higher concentration of specific secondary lipid oxidation products (namely, 4-hydroxy-2-nonenal to 4-hydroperoxy-2-nonenal) in the very small droplets compared to the whole emulsion (Chapter 9).

A comparison between emulsions prepared with microfluidics and conventional emulsification techniques was made in **Chapter 6**. In this chapter we used BODIPY 665/676 fluorescence measurements with confocal laser scanning microscopy to localise lipid oxidation, and to validate this method, BODIPY fluorescence was correlated to lipid oxidation product formation in monodisperse emulsions. The decrease in red fluorescence occurred at lower oxidation levels for Tween 20-stabilised emulsions than for WPI-stabilised emulsions. Lipid oxidation and most probably also protein oxidation increased with decreasing droplet size, which makes lipid oxidation in emulsions heterogeneous at the level of droplets. For WPI-stabilised monodisperse emulsions, the oil droplets were also found to oxidise in a heterogeneous way. In addition, extensive and highly heterogenous protein oxidation takes place in polydisperse emulsions, and to much lesser extent in monodisperse emulsions. This is expected to be intertwined with lipid oxidation, but it remains difficult to substantiate the intertwining given the heterogenous and complex nature of protein oxidation.

Besides reaction kinetics, mass transfer of components can play a role in the observed oxidation patterns. In **Chapter 7**, we found that short and hydrophilic lipid oxidation products, such as 4-hydroperoxy-2-nonenal, can be rapidly transferred between droplets, whereas the non-water-soluble triglycerides with a hydroperoxide group did not exchange between droplets. We found indications that the presence of 4-hydroperoxy-2-nonenal (0.2 mmol/kg oil) in fresh vegetable oil droplets can lead to slightly accelerated lipid oxidation, but that this is not always systematic nor reproducible. If the fresh droplets do not contain molecules that are sensitive to initiation reactions, then the provision of molecules that are sensitive to initiation reactions can subsequently cause oxidation via propagation reactions (H abstraction). On the other hand, if the 'fresh' droplets already contain molecules that are sensitive to initiation reactions, the provision of other sensitive molecules is not expected to have a large impact.

Emulsions are often dried to extend their shelf life, which results in a very different structure from wet emulsions. In such powder particles (~ 100 μm), the lipids are either encapsulated in the matrix or spread over the surface of the powder. In **Chapter 8**, we evaluated how antioxidant polarity affects lipid oxidation by assessing the effectiveness of phenolipid (gallic acid esters) antioxidants during processing and during storage based on their alkyl chain length. We found that for both the surface free fat and the encapsulated fat, the most polar gallic acid alkyl esters were ineffective, which we ascribed to their partitioning. We expect these hydrophilic antioxidants to (partly) end-up in the matrix, where they cannot counteract lipid oxidation. There is an 'optimal' polarity for the antioxidants, for which lipid oxidation is lowest. At lower polarity, lipid oxidation increases again slightly. When comparing encapsulated and free fat, we found that at high antioxidant polarity, the encapsulated fat oxidised slightly faster, whereas for a nonpolar antioxidant the free fat oxidised slightly faster. Even though the differences were always very small, there seems to be a switchover effect.

Finally, in **Chapter 9**, the findings of this thesis regarding droplet formation with microfluidic devices and lipid oxidation of the resulting droplets are discussed in a broader context. By doing so, we provide an answer to the compelling question: 'Is microfluidic emulsification only a powerful analytical tool, or can it also be a means to produce stable emulsions on larger scale?'

Since the first production of the 'Mahonaisse' in 1756, a lot of progress has been made in understanding emulsion formation, including instability mechanisms

such as lipid oxidation. This thesis has made a valuable contribution to our understanding of lipid oxidation, which was achieved by the highly advanced techniques that were used to make and analyse well-defined emulsions. Just to name a few insights that were obtained: (i) the role of droplet size including that of tiny droplets, (ii) the heterogeneity encountered in the emulsion systems, (iii) the effectiveness of antioxidants on lipid oxidation in spray-dried emulsions, and (iv) the transfer of low molecular weight small components. This has opened the way to an even deeper understanding of various effects that play a role during lipid oxidation, most notably: radical concentrations, reaction kinetics, transfer effects, and co-oxidising species.

Such insights are expected to contribute to further improvements in shelf life of emulsions products. The emulsion products made with whisk-like tools around 1756 were probably only stable for a couple of days at most, whereas the emulsion products that are prepared nowadays by homogenisers have a shelf life of > 1 year. As a next step monodisperse droplet production by microfluidics could be considered. This may sound like a futuristic tale, but the prototype upscaled microfluidic emulsification device presented in this ultimate chapter, and the fact that multiple start-ups have devoted themselves to upscaling this technology, indicates that industrial scale production of different emulsion product types by microfluidics lies within reach. This might lead to the next revolution in improved shelf life, and to the creation of added functionality for controlled release of active compounds (which is often droplet size-dependent), either for food or pharmaceutical applications. Until then, we will definitely continue to explore the use of microfluidic tools for an improved understanding of (oxidative) emulsion stability, given their unique control over droplet size.

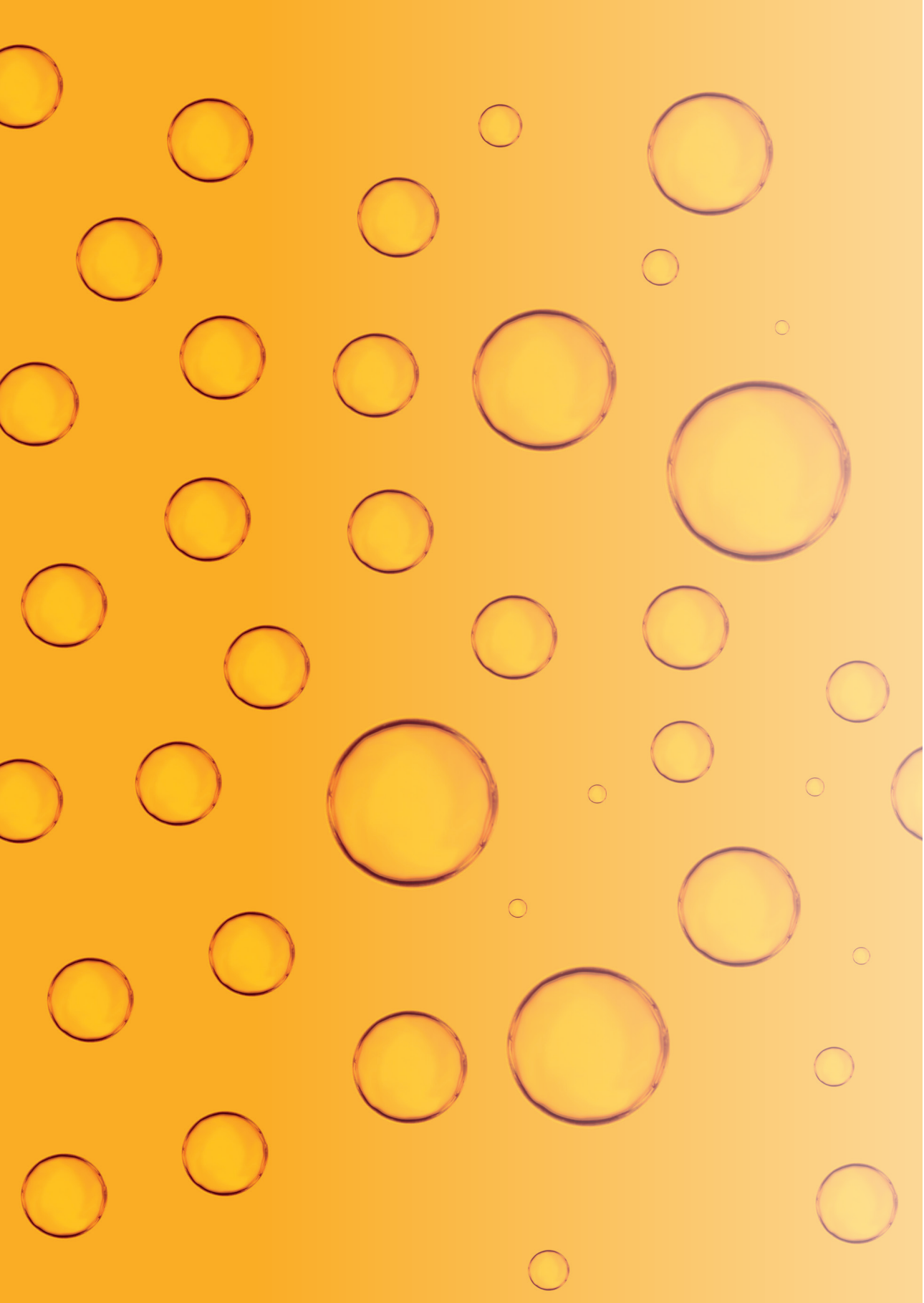

Appendix

Acknowledgements / Dankwoord
List of publications
Overview of completed training activities
About the author

Acknowledgements / Dankwoord

The involvement of and help by many people have not just made a major contribution to the quality of this work, but also to the fun that I experienced during my PhD. This makes that I am very happy to show my gratitude to everyone that was part of this journey. These people had different roles: some made this journey possible; others made this journey enjoyable; there are people that helped me to reach high peaks; and people that did drag me through dark and swampy valleys, therewith dropping me off at the foot of the next mountain; there are even people who I would like to thank for all of the above.

Ground control
First and foremost, I would like to thank my supervisors, **Claire** and **Karin**, who definitely belong to this last category. Thank you for always being so patient; thank you for always showing confidence in my capabilities; and thank you for always being understanding. Above all, I would like to thank you that I always felt welcome to share anything with you. The fun that we had during very insightful discussions are a perfect indication of how well we operated as a team. **Karin**, we first met during my BSc thesis, in 2015, and it is incredible how much I have learned from you ever since. It is inspiring how your unparalleled commitment always leads to outcomes that are beyond of what was considered achievable on forehand, and that certainly also counts for my PhD. I am especially very thankful for the great deal of motivation that you provided me with. **Claire**, I cannot express how happy I am that you decided to continue to work with FPE when you moved back to France. Your outstanding knowledge and unconditional support have not just added a lot to the content of my PhD, but have also made a positive contribution to the fun that I had during this PhD journey; I am still very grateful for the times that we could meet in person. Dear **Karin** and **Claire**, I cannot be thankful enough to both of you, and I sincerely hope that we keep in touch.

Leonie, bedankt dat je mij in de waardevolle coachsessies hebt geleerd dat plezier in je werk het allerbelangrijkste is en dat je daar zelf verantwoordelijk voor bent. Dit zal mij de rest van mijn leven bijblijven.

Journey guides at FPE
Technicians, **Maurice**, **Jos**, **Wouter**, **Martin**, **Lyneth** en **Jarno**, ontzettend bedankt voor jullie hulp en inzet; dit heeft de kwaliteit van mijn onderzoek enorm bevorderd. Jullie zijn ongelofelijk belangrijk in het onderhouden en verbeteren van de wegen die we bij FPE hebben en dat kan niet vaak genoeg benadrukt worden.

Marjan, **Ilona**, **Esther** en **Evelyn**, ik wil jullie graag hartelijk bedanken voor het in orde brengen van alle administratie (of in deze context: reisinformatie).

Journey guides / fellow travellers of License
It was great to be part of the LICENSE project during this journey, which has made a major contribution to the quality of my work. Within this project, we had many insightful project meetings and collaborations. I would like to thank **Machi** and **Suyeon**, for the great collaborations, which resulted in beautiful destinations (chapters) that I am very proud of: Chapter 5 & 6, respectively. Bedankt **Vincent** voor alle koffietjes die uiteindelijk altijd uitliepen op interessante onderzoek-gerelateerde besprekingen, met een hele mooie gezamenlijke publicatie (Chapter 4) als resultaat. Kijk jij ook zo uit naar de ontmoeting met de 'zeehond' van de WU aan het eind van de reis? **Katharina**, bedankt voor alles; it was very pleasant to have you around as a LICENSE-FPE-buddy, and it is awesome that our collaboration is also going to result in a very nice publication. **Khoa**, **Eleni**, and **Jianli**, thank you for the great time during all the LICENSE events. Of course, I would also like to thank the scientific staff involved in LICENSE: **John**, **Marie**, **Johannes**, **Remco**, **Heiner**, **Peter**, **Hans-Gerd**, and **Jean-Paul**, thank you for your valuable contributions to this work. I would like to thank everyone from Danone and Unilever involved in the LICENSE project: **Chris**, **Rayo**, **Silvia**, **Leonardo**, **Roland**, **Arend**, **Ewoud**, **Anne**, **Simeon**, and **Lia**. Thank you for your interest and participation in this research, and I happily acknowledge that this has improved the quality of this work. This consortium has often given me a nice boost of motivation.

I would also like to thank **Pierre**, **Erwann**, and **Claire** (**BL**) for the collaboration on Chapter 8, and I would like to thank **Jolet**, **Jelle** (hartelijk bedankt ook voor de schets van de cover!), and **Justin** for their valuable contributions to Chapter 2 and/or 3.

Fellow travellers at FPE/WUR
Throughout my PhD it has been very helpful to have other researchers around me, such as the Micro-team. If needed the help from the team was always very accessible for which I am very thankful to: **Boxin**, **Ivanna**, **Murat,** **Emma**, **Anja**, **Lingfeng**, **Kieke**, **Jiarui**, **Meinou**, **Herehau**, **Yhan**, **Fathinah**, **Asif**, **Justin**, **Jilu**, and **Pina**. Ik wil graag **Emma** in het bijzonder bedanken; ik heb het altijd heel fijn gevonden om mijn onderzoek met jou te bespreken. **Donny**, **Yanzhang**, and **Tatiana**, many thanks for all the NMR related help. The accessibility to the NMR measurements has not just improved the quality of my work, but has also saved me a lot of frustration; imagine that I would

have had to do all those measurements with the spectrophotometer instead...

Ik wil graag mijn talentvolle studenten **Lianne**, **Janna**, **Koen**, **Luuk**, **Pien**, **Niels** en **Isabelle**, bedanken voor jullie belangrijke bijdragen aan mijn onderzoek. Het was ontzettend leuk om met jullie samen te werken en mede dankzij jullie ging ik met veel plezier naar mijn werk.

Throughout the past four years, I have had a lot of fun with **many awesome friends at work**. It was amazing to organize the **PhD-trip** with such a fantastic committee. I would further like to thank my **office mates** for all the nice chats and fun office activities we had together. I am thankful to all my friends at WUR for all the fun times: from **coffee breaks** to **borrels**; from **power dumb*bellen*** to the **Veluweloop**; from enjoying lunch in the **cofFPEcorner** to lunches at **CP**; and from **group days / labuitjes** to awesome **trips** (e.g. Cork, France, Sofia, Singapore); I look back at all these moments with a big smile, and I will definitely miss that. **Loes** en **Patrick**, ik vind het ontzettend fijn dat ik mijn PhD mag gaan verdedigen met twee zulke goede maatjes aan mijn zijde. Ik ben jullie heel erg dankbaar voor alles wat jullie doen; zowel in voorbereiding als straks op de dag zelf.

Stay-at-home, yet important, folks
Wanneer je op reis bent, is het toch wel erg prettig om een fijn thuisfront te hebben waar je altijd op kunt terugvallen. Daarom wil ik hieronder graag mijn (**schoon**)**familie** en **vrienden** bedanken voor de afleiding en de support die ik afgelopen jaren heb gekregen.

Dit zijn vrienden waarmee ik heerlijk heb gesport (**Duurkamelen**, **Bende van Ellende**), vrienden waarmee ik allerlei activiteiten ondernam en vrienden waarmee we weekendjes / weekjes weggingen (**Vakantiefey, OnVerWagT, Jellies**, **Bestuur NA 2015, Clownerij**). Het deed me altijd goed dat jullie een beetje op de hoogte wilden blijven van mijn PhD.

Zonder de zorgeloze jeugd die ik dankzij mijn ouders heb mogen ervaren, had ik nooit de kans gekregen om aan dit avontuur te mogen beginnen, dus een bedankje naar jullie, **pa** en **mam**, is zeker op zijn plek. **Pa**, bedankt dat je me hebt bijgebracht dat dingen niet komen aanwaaien en dat als je iets moois wilt bereiken, je ervoor zult moeten werken. Dit is van onbeschrijfelijk groot belang geweest voor het behalen van mijn PhD. Daarnaast ook heel erg bedankt voor je hulp bij het ontwerpen van mijn cover, pa! **Mam**, bedankt dat je me hebt geleerd dat het heel belangrijk is naar je gevoel te luisteren en bedankt dat je me altijd

wil helpen om mijn gevoelens een plekje te geven. Dit heeft me ook tijdens mijn PhD enorm geholpen. Lieve zus **Irina**, en **Dennis**, bedankt voor jullie support tijdens mijn PhD. **Irina**, ik heb van jou mogen leren dat als je tegen iets opziet, dat je het maar beter zo snel mogelijk kan doen en dat je dan naderhand best een beetje trots mag zijn op jezelf; en dat zal ik zijn! En ten slotte wil ik mijn lieve vriendin **Wilke** ontzettend bedanken. Bedankt dat ik zowel persoonlijke als onderzoeks-technische opgaves met je kon bespreken; bedankt dat je altijd tijd vrijmaakte om te helpen; bedankt dat je stond te springen wanneer een van mijn papers geaccepteerd was; maar bovenal bedankt dat je me troostte als dat nodig was. Je was onwijs belangrijk gedurende mijn PhD. Nu de PhD-bestemming is bereikt, kijk ik er ontzettend naar uit om onze gezamenlijke reis te vervolgen.

List of publications:

This dissertation

S. ten Klooster, J. van Den Berg, C. Berton-Carabin, J. de Ruiter, and K. Schroën: **Upscaling microfluidic emulsification: the importance of sub-structure design in EDGE devices**, Chemical Engineering Science 261 (2022), 117993. (Chapter 2)

S. ten Klooster, C. Berton-Carabin, and K. Schroën: **Design insights for upscaling spontaneous microfluidic emulsification devices based on behaviour of the Upscaled Partitioned EDGE device**, Food Research International (2022), 112365. (Chapter 3)

S. ten Klooster, M. Takeuchi, K. Schroën, R. Tuinier, R. Joosten, H. Friedrich, and C. Berton-Carabin: **Tiny, yet impactful: Detection and oxidative stability of very small oil droplets in surfactant-stabilized emulsions**, submitted. (Chapter 5)

S. ten Klooster, K. Schroën, and C. Berton-Carabin: **Lipid oxidation products in model food emulsions: do they stay in or leave droplets, that's the question**, Food Chemistry 405 (2023), 134992. (Chapter 7)

S. ten Klooster, P. Villeneuve, C. Bourlieu-Lacanal, E. Durand, K. Schroën, and C. Berton-Carabin: **Alkyl chain length modulates antioxidant activity of gallic acid esters in spray-dried emulsions**, Food Chemistry 387 (2022), 132880. (Chapter 8)

Other publications

S. ten Klooster, S. Sahin, and K. Schroën: **Monodisperse droplet formation by spontaneous and interaction based mechanisms in Partitioned EDGE microfluidic device**, Scientific reports 9, no. 1 (2019): 1-12.

T. van de Laar, S. ten Klooster, K. Schroën, and J. Sprakel: **Transition-state theory predicts clogging at the microscale, Scientific reports 6**, no. 1 (2016): 1-8.

S. ten Klooster, V. Boerkamp, E. Lazaridi, S. Yang, M. Takeuchi, C. Berton-Carabin, K. Schroën, H.G Janssen, H. Friedrich, J. Hohlbein, J van Duynhoven, and H. Hennebelle: **Lipid Oxidation in Food Emulsions: Analytical Challenges and Recent Developments**, Lipid Oxidation in Food and Biological Systems (2022): 3-29.

Overview of completed training activities

Discipline specific activities	Organizer	Year
Edible Soft Matter (Le Mans)	LMU	2019
Bubble & Drop (Sofia)	BAS	2019
VLAG Online Lecture Series (online)	VLAG	2020
AOCS Annual Meeting (online)	AOCS	2020
3rd International Symposium on Lipid Oxidation and Antioxidants (online)	EFL	2020
Fundamentals of Nanotechnology (online)	UT	2021
AOCS Annual Meeting (online)	AOCS	2021
18th Euro Fed Lipid Congress and Expo (online)	UL	2021
AOCS Annual Meeting (online)	AOCS	2022
Edible Soft Matter (Wageningen)	WUR	2022
International MicroNano conference (Enschede)	UT	2022
General courses		
Adobe Indesign	WGS	2019
Brain Training	WGS	2019
VLAG PhD week	VLAG	2019
Supervising BSc and MSc students	WGS	2020
Scientific Writing	WGS	2020
Introduction to R	VLAG	2022
Career Perspectives	WGS	2022
Other		
Preparation of research proposal	WUR - FPE	2019
PhD study tour to Singapore	WUR - FPE	2022
Organizing PhD study tour to Singapore	WUR - FPE	2022
Weekly group meetings	WUR - FPE	2019 - 2023
FPE symposia	WUR - FPE	2019 - 2023

About the author

Sten ten Klooster was born on the 23rd of July, 1994, in Delft, the Netherlands. He obtained his VWO diploma in 2013, with a major in Nature and Health, at Christelijk Lyceum Delft.

Later that year, Sten started with a BSc Food technology at Wageningen University, and he graduated in 2016 with a minor in Environmental Engineering (Kaunas University of Technology, Lithuania). His BSc thesis was about clogging of microchannels. Sten continued with a master, also in Food Technology at Wageningen University, and he graduated with distinction in 2019. His MSc thesis was about producing emulsions with microfluidics. With this thesis, he won the 2018 Thesis Award in the domain of Agrotechnology and Food Sciences. His MSc internship was performed at Teagasc Moorepark (Fermoy, Ireland), where he worked on optimising a pilot-scale spray drying process of full fat milk.

In 2019, Sten started as a PhD-candidate at the Food Process Engineering department of Wageningen University, under supervision of prof. dr. ir. CGPH Schroën and dr. CC Berton-Carabin. His PhD research was about lipid oxidation in food emulsions, with a specific focus on producing well defined emulsions using microfluidics. The findings of this research are discussed in this thesis.

Cover: Roland ten Klooster (sketch),
Jelle van den Berg (sketch),
Farrukh Khan (final cover design)
Layout: ProefschriftMaken.nl
Printing: ProefschriftMaken.nl

This work was part of the LICENSE project, supported by the Dutch Research Council (NWO), grant number 731.017.301.